UNIVERSITY OF LEEDS

Amyloid Disease Models in *C. elegans*: insights into the toxicity of β_2-microglobulin and islet amyloid polypeptide

Sarah Catherine Good

Submitted in accordance with the requirements for the degree of Doctor of Philosophy

The University of Leeds
School of Molecular & Cellular Biology
Astbury Centre for Structural Molecular Biology

January 2021

The candidate confirms that the work submitted is their own, except where work which has formed part of jointly authored publications has been included. The contribution of the candidate and the other authors to this work has been explicitly indicated below. The candidate confirms that appropriate credit has been given within the thesis where reference has been made to the work of others.

Some of the work shown in Chapter 5 of the thesis has appeared in publications as follows:
O'Brien D., Jones L. M., Good S., Miles J., Vijayabaskar M. S., Aston R., Smith C. E., Westhead D. R., van Oosten-Hawle P.; 2018. A PQM-1-Mediated Response Triggers Transcellular Chaperone Signalling and Regulates Organismal Proteostasis. Cell Reports
For this work I performed paralysis assays on models overexpressing HSP-90 in either the body wall muscle, neurons or intestines of an Alzheimer's *C. elegans* model to demonstrate the effect of HSP-90 on amyloid-β aggregation. Furthermore, the effect of *pqm-1* knockdown by RNAi was assessed through paralysis assays in these models. All other work in this publication was performed by the co-authors and was not included in this thesis.
Lackie R. E., Marques-Lopes J., Ostapchenko V. G., Good S., Choy W-Y., van Oosten-Hawle P., Pasternak S. H., Prado V. F., and Prado M. A. M.; 2020 Increased levels of Stress-inducible phosphoprotein-1 accelerates amyloid-ß deposition in a mouse model of Alzheimer's disease. Acta Neuropathologica Communications
For this work I overexpressed STI-1 and performed RNAi knockdown of STI-1 in an Alzheimer's *C. elegans* model and performed paralysis assays to determine their effect on toxicity. All other work in this publication was performed by the co-authors and was not included in this thesis.

Acknowledgements

First and foremost, I'd like to thank my supervisor Dr Patricija van Oosten-Hawle and co-supervisor Professor Sheena Radford for their continued guidance and supervision throughout this project for which I have thoroughly enjoyed for the past four years. They have both provided tremendous support throughout this project in order to develop both my research and wider skills, and I will forever be thankful for the opportunities they have provided me throughout this time.

I would also like to thank the BBSRC for funding this research and to the members of the White Rose BBSRC management board for supporting my continued training and development throughout.

I would like to thank the other members of the van Oosten-Hawle and Radford groups for providing scientific support, encouragement and friendship and I have enjoyed working with them all. I would especially like to thank Jay Miles and Laura Jones for singing along to Absolute radio in the worm room with me and putting up with my mostly nonsensical chatter throughout the bulk of my time here; and to Sarah Townend and Albin Mejzini for taking over this mantle for the last year of my PhD. Thanks also to the other members of the Garstang building for providing a brilliant working environment and supporting my love of biscuits, doughnuts and the pub; in particular to Becky Foster and Georgia Pangratiou for being great friends, listening to my half-baked ideas and concerns, and overall being a massive support. I would like to also thank the Amyloiders for their scientific support and for providing purified β_2m and IAPP samples that I could use in my research.

I'd also like to thank my friends and family, whose support has been felt throughout my time. In particular, Penny whose reminder that this PhD wouldn't complete itself really spurred me to get working, and to Team for providing lots of fun. Finally, a massive thank you to Sam, for being so great and patiently listening to all the details of my project and for whom I am sure never wants to hear the words *C. elegans,* β_2m or IAPP ever again.

Abstract

The formation of amyloid fibres is associated with degenerative disorders including Alzheimer's, type II diabetes mellitus (T2DM) and dialysis related amyloidosis (DRA) amongst others. In order to study how amyloidogenic proteins can aggregate and cause toxicity, numerous *in vivo* disease models have been generated in the roundworm nematode *Caenorhabditis elegans*. Although many amyloid disease models for neurodegenerative disorders have been generated, models for systemic disorders such as T2DM and DRA are lacking. To address this, novel models of T2DM and DRA were generated to express variants of either IAPP (hIAPP, S20G IAPP or rat IAPP) or β_2-microglobulin (WT β_2m, D76N β_2m or ΔN6 β_2m). A range of behavioural phenotypes were explored in these models, including motility, development, lifespan, thermotolerance and ER stress. Disease models expressing IAPP or β_2m variants with high amyloidogenic aggregation propensity *in vitro* (S20G IAPP, D76N β_2m and ΔN6 β_2m) also confer to toxic phenotypes in the nematodes. *C. elegans* expressing variants that do not produce amyloid fibres under physiological conditions *in vitro* (WT β_2m and rat IAPP) displayed low toxicity. Furthermore, the role of the proteostasis network was explored in *C. elegans* disease models expressing amyloidogenic proteins. The role of HSP-90 in modulating amyloid-β toxicity was confirmed in an Alzheimer's disease strain, both cell-autonomously and cell-nonautonomously. Taken together, the results presented here demonstrate the utility of *C. elegans* in understanding the toxicity and aggregation of amyloid proteins; and present a platform on which future research studies on IAPP and β_2m can be built upon.

Table of Contents

List of Figures

List of Tables

Abbreviations

aSyn	a-synuclein
β_2m	β_2-microglobulin
Aβ	Amyloid-β
AβO	Amyloid-β oligomers
AD	Alzheimer's disease
ADP	Adenosine diphosphate
AFD	Amphid finger
AIY	Amphid Y
ALS	Amyotrophic lateral sclerosis
ApoAI	Apolipoprotein AI
ATF	Activating transcription factor
ATP	Adenosine triphosphate
BBPS	Body bends per second
BiP	Binding immunoglobulin protein
Bwm	Body wall muscle
CEPsh	Astrocyte-like sheath
CPE	Carboxypeptidase E
CRYAB	aB-crystallin
Cryo-EM	Cryo electron microscopy
CTD	C-terminal domain
DA neu	Dopaminergic neuron
DRA	Dialysis related amyloidosis
dsRNA	Double-stranded RNA
EM	Electron microscopy
ER	Endoplasmic reticulum
ERAD	ER-associated protein degradation
ERSE	ER stress elements
ESI-IMS-MS	Electrospray ionization-ion mobility spectrometry-mass spectrometry
ETC	Electron transport chain
FRAP	Fluorescence recovery after photobleaching
FTDP-17	Frontotemporal dementia with parkinsonism linked to chromosome 17
FUdR	Fluorodeoxyruridine
GAGs	Glycosaminoglycans
GCY	Guanylyl cyclase

GFP	Green fluorescent protein
Glut neu	Glutamatergic neuron
GPI	glycosylphosphatidylinositol
GRP94	Glucose-regulated protein 94
HD	Huntington's disease
HSE	Heat shock element
HSF	Heat shock factor
HSP	Heat shock protein
HSPG	Heparan sulfate proteoglycan
HSPs	Heat shock proteins
HSR	Heat shock response
Htt	Huntingtin
HttEx	Huntingtin exon
IAPP	Islet amyloid polypeptide
IRE1	Inositol requiring enzyme 1
L1	First stage larvae
L2	Second stage larvae
L3	Third stage larvae
L4	Fourth stage larvae
LB	Lysogeny broth
MC	Marker control
MD	Middle domain
MHC I	Major histocompatibility complex class I
MW	Molecular weight
NEF	Nucleotide exchange factor
Neu	Neuron
NFT	Neurofibrillary tangles
NGM	Nematode growth medium
NMR	Nuclear magnetic resonance
NTD	N-terminal domain
Pan-neu	Pan neuronal
PC	Proprotein convertase
PCR	Polymerase chain reaction
PD	Parkinson's disease
PDB	Protein Data Bank
PERK	Protein kinase-like ER kinase

PFD	Prefoldin
PN	Proteostasis network
polyQ	Polyglutamine
PrPc	Cellular prion protein
qPCR	Quantitative PCR
RFP	Red fluorescence protein
RNAi	RNA interference
ROS	Reactive oxygen species
RT-qPCR	Reverse transcription quantitative polymerase chain reaction
SAP	Serum amyloid P component
SBD	Substrate-binding domain
sHSPs	Small heat shock proteins
ssNMR	Solid state nuclear magnetic resonance
T2DM	Type II diabetes mellitus
TCS	Transcellular chaperone signalling
ThT	Thioflavin T
TNFAIP	Tumour necrosis factor-induced protein
TPR	Tetratricopeptide repeat
ts	Temperature-sensitive
TTR	Transthyretin
UCH-L1	Ubiquitin carboxyl-terminal hydrolase L1
Unc	Uncoordinated
UPR	Unfolded protein response
UPRE	Unfolded protein response element
UPR^{ER}	Unfolded protein response of the endoplasmic reticulum
UPR^{mito}	Unfolded protein response of the mitochondria
UPS	Ubiquitin proteasome system
WT	Wild type
XBP	X-box binding protein
YFP	Yellow fluorescent protein

Chapter 1. Introduction

1.1 Protein Folding

1.1.1 Introduction to Protein Folding

Proteins are considered one of the most essential components in biology as they are involved in virtually every cellular process that we depend on to live (Dobson, 2004). Proteins are synthesised as a string of different amino acids and are distinguished by the order in which these occur and their length. In order for this sequence of amino acids to be biologically functional, the majority of proteins need to fold into a compact conformational structure (Anfinsen, 1973). Nearly 60 years ago, work by Anfinsen and colleagues on the formation of the native ribonuclease A showed that proteins can fold spontaneously into structures without outside help (Anfinsen et al., 1961). This provided a foundation for future research in protein folding and founded the hypothesis that the only information required for proteins to fold is encoded in the primary amino acid sequence. It also led to many important questions; namely how do proteins fold? How does this amino acid sequence shape protein folding dynamics? And what happens when this goes wrong?

Evidence dictates that the native state of a protein is also that it is most stable under physiological conditions. However, the number of possible conformations a protein can form is so large that the time taken for exploration of each protein conformation by a random search would result in extremely slow protein folding and therefore not on a biologically relevant time-scale (Zwanzig et al., 1992). It was proposed therefore that proteins can navigate to their native state through a series of independent pathways (Levinthal, 1968). These pathways are kinetically controlled and guided by the rapid formation of local interactions which determine further folding of the chain and native-like local structures. This dramatically reduces the number of conformations sampled by each protein, representing a more relevant biological time-scale for folding.

Over the years, many models have been proposed to explain the mechanisms of protein folding and developed into the widely accepted protein folding funnel model. As correct native-like interactions are more likely to be stable than incorrect non-native interactions, proteins in principle must “know” and find the lowest energy structure for effective

performance (Englander and Mayne, 2017). This information is contained in the "energy landscape" of a protein, which describes the free energy of the polypeptide chain as a function of its conformational properties (Dobson, 2004). As the conformational space accessible to the polypeptide chain folding diminishes as the protein approaches its native state, this energy landscape is represented as a funnel. The funnel-shaped energy landscape is viewed as a "downhill" pathway, where unstructured high energy polypeptide sequences journey downhill to their more stable, lower energy native states, losing conformation entropy along the way (Englander and Mayne, 2017). Although studies of a group of small proteins containing less than 100 residues appear to follow this simplistic folding landscape (Jackson, 1998), in reality the majority of proteins employ "on-pathway" folding intermediates to achieve their native states. This is because the free-energy landscape is often rough, with high kinetic barriers and low kinetic traps along the folding pathway (Figure 1.1).

1.1.2 Protein misfolding

As well as "on pathway" folding intermediates, protein folding pathways are further complicated by "off pathway" structures which can form. These partially folded or misfolded proteins may become transiently populated, requiring substantial reorganisation to achieve their native state (Hartl et al., 2011). Moreover, these partially folded or misfolded states can become problematic as they are known to aggregate in a concentration-dependent manner (Eichner et al., 2011). Folding intermediates can undergo collapse leading to disorganised globular conformations or to intermediates that are stabilised by non-native interactions causing misfolded states (Hartl et al., 2011). Partially folded or misfolded proteins tend to expose hydrophobic amino acid residues that would normally be buried within the structure, driving aggregation of the protein resulting in amorphous aggregates. Moreover, fibrillar aggregates called amyloid may form. These are defined by β-strands running perpendicular to the long fibril axis, generating a highly ordered, thermodynamically stable cross-β structure (Almeida and Brito, 2020). These structures are normally accompanied by the formation of oligomeric intermediates, which have been shown to exert damaging effects *in vivo* (Tipping et al., 2015).

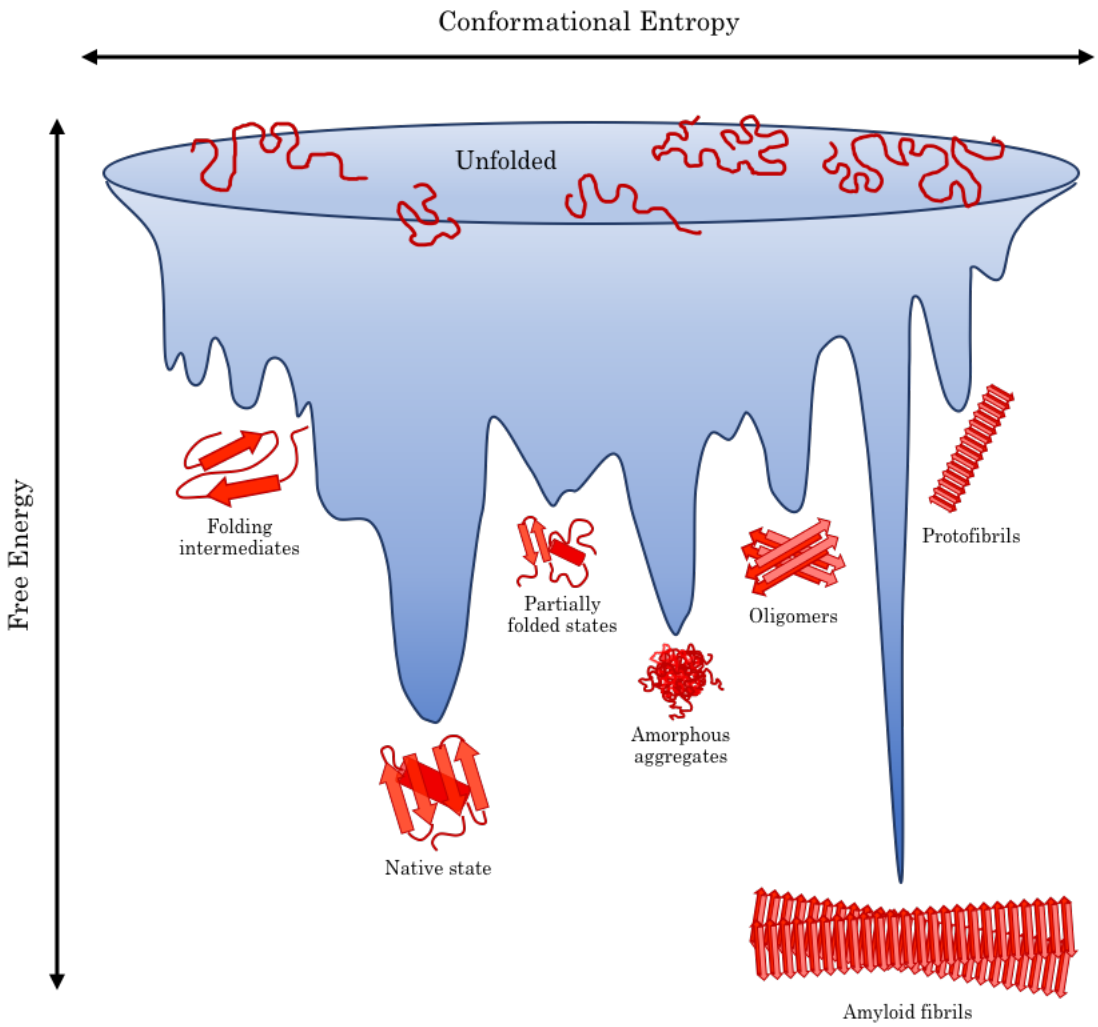

Figure 1.1 Free energy landscape of protein folding and aggregation.
Unfolded proteins funnel down towards a low energy native state. The surface of the energy landscape is rough and contains low energy troughs which can result in the accumulation of kinetically trapped conformations that need to overcome free-energy barriers to continue downwards. This energy landscape may overlap with the aggregation landscape where non-native states can traverse from folding to aggregation under specific conditions. This results in the formation of amorphous aggregates, oligomers, protofibrils and mature amyloid fibrils. Cross-β amyloid fibres have lower energy states than that of the folding landscape. Adapted from (Hartl et al., 2011)

Although many small proteins refold in the absence of components or an energy source; over the years, research has established that in the context of the complex and crowded cellular environment, many proteins require additional help from a number of auxiliary factors to fold efficiently on a biologically relevant timescale. These factors however do not determine the native structure and merely serve to assist natural folding pathways.

1.2 Proteostasis

The interior of the cell contains a complex environment comprised of proteins and other macromolecules. A typical mammalian cell expresses over 10,000 different proteins which are required to fold into their native state to function. This provides challenges to proteins whereby achieving – or remaining in – this native conformational state can be difficult, affecting ability to function. In order to preserve this functionality of the active states of these proteins, cells act to maintain a state of proteome balance within the cells – known as protein homeostasis (proteostasis). To do so, a large network of molecules act to fold and assemble proteins efficiently upon synthesis, as well as recognising aberrantly folded proteins in order to refold, disaggregate or clear them from the cell (Hipp et al., 2014). This network is called the proteostasis network (PN) and is comprised of molecular chaperones, their regulators and machineries of proteolytic degradation (Figure 1.2) (Labbadia and Morimoto, 2015). On top of the already highly complex system cells have to balance, additional stressors such as temperature, pH, reactive oxygen species, radiation, chemicals or infection can impact protein structure and folding, causing imbalance within the system for which cells have developed sensitive response mechanisms to combat. Moreover, the aberrant behaviour of some endogenous proteins such as Amyloid-β or β_2-microglobulin can give rise to disease, and therefore maintaining this delicate network is crucial to organismal and cellular health.

1.2.1 Molecular Chaperones

A central component of the PN is the molecular chaperones. Chaperones act within the cell to regulate client-substrate interactions, folding, disaggregation, degradation and trafficking (Hartl et al., 2011). Chaperones are highly conserved across eukaryotes and often known as stress proteins or heat-shock proteins (HSPs). In eukaryotes, they are broadly classified according to their molecular weight and grouped into the Hsp70, Hsp90, DNAJ/Hsp40, chaperonin/Hsp60, Hsp100 and small HSP (sHSPs) families. These classes cooperate together to form pathways and delicate networks across different cellular compartments in the cell (Mogk et al., 2015; Nillegoda et al., 2018; Tyedmers et al., 2010).

Chaperones that broadly act in *de novo* folding and refolding (Hsp70, Hsp90 and chaperonins) promote folding through ATP hydrolysis and cofactor binding cycles. These typically recognise hydrophobic exposed regions of the polypeptide sequence, and function

to fold or refold these proteins through kinetic partitioning. Chaperone binding and refolding prevents proteins from aggregating (Figure 1.1). These chaperones typically work alongside ATP-independent chaperones, such as sHSPs that function as 'holdases' to buffer aggregation (Hartl et al., 2011)

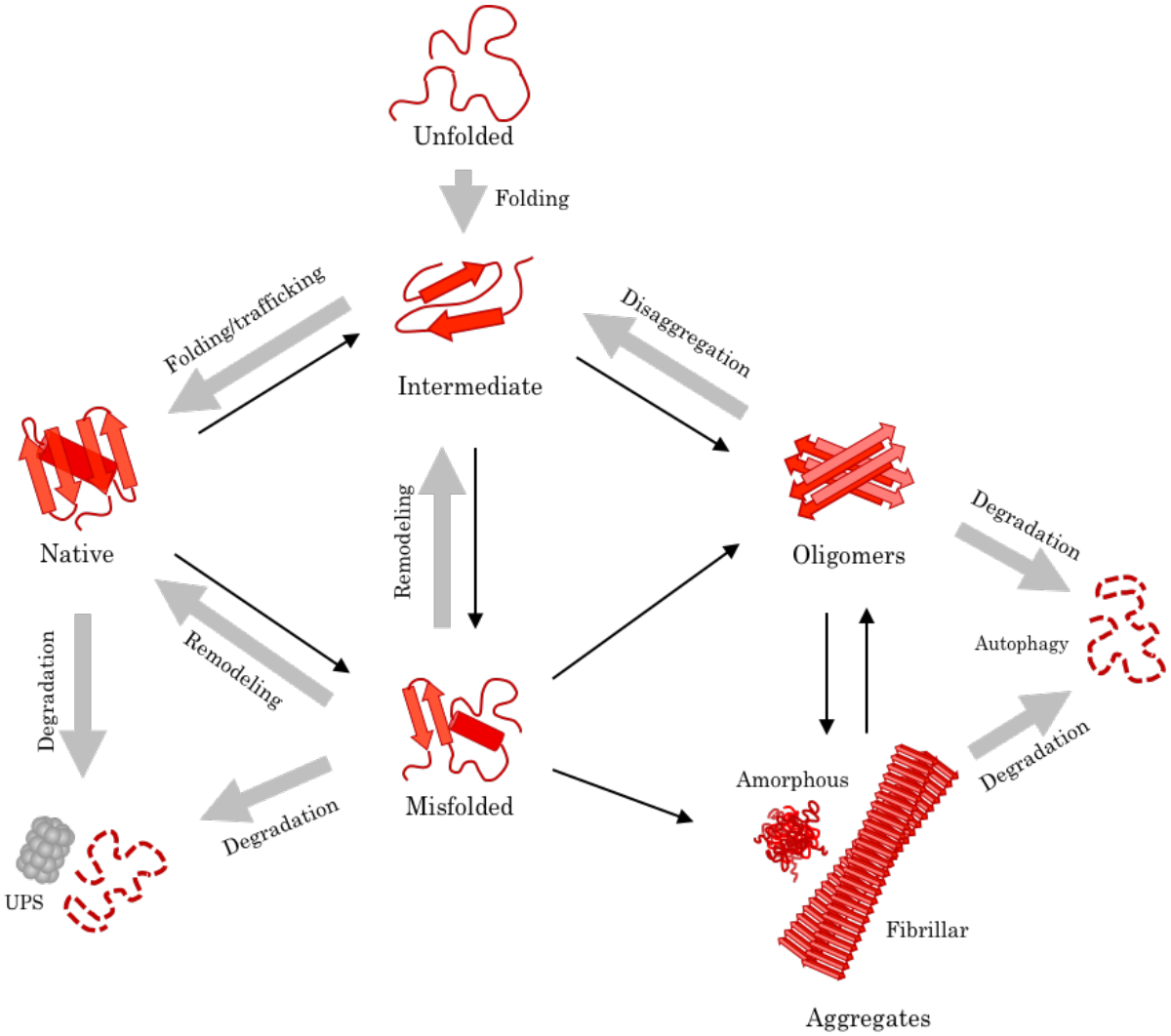

Figure 1.2 Functions of the Proteostasis Network.
The proteostasis network acts in order to maintain proper protein folding through the folding, trafficking, remodelling, disaggregation and degradation of proteins. The black arrows represent protein misfolding and aggregation, which the proteostasis network (grey arrows) acts to prevent. Adapted from (Hartl et al., 2011).

1.2.1.1 HSP70

The Hsp70 family act to fold and refold proteins and participate in protein disaggregation. Hsp70s act through an ATP-dependent client-binding and release cycles which is typically rather promiscuous. Binding and release by Hsp70 occurs through allosteric coupling at the Hsp70 ATPase domain with the C-terminal substrate-binding domain (SBD) (Kohler

and Andreasson, 2020). The SBD consists of a β-sandwich subdomain and α-helical lid segment. The β-sandwich subdomain recognises extended ~7 residue stretches enriched in hydrophobic amino acids (Rüdiger et al., 1997). These hydrophobic regions typically occur every 50-100 residues and correlate with a high propensity to aggregate (Rousseau et al., 2006). The α-helical lid regulates the affinity state for the peptide in an ATP-dependent manner.

Hsp70s never function alone and interact with a variety of co-chaperones and other factors to carry out function. These typically include a J protein (Hsp40), and almost always a nucleotide exchange factor (NEF) (Kampinga and Craig, 2010). The ATPase rate of Hsp70 is stimulated by the interaction with a J protein (Hsp40). The hydrolysis of ATP to ADP leads to lid closure and stable peptide binding. Hsp40 can also interact directly with unfolded polypeptide chains and recruit HSP70 to the substrate (Langer et al., 1992). After ATP hydrolysis has occurred, a NEF binds to the Hsp70 ATPase domain and catalyses the ADP-ATP exchange. This results in lid reopening and substrate release (Kampinga and Craig, 2010).

1.2.1.2 HSP90

The Hsp90 family controls numerous signalling pathways in eukaryotic cells, this includes functions in cell-cycle progression, telomere maintenance, apoptosis, mitotic signal transduction, vesicle-mediated transport, innate immunity and targeted protein degradation (Hartl et al., 2011). Hsp90 normally functions downstream of Hsp70, and cooperates with many regulators and co-chaperones to function in the structural maturation and regulation of numerous molecules (Taipale et al., 2010). Many of these assistant molecules utilise the tetratricopeptide repeat (TPR) domain to bind to Hsp90 and help to mediate conformational changes in the substrate proteins.

Like many other chaperones, Hsp90 function is driven through the hydrolysis of ATP. ATP binding on the N-terminal domain (NTD) of Hsp90 facilitates dimerisation of the two NTD domains (Schopf et al., 2017). This causes considerable structural rearrangement resulting in the compaction of the Hsp90 whereby the two domains twist around each other. After ATP hydrolysis, the ATPase domains dissociate and the individual monomers separate N-terminally (Schopf et al., 2017). Numerous co-chaperones assist with Hsp90 ATP hydrolysis and function. These include CDC37, which functions to deliver kinase substrates to Hsp90, HOP which inhibits N-terminal dimerization, AHA1 which

stimulates ATP hydrolysis and p23 which stabilises the dimerised form of Hsp90 before ATP hydrolysis (Gaiser et al., 2010; Guo et al., 2001; Lackie et al., 2017).

1.3 Cell-autonomous stress responses

Although delicate mechanisms are in place within the cell to maintain the cellular proteome, additional environmental challenges such as heat stress, chemical stress and oxidative stress aid to increase protein misfolding (Wallace et al., 2015). As environmental pressures are ever-changing, organisms have developed intricate networks to maintain and re-establish proteostasis in these times of cellular stress. Within the cell, surveillance mechanisms and signalling pathways have been established in different cellular compartments to detect and respond to protein-folding perturbations. These include the cytosolic heat-shock response (HSR), and unfolded protein response (UPR) of the endoplasmic reticulum (UPR^{ER}) and of the mitochondria (UPR^{mito}) (Hipp et al., 2019)..

1.3.1 Heat Shock Response (HSR)

Initially discovered in Drosophila as a transcriptional response to elevated temperatures (Ritossa, 1963), the HSR provides a mechanism to constantly monitor misfolded proteins in the cytosol of organisms. The response depends on the coordinated action of the master transcription factor and regulator Heat Shock Factor 1 (HSF1) (Baler et al., 1993; Sarge et al., 1993). Under normal cellular conditions, HSF1 is sequestered in the cytosol by a chaperone complex including the heat shock protein Hsp90, Hsp70 and TRiC (Bharadwaj et al., 1999; Guo et al., 2001; Neef et al., 2014). However, in times of cellular stress, levels of misfolded proteins accumulate. This leads to the dissociation of chaperones from HSF1 to facilitate folding or refolding of proteins (Figure 1.3) (Zou et al., 1998). HSF1 is therefore alleviated from repression and trimerises into its DNA binding form (Guo et al., 2001; Zou et al., 1998). HSF1 can now translocate to the nucleus and bind to heat shock element (HSE), driving transcription (Amin et al., 1988). HSEs are characterised by nGAAn repeats and are highly conserved throughout species (Lindquist, 1986). This leads to the rapid upregulation of numerous chaperone genes to deal with the misfolded proteins including Hsp90, Hsp70, Hsp40 and Hsp27 (Prodromou, 2016). The strong chaperone upregulation of molecular chaperone leads to increased protein folding in the cell, mitigating protein misfolding and returning the cells to a state of proteome balance. The resultant excessive molecular chaperone concentration in the cell provides negative feedback, sequestering HSF-1 in the cytosol and repressing transcription.

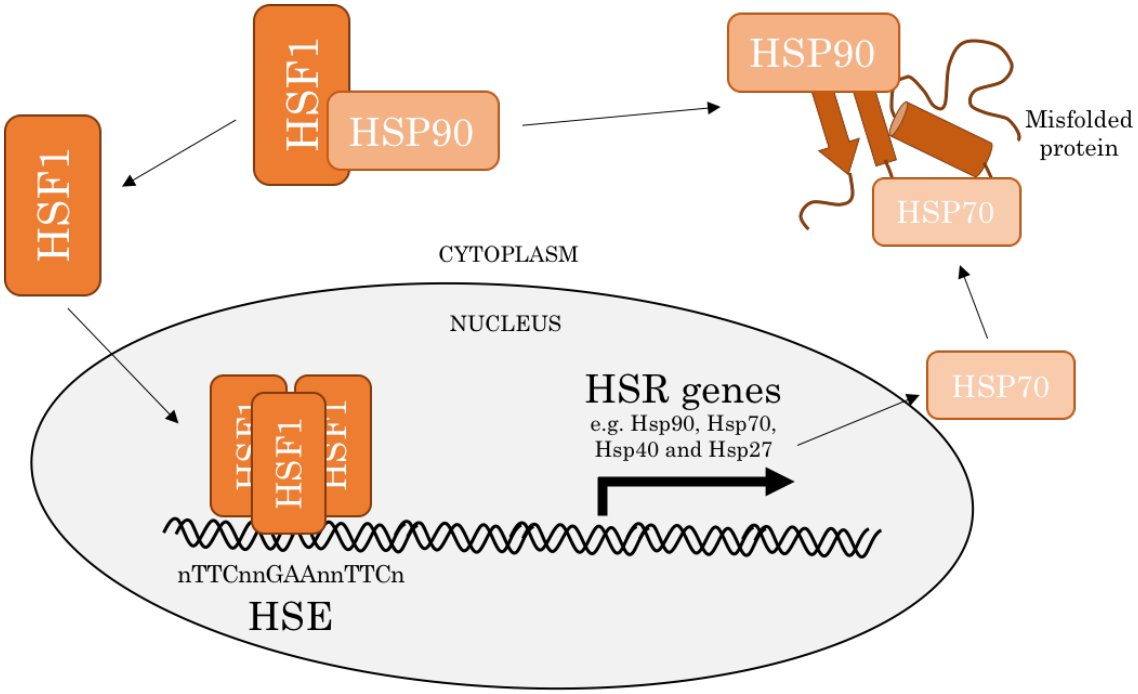

Figure 1.3 The Heat Shock Response.
Upon protein misfolding in the cytosol, HSP90 dissociates from HSF1 to refold misfolded proteins. HSF1 then trimerises and translocates to the nucleus where it binds to the HSE promoting expression of chaperone genes including HSP90, HSP70 and HSP40. The upregulated chaperones act to restore cellular proteome balance.

1.3.2 Unfolded protein response of the endoplasmic reticulum (UPR^{ER})

In order to be secreted extracellularly, proteins are trafficked through the endoplasmic reticulum (ER) before they are either delivered to other compartments, displayed on the cell surface or released extracellularly. During this process, proteins fold and mature into their native structures. Like the cytoplasm, the ER is also subjected to environmental pressures causing protein misfolding. In order to maintain proteostasis, a collection of conserved signalling pathways monitors the ER, and responds to any misfolding that occurs. This response is termed the unfolded protein response of the endoplasmic reticulum (UPR^{ER}).

The UPR^{ER} is comprised of three branches each controlled by a different signalling transducer (ATF6, PERK and IRE1) (Taylor and Dillin, 2011). These three branches work in parallel in order to maintain proteostasis. Under normal cellular conditions, the ER luminal domain of each signalling transducer is bound by the ER resident Hsp70 chaperone BiP (Schröder and Kaufman, 2005). Upon protein misfolding, BiP dissociates

from the signalling transducers in order to refold any non-native proteins. Dissociation enables the activation of each branch of the UPR^{ER}, which then mediate signalling and promote chaperone upregulation and decreased protein production (Hetz et al., 2011).

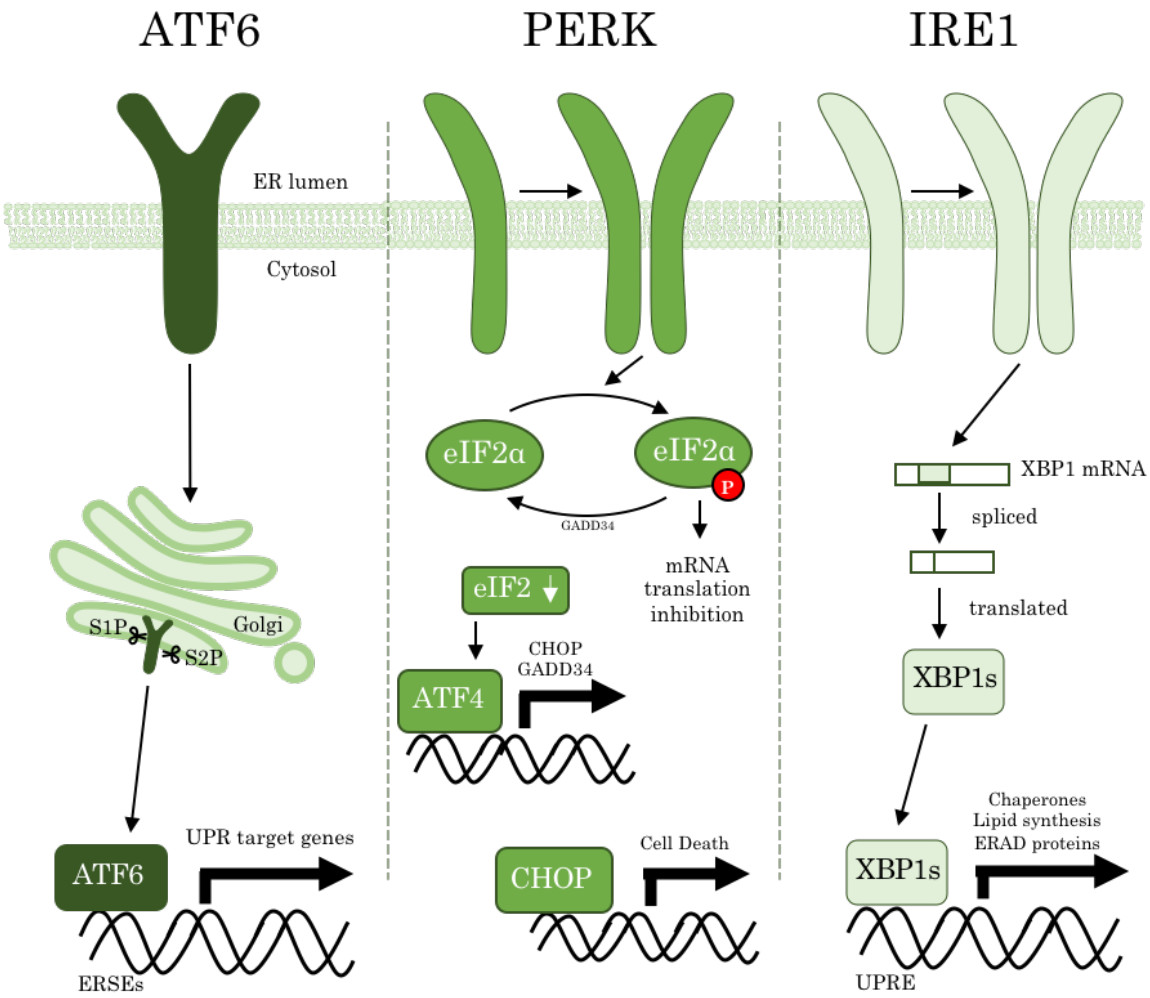

Figure 1.4 The three branches of the Unfolded Protein Response of the Endoplasmic Reticulum.
The three signal transducers (ATF6, PERK and IRE1) sense protein misfolding in the ER resulting in the induction of the UPR^{ER}. ATF6 sensing triggers vesicular transport to the Golgi, where ATF6 is cleaved by S1P and S2P to generate ATF6(N), a transcription factor that upregulates UPR target genes. PERK triggers the phosphorylation of eIF2a and subsequent decrease in eIF2, blocking mRNA translation and inhibition. It also conveys an increase in ATF4 leading to the transcription of XBP1 and CHOP. IRE1 activation leads to the splicing of XBP1 mRNA into XBP1s, a transcription factor that induces the expression of chaperone genes. Figure is adapted from (Walter and Ron, 2011).

Upon detection of accumulated of misfolded proteins, activating transcription factor 6 (ATF6) is delivered to the Golgi apparatus (Schindler and Schekman, 2009). Once there, it is proteolytically cleaved by S1P and S2P, removing the luminal domain and transmembrane anchor respectively (Haze et al., 1999; Ye et al., 2000). The remaining

cytosolic fragment is then free to move to the nucleus and bind to ER stress elements (ERSEs) in the promoters of UPR target genes. Amongst these genes are BiP, protein disulphide isomerase and glucose-regulated protein 94 (GRP94) (Walter and Ron, 2011).

Another branch of UPR^{ER} is mediated by double-stranded RNA activated protein kinase-like ER kinase, PERK. Upon activation, PERK oligomerises and undergoes phosphorylation. This causes the phosphorylation and inactivation of the ubiquitous translation initiation factor eIF2a leading the inhibition of mRNA translation (Harding et al., 2000). This inhibition helps to reduce the influx of proteins entering the ER, which aids to decrease the protein folding burden. When eIF2 activity is limited, the transcription factor ATF4 is preferentially translated. Two target genes of ATF4 include the transcription factor C/EBP homologous protein CHOP and growth arrest and DNA damage-inducible 34 GADD34. CHOP controls genes encoding components involved in apoptosis, and therefore strong levels of signalling can contribute to cell death pathways (Marciniak et al., 2004). Furthermore, GADD34 acts to dephosphorylate eIF2a, providing a negative feedback loop.

The final branch of the UPR^{ER} is defined by inositol requiring enzyme 1, IRE1. Conformational changes following IRE1 oligomerisation in the ER membrane activate its ribonuclease (RNase) function. IRE1 then cleaves the mRNA encoding the UPR-specific transcription factor X-box binding protein 1 (*xbp1*) into *xbp1s* (Sidrauski and Walter, 1997). Translation of this mRNA results in the production of the active transcription factor XBP1s which activates genes with an UPR element (UPRE) in the promoter. This includes the ER resident chaperone BiP (Yamamoto et al., 2005) and ER-associated degradation components (Reimold et al., 2001) which help to manage the increased protein burden in the ER, restoring proteostasis.

1.3.3 Unfolded protein response of the mitochondria (UPR^{mito})

Like the ER and cytosol, mitochondria have a specialised response to an imbalance in proteostasis termed the unfolded protein response of the mitochondria (UPR^{mito}). This response is coordinated by mitochondria-localised chaperones including a Hsp70 family member mtHsp70, GroEL (Hsp60) and GroES (Hsp10) (Neupert and Herrmann, 2007). Upon the accumulation of protein misfolding in the mitochondria, the mitochondrial matrix protease ClpXP degrades excess proteins into short peptides that are exported into the cytosol via the transporter HAF-1 (Haynes et al., 2010). This in turn activates the

transcription factor ATFS-1 and the complex DVE-1/UBL-5, which drives expression of mitochondrial chaperones such as Hsp60 and mtHsp70, mitochondrial import machinery and detoxification enzymes (Pellegrino et al., 2013). The action of these components aids in the restoration of mitochondria proteostasis.

1.4 Cell-non-autonomous stress responses

As well as intracellular responses to combat proteome imbalance, multicellular organisms also possess delicate inter-tissue stress responses. These act to coordinate protein quality control processes across tissues and organs in order to maintain organismal proteostasis. Transcellular activation of these responses is achieved by endo- and paracrine signalling pathways via hormones, cytokines, secreted peptides, neurotransmitters and neuropeptides amongst others. Due to the organismal nature of this response, nematodes have been heavily used as a model organism for the study of cell-non-autonomous stress responses; however, evidence of these responses has also been shown in invertebrates and vertebrates alike (Mahadevan et al., 2011; Miles et al., 2019).

1.4.1 The cell-non-autonomous HSR

The cell-non-autonomous activation of the HSR was first demonstrated in rats in the 1990s; where behavioural stress was demonstrated to induce an adrenal HSR through a neuroendocrine activation (Fawcett et al., 1994). Since then, numerous studies in *C. elegans* have demonstrated this response to be primarily controlled by the nervous system. In *C. elegans*, two amphid finger (AFD) neurons and their postsynaptic amphid Y (AIY) interneurons have been demonstrated to mediate a response to temperature change (Mori and Ohshima, 1995). These AFD neurons act via the transmembrane guanylyl cyclases GCY-8, GCY-18 and GCY-23 to enable the activation of a cGMP-gated ion channel (Inada et al., 2006; Ramot et al., 2008). This leads to the activation of organismal HSR via activation of the master HSR regulator HSF-1 in non-neuronal tissues, promoting increased chaperone expression, protein folding and survival (Prahlad et al., 2008; Tatum et al., 2015).

1.4.2 The cell-non-autonomous UPR^{ER}

The nervous system has also been shown to play a major role in the cell-non-autonomous regulation of the UPR^{ER}. In *C. elegans*, overexpression of the transcription factor XBP-1s, an ortholog of XBP1 in humans, in the neurons leads to BiP/HSP-4 induction in both the

neurons and intestines of the animal (Taylor and Dillin, 2013). This induction leads to increased stress resistance and longevity in the organism. The action of XBP-1 depends on functional neuronal vesicle release, mediated by UNC-13 which is required for neurotransmission involving small clear vesicles (Richmond et al., 1999). In addition, neuronal XBP-1 overexpression upregulates lysosomal genes and promotes lysosomal maturation and acidity. This has been shown to be required for the increased lifespan observed in neuronal XBP-1 overexpression mutants (Imanikia et al., 2019a; Taylor and Dillin, 2013). Similarly, when XBP-1 is overexpressed in the astrocyte-like sheath (CEPsh) glia, intestinal UPR^{ER} signalling is activated through *unc-13* dependent neuropeptide signalling and leads to an increase in lifespan (Frakes et al., 2020).

1.4.3 The cell-non-autonomous UPR^{mito}

Like both the cell-non-autonomous HSR and UPR^{ER} activation, the UPR^{mito} is also partially regulated by neuronal signalling. Mitochondrial stress in the neurons can activate the UPR^{mito} systemically; reduced expression of the ETC subunit, *cco-1*, in the neurons activates the expression of mtHSP70 in the intestine and extend the lifespan of nematodes (Durieux et al., 2011). This mtHSP70 induction was subsequently shown to be due to neuroendocrine signals via the neurotransmitter serotonin (Berendzen et al., 2016). Further studies have found that *cco-1* mediated mitochondrial stress results in Wnt-dependent induction of cell-non-autonomous UPR^{mito} in peripheral cells (Zhang et al., 2018). Finally, FLP-2 was also identified as a neuroendocrine signal involved in cell-non-autonomous UPR^{mito} activation; FLP-2 functions in a sub-circuit consisting of three types of sensory neurons and one interneuron to sense and transduce neuronal mitochondrial stress to peripheral tissues (Shao et al., 2016).

1.4.4 Transcellular chaperone signalling

Similarly to the cell-non-autonomous specific stress responses discussed previously, transcellular chaperone signalling (TCS) acts to coordinate a systemic stress response via intercellular signalling. Altered tissue expression of the molecular chaperone HSP-90 in *C. elegans* can cause activation of chaperones in other non-stressed tissue in the organism. This is exemplified through tissue specific overexpression of HSP-90 in the intestine or the neurons which can cause an upregulation of HSP-90 in the body wall muscle of the animal (Van Oosten-Hawle et al., 2013). This response was found to be controlled by the

zinc finger transcription factor PQM-1 and its downstream effectors *clec-41* and *asp-12* (O'Brien et al., 2018).

1.5 Amyloid

The misfolding and conversion of normally soluble, functional proteins into fibrillar amyloid structures is associated with over 50 disorders in humans. These disorders cause a multitude of symptoms and affect a wide range of functions in the body. Many amyloid disorders are strongly associated with ageing and due to the increase in life expectancy are becoming more common across the world. This encompasses several disorders that cause dementia in patients including Alzheimer's, Parkinson's and Huntington's Disease. It is estimated that in 2019 over 50 million people are living with dementia globally, which the Alzheimer's Disease International predicts is set to further increase to 152 million by 2050 (*World Alzhiemer's Report*, 2019). Other disorders associated with amyloid include those associated with lifestyle, including type II diabetes that affects more than 300 million individuals across the globe. Despite this increasing incidence in the global population, amyloid disorders are difficult to prevent or treat. This is due to abundance of intermediary species that occur on the pathway to self-assembly that make it difficult to pinpoint the originator of disease. In addition, many of these diseases impair the proteostasis network across ageing, leading to increased protein misfolding and further decline.

1.5.1 Brief History of Amyloid Research

The earliest reference to amyloid dates back to 1639, in the description of a lardaceous liver and white waxy deposits in the "sago spleen" (Reuben, 2004). Around 200 years later, it was the German pathologist Virchow that decreed the substance to be called amyloid, derived by the Greco-Latin word for starch flour, *amylum*. This was due to the similarities of iodine-staining between an amylaceous starch material found in plants and the staining of amylacea of the brain (Reuben, 2004). However, just 5 years after being coined, Friedrich and Kekule discovered that amyloid was predominantly proteinaceous and research shifted to the study of amyloid as a protein (Sipe and Cohen, 2000). Advances in light microscopy and histopathologic dyes such as Congo red and thioflavin shed new light on amyloid research, pointing towards an ordered sub microscopic structure (Puchtler et

al., 1961). Indeed, work in the 1960s by Shirahama and Cohen defined amyloid as composed of twisting protofilaments (Shirahama and Cohen, 1965), and further studies by Geddes, Aiken and colleagues using X-ray fibre diffraction revealed a distinct ~4.7A repeating feature along the fibril axis which was termed cross-β (Figure 1.5) (Geddes et al., 1968). Since then, numerous advancements in the study of amyloid have included the identification of precursor proteins in disease, high resolution structures of fibrils and advancements in our understanding of how amyloid elicits toxic damage.

1.5.2 Structure of Amyloid

Amyloid is associated with the misfolding of native proteins into intractable fibrillar aggregates that are associated with both the loss of function of the protein and the formation of toxic intermediates that elicit toxic damage. Protein fibres are characterised by protofilaments in which the β-strands align perpendicular to the long axis of the fibrils, termed cross-β amyloid fold (Geddes et al., 1968) (Figure 1.5). Amyloid fibrils are closely packed, highly ordered and confer to a high level of kinetic and thermodynamic stability as demonstrated by the deep energy trough they possess in the aggregation landscape in Figure 1.1. Due to the breakthroughs and development in cryo-electron microscopy (cryo-EM) as well as solid-state NMR spectroscopy (ssNMR), near-atomic detail of fibrils structures can now be achieved. This has revealed that although fibrils adopt the canonical cross-β structure, the fibrils are more complex and elaborate than previously thought and a wide variety of amyloid structures exist. As well as variety between fibrils containing different precursor proteins, it is now established that different growth conditions can dramatically affect the fibril structure.

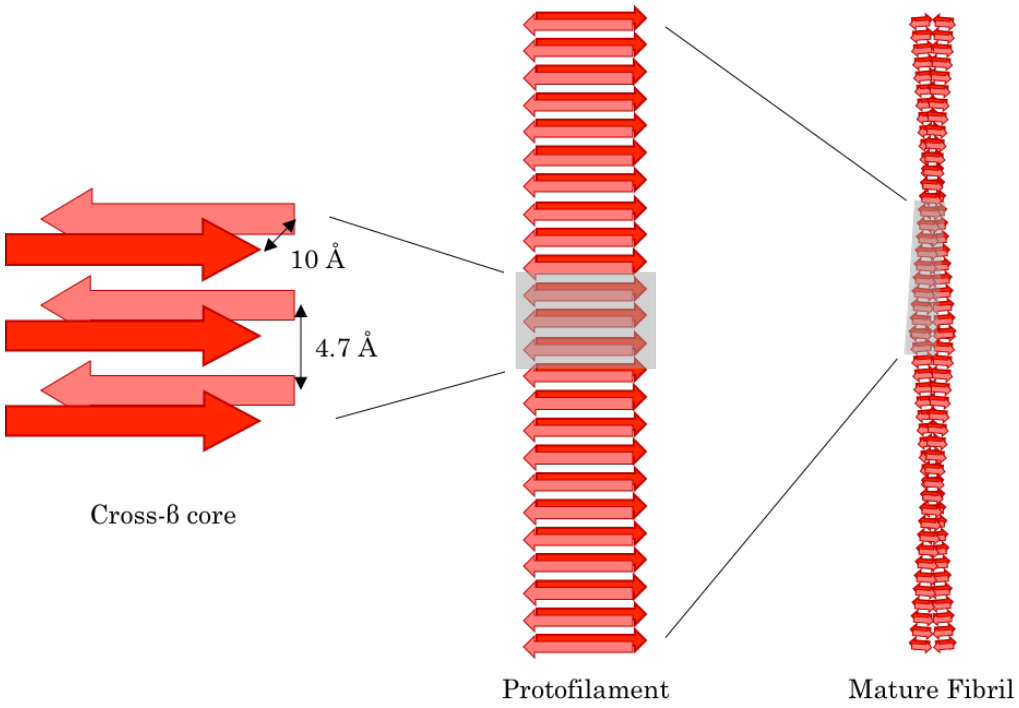

Figure 1.5 Cross-β amyloid fold.
The cross-β architecture of the amyloid protofilament core. Protofilaments structure self-assembles into mature fibrils with the common cross-β core.

Despite the common cross-β fold, there is remarkable diversity at the subunit level between different fibrils . A 10-residue peptide of transthyretin (TTR) forms antiparallel β-strand, where each peptide is the basis for one step along the cross-β ladder. Moreover, Amyloid-β (Aβ) 40 fibrils form distinct fibrils structures that have in-register parallel organisation of their β-strands but differ in the location of their β-loop β-motif (Lu et al., 2013; Paravastu et al., 2008). Furthermore, a complex arrangement has been observed in a structure of $A\beta_{42}$ fibrils, where the β-strands form Leu-Ser motifs that stack in a parallel arrangement on the fibril long axis. Other complex organisations of β-strands have been observed in fibril structures including those of α-synuclein and tau.

The morphology of the fibril is also determined by the number and arrangement of the protofilaments that form the fibrils, as well as the structure of the subunit itself. Although some fibrils contain just one protofilament (Wasmer et al., 2008), the majority of fibrils are made of multiple protofilaments that twist together (Iadanza et al., 2018). The organisation of these protofilaments can result in a variety of arrangements including cylinder (Andersen et al., 2010), flat ribbons (Dearborn et al., 2016), and pseudo-crystalline sheets (Reynolds et al., 2017). Amyloid fibrils of the same monomer can produce different arrangements as demonstrated by the 2A and 3Q fibrils of $A\beta_{40}$ in which different

morphologies correspond to different organisation of similar β-loop-β subunit motifs (Paravastu et al., 2008). Other fibril arrangements have been shown to arise from alternative packing of identical subunits, held together by different interactions. Evidence for this is provided by the cryo-EM structures of the paired helical and straight tau fibril polymorphs (Fitzpatrick et al., 2017), although it is thought that other proteins such as α-synuclein, $A\beta_{40}$, TTR and β_2m fibrils also display this alternative packing (Iadanza et al., 2018).

Structural analysis of Aβ fibrils from brain tissue, however, has revealed right-hand twisted fibrils that differ significantly from previously analysed *in vitro* Aβ fibrils (Kollmer et al., 2019). Both $A\beta_{40}$ and $A\beta_{42}$ *in vitro* derived fibrils display a left-hand twist, differing strongly from the analysis of brain-derived fibrils (Kollmer et al., 2019). This study highlights the importance of using patient-derived fibrils when investigating the structural basis for disease, indicating the *in vitro* conditions may not exactly match the conditions of fibril formation *in vivo*.

1.5.3 Mechanisms of Amyloid Formation

Amyloid is formed from the aggregation of monomeric protein precursors; this is initiated by a common nucleation growth mechanism (Knowles et al., 2014). Initially, precursor proteins may be unfolded or in a partially folded intermediate state (Figure 1.6), which then assemble into oligomeric species. Oligomers are highly dynamic, transient, heterogenous species that can have a varied structure (Glabe, 2006; Knowles et al., 2014). Association of oligomers can further produce higher-order species which are essential precursors for amyloid fibrils or are off-pathway assemblies that do not produce fibrils. Off-pathway species are still relevant to disease and have been shown to produce damaging toxic effects (Ferrone, 1999). During oligomerisation, a nucleus is formed and defined kinetically as the most unstable – and highest energy – species formed before the rapid polymerisation of the oligomers into amyloid fibrils. It is the likelihood of nucleus formation that determines the amount of time for amyloid assembly, and therefore the amyloidogenicity of the protein.

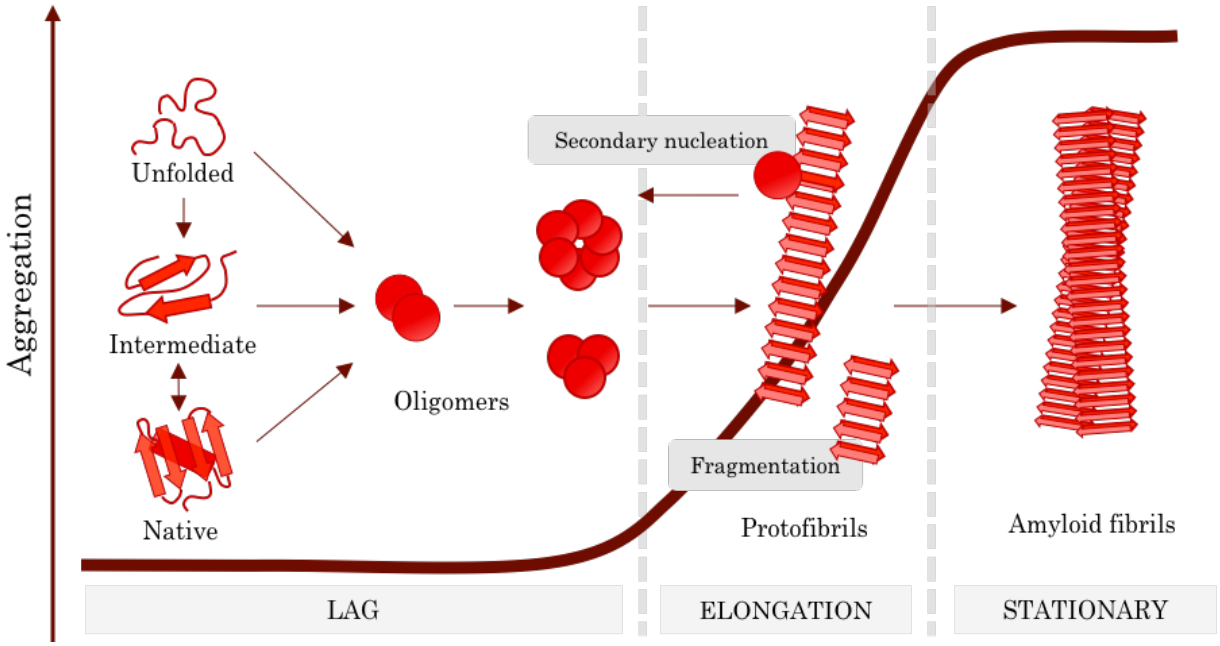

Figure 1.6 Mechanisms of aggregation of Amyloid.
Unfolded, intermediate or native structures form oligomeric structures which assemble to form higher-order fibrillar species (primary nucleation). The higher order fibrils can catalyse the formation of further oligomers or fragment to produce more fibril ends which monomers can recruit to (secondary nucleation). Adapted from (Iadanza et al., 2018).

As mentioned before, amyloid fibrils all contain a common cross-β fold. During self-assembly, each precursor protein undergoes a structural transformation in order to form this β-strand rich structure (Figure 1.5). Once this has been formed, fibrils can fragment which produces more fibril ends from which monomers can be recruited to. This eliminates the length of time required for the lag phase, causing exponential growth (elongation phase) (Figure 1.6) (Meisl et al., 2016). Other mechanisms of elongation include secondary nucleation; this occurs when oligomer formation is catalysed on the surface of the fibril, enhancing the rate of fibril formation (Ferrone, 1999; Linse, 2017).

1.5.4 Amyloid and disease

Amyloid was first associated with disease in 1901, when Alois Alzheimer reported the first case of Alzheimer's Disease (AD) which included Congo-red-positive plaques in the brain. Since then over 50 disorders have been associated with amyloid, including Huntington's Disease (HD), Parkinson's Disease (PD), amyotrophic lateral sclerosis (ALS), dialysis related amyloidosis (DRA), and type II diabetes mellitus (T2DM). These diseases are classically associated with neurodegenerative disorders such as AD, HD and PD; however,

they can also affect other tissues such as in T2DM (islet of Langerhans) and DRA (osteoarticular tissue). Although over 50 disorders have been associated with amyloid disease, only 37 peptides or proteins have been identified as the precursor protein in these diseases. Certain precursors such as TTR can be associated with many disorders including senile systemic amyloidosis, familial amyloidotic polyneuropathy, familial amyloid cardiomyopathy and leptomeningeal amyloidosis (Chiti and Dobson, 2017).

A central question to amyloid research is how and why do these proteins aggregate and what initiates the onset of disease? Many amyloidogenic precursor proteins are endogenous and have functional roles within an organism; however, they aggregate in the instance of disease to cause devastating effects. A key contributor to the progression of several amyloid diseases is ageing. The maintenance of proteostasis – and therefore the prevention of amyloid aggregation – is closely linked to ageing. As organisms age, components of the PN decline in function, and the expression of stress-inducible chaperones are impaired (Ben-Zvi et al., 2009), leading to protein aggregation (Morley et al., 2002). Due to the increased life expectancy in many countries, this has consequences on the incidence of diseases such as AD and PD, which are set to rise and estimate to cost €357 billion in Europe by 2050 (Iadanza et al., 2018).

Although some precursor proteins are wild type, mutations in the protein sequence can enhance the amyloidogenicity of these proteins and promote an earlier onset of the disease. Examples of this includes mutations such as A30P or A53T in α-synuclein in PD (Li et al., 2001) and E22Δ or E22K in Aβ in AD (Krone et al., 2008). Mutations typically occur in the polypeptide chain that undergoes aggregation, affecting aggregation propensity. For example, there are more than 100 mutations that have been linked to hereditary forms of transthyretin amyloidosis which destabilise the native tetrameric form of the protein (Sekijima et al., 2005). Similarly, there are 19 mutations associated with systemic apolipoprotein A-1 (ApoAI) amyloidosis, which destabilise the protein and increase solvent exposure of the strand that initiates aggregation (Das et al., 2014; Gursky et al., 2012). Other examples of mutations include trinucleotide repeat diseases including the expansion of polyglutamine (polyQ) in polyQ-associated ataxias such as Huntington's disease (Fan et al., 2014), poly-alanine in oculopharyngeal muscular dystrophy (Brais et al., 1998; Scheuermann et al., 2003), and poly-GlyAla expansions in the gene *C9orf72* associated with genetic forms of ALS and frontotemporal dementia (Renton et al., 2011).

A small proportion of amyloid-associated diseases are a result of medical treatment. In patients undergoing haemodialysis, the inability to effectively remove circulating wild type β_2m from the system causes a ~50-fold increase in the concentration of β_2m leading to aggregation and disease (Scarponi et al., 2016). Furthermore, in iatrogenic Creutzfeldt-Jakob disease, organ transplants or treatment with biological derivatives extracted from cadavers contaminated with aggregated PrP can also lead to disease.

1.5.5 Cytotoxicity of Amyloid

Since the discovery of the association between amyloid fibres and disease there has been a lot of debate over the cytotoxic nature of the species. Originally it was thought that amyloid fibrils themselves were toxic in nature and the causative agent in disease. However, over the last 20 years the evidence has shifted the focus from amyloid fibrils to oligomeric species as the main culprit in the toxic damage observed. That being said, there is still evidence that amyloid fibres can still elicit toxicity themselves. Amyloid fibres of β_2-microglobulin, α-synuclein, Huntingtin and lysozyme have all been observed to induce cellular toxicity (Pieri et al., 2012; Xue et al., 2009). It has been shown that β_2m fibrils interact with and disrupt lipid vesicles (Sheynis et al., 2013), where changes in pH can cause a reduction in fibre length and enhance the membrane disruptive capacity of amyloid fibrils (Goodchild et al., 2014; Jakhria et al., 2014). Furthermore, fibres of the polyQ-expanded Huntingtin exon 1 (HttEx1) or α-synuclein can bind to and permeabilise lipid vesicles, altering Ca^{2+} homeostasis (Pieri et al., 2012). Other studies have reported the interaction between Aβ and membranes inhibits long-term potentiation in mice hippocampal brain slices; these Aβ fibres have also been shown to interact with membranes and cause the resolubilisation of fibres into 'reverse' oligomers that are indistinguishable from other oligomers and cause toxic damage to primary neurons (Martins et al., 2008).

Numerous studies have detailed the cytotoxic nature of oligomeric species in amyloid disease progression. Studies in AD patients have shown the cognitive decline is not associated with amyloid plaque burden, suggesting that the pre-fibrillar aggregates are the cause of toxicity and disease (Nelson et al., 2012). Much like fibrillar toxicity studies, oligomers have been postulated to exert toxic effects through membrane disruption. In 1993, it was proposed that amyloid aggregates could exert toxicity through the formation of non-specific pore-like channels in the membranes of exposed cells (Arispe et al., 1993).

Since then, studies on synthetic phospholipid bilayers and cell membranes have demonstrated that membrane protein function is compromised through the interaction with oligomers (Kourie and Henry, 2002).

A key observation in cellular and organismal models of protein misfolding diseases has been the effect of protein misfolding on components of the proteostasis network (PN). Although it is not clear in the majority of cases how amyloid species impairs the capacity of the PN, it is generally considered that amyloid species sequester components of the PN, making them unavailable to other vital client proteins. Furthermore, protein aggregation can compromise the ubiquitin proteasome system (UPS). For example, expression of aggregation-prone proteins can prevent the proteasomal degradation of other endogenous proteins, as was shown in cells expressing polyQ-expansion proteins (Bennett et al., 2007; Hipp et al., 2012), Prp^{sc} (Kristiansen et al., 2007) and mutants of SOD1 (Urushitani et al., 2002). In a yeast model of Huntington's Disease, polyQ aggregates have been shown to sequester the Hsp40 chaperone Sis1p leading to proteasomal degradation inhibition (Park et al., 2013). Furthermore, aggregates of SOD1 have been demonstrated to sequester Hsc70 and its nucleotide exchange factor Hsp110 (J. Wang et al., 2009b).

1.6 *Caenorhabditis elegans*

In 1963, Sydney Brenner first proposed the roundworm nematode *Caenorhabditis briggsae* to be an ideal model to aid in the understanding of molecular biology, most notably development and the nervous system. Later on, he eventually settled on the related nematode *C. elegans*, as the strain grew better than the *C. briggsae* isolate in Brenner's laboratory. It wasn't until the early 1970s, however, that Brenner, together with John Sulston, published their pioneering work on the genetics of *C. elegans* (Bailey and Peddie, 1985; Brenner, 1974). This work led to the mapping of the entire *C. elegans* cell lineage (Sulston et al., 1983), and further to the sequencing of its entire genome – the first multicellular organism to have the honour. 50 years on, *C. elegans* research occurs throughout laboratories across the world, and some of the fundamental concepts of molecular biology are attributed to this simple organism.

1.6.1 Key Features of *C. elegans*

C. elegans is a free-living, non-parasitic nematode. The adult nematode is ~1mm in length, meaning the use of a dissecting microscope is needed to visualise these organisms. As *C. elegans* are transparent, tissues, individual cells and subcellular detail can be visualised under increased magnification (Figure 1.8). It's transparency also has other benefits; the use of fluorescent proteins to label proteins can discern further enhanced detail in the animals; this includes studying developmental processes, screening mutants, isolating cells and characterising protein interactions *in vivo*. The *C. elegans* genome is ~100 megabases long and contains over 20,000 protein coding genes (WormBase release WS275; The *C. elegans* Sequencing Consortium 1998). It is estimated that around 60-80% of all human genes and 42% of human disease genes possess an ortholog in *C. elegans*. (Markaki and Tavernakis, 2010).

A major benefit to *C. elegans* research is its rapid reproductive cycle and short lifespan (Brenner, 1974), allowing for ease of large scale propagation. *C. elegans* exists primarily as a self-fertilising hermaphrodite, which when propagated at 20°C develops from eggs to egg-laying adult in 3 days, and lives for 2-3 weeks on average. An hermaphrodite has a defined lineage of 959 somatic cells of which 302 are neurons (Sulston et al., 1983). At 20°C, *C. elegans* embryogenesis takes ~16 hours, where partial development occurs inside the mother. When hatched, the hermaphrodite embryo contains 558 nuclei and develops into the first stage (L1) larvae. The L1 stage lasts ~16hr, with a period of inactivity (lethargus) occurring at the end of the stage in which a new cuticle is formed and the old cuticle is molted. As shown in Figure 1.7, there are four larval stages of development (L1-L4) in which lethargus occurs at the end of each (Raizen et al., 2008). Approximately 12 hours after the L4 molt, the young adult hermaphrodite will then start to produce eggs, renewing the cycle. An adult hermaphrodite will produce eggs for 2-3 days until they no longer have any self-produced sperm to fertilise with. If there is a lack of food source in the second stage (L2) larvae, an alternate life cycle is activated whereby animals molt into an alternative L3 stage called "dauer" larva. In dauer larva, there is a cuticle completely surrounding the animal, plunging it into arrested development. Dauer larva have an enhanced resistance to environmental stresses and can survive for many months. When they encounter a food source, the animals molts and continues development into the L4 stage.

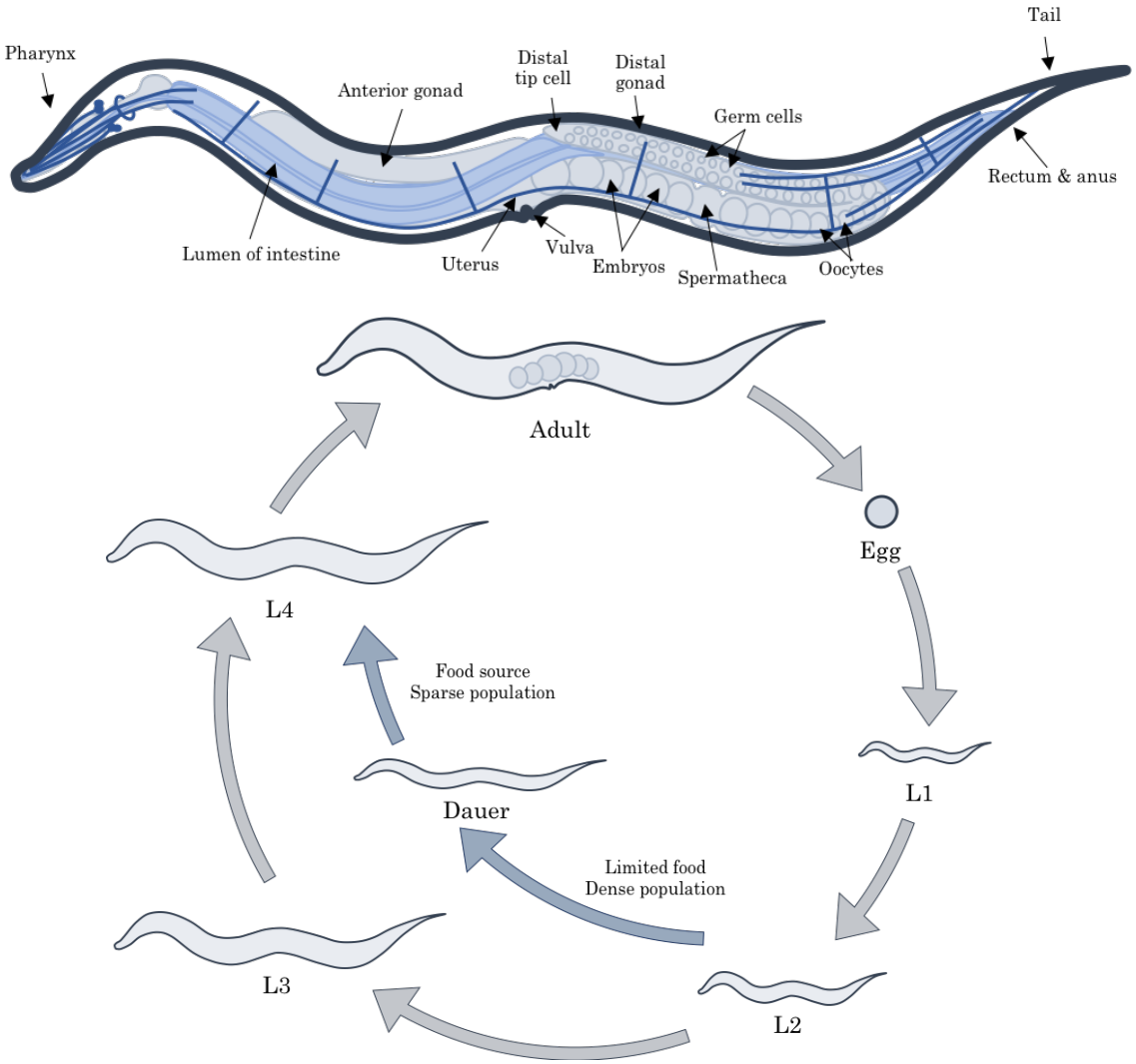

Figure 1.7 Tissues and lifecycle of *Caenorhabditis elegans*.
Top: Diagram of an adult hermaphrodite *C. elegans* with selected anatomical features highlighted. Bottom: Life cycle of the self-fertilising *C. elegans* hermaphrodite. Adults lay eggs, which hatch into the L1 stage. If conditions are favourable, the larvae continue through developmental stages into reproductive adults. If conditions are not favourable they enter the dauer stage, an alternative L3 stage.

1.7 *C. elegans* as a model for Amyloid Disease

Although *in vitro* research provides a wealth of information about the aggregation of amyloidogenic proteins, it cannot exactly replicate the complexity of a cellular, multi-tissue, *in vivo* environment. Therefore, over two decades ago the first study expressing an amyloidogenic protein in the model organism *C. elegans* was performed. In this study, Amyloid-β was expressed in the body wall muscle of *C. elegans* and animals displayed muscle-specific anti-β immunoreactive deposits (Link, 1995). Since then, *C. elegans* has

been utilised in numerous studies to express and study the aggregation of amyloidogenic proteins including Amyloid-β (Link, 1995), transthyretin (Madhivanan et al., 2018), α-synuclein (Van Ham et al., 2008), β_2-microglobulin (Diomede et al., 2012), and Huntingtin (Morley et al., 2002) amongst others. These resultant disease models have been instrumental in aiding our understanding of amyloid aggregation *in vivo*, furthering our knowledge of not just how aggregation-prone proteins accumulate but the delicate proteostasis systems in place in organisms to combat this.

1.7.1 Genetic manipulation

As well as its ease of propagation and economical value, a number of features mark *C. elegans* as a suitable disease model for the study of Amyloid. Genetic manipulation of *C. elegans* including forward genetic screens, RNAi knockdown, rapid mutation mapping and transgenic animal generation provide *C. elegans* researchers a powerful genetic toolbox to utilise. Transgenic animal generation has been the basis for the majority of *C. elegans* amyloid studies, where different proteinopathies have been modelled using specific promoters that target different tissues and cells including neurons, intestines and body wall muscle. Moreover, as the generation of novel transgenic animals is relatively straight-forward, information can be gathered about the drivers of aggregation through modifying the sequence of amino acids. This is exemplified through work by Doherty and colleagues, who identified stretches of the α-synuclein sequence that were aggregation prone: P1 (36-42) and P2 (45-57). By removing P1 and P2 from the α-synuclein transgene and generating a novel *C. elegans* strain, the age-dependent foci accumulation and motility phenotype seen in animals expressing wild type α-synuclein was ameliorated (Doherty et al., 2020).

A useful feature to *C. elegans* as a disease model is the ability to temporally control gene expression using RNA interference (RNAi) (Fire et al., 1998; Montgomery et al., 1998) making reverse genetic screens relatively easy to perform in the organism. Double-stranded RNA (dsRNA) can be applied to animals through feeding or soaking, systemically knocking down target genes throughout the organism due to transmembrane dsRNA transporter SID-1 which facilitates uptake of cellular dsRNA (Winston et al., 2002). RNAi screens have been performed on several *C. elegans* models of protein misfolding diseases including those expressing α-synuclein (Kuwahara et al., 2008; Van Ham et al., 2008), tau (Kraemer et al., 2006), amyloid-β (Brehme et al., 2014) and polyglutamine repeats (Lejeune et al., 2012).

1.7.2 Fluorescently tagged proteins

Another major benefit to amyloid researchers has been the transparency of the *C. elegans* system, allowing proteins to be tagged with fluorescent tags and easily visualised and tracked in the organism. As many amyloidogenic proteins self-assemble into aggregates in an age-dependent manner (Hipp et al., 2014), tagging proteins with fluorescent proteins has enabled researchers to track, visualise and quantify protein aggregation throughout ageing in real-time. A well-researched example of this includes the polyglutamine (polyQ) disease models created by Morley and colleagues that were designed to express different length polyQ repeats tagged with yellow fluorescent protein (YFP) in the body wall muscle of the animals (Morley et al., 2002). As well as confirming the aggregation threshold of 35-40 polyQ repeats in the model, the number of aggregates were recorded throughout ageing demonstrating age-related aggregation in the models (Morley et al., 2002). Fluorescent tagging of amyloidogenic protein in *C. elegans* can also provide information on the nature of the aggregates through the use of fluorescence recovery after photobleaching (FRAP) analysis, which measures the mobility of fluorescent molecules within a defined area. For example, in a *C. elegans* model expressing α-synuclein tagged with YFP in the body wall muscle, animals developed mobile inclusions during ageing (Figure 1.8), until day 11 when a proportion of the inclusions were immobile and this increased with age (Van Ham et al., 2008).

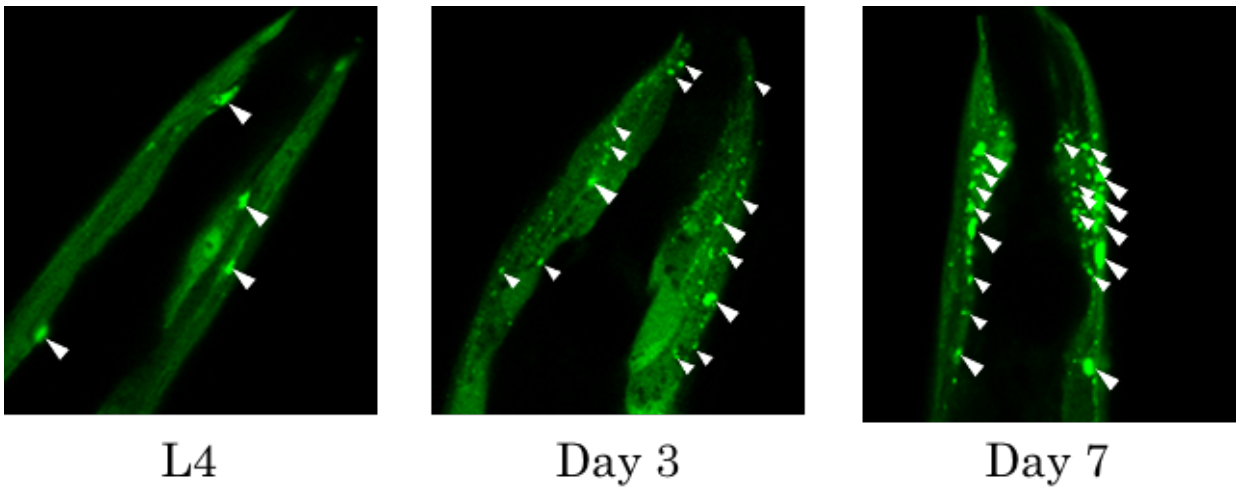

Figure 1.8 Aggregation of WT αSyn::YFP foci throughout ageing in *C. elegans*.
Images of the WT αSyn::YFP body wall muscle model (Van Ham et al., 2008) at L4 stage, day 3 of adulthood and day 7 of adulthood.

1.7.3 Behavioural phenotypes

Due to the relatively simple nature of *C. elegans*, any toxic damage caused by the aggregation of amyloidogenic proteins can be easily determined through phenotypic changes to the animal as detailed in Table 1.1. A common example of phenotypic readout is the measurement of locomotion through the uncoordinated (Unc) phenotype, paralysis or a reduction in the thrashing rate of animals in liquid. These locomotion phenotypes are present in both animals that express aggregation-prone proteins in the body-wall muscle or in the neurons (Pir et al., 2017). Other phenotypic readouts of toxic damage in *C. elegans* include chemotaxis phenotype - such as those observed when Aβ is expressed pan-neuronally (Wu et al., 2006) – and the loss of the touch nose response, as observed when tau is expressed in the mechanosensory neurons (Miyasaka et al., 2005).

1.7.4 Limitations of *C. elegans* as a model

Although it is an established model in amyloid research and provides a wealth of *in vivo* data for amyloid researchers, the use of *C. elegans* in amyloid research is not without its limitations and pitfalls. Erroneous expression of transgenes can impact upon the proteins expression; this is exemplified by the original Alzheimer's disease strain CL2006. Originally designed to express the full-length amyloid-β protein $A\beta_{1-42}$ (Link, 1995), it was discovered some time later to instead express a 3-42 truncation product due to aberrant cleavage of the Aβ peptide within the organism (McColl et al., 2009). Researchers then generated a new model to express the full-length $A\beta_{1-42}$, which displayed similar locomotion phenotypes to the original model (McColl et al., 2012). Further, mosaic expression from extrachromosomal arrays and leaky expression of transgenes can cause problems and yield misleading results for researchers (Pir et al., 2017). It is therefore important that data from studies are appropriately substantiated through further experiments such as immunohistochemistry or western blot analysis. Furthermore, it is important to appreciate that while the use of *C. elegans* to study amyloid disease provides a simple *in vivo* environment from which to study the effects of amyloid aggregation, it cannot completely reflect the *in vivo* factors of disease in humans. This is reflected throughout the majority of protein misfolding disease that are modelled, where some components of tissues are not represented in *C. elegans* such as visceral tissue. Nevertheless, *C. elegans* as a model does provide a lot of information about aggregation kinetics in an organismal context.

Disease	Protein	Tissue	Genotype	Phenotype	Reference
AD	Aß	Bwm	*unc-54::human Aβ$_{1-42}$*	Accumulation of amyloid deposits, rapid paralysis	(McColl et al., 2012)
		Bwm	*unc-54::human Aβ$_{3-42}$*	Accumulation of amyloid deposits, progressive paralysis	(Link, 1995; McColl et al., 2009)
		Bwm	*unc-54::human L17P Aβ$_{3-42}$*	No amyloid deposition	(Fay et al., 1998)
		Bwm	*myo-3::human Aβ$_{3-42}$:: let-851*	Paralysis	(Link et al., 2003)
		Glut neu	*eat-4::human Aβ*	Loss of glutamatergic neurons	(Treusch et al., 2011)
		Pan-neu	*snb-1::human Aβ$_{1-42}$*	Reduced chemotaxis, hypersensitive to 5-HT	(Wu et al., 2006)
	Tau	Pan-neu	*aex-3::human IN4R-MAPT*	Uncoordinated	(Kraemer et al., 2003)
		Pan-neu	*aex-3:: human P201L MAPT*	Severe uncoordinated phenotype and progressive neurodegeneration	(Kraemer et al., 2003)
		Pan-neu	*aex-3:: human V337M MAPT*	Server uncoordinated phenotype and progressive neurodegeneration	(Kraemer et al., 2003)
		Sensory neu	*mec-7::human tau*	Age-dependent loss of touch nose response	(Miyasaka et al., 2005)
		Sensory neu	*mec-7::P301L tau*	Severe and progressive loss of touch nose response	(Miyasaka et al., 2005)
		Sensory neu	*mec-7::R406W tau*	Severe and progressive loss of touch nose response	(Miyasaka et al., 2005)
		Pan-neu	*F25B3.3::human tau*	Age-dependent uncoordinated locomotion	(Brandt et al., 2009)
		Pan-neu	*F25B3.3::human PHP tau*	Age-dependent uncoordinated locomotion, defective motor neuron development	(Brandt et al., 2009)
		Pan-neu	*Snb-1::human 2N4R tau*	Mild late-onset uncoordinated phenotype	(Pir et al., 2016)
		Pan-neu	*Snb-1::human 2N4R A152T tau*	Early-onset paralysis, reduction of lifespan, neuronal dysfunction	(Pir et al., 2016)
PD	α-Syn	Bwm	*unc-54::human α-Syn::YFP*	Progressive accumulation of deposits, reduction in motility	(Van Ham et al., 2008)
		Bwm	*unc-54::human α-Syn::GFP*	Progressive accumulation of deposits	(Hamamichi et al., 2008)
		DA neu	*dat-1::human α-Syn::GFP*	DA loss and dendritic breaks	(Lakso et al., 2003)
		DA neu	*dat-1::A53T α-Syn*	DA loss and dendritic breaks	(Lakso et al., 2003)
		Pan-neu	*aex-3::human α-Syn*	Reduced thrashing rate, DA loss and dendritic breaks	(Lakso et al., 2003)
		Pan-neu	*aex-3::A53T α-Syn*	Reduced thrashing rate, DA loss and dendritic breaks	(Lakso et al., 2003)
		Motor neu	*acr-2::human α-Syn*	Reduced thrashing rate	(Lakso et al., 2003)
		Motor neu	*acr-2::A53T α-Syn*	Reduced thrashing rate	(Lakso et al., 2003)
		DA neu	*dat-1::A30P α-Syn*	Neurite defects	(Karpinar et al., 2009)
		DA neu	*dat-1::A53T α-Syn*	Neurite defects	(Karpinar et al., 2009)
		DA neu	*dat-1::A56P α-Syn*	Severe neurite defects	(Karpinar et al., 2009)
		Pan-neu	*unc-51::human α-Syn*	No obvious phenotype	(Kuwahara et al., 2008)
		Pan-neu	*unc-51:: A53T α-Syn*	No obvious phenotype	(Kuwahara et al., 2008)
		Pan-neu	*unc-51:: A30P α-Syn*	No obvious phenotype	(Kuwahara et al., 2008)

HD	Htt-PolyQ	Bwm	*unc-54::GFP-Htt-polyQ*	Reduced thrashing rate	(H. Wang et al., 2009)
		Sensory neu	*mec-3::Htt-polyQ::GFO*	Neurodegeneration	(Wang et al., 2006)
		Sensory neu	*osm-10::Htt-Q2 polyQ*	No sensory neuron phenotype	(Faber et al., 2002)
		Sensory neu	*osm-10::Htt-Q23 polyQ*	No sensory neuron phenotype	(Faber et al., 2002)
		Sensory neu	*osm-10::Htt-Q95 polyQ*	Progressive defective sensory neuron endings	(Faber et al., 2002)
		Sensory neu	*osm-10::Htt-Q150 polyQ*	Progressive sensory neuron defect, and death, progressive aggregate accumulation	(Faber et al., 2002)
		Bwm	*unc-54::Q0-YFP*	Diffuse fluorescence distribution and no motility defects	(Morley et al., 2002)
		Bwm	*unc-54::Q19-YFP*	Diffuse fluorescence distribution and no motility defects	(Morley et al., 2002)
		Bwm	*unc-54::Q29-YFP*	Diffuse fluorescence distribution and no motility defects	(Morley et al., 2002)
		Bwm	*unc-54::Q33-YFP*	Age-dependent foci formation and motility defect	(Morley et al., 2002)
		Bwm	*unc-54::Q35-YFP*	Age-dependent foci formation and motility defect	(Morley et al., 2002)
		Bwm	*unc-54::Q40-YFP*	Age-dependent foci formation and severe motility defect	(Morley et al., 2002)
		Bwm	*unc-54::Q44-YFP*	Localised discrete fluorescent foci	(Morley et al., 2002)
		Bwm	*unc-54::Q64-YFP*	Localised discrete fluorescent foci	(Morley et al., 2002)
		Bwm	*unc-54::Q82-YFP*	Localised discrete fluorescent foci and severe motility defect	(Morley et al., 2002)
		Pan-neu	*F25B3.3::Q0-CFP*	Diffuse fluorescent distribution, no motility defect	(Brignull et al., 2006)
		Pan-neu	*F25B3.3::Q19-CFP*	Diffuse fluorescent distribution, no motility defect	(Brignull et al., 2006)
		Pan-neu	*F25B3.3::Q35-CFP*	Diffuse fluorescent distribution, motility phenotype	(Brignull et al., 2006)
		Pan-neu	*F25B3.3::Q40-CFP*	Diffuse fluorescent distribution in the neurons, motility phenotype	(Brignull et al., 2006)
		Pan-neu	*F25B3.3::Q67-CFP*	Localised discrete fluorescent foci, severe motility phenotype	(Brignull et al., 2006)
		Pan-neu	*F25B3.3::Q86-CFP*	Localised discrete fluorescent foci, severe motility phenotype	(Brignull et al., 2006)
SCA	MJD1-PolyQ	Pan-neu	*unc-119::MJD1-17Q-GFP*	Diffuse fluorescence distribution	(Khan et al., 2006)
		Pan-neu	*unc-119::MJD1-91Q-GFP*	Diffuse fluorescence distribution	(Khan et al., 2006)
		Pan-neu	*unc-119::MJD1-130Q-GFP*	Age-dependent aggregation	(Khan et al., 2006)
ALS	SOD 1	Ubiquitous	*hsp16.2::human SOD1*	No sensitivity to paraquat under heat shock conditions	(Oeda et al., 2001)
		Ubiquitous	*hsp16.2::A4V SOD1*	Increased sensitivity to paraquat under heat shock conditions	(Oeda et al., 2001)
		Ubiquitous	*hsp16.2:: G37V SOD1*	Increased sensitivity to paraquat under heat shock conditions	(Oeda et al., 2001)
		Ubiquitous	*hsp16.2::G93A SOD1*	Increased sensitivity to paraquat under heat shock conditions	(Oeda et al., 2001)
		Bwm	*unc-54::human SOD1::YFP*	Diffuse fluorescence, no motility defects	(Gidalevitz et al., 2009)
		Bwm	*unc-54::G85R SOD1-YFP*	Punctate fluorescent pattern, reduction in thrashing rate	(Gidalevitz et al., 2009)
		Bwm	*unc-54::G93A SOD1-YFP*	Punctate fluorescent pattern, reduction in thrashing rate	(Gidalevitz et al., 2009)
		Pan-neu	*snb-1::human SOD1*	No motility defect	(J. Wang et al., 2009a)

		Pan-neu	*snb-1::G85R SOD1*	Severe motility defect, decreased number of neuromuscular junctions and synaptic vesicles	(J. Wang et al., 2009a)
		Motor neu	*unc-25::human SOD1*	Progressive locomotion defect and paralysis phenotype	(Li et al., 2013)
		Motor neu	*unc-25::G93A SOD1*	Progressive locomotion defect and paralysis phenotype	(Li et al., 2013)
		Ubiquitous	MosSCI *A4V SOD1*	Increased SOD1 protein accumulation, oxidative stress induced neurodegeneration	(Baskoylu et al., 2018)
		Ubiquitous	MosSCI *H71Y SOD1*	Increased SOD1 protein accumulation, oxidative stress induced neurodegeneration	(Baskoylu et al., 2018)
		Ubiquitous	MosSCI *G85R SOD1*	Increased SOD1 protein accumulation, oxidative stress induced neurodegeneration	(Baskoylu et al., 2018)
	TDP-43	Pan-neu	*snb-1::human TDP-43*	Uncoordinated phenotype, abnormal motor neuron synapses	(Ash et al., 2010)
		Pan-neu	*snb-1::human TDP-43*	Moderate motor defect, shortened lifespan	(Liachko et al., 2010)
		Pan-neu	*snb-1::G290A TDP-43*	Severe motor dysfunction, degeneration of GABAergic neurons, shortened lifespan	(Liachko et al., 2010)
		Pan-neu	*snb-1::A315T TDP-43*	Severe motor dysfunction, degeneration of GABAergic neurons, shortened lifespan	(Liachko et al., 2010)
		Pan-neu	*snb-1::M337V TDP-43*	Severe motor dysfunction, degeneration of GABAergic neurons, shortened lifespan	(Liachko et al., 2010)
		Pan-neu	*snb-1::human TDP-43::YFP*	Severe locomotion defects, formation of fluorescent insoluble foci	(Zhang et al., 2011)
		Pan-neu	*snb-1::Q331K TDP-43::YFP*	Severe locomotion defects, formation of fluorescent insoluble foci	(Zhang et al., 2011)
		Pan-neu	*snb-1::M337V TDP-43::YFP*	Severe locomotion defects, formation of fluorescent insoluble foci	(Zhang et al., 2011)
SSA and FAP	TTR	Bwm	*unc-54::TTR::EGFP*	Diffuse fluorescence, decreased lifespan	(Tsuda et al., 2018)
		Bwm	*unc-54::TTR$_{1-80}$::EGFP*	Diffuse fluorescence	(Tsuda et al., 2018)
		Bwm	*unc-54::TTR$_{49-127}$::EGFP*	Localised fluorescent foci, decreased lifespan	(Tsuda et al., 2018)
		Bwm	*unc-54::TTR$_{81-127}$::EGFP*	Localised fluorescent foci, decreased lifespan	(Tsuda et al., 2018)
		Bwm	*unc-54:: V30M TTR*	Impaired nociception, defective dendritic morphology, impaired locomotion	(Madhivanan et al., 2018)
		Bwm	*unc-54:: D18G TTR*	Impaired nociception, Impaired locomotion	(Madhivanan et al., 2018)
DRA	ß$_2$m	Bwm	*unc-54::WT β$_2$m*	Increased paralysis, delayed larval growth	(Diomede et al., 2012)
		Bwm	*unc-54:: ΔN6 β$_2$m*	Increased paralysis, delayed larval growth	(Diomede et al., 2012)
		Bwm	*unc-54:: P32G β$_2$m*	Increased paralysis, delayed larval growth	(Diomede et al., 2012)
		Bwm	*D76N β$_2$m*		(Faravelli et al., 2019)
Type II diabetes	IAPP	Ubiquitous	*Hsp-16.2::hIAPP*	Defects in chemotaxis	(Aldras et al., 2019)
		Pan-neu, Bwm, + pharynx	*Lev-11::hIAPP::YFP; tnt-4:: hIAPP::YFP; aex-3::hIAPP::YFP*	Insoluble aggregate formation; growth retardation	(Rosas et al., 2016)

Table 1.1 *C. elegans* amyloid disease models
Bwm= body wall muscle; DA neu = dopaminergic neurons; glut neu= glutaminergic neurons; motor neu= motor neurons; pan-neu= all neurons; sensory neu= sensory neuro

1.8 *C. elegans*, Proteostasis and Amyloid Disease

Like humans, other organisms are also constantly under threat from misfolded proteins that can occur due to stressors such as heat, oxidative stress, nutrient starvation and metabolic imbalances. Therefore the proteostasis network is highly conserved from humans to *C. elegans* in order to facilitate the folding, refolding and degradation of any aberrantly folded proteins to ensure proteome balance (Labbadia and Morimoto, 2015). *C. elegans* possess 219 chaperone genes that represent every major functional human chaperone family including Hsp90, Hsp70, Hsp60, Hsp40, prefoldin (PFD), sHsps, TPR-domain containing chaperone families as well as ER- and mitochondria-specific chaperones (Brehme et al., 2014). Stress response mechanisms are also conserved in *C. elegans* including the HSR, the UPR^{ER} and the UPR^{mito} (Balchin et al., 2016).

As amyloid diseases are based on the misfolding of precursor proteins, it is particularly important to understand the interplay between aggregation of the molecules and the proteostasis network. Although *in vitro* cellular studies can replicate the intracellular conditions of protein folding, *in vivo* models are necessary in order to understand how the intricate inter-tissue networks maintain the cellular proteome.

1.8.1 Molecular chaperones

Several chaperones have been shown to be associated with the expression of amyloidogenic proteins in *C. elegans*. Mass spectrometry analysis of proteins in an Aβ-expressing *C. elegans* disease model identified several chaperones that interact with intracellular Aβ including two members of the Hsp-70 family and three aB-crystallin related sHsps (Fonte et al., 2002). Furthermore, HSP-16 has been shown to colocalise with Aβ intracellular deposits and when overexpressed partially suppresses Aβ toxicity (Fonte et al., 2008, 2002).

Studies have also explored the impact of cell-non-autonomous stress responses in modulating aggregation in protein misfolding *C. elegans* disease models. Expression of HSP-90 in the neurons or the intestine was sufficient to alleviate the toxic paralysis phenotype associated with Aβ expression in the body wall muscle of animals, demonstrating the transcellular chaperone signalling can ameliorate protein aggregation in the model (O'Brien et al., 2018).

Similarly to humans, nematodes contain a disaggregase complex comprising of Hsp-110, Hsp-70 and J-proteins (Nillegoda et al., 2015). This complex has been shown to act upon polyglutamine aggregation in a *C. elegans* model, whereby knockdown of both a class A J-protein and the class B J-protein *dnj-13* promoted polyQ aggregation, indicating mixed-class cooperation (Kirstein et al., 2017). Moreover, knockdown of the *hsp-1*, a Hsp-70 chaperone, or *hsp-110* resulted in the increased number of aggregates in several polyglutamine models (Q35, Htt513Q15, AT3CTQ45, AT3CTQ63) (Scior et al., 2018). These results were replicated in HD patient derived neural cells, where the overexpression of a J-protein DNAJB1 reduced HttExon1Q97 aggregation (Scior et al., 2018).

Gene expression analysis has identified numerous genes related to the proteostasis network to be up-regulated in response to the expression of amyloidogenic proteins. In a genetic analysis of a temperature-inducible Aβ-expressing strain, 67 genes were identified to be upregulated including aB-crystallin (CRYAB) and tumour necrosis factor-induced protein 1 (TNFAIP1) (Link et al., 2003). An RNAi screen of all *C. elegans* chaperone genes in both an AD and a polyQ disease model further identified a core set of 7 chaperone genes which act as suppressors of Aβ associated toxicity in both models including *Hsc-70*, *Hsp-90*, *hsp-40* and *Sti-1* (Brehme et al., 2014). Several RNAi screens in α-synuclein expressing *C. elegans* models have identified modifiers of disease; these include genes involved in the ubiquitin proteasome system (UPS) (Vartiainen et al., 2006), mitochondrial genes (Vartiainen et al., 2006), endocytic pathway (Kuwahara et al., 2008) and protein quality control in the ER/Golgi complex (Van Ham et al., 2008). Another RNAi screen in an α-synuclein body wall muscle model identified 20 modifiers of aggregation that also protected against neurodegeneration induced in a PD dopaminergic model, demonstrating the common mechanism of protection between tissues (Hamamichi et al., 2008).

1.8.2 HSR

The interplay between the heat shock response and amyloid aggregation has also been studied using *C. elegans*. Heat shock treatment applied to a neuronal Aβ-expressing *C. elegans* model has been shown to alleviate Aβ toxicity and reduce Aβ oligomerisation (Wu et al., 2010). Expression of the Spinocerebellar ataxia-related amyloidogenic protein AT3(Q130) in the background of a *hsf-1* – the master regulator of HSR - mutant caused a deleterious phenotype to the animal (Teixeira-Castro et al., 2011). Moreover, in a model overexpressing expanded polyQ repeats, mutations in AFD/AIY thermosensory neurons

inhibited organismal HSR, and suppressed protein aggregation (Prahlad and Morimoto, 2011).

1.8.3 UPR^{ER}

Knockdown of the UPR^{ER} transcription factors *xbp-1* and *atf-6* was found enhance frontotemporal dementia with parkinsonism linked to chromosome 17 (FTDP-17) tau and tau-related behavioural defects (Kraemer et al., 2006; Waldherr et al., 2019). Constitutive activation of neuronal XBP-1 suppressed the loss of chemotaxis in a neuronal polyglutamine model and the loss of neurons observed in a tau-expressing *C. elegans* model (Imanikia et al., 2019b; Waldherr et al., 2019). Although tau protein was not observed in the ER of the model, it was shown that the ERAD was required for the suppression observed (Waldherr et al., 2019). Furthermore, expression of *xbp-1* in the neurons was also sufficient to alleviate aggregation of polyQ in the body-wall muscle of animals, demonstrating the cell-non-autonomous action of this PN component in protein misfolding (Imanikia et al., 2019a). DNJ-27, another ER luminal protein has been shown to have a protective role against Aβ aggregation when overexpressed, ameliorating the associated deleterious paralysis phenotype (Muñoz-Lobato et al., 2014).

1.8.4 UPR^{mito}

Increasingly, research has linked the UPR^{mito} and various amyloid-associated diseases. Data from AD patients has revealed a strong correlation to genes in the UPR^{mito} pathway (Sorrentino et al., 2017). This upregulation of mitochondrial stress response genes was also observed in an AD *C. elegans* disease model that displayed age-dependent amyloid aggregates. Conversely, upregulation of the UPR^{mito} transcription factor *atfs-1* in the same model was able to reduce the number of amyloid aggregates in the model (Sorrentino et al., 2017). Expression of 40 polyglutamine repeats in the neurons of *C. elegans* induced both cell-autonomous and cell-non-autonomous upregulation of mtHsp70/HSP-6 in distal tissues (Berendzen et al., 2016).

1.9 Thesis Overview and Aims

The aim of this research was to investigate amyloid aggregation and mechanisms of amyloid toxicity *in vivo*. To achieve this, the roundworm nematode *Caenorhabditis elegans* was utilised as a model for the expression of amyloidogenic proteins, and the consequences of chaperone involvement in aggregation were explored. *C. elegans* has been used as a useful tool to study amyloid aggregation *in vivo*. This includes the expression of amyloidogenic proteins β_2-microglobulin and IAPP which are involved in the protein misfolding diseases dialysis related amyloidosis and type II diabetes mellitus respectively. Although *C. elegans* models expressing β_2-microglobulin and IAPP have been generated previously, each have their limitations, and are therefore subject to improvements.

Previous *C. elegans* models of β_2-microglobulin aggregation have been generated to express wild type, D76N and ΔN6 β_2m (Diomede et al., 2012; Faravelli et al., 2019). To study the differences between the toxic damage caused by each β_2m variant, it was necessary to generate three similar *C. elegans* disease models, each expressing a variant of β_2m. **Chapter 3** outlines the generation and characterisation of each disease model, including the exploration of protein aggregation within the model and the effects of aggregation on the proteostasis network.

IAPP aggregation has been previously modelled in *C. elegans* through the expression of human IAPP simultaneously in the neurons, body wall muscle and pharynx (Rosas et al., 2016), or an inducible neuronal model (Aldras et al., 2019). To elucidate the cell-autonomous and cell-non-autonomous effects of IAPP aggregation, the research presented in **Chapter 4** explores a newly generated model, expressing IAPP in the body wall muscle of animals alone. To discriminate the toxic effects of IAPP *in vivo*, models expressing other variants of varying amyloidogenicity were also generated. **Chapter 4** further outlines the generation of these IAPP-expressing models and the characterisation of any aggregation or toxic damage during development and aging of the organism. As IAPP is known to affect Aβ aggregation, the generated IAPP models were also crossed into Aβ expressing *C. elegans* models in order to further explore this relationship *in vivo*.

The proteostasis network has been demonstrated to be vital in maintaining proper protein folding and prevent the aggregation of peptides into amyloid species. The molecular chaperone, *hsp-90* is essential for the folding of metastable client proteins as well as

preventing aggregation of amyloid beta (Brehme et al., 2014; Evans et al., 2006). **Chapter 5** explores this relationship further, to gain understanding of the cell autonomous and cell-non-autonomous relationship of HSP-90 and the aggregation of the AD protein, Amyloid-β in *C. elegans*.

Chapter 2. Materials and Methods

2.1 *Caenorhabditis elegans* strains and maintenance

Unless otherwise stated, strains were maintained at 20°C on 60 mm NGM agar plates seeded with OP50-1 *Escherichia coli* as a food source. All strains were maintained on NGM plates with plenty of food source and transferred to a new plate every few days using a platinum wire pick to ensure a food source was maintained.

2.1.1 Preparation of Nematode Growth Medium (NGM) or RNAi plates

Nematode growth medium (NGM) was prepared using protocols recommended by WormBook (Stiernagle, 2006). Briefly, agar medium was prepared as 1.7% (w/v) agar, 50 mM NaCl and 0.25% (w/v) bactopeptone and sterilised by autoclaving. Following autoclaving additional supplements were added to the medium including 25 mM KPO_4 pH 6.0, 1 mM $CaCl_2$, 1 mM $MgSO_4$, 5 µg/mL cholesterol, and 200 µg/mL streptomycin. Agar medium was dispensed into 60 mm petri dishes under sterile condition and plates were left overnight to dry. The next day NGM plates were seeded with 250 µL bacterial cultures of OP50-1 *E. coli*.

Bacterial cultures of OP50-1 *E. coli* were prepared my inoculating lysogeny broth (LB) with a small amount of OP50-1 glycerol stocks. LB was prepared to contain streptomycin at a final concentration of 1 mg/mL and the cultures were incubated overnight at 37°C shaking. Glycerol stocks of bacterial cultures were made by thoroughly combining 600 µL of bacterial culture with 300 µL of 60% glycerol and stored at -80°C until use.

2.1.2 Genetic crosses

To generate genetic crosses between two strains, males of one of the strains were generated. As males represent a low incidence in a normal *C. elegans* population, the strains were subjected to heat shock to increase the probability of X chromosome non-disjunction (Rose and Baillie, 1979). To obtain males, three plates of 10 L4-stage hermaphrodites were placed at 35°C for 3 hours, and then returned to 20°C to recover. Plates were checked every day for the presence of male progeny until a sufficient amount

of males could be detected. To initiate the genetic cross, seven adult males of one strain were placed onto an NGM plate with two L4-stage hermaphrodites of the second strain and allowed to cross-fertilise for two days. Males were then removed from the plate to avoid potential mating with the progeny.

Plates were checked daily for the presence of F1 progeny containing the appropriate phenotypes of each strain. Four L4-stage hermaphrodite F1 progeny were moved to a new NGM plate and allowed to self-fertilise. The progeny of the F1s were checked daily for the development of F2 progeny containing the appropriate phenotypes (e.g. fluorescent transgenic marker) of both strains. 20 F2 progeny were selected and isolated onto separate NGM plates, allowed to self-fertilise and the population to grow. The F2 populations were monitored for population homozygosity. Identified homozygous populations were maintained for future use.

2.1.3 Generation of transgenic strains via microinjection

L4-stage N2s were isolated onto an NGM plate and left overnight to develop. Day 1 young adult animals were transferred onto 2% agarose pads containing a drop of microinjection oil in order to immobilise the nematode. Injection needles were loaded with 1 µL of transgenic DNA solution (5 ng/µl myo-2p::mCherry, 10 ng/µl DNA in dH_2O). The injection needle was fitted onto a Zeiss Axioscope with a DIC filter and a needle arm for injections. The gonad arm of the nematode was brought into focus using the 40X objective and the needle gently lowered into focus at a 15-45° angle. The N_2 gas was turned on until noticeable swelling of the organism from the DNA solution could be seen. Nematodes were recovered using M9 buffer and placed onto new NGM plates for recovery. Three to five days later, plates were checked for successful transgenic progeny. Any successful transgenic animals were isolated onto new NGM plates and checked daily to ensure a stable extrachromosomal transgenic line had been established.

2.1.4 Synchronisation of populations and ageing

Populations of strains were synchronised by either bleaching or egg-laying. Unless stated otherwise, stains were synchronised by egg-laying methods. 10 gravid adults were selected from the strain and placed onto new NGM plates and allowed to lay eggs for 6 hours.

Following this, all 10 adults were removed from the plate, and the remaining eggs were allowed to develop.

To bleach synchronise strains, a population was grown on NGM plates until a large population of eggs and non-starved gravid adults were present. The nematodes were washed from the plate using M9 buffer into a 15 mL microcentrifuge tube and pelleted by centrifugation at 1000 rpm for 1 minute. M9 supernatant was removed carefully to not disturb the nematode pellet, and 10 mL of bleach solution (1% sodium hypochlorite (v/v), 0.25M NaOH) was added to the pellet. The tubes were inverted for 5 minutes then centrifuged to pellet. The bleach supernatant was removed and the pellet was washed three times with 15 mL M9 buffer to remove any trace of bleach solution. The pellet was suspended in 1 mL of M9 buffer and placed on a rotator overnight for the eggs to hatch. The following day the hatched larvae were added to NGM plates to further develop.

To age animals, L4-stage animals were selected onto NGM plates and transferred daily to new NGM plates until the desired stage was reached. Animals were transferred daily to ensure any progeny did not infiltrate the strain population. Alternatively, where stated animals were also aged from L4 stage on NGM Agar plates supplemented with 50 µM fluorodeoxyuridine (FUdR). The addition of FUdR to plates induces sterility by preventing eggs from hatching. Therefore nematodes grown on FUdR were not moved daily and grown until the required age. If the food source was limited on the plates, animals were washed using M9 buffer and transferred to a new FUdR NGM plate.

2.2 Phenotypic *C. elegans* assays

2.2.1 Developmental assay

Ten gravid adult nematodes were placed on an NGM plate with OP50-1 as a food source and allowed to lay eggs for 2 hours then removed. Eggs were left to develop for 65 hours after removal and animals on the plate were assessed for developmental stage and recorded. Three independent experiments were performed for each strain.

2.2.2 Fecundity assay

Thirty L4-stage nematodes were transferred onto separate individual NGM plates supplemented with OP50-1. At time-points of 24-, 48-, 72- and 96- hours, individual animals were transferred onto a new NGM plate using a sterilised platinum wire, and the number of eggs laid over the previous 24 hours were counted and recorded.

2.2.3 Lifespan assay

Animals were synchronised by egg-laying, and 80 L4-stage animals were selected per strain and transferred onto four NGM plates with 20 animals per plate. Every other day each nematode was assessed for survival, death or censored and numbers were recorded. Animals were assessed as dead if they did not display movement when gently touched on the nose using a platinum wire, and no pharyngeal pumping could be observed. Animals were censored if they crawled up the edge of the plate and became desiccated, burrowed into the agar, displayed the 'bag of worms' phenotype where eggs hatched internally, or if they could not be found. Any dead or censored animals were recorded and left on plates, while alive animals were transferred onto a new NGM plate. Data was analysed using OASIS 2 online software (Han et al., 2016)

2.2.4 Paralysis assay

Animals were synchronised using egg-laying methods, and 100 L4-stage nematodes were transferred onto five NGM plates with OP50-1 (20 animals per plate). Every 24 hours for 8 days, each nematode was assessed by the touch-nose response for paralysis and the numbers of mobile, paralysed or censored animals were recorded. Nematodes were identified as mobile if they were able to move freely, either when touched by a platinum wire, or when unprompted. Nematodes were assigned as paralysed if little movement was seen when touched by a platinum wire, but still displayed minimal movement or pharyngeal pumping to indicate they were still alive. Censored nematodes included nematodes that had died, displayed the 'bag of worms' phenotype, crawled up the side of the plate, or could not be identified. Mobile nematodes were moved onto a new plate each day to ensure any progeny did not influence the results. Wilcoxon signed-rank test was used to compared populations.

2.2.5 Thrashing assay

Animals were synchronised by egg-laying and aged to either day 1 or day 8 of adulthood by picking. At the appropriate time point, 15-20 nematodes of each strain were transferred into a 24-well plate containing 1 mL M9 buffer. Animals were left to recover for 30 seconds, then video recorded for 30 seconds using a WiFi camera attached to a Microtec light microscope. At least three videos of each strain were recorded. Videos are analysed in ImageJ using the WrmTrck plugin (Nussbaum-Krammer et al., 2015) to quantify the number of body bends per second (BBPS) an animal performed.

2.2.6 Thermotolerance assay

Progeny were synchronised by egg-laying and 50 L4-stage animals were selected and placed onto an NGM plate. The next day (day 1 adults), plates were incubated at 35°C for 6 hours then moved immediately into a 20°C incubator. Plates were left for 16 hours for recovery, then survival of animals were scored. Animals were scored as alive if movement or pharyngeal pumping was observed and dead otherwise. The percentage of alive and dead animals was calculated and mean survival rates were determined using Student's t test.

2.2.7 ER stress assay

Nematodes were synchronised by egg-laying and L4-stage animals were selected and placed onto new NGM plates. Nematodes were left overnight to grow and 50 day 1 adult stage were transferred using a sterilised platinum wire into M9 buffer containing 50 µg/mL tunicamycin. Animals were incubated in tunicamycin for 6 or 10 hours at 20°C on a rotator. After incubation, nematodes were washed three times in M9 buffer and plated onto NGM plates. After 16 hours of recovery, animals were scored for survival. Alive animals were determined by their ability to move spontaneously or when stimulated by touch, or pharyngeal pumping was observed. Dead animals were determined through lack of movement or pharyngeal pumping. Percentages of alive and dead animals were calculated and plotted.

2.3 Imaging techniques

2.3.1 Immunostaining

Nematodes were synchronised by egg-laying and aged according to experimental needs. When animals reached the relevant age but were not starved, they were washed off the plate using M9 buffer and transferred into 1.5 mL microcentrifuge tubes using a glass pipette. The animals were pelleted by centrifugation at 1000 rpm for 1 minute, supernatant removed and washed three more times using M9 buffer. As much supernatant was removed as possible without disturbing the pellet, and 500 µL M9 buffer supplemented with 40 µL Pulsin (PolyPlus transfection SA) and an antibody against Amylin (R10/99) tagged with Alexa 647 or β_2-microglobulin (Dako). To tag Alexa 647 onto R10/99, the Alexa 647 Antibody Labelling Kit (A20186) was used (Invitrogen). Animals were incubated in Pulsin and appropriate antibody for 6 hours, and then imaged.

2.3.2 X-34 staining

Nematodes were synchronised by egg-laying and aged to the relevant stage by transferring the animals onto a new NGM plate everyday using a platinum wire pick. Animals were transferred off the plate into 500 µL M9 buffer and washed three times in M9 buffer to remove as much bacterial contaminant as possible. The pellet was resuspended in M9 buffer containing 1 mM X-34 (stored in 10 mM Tris pH 8.0). Animals were incubated at 20°C for 2 hours on a rotator. Animals were washed three times in M9 buffer and transferred to a new NGM plate using a glass pipette. Plates were incubated at 20°C for 12-16 hours and animals were imaged (excitation 400-410 nm, emission 455 nm).

2.3.3 Confocal Microscopy

Individual nematodes where transferred into a drop of 5 mM levamisole on a 2% (w/v) agarose glass slide to anaesthetise. Slides were left to dry for a 1-2 minutes before a glass coverslip was placed on top of the slide. Images were taken of the slides using an upright Zeiss LSM880 laser scanning confocal microscope and Zen software. Images were taken at magnifications of 10X, 20X and 40X. Images were taken together for each experiment, and identical settings were used.

2.4 Quantitative Reverse Transcription PCR (RT-qPCR)

2.4.1 Sample Preparation

Samples were prepared from ~100 L4-stage nematodes which were collected into 250 µL of M9 buffer in a 1.5 mL microcentrifuge tube. The nematodes were centrifuged at 1000 rpm for 1 minute and supernatant removed. The nematode pellets were washed in M9 buffer twice more to remove as much bacterial contamination as possible. Upon the final wash, as much supernatant was removed as possible without disturbing the nematode pellet. The pellets were then frozen at -80°C for at least a day. To homogenise the samples, the Zymo Direct-Zol RNA MiniPrep kit was followed. Briefly, 50 µL of TRIzol (Ambion) was added to the frozen pellet and using a pellet grinder the nematodes were ground on ice three times for 30 seconds each. A further 150 µL of TRIzol was added to the samples and the solution was vortexed at 4°C for 10 minutes. To facilitate salt formation, 200 µL of 100% ethanol was added to the sample and the reaction was transferred to a Zymo-Spin IICR column with collection tube. The sample column was centrifuged for 13,000 rpm for 30 seconds, and the flow-through was discarded. Samples were washed using RNA Wash Buffer and then treated with DNase I and DNA Digestion Buffer. Samples were further washed and eluted using RNase-free water. A Thermo Scientific NanoDrop One was used to record the RNA concentration of the samples, and they were stored at -80°C until further use.

2.4.2 cDNA synthesis

Each sample was reverse transcribed into cDNA using a Bio-Rad iScript cDNA synthesis kit. Briefly, reactions were set up in PCR tubes to contain 250 ng RNA sample, 4 µL iScript 5X mix, 1 µL reverse transcriptase and nuclease-free water to a final volume of 20 µL. The reactions were placed into an Applied Biosystems Veriti 96-Well Thermal Cycler for the following profile: 5 minutes at 25°C, 20 minutes at 46°C, 1 minute at 95°C then held at 4°C. cDNA samples were stored at 4°C for short-term storage and -80°C for long term storage.

2.4.3 Quantitative PCR (qPCR)

Quantitative PCR was set up in 96-well plates in a reaction volume of 20 µL. Reactions were set up to contain 1 µL of cDNA sample, 8µL nuclease-free water, 0.5 µL 10µM forward primer, 0.5 µL reverse primer, 10 µL 2X Bio-Rad SsoAdvanced Universal SYBR Green mix. qPCR was performed in a Bio-Rad CFX Connect Real-Time System using the programme described in Table 2.1.

Step		**Temperature (°C)**	**Duration (seconds)**
Denaturation		95	180
40X	Denaturation	95	15
	Primer annealing	56	30
	Extension	72	30
Final Extension		72	60
Melt curve		55-95	10

Table 2.1 qPCR thermal cycler programme.

2.4.4 Primers

Gene	Sequence	
	Forward	Reverse
C12C8.1	GATCAAGCCGCTCGTAATCC	AACCTCAACAACGGGCTTTC
cdc-42	TGTCGGTAAAACTTGTCTCCTG	ATCCTAATGTCTATGGCTCGC
GFP	AGTCCGCCCTGAGCAAAGA	TCCAGCAGGACCATGTGATC
hIAPP	ATTGAGTCACATCAAGTGGAGAA	GCTAGACAGAATAGCACCGAAAT
hsp-1	ACTTCTACACCAACATCACTCG	CAAGGACGATGTCATGAACTTG
hsp-4	GTGGCAAACGCGTACTGTGATGA	CGCAACGTATGATGGAGTGATTCT
hsp-90	GACCAGAAACCCAGACGATATC	GAAGAGCACGGAATTCAAGTTG
rIAPP	TCAGGTGGACAAACGGAAGT	TGCCACATTCCTCTTCCCAT
sti-1	CTTGCCTATATCAATCCAGAGCTT	GGATGTATCCCTTGTAAATTTCG

WT B2m	CAACTTCCTGAACTGCTATGTTTC	ACAAGAGGTAGAACGACCAATC

Table 2.2 qPCR primers

Chapter 3. Expression of β2-microglobulin in *C. elegans*

3.1 Abstract

Amyloid is associated with numerous misfolding diseases and can cause a range of localised or systemic disorders. This includes dialysis related amyloidosis, a disease caused by the aggregation and deposition of β2-microglobulin in haemodialysed patients. Although the aggregation of β2m into amyloid has been studied extensively *in vitro*, *in vivo* models of β2m are comparatively lacking. To address this, three new transgenic *C. elegans* strains were generated to express either the wild type (WT) human β2m, or two of its highly amyloidogenic naturally occurring variants: D76N and ΔN6, in the body wall muscle of the nematodes. In this chapter, the effects of β2m expression in *C. elegans* were characterised throughout ageing. Strains expressing the more amyloidogenic variants, D76N and ΔN6 exhibit increased amounts of protein aggregation compared with WT β2m-expressing animals. This increased protein aggregation correlated with the severity of toxicity observed in animals and included increased paralysis, reduced thrashing rate, delayed development and shortened lifespan. A reduced capacity to cope with ER stress and decreased basal expression of the ER chaperone *hsp-4* was observed in all three β2m-expressing strains. Furthermore, WT β2m and D76N β2m but not ΔN6 β2m expressing strains were observed to not upregulate *hsp-4* transcripts in response to ER stress. These data suggest a possible link between β2m toxicity, and the unfolded protein response of the ER.

3.2 Introduction

The misfolding of proteins has been associated with many different diseases in humans; of which a large number are associated with the formation of amyloid fibres, including Alzheimer's Disease, Parkinson's Disease and Dialysis Related Amyloidosis (Hartl et al., 2011; Hipp et al., 2019, 2014). Amyloid diseases are characterised by the formation of insoluble fibres containing a cross-β fold and are the result of aberrant misfolding of the protein involved (Hipp et al., 2014). Many of these diseases involve the self-assembly of different proteins which do not share a common native structure or amino acid sequence;

however, the chemical properties of the amino acid sequence, the conformational stability of its folded state and its cellular concentrations allow these proteins to misfold into the generic amyloid fibres associated with disease (Hipp et al., 2019, 2014; Knowles et al., 2014).

This chapter focuses on one of these proteins, β_2-microglobulin (β_2m), which is the non-covalently bound light chain of the major histocompatibility complex class I (MHC I). β_2m is composed of 99-residues and contains a characteristic β-sandwich immunoglobulin fold, which consists of seven β-strands and one intrachain disulphide bond (Strominger et al., 1987; Verdone et al., 2009). In patients on long-term dialysis, β_2m can cause severe complications as it is not properly removed from the system, and therefore concentrations of β_2m in the plasma increase up to >60-fold compared with healthy individuals (Gejyo et al., 1985). Aggregation of human wild type (WT) β_2m initiates the formation of amyloid in osteoarticular tissues leading to the condition known as dialysis-related amyloidosis (DRA). Amyloid deposits of β_2m are mainly composed of wild type (WT) β_2m (~70%), but also contain truncation products, of which the majority represent a six amino acid N-terminal truncation, ΔN6 (~30%) (Esposito et al., 2000).

3.2.1 WT β_2m

The aggregation of β_2m into amyloid has been extensively studied *in vitro* (Jadoul and Drüeke, 2016; Karamanos et al., 2019, 2014; Scarponi et al., 2016). Although it is the major component of the amyloid deposits found in DRA, WT human β_2m cannot aggregate under physiological conditions *in vitro*, and requires partial unfolding which involves the *cis-trans* isomerisation of Pro32 and the formation of a non-native, unstable state (Chiti et al., 2001; Eichner and Radford, 2009; Smith et al., 2020). This partial unfolding and subsequent amyloid formation can be achieved *in vitro* via the lowering of pH or the addition of additives such as Cu^{2+} ions, detergents or organic solvents (Benseny-Cases et al., 2019; Yamamoto et al., 2005). Although the mechanism of recruitment of WT β_2m to osteoarticular tissues is not fully understood, extracellular matrix components present in these tissues such as collagen, apolipoprotein E and the glycosaminoglycans (GAGs) heparin and hyaluronic acid have been found to enhance amyloid formation *in vitro* (Benseny-Cases et al., 2019; Hoop et al., 2020; Myers et al., 2006; Relini et al., 2008, 2006; Wyatt et al., 2012).

3.2.2 D76N β_2m

Mutations in β_2m can also affect characteristics of its aggregation. The single point mutation Asp76Asn (D76N) of β_2m has been implicated in a rare hereditary systemic amyloidosis. Unlike WT β_2m deposition in DRA, patients with D76N β_2m develop extensive amyloid deposits in visceral tissues that are not a result of dialysis complications (Valleix et al., 2012). Comparison of the three-dimensional structures of WT and D76N β_2m shows that they are almost identical (Figure 3.1). However, D76N β_2m is less thermodynamically stable, and forms fibrils under physiological conditions (Mangione et al., 2013; Valleix et al., 2012). NMR experiments have also revealed that D76N β_2m possesses enhanced molecular dynamics, and a loss of rigidity (Valleix et al., 2012). It was shown i*n vitro* that D76N β_2m can also recruit WT β_2m into amyloid fibrils. However, WT β_2m is absent from D76N fibrils *in vivo* and this is speculated to be due to inhibition by chaperone activity (Mangione et al., 2013).

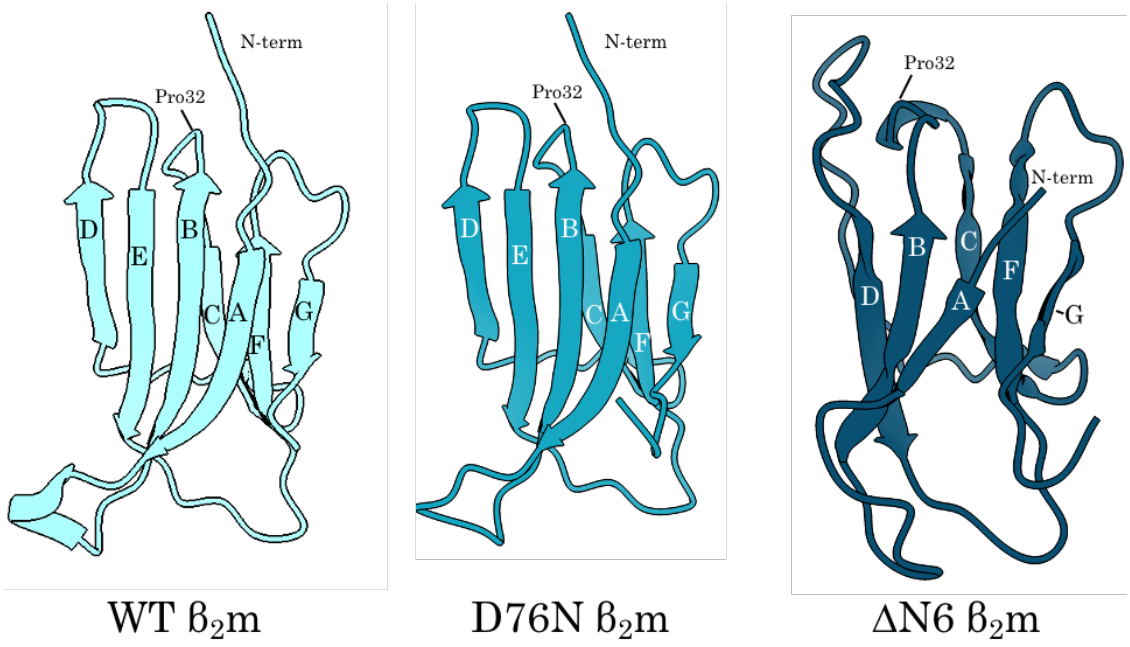

Figure 3.1 Monomeric structures of WT β_2m, D76N β_2m and ΔN6 β_2m.
Structures of WT β_2m (Protein Data Bank (PDB) ID code 2XKS), D76N β_2m (PDB ID code 4FXL) and ΔN6 β_2m (PDB ID code 2XKU) (Eichner et al., 2011; Valleix et al., 2012). Structures generated using ChimeraX software.

3.2.3 ΔN6 β_2m

As previously mentioned, the 6 amino acid truncation of WT β_2m, ΔN6, is present in ex-vivo DRA deposits (Esposito et al., 2000). Previous studies have shown that ΔN6 β_2m can induce amyloid formation of WT β_2m *in vitro* (Eichner et al., 2011) and can co-assemble

with WT β_2m into amyloid fibrils (Sarell et al., 2013b). In contrast to WT β_2m, ΔN6 is highly amyloidogenic, and can readily aggregate into amyloid *in vitro* at the physiological pH of 6-7 in the absence of any additives or fibril-seeds (Eichner et al., 2011; Karamanos et al., 2016; Myers et al., 2006). It is thought that ΔN6 is a structural mimic of the partially unfolded state of WT β_2m, the precursor to amyloidosis. This is because the ΔN6 β_2m protein contains a *trans* His-Pro peptide bond at residue 32 (in contrast to the native *cis* isoform (Figure 3.1), which facilitates rapid aggregation (Eichner et al., 2011). ΔN6 forms amyloid in a specific assembly mechanism that involves the formation of head-to-head dimers that pack into symmetric hexamers. These hexamers are not cytotoxic, retain the immunoglobulin fold of native β_2m and appear to be primed for further conformational change into the cross-β structure of amyloid (Karamanos et al., 2019).

3.2.4 β_2m toxicity in cells

Numerous studies have sought to uncover the mechanism by which β_2m exerts its toxic effects. It has been established that the oligomeric intermediates of amyloid assembly can be cytotoxic, and this has been demonstrated both *in vitro* and *in vivo* for several amyloidogenic proteins (Tipping et al., 2015). In contrast, amyloid fibrils in general are thought to have little cytotoxic activity, and therefore have been proposed by some researchers to instead represent inert end-stage products of amyloid assembly (Tipping et al., 2015). In contrast to this, research on the toxicity of β_2m has mainly focussed on the cytotoxic effects of fibrils. Amyloid fibrils of β_2m formed *in vitro* were observed to disrupt artificial lipid membranes, where fragmentation of the fibrils disrupted membranes to a greater extent than in the longer unfragmented precursors (Xue et al., 2009). Cryo-electron tomography of the fragmented β_2m fibrils in the presence of liposomes revealed fibril-lipid interactions occur primarily at the fibril ends and result in membrane distortion (Milanesi et al., 2012), and this is modulated by lipid composition and pH (Goodchild et al., 2014). Subsequently, it was shown that these fragmented fibrils were more readily internalised by cells, accumulating in lysosomes, inhibiting protein degradation by lysosomes and perturbing trafficking in the endolysosomal pathway (Jakhria et al., 2014).

Macrophages have also been implicated in the progression of DRA, and have been shown to be present in β_2m deposits (Argilés et al., 1994). Indeed, β_2m has also been reported to be cytotoxic to monocytes, the precursor to macrophages (Porter et al., 2011). Moreover,

bone resorbing osteoclasts – cells of the monocyte/macrophage lineage – have been suggested to be responsible for osteolytic lesions in DRA (Menaa et al., 2008; Porter et al., 2011). Indeed, human β_2m has been shown to promote osteoclastogenesis in murine macrophages (Menaa et al., 2008), and inhibit the formation of osteoclasts (Porter et al., 2011).

Similar to WT β_2m, D76N β_2m also induces cytotoxicity. When applied to human neuroblastoma cells, fibrillar D76N induced MTT cytotoxicity, increased Ca^{2+} and ROS levels, leading to necrotic cell death. This cytotoxicity was dependent on interactions of D76N β_2m with the cell membrane (Leri et al., 2016).

3.2.5 *In vivo* models of β_2m associated amyloidosis

The roundworm nematode *C. elegans* has been used previously to investigate the toxicity of several different amyloid disease-related proteins *in vivo*. Its small size, short life-cycle and ease of maintenance make *C. elegans* an excellent model for biological research. Moreover, *C. elegans* shares many characteristics with mammalian systems, and roughly 60% of human genes possess a *C. elegans* ortholog (Shaye and Greenwald, 2011). In addition, genetic manipulations of the organism are performed easily, including forward genetic screens, RNAi screens, rapid mutation mapping and transgenic animal generation (Nance and Frøkjær-Jensen, 2019). Due to the transparent nature of the nematode, previous studies have also utilised fluorescent protein tags to study the aggregation of amyloidogenic proteins in real time (Morley et al., 2002; Van Ham et al., 2008).

Although *C. elegans* has been widely utilised to study neurodegenerative amyloid diseases such as Alzheimer's disease (Link, 1995) and Huntington's disease (Morley et al., 2002), research on systemic amyloidoses is lacking in comparison. That being said, a few models have been generated to mimic these systemic diseases *C. elegans*, including models expressing transthyretin (TTR) (Link, 1995; Madhivanan et al., 2018), or β_2m (Diomede et al., 2012; Faravelli et al., 2019). In regards to β_2m models, Diomede and colleagues generated three new transgenic *C. elegans* strains expressing either wild type (WT) β_2m, the six amino acid truncated variant ΔN6, or P32G a non-naturally occurring variant in the body wall muscle of animals (Diomede et al., 2012). Expression of the highly amyloidogenic variants ΔN6 and P32G affected larval growth and shortened lifespan, while expression of all three variants caused a reduction in the number of body bends, and

this was rescued by tetracyclines (Diomede et al., 2012). The naturally occurring familial variant of β_2m, D76N has also been expressed in *C. elegans*, and caused a growth and motility phenotype in the model which was also rescued by tetracyclines (Faravelli et al., 2019). Although models of β_2m have been generated in *C. elegans* before, the characterisation of these models was limited to cell autonomous locomotion phenotypes, and the mechanisms of the toxicity observed were not explored. Thus, this study sought to generate new improved models from which novel insights about the mechanisms of toxicity of these proteins *in vivo* could be uncovered.

3.2.6 Protective cellular stress response pathways and amyloid diseases

Cells employ stress response and clearance pathways to combat the accumulation of misfolded amyloid proteins (Hipp et al., 2019; Rendleman et al., 2018). These include the ubiquitin-proteasome system (UPS), and autophagy which facilitate degradation of misfolded proteins, and signalling cues that upregulate the expression of protective protein quality control components, including the heat shock response (HSR) (Hajdu-Cronin et al., 2004), and the unfolded protein response (UPR) of the endoplasmic reticulum (UPR^{ER}) and the mitochondria (UPR^{mito}) (Neupert and Herrmann, 2007). Of these signalling responses, the UPR^{ER} maintains the proteome in the endoplasmic reticulum. It is defined by three ER transmembrane stress sensors IRE1, PERK and ATF6 that are regulated by the interaction and dissociation of the molecular chaperone BiP. PERK activation inhibits general protein translation and activates the activating transcription factor 4 (ATF4), which leads to expression of genes involved in autophagy, amino acid metabolism, antioxidant responses and apoptosis (Walter and Ron, 2011). IRE1a activation leads to the splicing of the transcription factor *XBP1* which controls regulation of genes related to protein folding, ER-associated protein degradation (ERAD), protein translocation and lipid synthesis (Hetz et al., 2011). Moreover, activation of ATF6 leads to activations of ERAD genes, and the master transcription factor *XBP1s* (Walter and Ron, 2011a). In *C. elegans*, the IRE1a/XBP1 branch is involved in ageing (Taylor and Dillin, 2013). For example, the constitutive activation of XBP-1s can extend lifespan (Taylor and Dillin, 2013) and has been shown to ameliorate toxicity associated with a tau model (Waldherr et al., 2019). Other components upregulated by stress response pathways have also been shown to ameliorate toxicity associated with amyloidogenic protein expression, including the HSP-70, HSP-16, DNJ-27 and HSP-90 (Fonte et al., 2008; Muñoz-Lobato et al., 2014; O'Brien et al., 2018)

3.3 Aims of the chapter

In Chapter 3, I sought to generate and characterise three new transgenic *C. elegans* disease models expressing different variants of β_2m: wild type (WT) β_2m, D76N β_2m and ΔN6 β_2m. Through characterising the toxic phenotypes observed in these transgenic disease models and determining the aggregation characteristics of the models I aimed to gain further insight into how these proteins cause toxic damage. Further, I aimed to uncover any mechanisms through which toxicity of the proteins was exerted on the animals, in particular whether expression of these proteins caused effect to the proteostasis network.

3.4 Methods

3.4.1 *C. elegans* strains

Strain name	Genotype
N2 (Bristol)	Wild type
PVH69	*pccEx007[myo3::WT hβ2m::GFP::unc-54 3'UTR + myo2::RFP]*
PVH177	*pccEx009[myo-3p::WT hβ2m::unc-54 3'UTR + myo-2p::RFP]*
PVH178	*pccEx010[myo-3p::D76N β2m::unc-54 3'UTR + myo-2p::RFP]*
PVH179	*pccEx011[myo-3p::ΔN6 β2m::unc-54 3'UTR + myo-2p::RFP]*
PVH182	*pccEx024[myo-2p*::RFP]

Table 3.1 *C. elegans* strains used in Chapter 3 and their genotypes

3.4.2 Generation of a β2m-expressing transgenic vector

The expression vector pPD95_75 (Fire lab, Addgene) was digested with AgeI and EcoRI, blunt-ended and ligated to generate an expression vector without the GFP cDNA. The *myo-3p* body-wall muscle promoter was ligated into the pPD95_75 vector using HindII and SalI sites. Ligations were transformed into DH5α cells and analysed through colony restriction digestion using HindII and SalI. Successful colonies were sent for sequencing.

The signal sequence for human WT ß2m was generated by oligonucleotide annealing of SalI-signalpeptideB2m-for (Table 3.2) and BamHI-signalpeptideB2m-rev (Table 3.2). Oligos were mixed in a 1:1 ratio in 10 µL, then placed at 94ºC and allowed to cool until they reached less than 30ºC. Serial dilutions of the oligos were made (1:5, 1:10, 1:50, 1:100). 5 µL of the undiluted oligos and the serial dilutions were ligated into the successfully sequenced myo-3p-pPD95_75 vector. Ligations were transformed into DH5α cells. Colony restriction digestion was performed using BamHI and SalI restriction enzymes and analysed for a 100 bp band, successful constructs were sent for sequencing using the AgeI-ß2m-rev primer.

Finally, Human WT, D76N and ΔN6 ß2m cDNA (Radford lab) were PCR amplified using BamHI-B2m-for (Table 3.2) and MscI-B2m-rev (Table 3.2) to contain BamHI and MscI restriction sites and ligated into the myo-3p-ss-pPD95_75 vector. Ligations were transformed into DH5α cells. Colony restriction digestion was performed using BamHI

and MscI restriction enzymes and successful colonies containing a 300 bp band were analysed for sequencing using the MscI-B2m-rev primer.

3.4.3 Single nematode PCR

5 µL of nematode lysis buffer (100 µg/mL proteinase K, 50mM KCl, 10 mM Tris pH8.3, 2.5 mM $MgCl_2$, 0.45% (v/v) NP-40, 0.45% (v/v) Tween-20, 0.01% (w/v) gelatin) was added to the bottom of a PCR tube. Between 5-10 nematodes were picked directly into the tube with lysis buffer. Nematodes were frozen at -80°C. Nematodes were lysed and genomic DNA released by heating the tube to 65°C for 60 minutes, then proteinase K was inactivated by heating to 95°C for 15 minutes.

Standard PCR procedure was performed on the resultant DNA, where the following reagents were added to a PCR tube: 5 µL 10X Taq buffer; 1.25 µL BamHI-β_2m forward primer (Table 3.2); 1.25 µL MscI-β_2m reverse primer (Table 3.2); 1 µL dNTPs; 0.5 µL Taq polymerase; 0.5 µL Template DNA; 40 µL dH_20. The reaction was run on a thermocycler at 95°C for 5 minutes. Then 35 cycles of amplification at 95°C for 30 seconds, 58°C for 30 seconds and 72°C for 30 seconds was performed. The reaction was then run at 72°C for 5 minutes and kept at 4°C until further use. The resultant amplified DNA was run on an 1% (w/v) agarose gel and analysed for successful 300bp DNA bands.

Gene	Sequence
BamHI-B2m-for	AAAGGATCCATTCAAAGAACTCCAAAAATTC
MscI-B2m-rev	AAATGGCCATTACATGTCTCGATCCCACTTA
SalI-signalpeptide B2m-for	TCGACAAAAATGTCTCGCTCCGTGGCCTTAGCTGTGGCCTTA GCTGTGCTCGCGCTACTCTCTCTTTCTGGCCTGGAGGCTG
BamHI-signalpeptide B2m-rev	GATCCAGCCTCCAGGCCAGAAAGAGAGAGTAGCGCG AGCACAGCTAAGGCCACGGAGCGAGACATTTTTG

Table 3.2 Primer sequences used in Chapter 3

3.4.4 Soluble/insoluble protein fractionation

Animals were aged to day 1 or day 8 adults using FUdR plates (Chapter 2.1.4). Nematodes were collected using M9 buffer, and resuspended in lysis buffer (20 mM Tris, pH 7.5, 10

mM β-mercaptoethanol, 0.5% (v/v) Triton X-100, complete protease inhibitor (Roche)). Extracts were shock frozen in liquid nitrogen, and the frozen nematode pellet was ground using a motorized pestle, then lysed on ice in the presence of 0.0025 U/mL benzonase (Sigma). Lysates were centrifuged at 1000 rpm for 1 min in a tabletop centrifuge and the supernatant was extracted. 2% (v/v) N-Lauroylsarcosine was added to the supernatant and was ultracentrifuged at 100,000 *g* for 1 hour at 4°C. The supernatant was removed, and the resulting pellet was resuspended in the same volume of dH_2O as the supernatant.

3.4.5 Silver-Stain

Nematode extracts were run on an 4-20% (w/v) SDS-PAGE gel (BioRad). The gel was fixed in solution A (50% (v/v) ethanol, 10% (v/v) acetic acid) for 30 minutes, then incubated in solution B (5% (v/v) ethanol, 1% (v/v) acetic acid) for 15 minutes on a gentle rocker. The gel was washed in dH_2O three times for 5 minutes, and then incubated in solution D (0.02 g sodium thiosulphate in 100 mL dH_2O) for 2 minutes while gently rocking. The gel was washed again in dH_2O three times for 30 seconds, then incubated in solution E (0.2 g silver nitrate, 75 µL formaldehyde in 100 mL dH_2O) for 20 minutes. After three washes in dH_2O for 20 seconds, the gel was developed in solution F (6 g sodium carbonate, 50 µL formaldehyde, 0.2 mL solution C in 100 mL dH_2O) until protein bands could be visualised and the reaction was stopped using solution G (5% (v/v) acetic acid). The gel was then stored in dH_2O and imaged.

3.4.6 Western blot

Nematodes were collected and lysed on ice using a motorised pestle in lysis buffer (150mM NaCl, 50 mM Tris pH 7.4, 1 mM EDTA, 0.1% (v/v) NP-40). Extracts were centrifuged at 13,000 rpm for 1 minute to pellet the carcasses and the supernatant collected. The protein extract was run on a 10% (w/v) Tris-Tricine gel and proteins were electro-transferred to 0.22 µM nitrocellulose membranes. The blots were blocked using 5% (w/v) milk overnight, washed four times in PBS/Tween (0.1%) for 5 minutes, then probed with primary anti-human $ß_2m$ rabbit polyclonal antibody (Dako) at a 1:1000 (v/v) dilution in PBS/Tween (0.1%) and 1% (v/v) milk for 2 hours. Blots were washed then probed with 1:10000 (v/v) dilution HRP-conjugated goat anti-rabbit secondary antibody for 1 hour. Blots were developed using ECL (Fisher) and images were exposed onto film.

Methods for the following experiments can be found in the Methods chapter (Chapter 2):

C. elegans maintenance	Chapter 2.1
Developmental assay	Chapter 2.2.1
Fecundity assay	Chapter 2.2.2
Lifespan	Chapter 2.2.3
Paralysis assay	Chapter 2.2.4
Thrashing assay	Chapter 2.2.5
Thermotolerance	Chapter 2.2.6
ER stress	Chapter 2.2.7
Immunostaining	Chapter 2.3.1
X-34 staining	Chapter 2.3.2
RT-qPCR	Chapter 2.4

3.5 Results

3.5.1 Generation of a β2-microglobulin-expressing *C. elegans* strain

To study the aggregation of β2m and the effects of its proteotoxicity *in vivo*, three new strains of *C. elegans* expressing different variants of β2m were generated, including wild type human β2m, the single point familial mutation D76N and the N-terminal 6aa truncated variant ΔN6. For this, the *C. elegans* expression vector pPD95_75 (Addgene, Fire Lab) which contains a GFP sequence positioned upstream of the *C. elegans unc-54* 3'UTR was used. The *C. elegans* body wall muscle promoter sequence *myo-3p* followed by the β2m variant sequences was cloned upstream of the GFP sequence in order to direct expression of the C-terminally tagged β2m proteins to the muscle of the animal (Figure 3.2a). Expression of β2m variants in the body wall muscle allows the measure of toxicity based on locomotion phenotypes. In addition, the signal peptide sequence of the protein was included in the transgene to secrete the protein, in order to replicate the natural environment of aggregation in extracellular tissue.

The *myo-3p*::*β2m*::GFP transgene was microinjected into wild type (N2) *C. elegans* animals, along with a *myo-2p*::RFP co-injection marker that causes the expression of RFP in the pharynx of animals. Extra-chromosomal lines were established; however, only the co-injection marker was observed and no GFP fluorescence could be observed in the body wall muscle of the animals (Figure 3.2b). To investigate whether the resulting transgenic nematodes did indeed contain the *β2m*::GFP transgene, mRNA levels of β2m and GFP were measured using quantitative real time PCR (qRT-PCR). An 80-fold upregulation in β2m expression and a 40-fold upregulation in GFP expression compared with the wild type (N2) control strain was observed in the transgenic *myo-3*::*β2m*::GFP strain (Figure 3.2c), confirming the presence of the transgene in the animals.

To validate whether the transgene contained the correct sequence for either the *myo-3p* body wall muscle promoter or the GFP fluorescent tag, a new vector was created whereby the human β2m and signal sequence was removed. This generated a transgene containing the GFP sequence under the control of the *myo-3p* promoter (*myo-3p*::GFP) (Figure 3.2d). Microinjection of this transgene vector in *C. elegans* resulted in the expression of GFP in the body wall muscle of the animal and was clearly observed when imaged (Figure 3.2e). It was postulated that as protein folding is essential for the chromophore formation and fluorescence of GFP, the absence of GFP fluorescence observed in β2m fused to C-terminal

GFP could be due to improper folding of the β2m-GFP fusion protein. Furthermore, the large GFP tag (~27 kDa) on the relatively small protein β2m (~11 kDa) could affect the folding and aggregation potential of β2m in this *in vivo* environment.

As GFP could not be visualised when a β2m::GFP fusion protein transgene was expressed under the control of the body wall muscle promoter *myo-3p* (Figure 3.2b), the β2m expression construct was redesigned. A new construct without the GFP tag was engineered, which contained the human wild type β2m signal peptide followed by a variant of β2m (WT, D76N or ΔN6) under the control of the body wall muscle specific promoter *myo-3p* (Figure 3.3). Firstly, the GFP transgene was removed from the vector pPD95_75 using the AgeI and EcoRI restriction sites. Using the HindIII and SalI restriction sites the *myo-3p* body wall muscle promoter was then cloned into the vector. The resultant vector was then subjected to SalI and BamHI treatment and the human wild type β2m signal peptide sequence was ligated into the vector. Finally, the BamHI and MscI restriction sites were utilised to clone in one of three β2m variants (Figure 3.3a and 3.3b). Three different variants of β2m (WT, D76N and ΔN6) were chosen to be expressed in *C. elegans* in order to further understand the relationship of protein aggregation and toxicity. The three β2m transgenes (Figure 3.3b) were microinjected into wild type *C. elegans*, and stable extrachromosomal lines were established for each expressed transgene using the *myo-2p*::RFP co-injection marker.

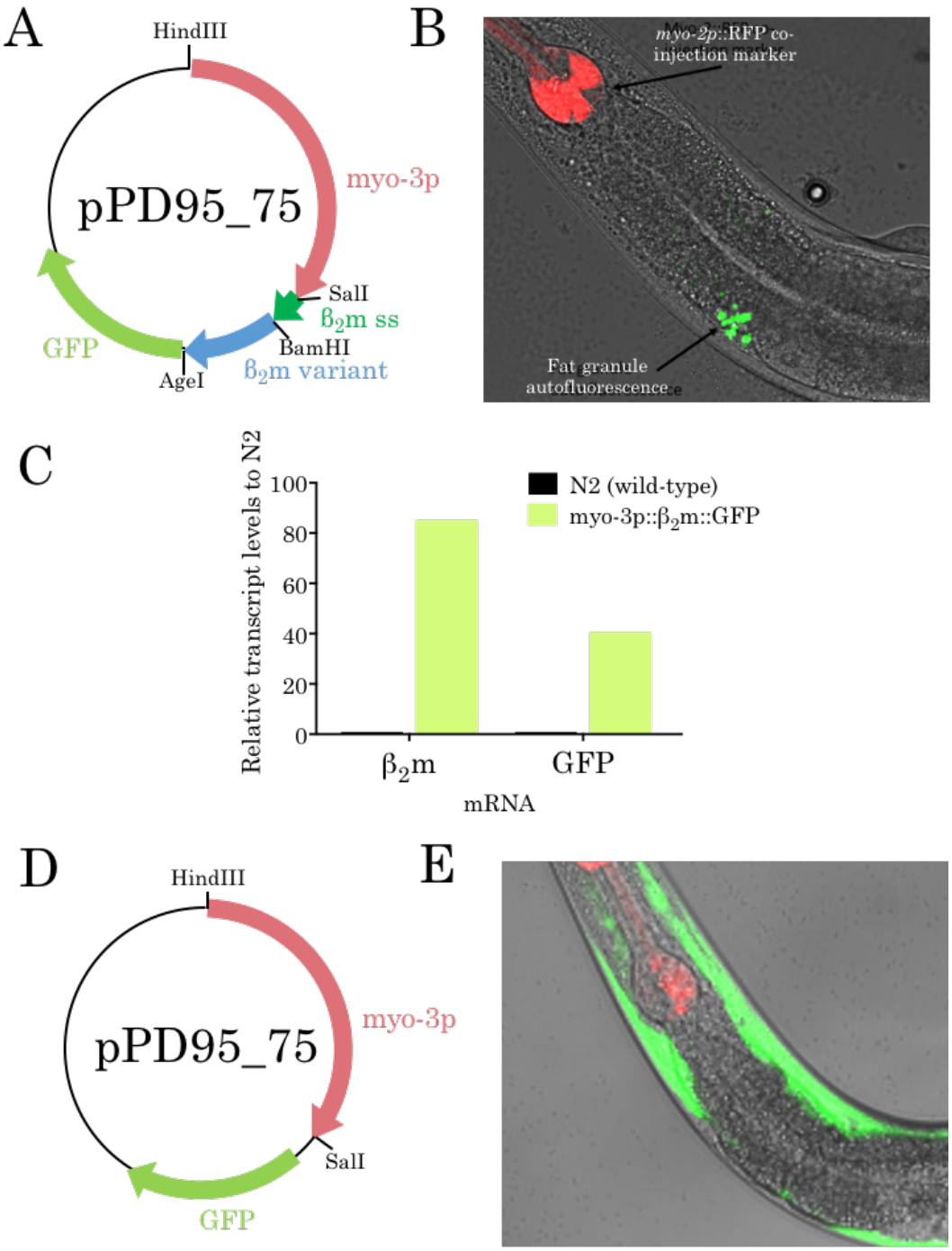

Figure 3.2 Generation of a transgene expressing β₂-microglobulin tagged with Green Fluorescent Protein (GFP).
A) Schematic of the transgene *myo-3p*::β2m::GFP, designed to express human wild type β2m tagged with GFP under the control of the body-wall muscle promoter *myo-3p*. β2m ss = β2m signal sequence B) Representative confocal image of *C. elegans* expressing the transgene *myo-3p*::β2m::GFP. Expression of the co-injection marker *myo-2p*::RFP is highlighted, as well as fluorescence in the intestine of the animal produced by the autofluorescence of fat granules. C) Transcript levels of β2m or GFP in the *myo-3p*::β2m*::GFP* strain compared with a wild type (N2) control. D) Schematic of the transgene of *myo-3p*::GFP, where the fluorescent protein GFP in under control of the body wall muscle promoter *myo-3p*. E) Representative confocal image of *C. elegans* expressing the transgene *myo-3p*::GFP. Images were collected using the LSM880 Confocal Zeiss Microscope.

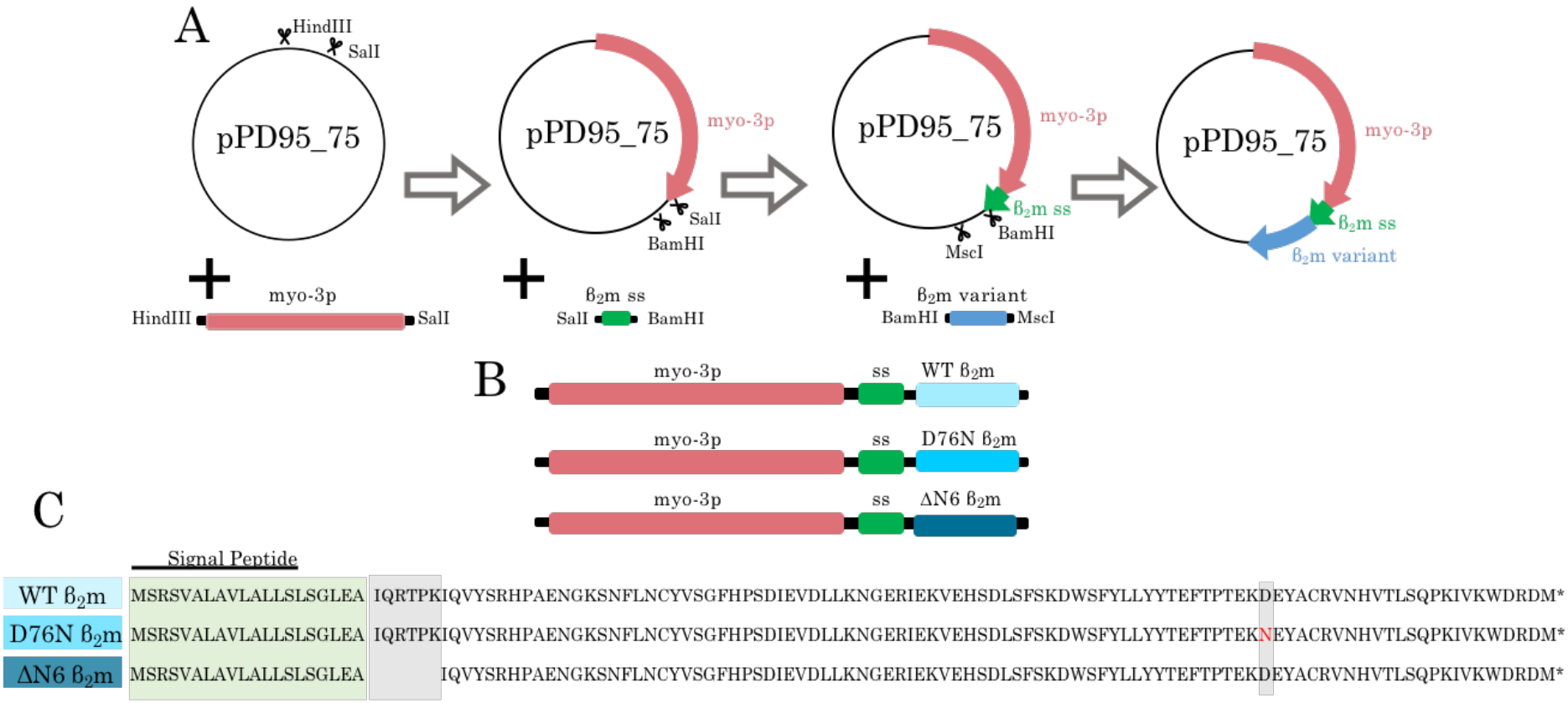

Figure 3.3 Generation of plasmids for the expression of β2m in the body wall muscle of *C. elegans*.
A) Cloning strategy for the generation of a plasmid encoding variants of ß2m under the control of the body wall muscle promoter *myo-3p*. The promoter *myo-3p* was cloned into the HindIII and SalI restriction sites of the pPD95_75 *C. elegans* vector. The resulting constructs were digested with SalI and BamHI and the signal peptide of ß2m was cloned in. cDNA of the human WT ß2m, D76N ß2m or ΔN6 ß2m were then cloned into the BamHI and MscI sites to generate the WT ß2m, D76N ß2m and ΔN6 ß2m transgenes. B) WT ß2m, D76N ß2m and ΔN6 ß2m transgenes generated for the expression of ß2m in *C. elegans*. C) WT ß2m, D76N ß2m and ΔN6 ß2m with the human β2m signal peptide amino acid sequences. The signal peptide amino acid sequence (1-20) is highlighted in green. Any differences between the amino acid sequences are highlighted in grey. Mutations between the amino acid sequences are in red.

3.5.2 Genotypic characterisation of β2m-expressing *C. elegans* strains

The transgenic β2m strains were first confirmed for the expression of the β2m transgene through quantitative RT-PCR and single nematode PCR methods (Figure 3.4). Quantitative RT-PCR against the β2m gene revealed an upregulation of ~13,000-fold, ~4,000-fold and ~2,000-fold in the WT β2m, D76N β2m and ΔN6 β2m strains respectively, compared with the N2 control that does not express the transgene (Figure 3.4a). A strain expressing the *myo-2p*::RFP co-injection marker only (marker control; MC) was generated as an additional control. As expected, an upregulation of the β2m transgene was not observed in marker control animals compared with wild type (N2) animals (Figure 3.4a). Next, single nematode PCR was performed on transgenic strains to further validate these results. Using primers (Table 3.2) for the full length β2m gene and signal peptide sequence, the expected ~360bp (WT β2m or D76N β2m) or ~340bp (ΔN6 β2m) product was observed in the corresponding strains (Figure 3.4b), but not in the control strains, N2 and MC (Figure 3.4b). Taken together, these results indicate that the β2m transgene is transcribed in the newly generated *C. elegans* strains expressing WT, D76N or ΔN6 β2m.

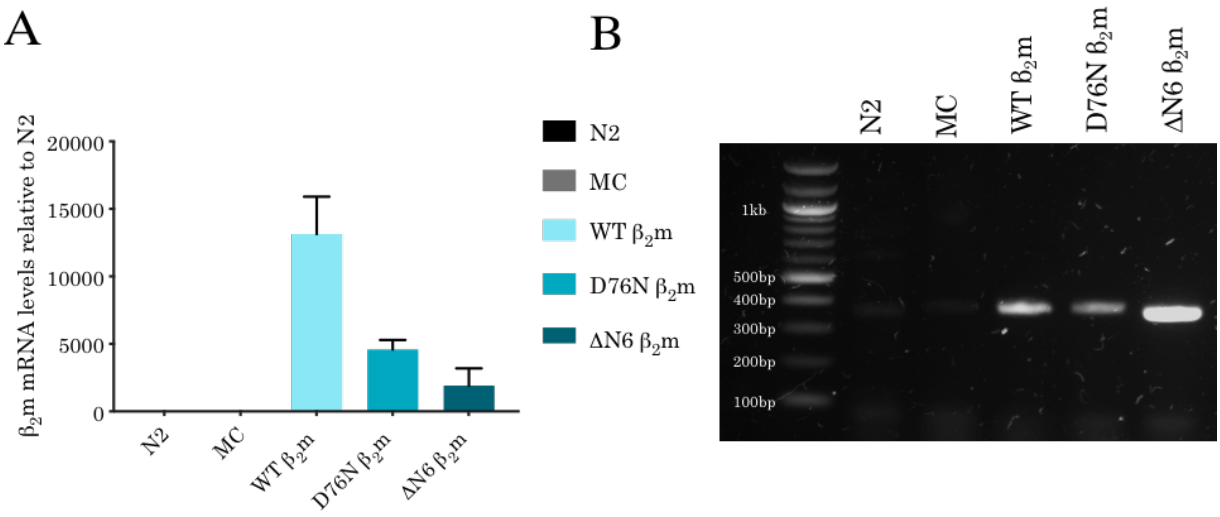

Figure 3.4 Confirming β2m gene expression in transgenic *C. elegans*
A) RT-qPCR of adult transgenic animals transfected with the marker control (MC) or vectors for the expression of WT β2m, D76N β2m or ΔN6 β2m compared with a wild type (N2) control. Data represent the mean of three independent experiments. Error bars = SEM. B) PCR confirmation of adult transgenic animals expressing WT β2m, D76N β2m or ΔN6 β2m compared with wild type (N2) and MC control nematodes expressing the *myo-2p*::mCherry co-injection marker only. Single nematode PCR was performed on each strain using primers encompassing the signal peptide and full-length sequence. The expected size of the PCR product was 360bp (WT β2m and D76N β2m) or 342bp (ΔN6 β2m).

3.5.3 Expression of β2m in *C. elegans* causes age-dependent protein aggregation

As expression of the WT β2m, D76N β2m or ΔN6 β2m transcripts was observed in the new transgenic lines, next protein expression was assessed. For this, nematode lysates from the corresponding strains were prepared and analysed by western blot methods using polyclonal anti-human β2m antibody (Dako). In the control N2 and marker control strains, β2m protein expression was not observed (Figure 3.5a). By contrast, β2m protein was detected in all three β2m variant-expressing strains (Figure 3.5a). The amount of β2m detected was considerably higher in the WT β2m lysates and D76N β2m than the ΔN6 β2m samples. This indicates that steady-state WT β2m and D76N β2m protein expression is higher than the ΔN6 variant and could suggest potential degradation of ΔN6 β2m protein (Figure 3.5a). Furthermore, recombinant protein samples of WT β2m, D76N β2m and ΔN6 β2m (gift from the Radford lab) which do not contain the signal sequence were used as a positive control alongside the nematode protein extracts (Figure 3.5a). Because the β2m variants of the recombinant protein samples and the nematode protein extracts are observed at the same molecular weight on the western blot (Figure 3.5a), this indicates that β2m detected in the lysates does not contain the signal sequence and suggests it is cleaved.

As β2m has been shown to aggregate and form toxic species over time *in vitro* (Karamanos et al., 2019; Sarell et al., 2013b) and *in vivo* (Diomede et al., 2012; Faravelli et al., 2019), the amount of β2m protein that is soluble or insoluble was assessed throughout aging in *C. elegans*. Nematode lysates of age-synchronised day 8 adults of wild type (N2), WT β2m and D76N β2m expressing animals were prepared and separated into insoluble and soluble fractions by ultra-centrifugation. β2m protein levels in each fraction were then assessed by western blot. β2m was detected in the soluble fraction of WT β2m animals, and a low amount of β2m protein was also present in the insoluble fraction (Figure 3.5b). A larger proportion of D76N β2m protein was found in the insoluble fraction of D76N expressing nematodes compared with WT β2m (Figure 3.5b and 3.5e). The presence of more D76N β2m protein in the insoluble fraction could be a reflection of increased protein aggregation of this variant *in vivo*. D76N can readily aggregate into oligomeric and fibrillar species *in vitro,* while WT β2m does not aggregate under physiological conditions *in vitro* (Mangione et al., 2013), and therefore the observation of a higher amount of aggregated β2m species are observed when D76N is expressed *in vivo* correlates with the protein's behaviour *in vitro*. Further experiments to detect the amount of β2m in soluble and insoluble fractions

in the ΔN6-expressing strain should also be performed in order to compare between strains.

Next, whether the expression of β_2m variants affected aggregation of endogenous proteins in *C. elegans* in an age-dependent manner was assessed. For this, soluble and insoluble fractions of day 1 and day 8 adults of each the β_2m-expressing strains and two controls (N2 and MC), were prepared and examined using SDS-PAGE. Silver staining was used to visualise the total amount of protein present in each sample. The density of protein in the insoluble and soluble fractions of each sample was analysed in ImageJ, and the proportion of insoluble protein was calculated by dividing the density of the insoluble sample by the combined density of the insoluble and soluble samples [density of insoluble]/[density of soluble + density of insoluble] to achieve the ratio of insoluble protein in the sample. At day 1 of adulthood, a lower proportion of total protein was found in the insoluble fraction of the lysate than the soluble fraction of all samples (Figure 3.5c and 3.5f). At day 8 of adulthood however, a larger proportion of protein was detected in the insoluble fraction of lysates prepared from D76N β_2m (0.64 ±0.13) and ΔN6 β_2m (0.60 ±0.08) expressing animals compared with N2 day 8 adults (Figure 3.5d and 3.5f). In contrast, lysates prepared from WT β_2m expressing animals showed a similar ratio of total protein present in the insoluble day 8 fractions compared with N2 day 8 adults (0.51 ±0.07 compared with 0.48 ±0.11). These results suggest that expression of the D76N β_2m and ΔN6 β_2m variants are causing widespread endogenous protein aggregation. Although expression of β_2m is higher in WT β_2m-expressing animals (Figures 3.4 and 3.5a), this protein remains soluble until old age (day 8 of adulthood) (Figure 3.5b) and leads to little aggregation of endogenous total protein *in vivo* during aging (Figure 3.5c and 3.d). This is consistent with *in vitro* observations demonstrating that D76N β_2m and ΔN6 β_2m are more highly amyloidogenic (Eichner et al., 2011; Mangione et al., 2013). The analysis of total protein content in the soluble and insoluble fractions clearly provides an insight into the possible effects of β_2m aggregation *in vivo* and during aging.

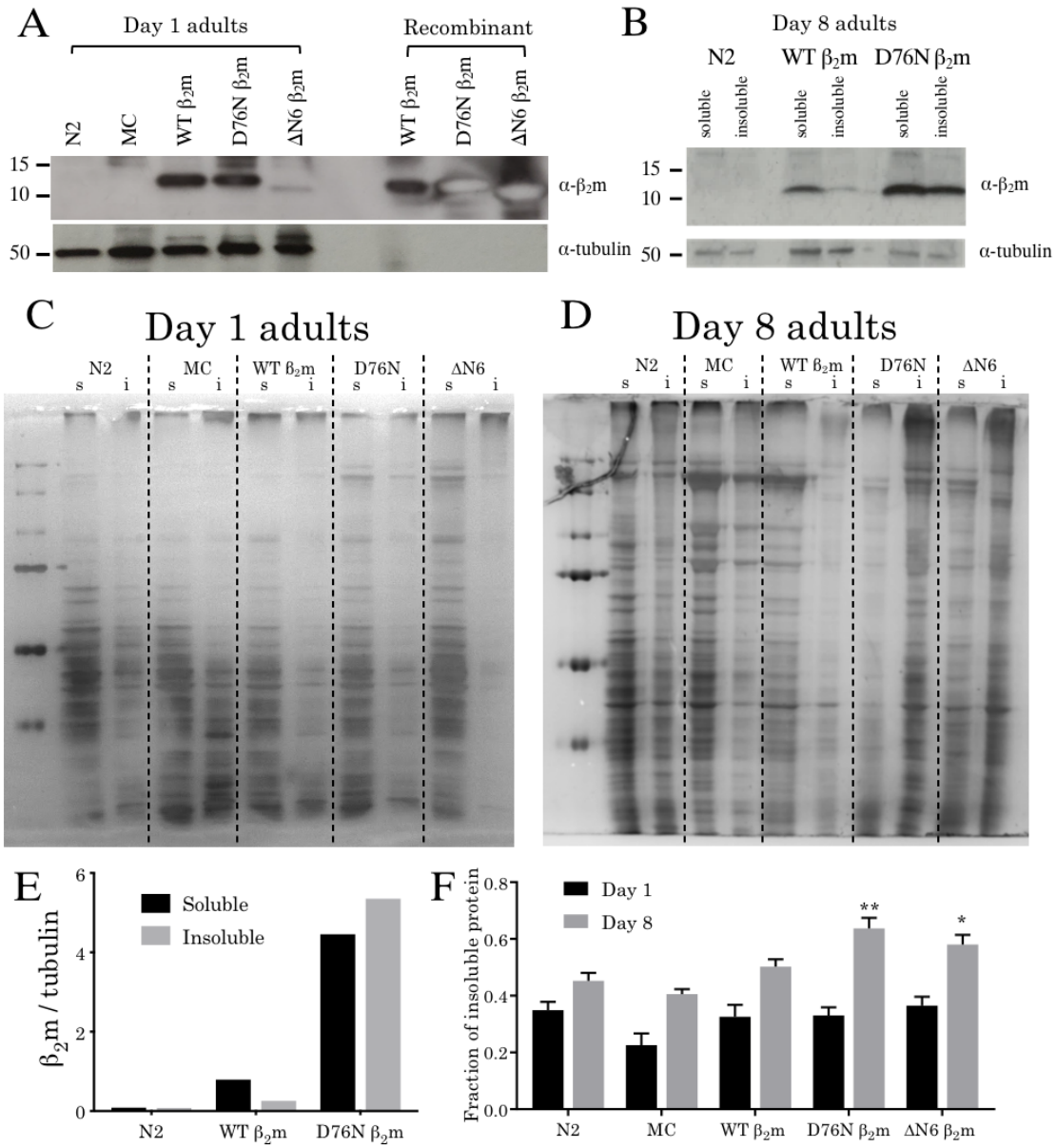

Figure 3.5 Expression of β2m causes age-dependent aggregation in *C. elegans*.
A) Western blot of day 1 adults wild type (N2), marker control (MC), WT ß2m, D76N ß2m and ΔN6 ß2m transgenic *C. elegans* strains alongside recombinant samples of WT ß2m, D76N ß2m and ΔN6 ß2m (Gift from Radford lab). Whole nematode extracts of day 1 adults were immunoblotted with polyclonal anti-human ß2m antibody (Dako) and anti-human tubulin antibody (Invitrogen). B) Western blot of the soluble and insoluble fractions of wildtype (N2), WT ß2m and D76N ß2m transgenic *C. elegans* strains. Nematode extracts of 8-day old adults were collected and 50 µg of protein was ultracentrifuged for 100,000 *g*. The soluble fraction (s) and insoluble fraction (i) were immunoblotted with a polyclonal anti-human ß2m antibody (Dako) and anti-human tubulin antibody (Invitrogen). C and D) Silver stain of the soluble and insoluble fractions of day 1 (C) and day 8 (D) adult nematodes. Samples were run as detailed in B) and stained using silver nitrate and imaged. E) Quantification of protein levels collected in B. Gels were analysed in ImageJ and data represents density of indicated bands normalised to the density of tubulin detected (n=1). F) Quantification of total protein levels in C and D. Density of lanes were analysed in ImageJ, and fraction of insoluble protein calculated using [density of insoluble]/[density of soluble + density of insoluble] (n=3). P-values represent significance compared with Day 8 N2 extracts. p*<0.05; p**<0.001

3.5.4 Localisation of β_2m protein could not be determined in β_2m-expressing transgenic animals

As β_2m protein was detected in the transgenic β_2m-expressing strains (Figure 3.5a), the location of the protein throughout the animal was next questioned. To achieve this, wild type (N2), WT β_2m- and D76N β_2m- expressing animals were fixed and immunostained using an antibody against human β_2m (Dako). However, the antibody appeared to bind non-specifically, as a fluorescence signal was observed in wild type (N2) animals (Figure 3.6a). This inconclusive staining is in contrast with the previous WT β_2m- and ΔN6 β_2m-expressing models that have been produced; where staining was shown in the vulva and anal sphincter in WT β_2m-, P32G β_2m- and ΔN6 β_2m-expressing animals, but consistent with the previous D76N models where staining could not be observed (Diomede et al., 2012; Faravelli et al., 2019).

Previous transgenic *C. elegans* models expressing amyloidogenic proteins have used amyloid binding dyes to both confirm the presence of amyloid fibres and visualise the localisation of the deposits in the animal (Link et al., 2001; Olzscha et al., 2011). Here, the amyloid binding dye X-34 (Sigma) was used to locate amyloid deposits in the β_2m-expressing strains. Due to the short excitation and emission wavelength of this dye, a lot of autofluorescence was observed throughout wild type (N2) animals, in particular in the intestine (Figure 3.6b). Transgenic *C. elegans* expressing WT β_2m displayed a similar pattern of fluorescence to wild type (N2) animals, suggesting there is little amyloid deposition in the animal. However, in transgenic animals expressing D76N β_2m, the presence of foci was observed surrounding the pharyngeal bulb. This could represent the deposition of amyloid in the muscle tissue; however, as some foci were also observed in wild type (N2) animals (Figure 3.6b) this is not conclusive. As inconclusive immunostaining and X-34 images were obtained for both WT β_2m- and D76N β_2m-expressing animals, staining and imaging of marker control (MC) or ΔN6 β_2m-expressing animals was not further explored.

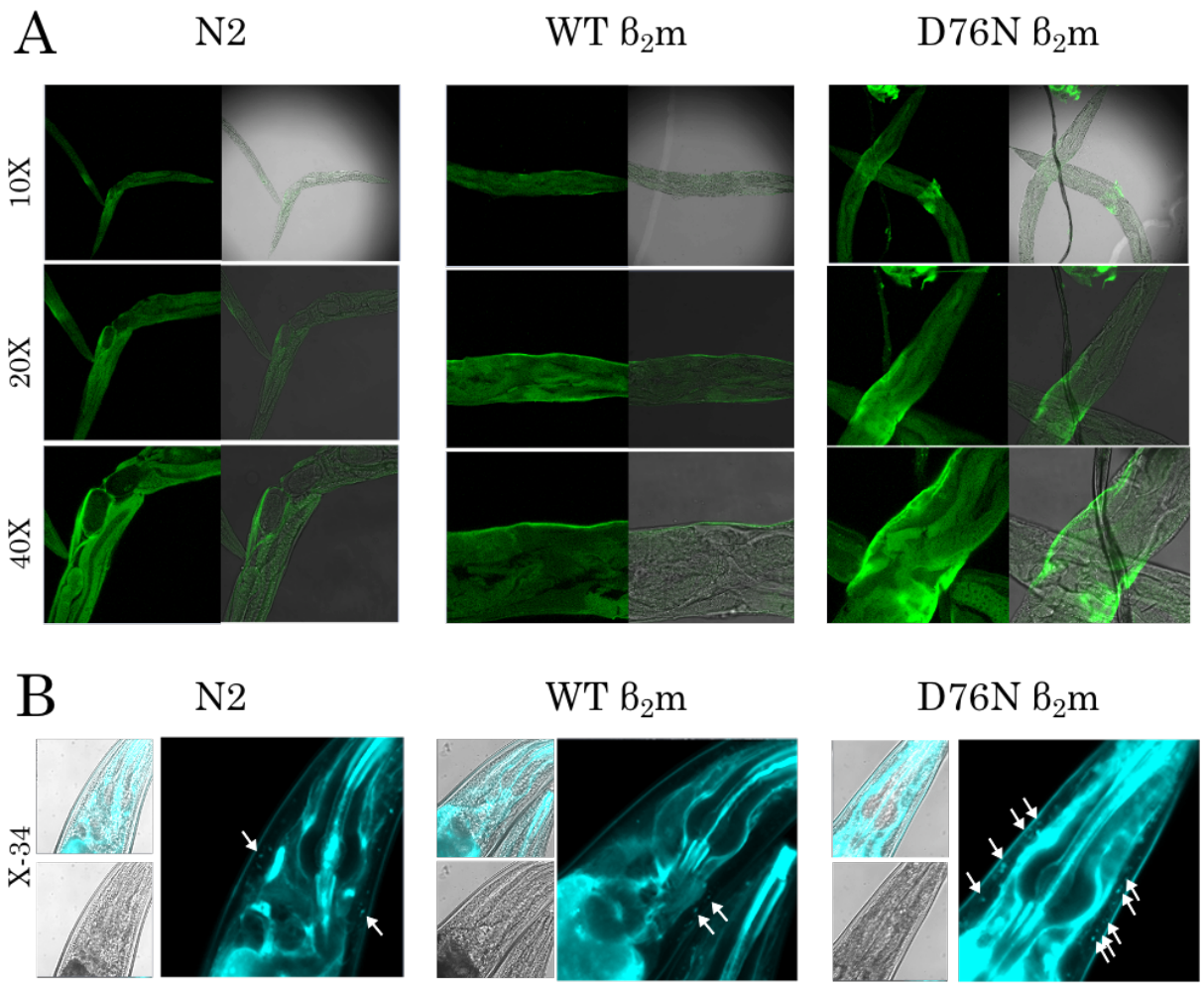

Figure 3.6 Localisation of β2-microglobulin in β2-microglobulin expressing transgenic strains.
A) Representative confocal microscopy images of day 1 adult wild type (N2), WT β2m- and D76N β2m-expressing transgenic strains immunostained with anti-β2m antibody (Dako) and anti-rabbit Alexa-647. Images shown are for 10X, 20X and 40X, and depict immunofluorescence and overlay of bright field and immunofluorescence. B) Representative images of X-34 staining of day 4 adult wild type (N2), WT β2m- and D76N β2m-expressing transgenic animals. Immunofluorescence images, bright field images and overlay are depicted. White arrows indicate foci. All images were obtained using a Zeiss LSM880 confocal microscope.

3.5.5 Expression of D76N β2m and ΔN6 β2m variants but not WT β2m in *C. elegans* causes a developmental delay and reduces lifespan

Expression of D76N and ΔN6 β2m in *C. elegans* correlated with an increase in age-dependent aggregation *in vivo* (Figure 3.4), reflecting the increased aggregation propensity of these proteins *in vitro* (Esposito et al., 2000; Mangione et al., 2013). Therefore, it was questioned whether this increased protein aggregation also correlated with increased toxicity. For example, fibrillar ß2m has been shown previously to be proteotoxic to human SH-SHY5Y cells when added extracellularly (Jakhria et al., 2014; Xue et al., 2009). To investigate whether expression of ß2m in *C. elegans* causes organismal toxicity, the development and lifespan of the *C. elegans* models was first explored.

To assess whether expression of ß2m variants caused a developmental delay, the developmental stage of animals was recorded 65 hours after eggs were laid. At this time point the majority of wild type (N2) animals were adults and only 6.8 ±2.0% of animals were at the L3-L4 stage of development (Figure 3.7a). The marker control (MC) strain did not significantly affect the development of the animals compared with wild type (N2), where 8.4 ±2.3% of animals also remained in the L3-L4 stage after 65 hours. Remarkably, the expression of either of the highly amyloidogenic proteins D76N ß2m or ΔN6 ß2m resulted in a delay in the percentage of animals reaching adulthood, whereby 22.7 ±2.0% and 32.3 ±4.6% of animals respectively did not reach adulthood 65 hours after hatching (Figure 3.7a) compared with just 6.8 ±2.0% of wild type (N2) animals that were not adults after 65 hours. Interestingly, expression of WT ß2m did not significantly affect the development of the animals compared with the wild type (N2) control. Thus, these observations indicate that expression of D76N ß2m or ΔN6 ß2m impair the development of *C. elegans*, while expression of the less amyloidogenic variant WT ß2m did not affect this phenotype in the animals.

As the development of animals expressing either D76N ß2m or ΔN6 ß2m was delayed, it was hypothesised that the fecundity of the animals could also be affected. To test this, the number of eggs laid each day was analysed for 4 days after the appearance of the vulva. In the wild type (N2) and marker control strains, on average ~200 eggs and ~190 eggs respectively had been laid after 96 hours (Figure 3.7b). By contrast, animals which expressed either WT ß2m, D76N ß2m or ΔN6 ß2m had laid a significantly fewer of eggs (~140 eggs after 96 hours) than the wild type (N2) control (Figure 3.7b). These results

indicate that the expression of WT ß$_2$m, D76N ß$_2$m or ΔN6 ß$_2$m causes a decrease in fecundity in *C. elegans*. It is however not clear whether the reduced fecundity is the result of a reduced brood size or whether this was due to a deficient vulval muscle, resulting in reduced egg-laying.

Developmental and egg laying deficiencies provide a picture of the early-stage consequences of expression of ß$_2$m variants. Earlier in this chapter, it was demonstrated that protein aggregation was present in aged D76N β$_2$m- and ΔN6 β$_2$m-expressing animals (Figure 3.5). Whether D76N β$_2$m and ΔN6 β$_2$m variants also affected the survival and long-term lifespan of the animals was also investigated. Lifespan experiments were therefore conducted on β$_2$m-expressing transgenic strains and control animals (N2 and MC). Wild type (N2) nematodes lived for a maximum of approximately 37 days and had a mean lifespan of 18.70 ±0.58 days (Figure 3.7c and 3.7d). This was similar to the strains expressing either the marker control (MC) or WT ß$_2$m where the mean lifespan was 17.55 ±0.53 and 17.76 ±0.70 respectively, and a maximum lifespan of 33 days was observed in both strains. A significant decrease in mean lifespan was observed in animals expressing the ß$_2$m variants D76N or ΔN6 compared with the wild type (N2) strain, where the mean lifespan was 13.81 ±0.59 and 13.87 ±0.80 respectively (Figure 3.7c and 3.7d). These results indicate that the expression of D76N ß$_2$m or ΔN6 ß$_2$m reduces lifespan, while the expression of WT ß$_2$m does not affect the survival of animals.

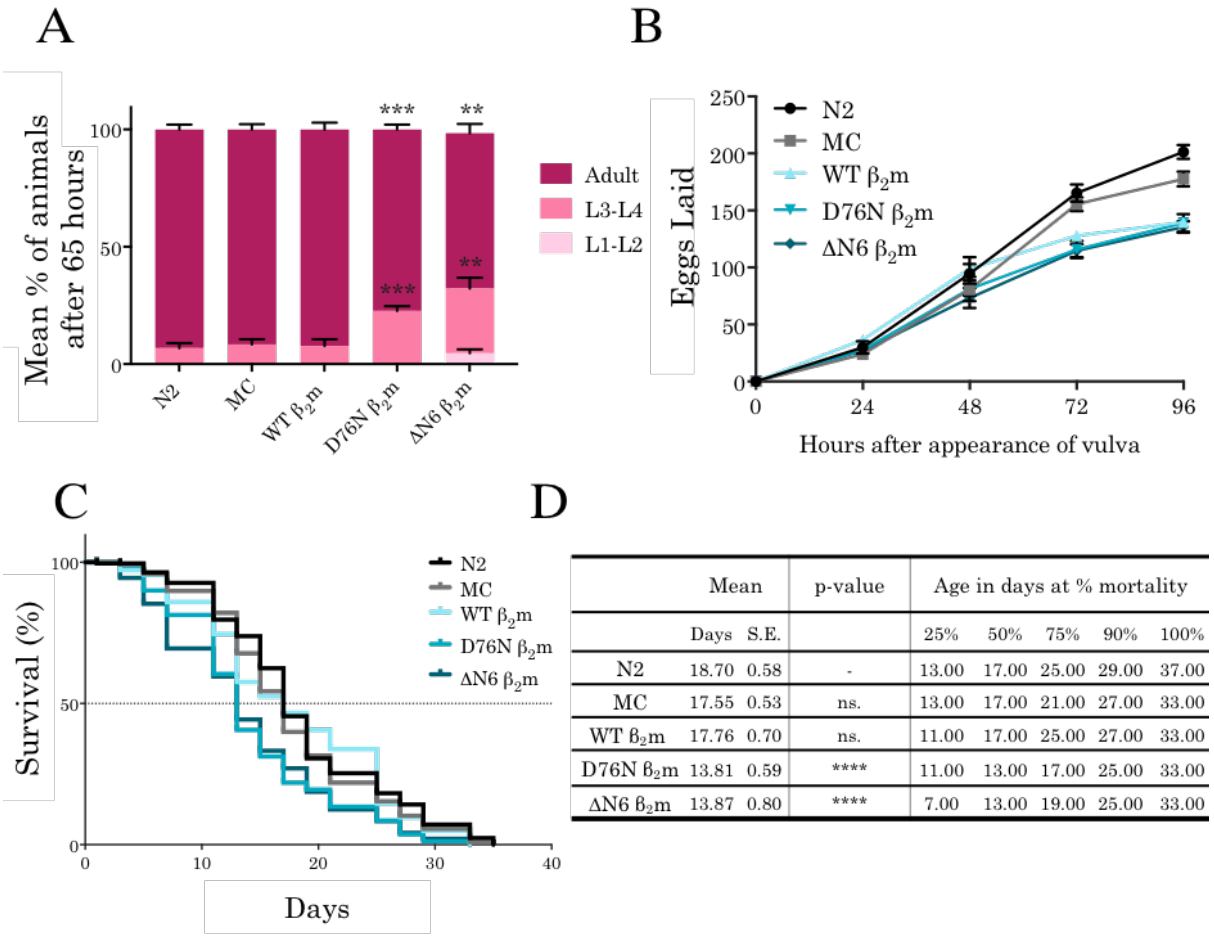

	Mean		p-value	Age in days at % mortality				
	Days	S.E.		25%	50%	75%	90%	100%
N2	18.70	0.58	-	13.00	17.00	25.00	29.00	37.00
MC	17.55	0.53	ns.	13.00	17.00	21.00	27.00	33.00
WT β2m	17.76	0.70	ns.	11.00	17.00	25.00	27.00	33.00
D76N β2m	13.81	0.59	****	11.00	13.00	17.00	25.00	33.00
ΔN6 β2m	13.87	0.80	****	7.00	13.00	19.00	25.00	33.00

Figure 3.7 Expression of β2m variants leads to a developmental delay and reduces lifespan.
A) Development of WT β2m, D76N β2m and ΔN6 β2m-expressing transgenic nematodes compared with wild type (N2) and marker control (MC) nematodes 65 hours after eggs have been laid. Data are expressed as the percentage of total nematodes on the plate at each developmental stage. Three independent experiments were performed (n=100 animals per experiment). **p<0.005 ***p<0.001 B) Number of eggs laid by wild type (N2), marker control (MC), WT β2m, D76N β2m and ΔN6 β2m transgenic *C. elegans* 24, 48, 72 and 96 hours after the appearance of the vulva. Three independent experiments were performed (n=30 animals per experiment).C) Survival curves of wild type (N2), marker control (MC), WT β2m, D76N β2m and ΔN6 β2m transgenic *C. elegans*. Adults were placed on seeded NGM plates (Chapter 2.1.1) from L4 stage, cultured at 20°C and transferred every other day. Survival rate was scored and expressed as percentage survival. Plots are representative of three independent experiments (n=80). D) Mean lifespan of wildtype (N2), marker control (MC), WT β2m, D76N β2m and ΔN6 β2m transgenic *C. elegans*. Data from C) were analysed using OASIS 2 (Han et al., 2016) and mean lifespan, standard error, p-value and age in days at 25%, 50%, 75%, 90% and 100% mortality is displayed. P-value represents significance compared with the wild type (N2) control strain, ns. = not significant, **** p<0.0001

3.5.6 Expression of β2m in *C. elegans* in the body wall muscle reduces motility

Expression of D76N β2m and ΔN6 β2m in the body wall muscle delays development and reduces fecundity and lifespan, suggesting that the expression of these proteins are toxic at an organismal level. As β2m was expressed in the body wall muscle of the animals, an obvious phenotype of toxic damage from the expression of WT β2m, D76N β2m or ΔN6 β2m would be in the movement of the animals. To address this, the paralysis of transgenic animals was monitored for 8 days. Wild type (N2) animals displayed an age-dependent increase in paralysis, whereby ~10% of animals were paralysed at day 8 of adulthood (Figure 3.8a). In animals expressing either the marker control (MC) or WT β2m, ~15% of animals were observed to be paralysed after 8 days, which was not significantly different to the wild type (N2) control (Figure 3.8a). In nematodes expressing D76N β2m, 30% of animals were paralysed at day 8 of adulthood, a significant increase of 20% compared with wild type (N2) animals (Figure 3.8a). Interestingly, animals that expressed the 6 amino acid truncated variant of human β2m, ΔN6, started to paralyse at day 2 of adulthood, and displayed a significantly higher percentage of paralysed animals (~30%) at day 8 of adulthood compared with the wild type (N2) control (Figure 3.8a). These observations suggest that expression of D76N and ΔN6 are proteotoxic to muscle cells, leading to muscle cell collapse and increased paralysis in the animals.

From these observations it can be postulated that expression of either D76N β2m or ΔN6 β2m reduces locomotion in an age-dependent manner. To explore this further, whether expression of these proteins also impairs the frequency of body bends throughout aging was assessed. While the percentage of paralysed animals can provide information on the total muscle cell collapse occurring in a population, the frequency of body bends will disseminate more subtle changes and damage to muscle cells. The number of body bends per second (BBPS) an animal could perform in M9 media was analysed at days 1 and 8 of adulthood to distinguish age-related effects of expression of the proteins. Wild type (N2) and marker control (MC) animals displayed an average of 1.12±0.05 and 1.07±0.07 BBPS in day 1 adults, and this decreased to 0.90 ±0.05 BBPS and 0.85 ±0.06 BBPS respectively in day 8 adults. Animals which expressed either WT β2m or D76N β2m in the body wall muscle performed on average 1.27 ±0.04 and 1.07 ±0.08 BBPS at day 1 of adulthood, which was not significantly different to wild type (N2) animals. In contrast at day 8 of adulthood WT β2m or D76N β2m animals displayed a significantly decreased thrashing rate of 0.65 ±0.04 BBPS and 0.56 ±0.08 BBPS respectively (Figure 3.8b). Expression of ΔN6 β2m in *C.*

elegans displayed a slightly decreased number of BBPS (0.93 ±0.10) compared with wild type animals (N2) at day 1 of adulthood, although this was not significant. At day 8 of adulthood, however, animals expressing ΔN6 β2m displayed 0.18 ±0.04 BBPS, a significant a decrease compared with the wild type (N2) control (Figure 3.8b). These results indicate that the expression of either ΔN6 β2m and to a lesser extent WT β2m and D76N β2m in the body wall muscle of *C. elegans* leads to muscle damage and suggests an association with the aggregation of the proteins to the proteotoxic effects observed. This is consistent with previous research, whereby expression of either WT β2m, D76N β2m or ΔN6 β2m in *C. elegans* was associated with a decrease in the thrashing rate of the animals (Diomede et al., 2012; Faravelli et al., 2019). Taken together the results displayed in Figures 3.8a and 3.8b indicate that expression of D76N β2m and ΔN6 β2m cause strong proteotoxicity to muscle cells. Expression of WT β2m is associated with only a mild thrashing phenotype, suggesting a milder proteotoxic effect of this protein.

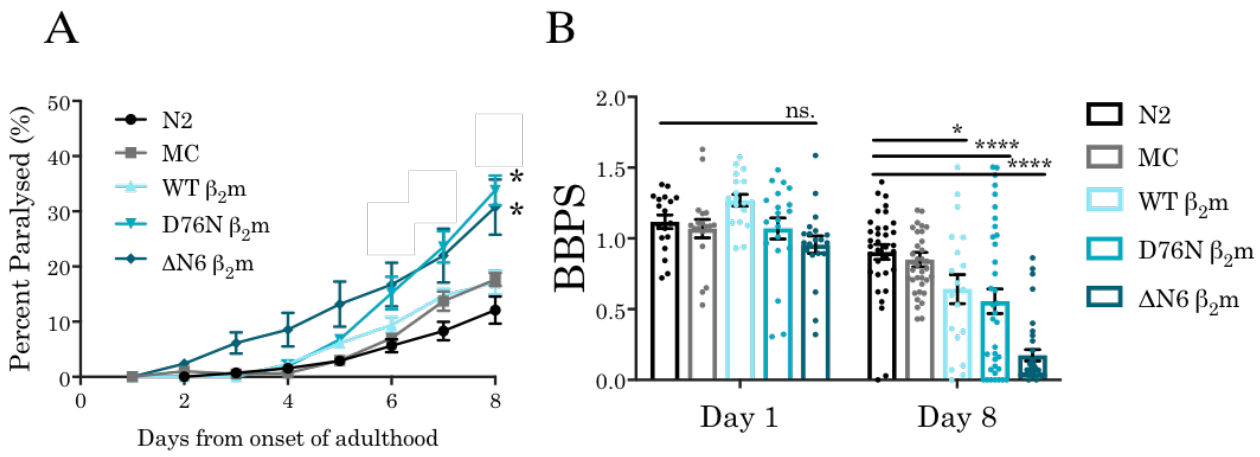

Figure 3.8 Locomotion phenotypes of β2m-expressing *C. elegans* strains.
A) Paralysis assays of *C. elegans* expressing either WT ß2m, D76N ß2m, ΔN6 ß2m or the marker control (MC) compared with wild type (N2) animals at 20°C. Paralysis data represents the SEM of 3 independent biological repeats (n=100 animals). Statistical significance was determined using the Wilcoxon matched-paired signed rank test. *p<0.05 B) Thrashing rates of wild type (N2), marker control (MC), WT ß2m, D76N ß2m and ΔN6 ß2m transgenic *C. elegans* at day 1 and day 8 of adulthood. Data represent the number of full body bends per second (BBPS) in M9. Three independent experiments were performed (n=20 animals). Data are given as a mean of the number of body bends per second ±SEM. A student's t test was used to assess significance: **p<0.01, ***p<0.005

3.5.7 *C. elegans* expressing variants of β2m have reduced stress survival

The proteostasis network (PN) has several stress response pathways to cope with the increased burden of misfolded and aggregated proteins throughout aging and acute environmental stresses (Åkerfelt et al., 2010; Hipp et al., 2019; Tyedmers et al., 2010). Two of these stress response pathways are the heat shock response (HSR) and the unfolded protein response of the ER (UPR^{ER}). Because expression of D76N β2m or ΔN6 β2m led to proteotoxicity compared with wild type (N2) and WT β2m-expressing animals, whether the impairment of these stress responses could be responsible at least in part for this effect was next explored.

The ability of animals to cope with heat stress was first investigated. Control strains (N2) and marker control (MC) displayed a survival rate of 30 ±2.9% and 27 ±0.5%, respectively, after a 6-hour heat shock at 35°C (Figure 3.9a). In comparison, nematodes expressing WT β2m and D76N β2m exhibited a survival rate of 15 ±1.5% and 9 ±1.5%, respectively (Figure 3.9a). Interestingly, the expression of ΔN6 β2m did not significantly affect the survival of the animals compared with wild type (N2) animals, where 24 ±4.9% of animals survived heat shock treatment (Figure 3.9a). This shows that expression of WT β2m and D76N β2m affects the ability of animals to deal with heat stress and could indicate a different mechanism of toxicity between these β2m variants and nematodes expressing ΔN6 β2m.

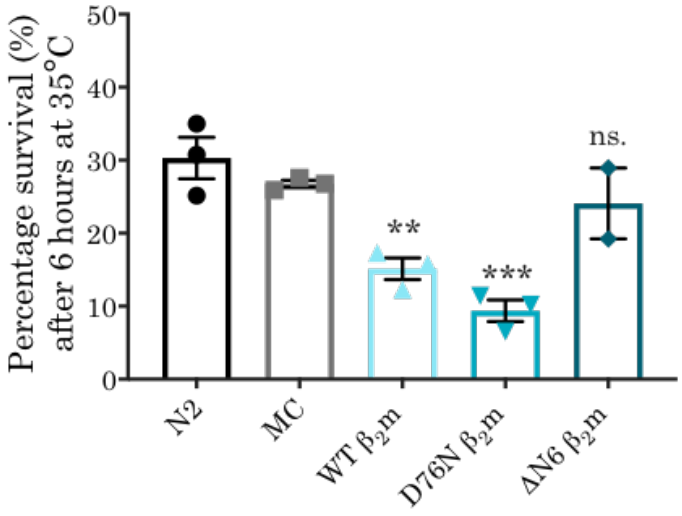

Figure 3.9 β2m-expressing strains have a reduced capacity to thermal stress
A) Survival rates of wild type (N2), marker control (MC), WT β2m, D76N β2m and ΔN6 β2m strains after thermal stress. Day 1 adults were placed onto seeded OP50-1 and incubated at 35°C for 6 hours. Animals were left to recover for 16 hours and scored for survival. Three independent experiments were performed (n=50 animals per experiment). Error bars indicate ±SEM. A student's t test was used to assess significance **p<0.005 ***p<0.001 ns. = not significant

As the expression of WT β_2m and D76N β_2m affected the ability of animals to deal with heat stress, it was next investigated whether other stress response pathways could also be affected in these animals. In particular, all the β_2m variants contain a signal peptide to direct the protein to be secreted via the ER (Figure 3.2), and this is cleaved in our models indicating that the protein is entering the ER (Figure 3.5). Therefore, the UPR^{ER} pathway could be affected. This was investigated by treatment with tunicamycin, an inhibitor of N-linked glycosylation that induces ER stress (Taylor and Dillin, 2013). Wild type and marker control animals treated with 50 µg/mL tunicamycin cultures for 6 hours and showed an 86.3% (±0.850) and 86.4% (±2.365) survival rate respectively; when treated with tunicamycin for a longer 10-hour time period, these strains showed reduced survival rates at 81.6% (±1.212) and 80.2 (±4.416) respectively (Figure 3.9b). Although expression of either WT β_2m or D76N β_2m did not affect the survival of the nematodes after 6 hours incubation in tunicamycin compared with the wild type (N2) strain; when incubated for the longer 10-hour time period the percentage of animals surviving was significantly reduced to 62.1% (±6.775) and 58.4% (±4.726) respectively. Furthermore, ER stress survival was slightly but significantly decreased in ΔN6 β_2m-expressing strains after both 6 hours (79.4 ±1.027) and 10 hours (59.5 ±12.271) of tunicamycin treatment (Figure 3.9b). Together, these results indicate that expression of β_2m affects the PN in the ER and disrupts the organism's ability to deal with ER stress.

The observation that expression of different variants of β_2m disrupted the ability of the nematodes to cope with ER stress was intriguing. In order to gain further understanding of this phenomenon, expression of the ER resident Hsp70 chaperone, *hsp-4*, was explored. *hsp-4* is a homolog of the ER Hsp70 chaperone BiP, and is upregulated upon ER stress in an IRE-1- and XBP-1- dependent manner (Calfon et al., 2002; Taylor and Dillin, 2013). Using quantitative RT-PCR, mRNA levels of *hsp-4* were measured during basal conditions and during ER stress, using tunicamycin as a stressor (Figure 3.10). As expected, *hsp-4* transcript levels in the marker control strain (MC) were similar (0.947± 0.090) compared with the wild type (N2) control during basal conditions (Figure 3.10a). However, *hsp-4* transcripts were reduced to 0.641 (±0.039) in the WT β_2m strain, 0.702 (±0.050) in D76N β_2m expressing animals, and 0.506 (±0.069) in the ΔN6 strain compared with the wild type control strain (Figure 3.10a). ER stress resulted in a 2.7-fold (±0.526) upregulation of *hsp-4* transcript levels in wild type (N2) animals and a 2.5-fold (±0.408) induction in the marker control strain compared with basal N2 *hsp-4* transcript levels (Figure 3.10b). *hsp-4* transcripts were induced 1.4-fold (±0.130) following ER stress in the ΔN6 strain, however

upon tunicamycin treatment no *hsp-4* induction was observed in the WT β_2m and D76N β_2m strains (Figure 3.10b). This indicates that expression of β_2m variants WT β_2m and D76N β_2m variants could impair the activation of UPR^{ER} in response to ER stress, which is also reflected by the reduced survival rates (Figure 3.10a). While the UPR^{ER} can be induced in ΔN6 expressing animals (Figure 3.10a), the magnitude of UPR^{ER} dependent *hsp-4* induction is lower when compared with control animals (N2 and MC strains). It is nevertheless puzzling that animals expressing ΔN6 can induce *hsp-4* following ER stress, whereas *C. elegans* expressing WT and D76N β_2m cannot. Furthermore, the differences in effect of the β_2m variants on *hsp-4* induction indicates a possible different mechanism of toxicity between β_2m variants, whereby expression of WT β_2m and D76N β_2m act to impair *hsp-4* ER stress response while ΔN6 does not.

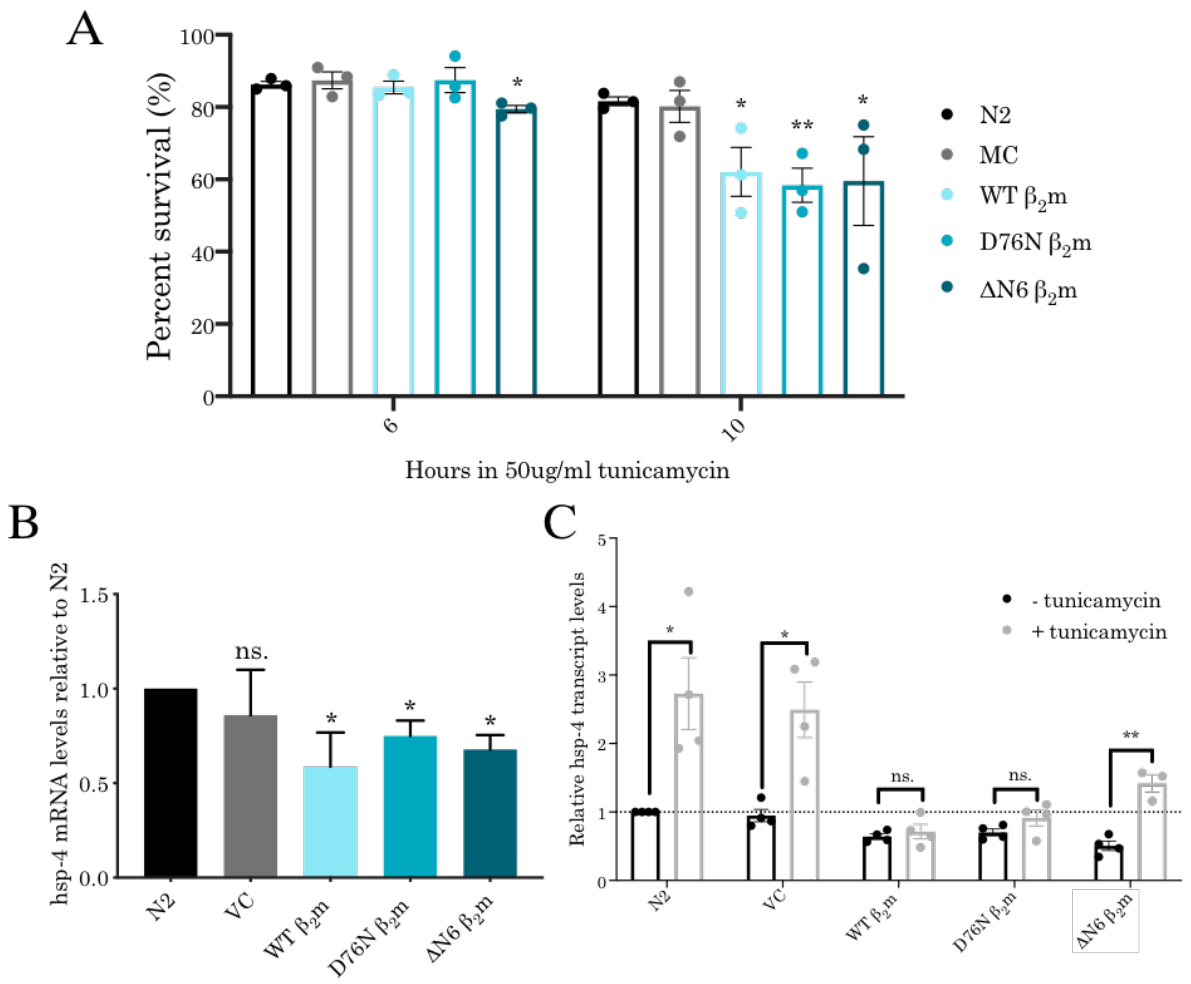

Figure 3.10 β2m-expressing strains have a reduced capacity to ER stress.
A) Survival rates of wild type (N2), marker control (MC), WT ß2m, D76N ß2m and ΔN6 ß2m strains after 6- and 10-hours ER stress. Day 1 adults were incubated in 50 µg/mL tunicamycin for either 6 or 10 hours then recovered on plates for 16 hours, and survival was scored. Three independent experiments were performed (n=40 animals per experiment). Error bars represent mean ±SEM. B) Transcript levels of *hsp-4* in day 1 adult marker control (MC), WT ß2m, D76N ß2m and ΔN6 ß2m transgenic *C. elegans* compared with wild type (N2). Levels were measured through quantitative RT-PCR and are given relative to transcript levels in N2 animals, with error bars indicating mean ±SEM. Three independent experiments were performed. C) Transcript levels for *hsp-4* with (+) or without (-) tunicamycin treatment in day 1 adult marker control (MC), WT ß2m, D76N ß2m and ΔN6 ß2m transgenic *C. elegans* compared with wild type (N2). Day 1 adult animals were incubated in 50 µg/mL tunicamycin cultures for 2 hours, RNA was extracted, and quantitative RT-PCR was performed. Transcript levels shown are relative to N2 animals, with error bars indicating mean ±SEM. Three independent experiments were performed. Experiments were performed and data are displayed as in B). A student's t test was used to assess all significance: *p<0.05 **p<0.001 ns. = not significant

3.6 Discussion

Previous research has demonstrated the cytotoxic nature of the amyloidogenic protein β2m both *in vitro* (Karamanos et al., 2014; Scarponi et al., 2016) and *in vivo* (Diomede et al., 2012; Faravelli et al., 2019). However, *in vivo* analysis of β2m toxicity at the organismal level is comparatively lacking. I set out to further understand the relationship of β2m aggregation and toxicity *in vivo* by generating three new *C. elegans* disease models expressing different variants of β2m in the body wall muscle of the roundworm nematode *C. elegans*. A correlation between the expression of the highly amyloidogenic variants D76N β2m and ΔN6 β2m, protein aggregation and toxic phenotypes in the animals was observed. In contrast, expression of WT β2m resulted in little toxicity and no protein aggregation. This is consistent with *in vitro* data demonstrating that WT β2m does not readily form amyloid fibres under physiological conditions *in vitro* (Chiti et al., 2001; Eichner et al., 2011). This suggests that the amyloidogenic propensity of the protein *in vitro* reflects the toxicity of the protein in an *in vivo* organismal animal model.

3.6.1 The β2m-expressing transgenic models generated throughout this study display similar phenotypes to previous disease models

In this chapter, a new transgenic *C. elegans* disease model expressing the naturally occurring β2m variant D76N β2m was described. Although a similar D76N β2m-expressing *C. elegans* disease model was generated previously, referred to as CPV27 (Faravelli et al., 2019); the model in this thesis work differs from CPV27 in a number of ways. Firstly, in the model presented in this chapter, D76N β2m was directly expressed under the control of the body-wall muscle promoter. In comparison, the CPV27 strain used the *smg* inducible system and the authors of the study observed early stage lethality when D76N β2m was directly expressed. It would therefore be interesting to explore embryonic lethality in the D76N β2m-expressing strain generated in this chapter to explore whether this phenotype could also be observed. A possible explanation for the difference in complete embryonic lethality could be that the strain generated in this study expressed a lower copy number of the D76N β2m transgene than in the CPV27 strain, and therefore expressed a lower amount of protein which negated the embryonic lethality observed. Analysis of the CPV27 strain also observed little β2m protein in the insoluble fraction of nematode lysates at day 5 of adulthood (Faravelli et al., 2019) whilst the strain generated in this thesis contained an increased amount of β2m in the insoluble fraction at day 8 of adulthood (Figure 3.4). This could be due to differences in age and expression levels of D76N β2m in the two

models, therefore affecting the aggregation of the protein. The phenotypes associated with CPV27 were however consistent with the phenotypes observed in the D76N β_2m disease model of this study. These included reduced motility, lifespan and fecundity and thus indicate that expression of D76N β_2m *in vivo* results in toxicity.

3.6.2 Locomotion defects are associated with the expression of β_2m in *C. elegans*

Expression of amyloidogenic proteins in the body wall muscle of nematodes has been widely reported to cause motility defects shown through analysis of the frequency of body bends in animals, including in models expressing amyloid-β (Link, 1995; McColl et al., 2012; Sorrentino et al., 2017), α-synuclein (Doherty et al., 2020; Hamamichi et al., 2008; van Ham et al., 2010; Van Ham et al., 2008), huntingtin (Brehme et al., 2014; Morley et al., 2002; H. Wang et al., 2009) and previously generated β_2m models (Diomede et al., 2012; Faravelli et al., 2019). Consistent with the previous literature, the expression of WT β_2m, D76N β_2m and ΔN6 β_2m also caused defects in the frequency of body bends in the animals. Therefore, the expression of these amyloidogenic proteins in the muscle is cytotoxic and could represent a generic mechanism of proteotoxicity across species.

To further complement the thrashing rate analysis in all β_2m-expressing strains, paralysis of the animals throughout aging was also monitored. Measurement of paralysed animals represents the end-point total collapse of the muscle cell, as opposed to muscle cell damage observed through measurement of the frequency of body bends. Animals expressing D76N β_2m and ΔN6 β_2m displayed increased paralysis during aging, which reflected the reduced thrashing rates. In contrast, WT β_2m-expressing animals showed little paralysis throughout aging (Figure 3.8). The increased paralysis in both D76N β_2m- and ΔN6 β_2m-expressing nematodes correlates with the increased protein aggregation in the same animals. This suggests that the age-dependent accumulation of aggregated species in these animals is cytotoxic. This is consistent with *in vitro* studies which positions both D76N β_2m and ΔN6 β_2m as highly amyloidogenic proteins (Eichner et al., 2011; Valleix et al., 2012)., and demonstrates a correlation between their ability to aggregate *in vitro* to their toxicity *in vivo.*

In contrast, expression of WT β_2m - although higher than D76N β_2m- and significantly higher than in ΔN6 β_2m-expressing animals (Figure 3.4 and Figure 3.5) – did not cause paralysis, suggesting there is less toxic damage occurring in this model. Further, an

increased amount of WT β2m protein aggregation was not observed in the insoluble fraction of aged animals (Figure 3.5). Therefore, it could be postulated that WT β2m may not be aggregating in this *in vivo* model, which is consistent with *in vitro* findings that WT β2m does not aggregate under physiological conditions (Eichner and Radford, 2009; Scarponi et al., 2016). Aggregation of WT β2m has been shown to require conversion to a partially unfolded state via lowering of pH or additives including collagen and glycosaminoglycans among others (Myers et al., 2006; Relini et al., 2008, 2006; Smith et al., 2020). Although both collagen and glycosaminoglycans are present in the basement membrane of the *C. elegans* muscle system (Hutter et al., 2000), the results here suggest that the *in vivo* environment in the WT β2m-expressing model is not sufficient to initiate aggregation. As 30% of *ex vivo* β2m deposits are made of ΔN6 β2m (Esposito et al., 2000), and ΔN6 β2m has been shown to induce WT β2m aggregation (Eichner et al., 2011), it might be interesting to generate a model that expresses both WT β2m and ΔN6 β2m to initiate WT β2m amyloidogenesis and fibril formation, and provide further insight into the aggregation of this protein *in vivo*.

3.6.3 Expression of β2m in *C. elegans* causes cell non autonomous toxicity

Expression of D76N β2m or ΔN6 β2m led to a developmental delay, while expression of WT β2m caused no developmental effect (Figure 3.7). This suggests that the aggregation of the amyloid proteins might be occurring early on in development. A similar effect on early stage development was also observed in the β2m variant strains generated by Diomede and colleagues, which they postulated to be caused by changes in mitochondrial efficiency (Diomede et al., 2012). Indeed, mitochondria have been shown previously to be a sensitive target of other amyloidogenic protein aggregates (Ashkavand et al., 2020; Eckert and Pagani, 2011; Sorrentino et al., 2017; Teo et al., 2019), and also play a crucial role in larval development (Tsang and Lemire, 2003). It would therefore be interesting to explore the role of oxidative stress and ROS species in the models generated in this chapter further and uncover whether animals have enhanced phenotypes under oxidative stress.

As well as a developmental delay, the animals expressing β2m variants also produced a reduced number of eggs over 3 days (Figure 3.7b). Egg-laying in *C. elegans* is controlled by dopamine, whereby exposure to environmental toxins can cause changes in dopamine signalling, and alter fecundity or brood size in the animals (Weinshenker et al., 1995). Expression of β2m in *C. elegans* could therefore be disrupting this neuronal signalling

pathway and cause a reduction in the egg-laying capabilities of the strains. Furthermore, this response could be due to an effect in the vulval muscles, whereby eggs cannot be laid. This leads to a "bagging" phenotype in animals, as the eggs hatch inside the parent nematode. To further explore whether this is occurring in the animals, the number of nematodes that display the "bagging" phenotype needs to be assessed in the strains. This would distinguish whether this phenomenon is due to reduced function of the vulval muscle, or it is indeed due to a reduced dopamine signalling.

3.6.4 Widespread proteome aggregation occurs when D76N and ΔN6 β_2m are expressed in *C. elegans*

As organisms age, the protein quality control network that responds to stress associated with proteostasis becomes compromised (Ben-Zvi et al., 2009; Hipp et al., 2019; Ji et al., 2020; Walther et al., 2015). This process is further exacerbated under increased proteostasis stresses, such as the expression of aggregation-prone proteins (Gidalevitz et al., 2006; Sui et al., 2020). Results in this chapter revealed the expression of the amyloidogenic proteins D76N β_2m and ΔN6 β_2m to correlate with increased global protein aggregation in aged animals (Figure 3.5). This is consistent with other studies in *C. elegans* demonstrating that expression of another amyloidogenic protein containing a polyglutamine expansion disrupts the global balance of the PN, and therefore animals display aberrant folding of the metastable protein paramyosin (Gidalevitz et al., 2006). Further, different proteotoxic stresses, such as expression of amyloidogenic proteins, modulation of chaperone expression and oxidative stress have been shown to induce highly specific proteome changes (Sui et al., 2020). Therefore, widespread proteome changes demonstrated in D76N β_2m- and ΔN6 β_2m-expressing nematodes could be responsible for the toxic phenotypes observed. It would therefore be interesting to explore and compare the differences in protein remodelling observed in D76N β_2m- and ΔN6 β_2m-expressing animals through proteomic analysis. This could potentially lead to further understanding in the differences in phenotypes observed in these strains.

Although proteome changes and the presence of β_2m was observed in the insoluble fraction of aged β_2m-expressing strains (Figure 3.5), the nature of these aggregated species in the models is still yet to be determined. The majority of β_2m cytotoxicity studies published to date have focussed on the proteotoxic nature of short β_2m fibrils which have been shown to disrupt membranes and inhibit the endolysosomal pathway (Goodchild et al., 2014; Jakhria et al., 2014; Xue et al., 2009). Therefore, determining the species of aggregated

β2m formed in the transgenic strains could provide further insight into the toxic mechanisms by which β2m exerts its cytotoxicity. Attempts were made to stain the *C. elegans* β2m disease models with X-34, an amyloid-specific dye that binds to amyloid fibrils (Link et al., 2001); however, staining was not reproducible and inconclusive in the models (Figure 3.6b). Further research utilising anti-amyloid antibodies - such as WO1 (O'Nuallain and Wetzel, 2002) - or anti-oligomer antibodies – such as A11 (Kayed et al., 2007) - to immunoblot lysates of the β2m models generated in this study would be useful to provide a clearer picture of the mechanisms of toxicity observed.

A major drawback of the data presented in this chapter was the lack of visualisation of β2m localisation in the animals. Western blot analysis using anti-β2m antibodies detected the presence of β2m in the strains (Figure 3.5). However, when using standard *C. elegans* immunostaining techniques, reproducible antibody staining of β2m in the animals could not be visualised (Figure 3.6a). This is in contrast with the previous studies expressing β2m variants, where staining was observed in only the anal sphincter and vulva in animals expressing WT β2m or ΔN6 β2m in the body wall muscle; however, staining could not also be observed in previous models expressing D76N β2m (Diomede et al., 2012; Faravelli et al., 2019). As the signal peptide sequence was included in the expressed β2m transgene and this was found to be cleaved, it is expected that the protein is extracellularly secreted. However, lack of visualisation is limiting this conclusion. Further immunofluorescence studies need to therefore be developed and will be important to elucidate the pathology of the β2m-induced phenotypes observed in the models.

3.6.5 The ER stress response could be contributing to toxicity associated with β2m expression in *C. elegans*

In this chapter, it was demonstrated that expression of β2m variants impaired the ability of *C. elegans* to deal with heat and ER stress. It is particularly interesting to note that WT β2m and D76N β2m expression led to both reduced survival under heat stress and ER stress conditions, while animals expressing ΔN6 β2m were unaffected by heat stress (Figure 3.9). This difference between D76N β2m and ΔN6 β2m expression is particularly interesting as both are highly amyloidogenic *in vitro* and suggests a different mechanism of toxicity between the two proteins. Indeed, clinically these two proteins are associated with different pathologies in patients; D76N β2m deposits are found in visceral tissues (Mangione et al., 2013), while ΔN6 β2m is found in β2m deposits in osteoarticular tissue (Esposito et al., 2000). Moreover, in WT β2m- and D76N β2m-expressing animals, induction

of the UPR^{ER} in response to protein folding stress in the ER is reduced at day 1 of adulthood. The expression of ER chaperones are downregulated during aging (Ben-Zvi et al., 2009; Taylor and Dillin, 2013). Therefore, a possible explanation of these results could be that expression of either WT β_2m or D76N β_2m could be triggering early proteostasis collapse of the UPR^{ER} in young animals. Constitutive upregulation of other UPR^{ER} components such as XBP-1 have been shown to ameliorate this collapse, improving ER stress resistance and the longevity of animals (Taylor and Dillin, 2013). It would therefore be interesting to further explore whether upregulation of UPR^{ER} components such as IRE-1, XBP-1 or ATF6 could also ameliorate the toxic phenotypes observed in the models.

It is particularly puzzling that ΔN6 expressing animals can induce the UPR^{ER}, albeit lower than control samples, while WT β_2m and D76N β_2m expressing animals cannot (Figure 3.10). It would be interesting to investigate the molecular and structural reasons underlying this result in more detail, such as investigating binding studies of ΔN6 β_2m to the human *hsp-4* homolog BiP (Taylor and Dillin, 2013). It is also worthwhile noting that steady-state levels of ΔN6 β_2m are reduced, which could be indicative of increased degradation of this β_2m variant. Thus, future studies could include the role of ER associated degradation (ERAD) in this process of β_2m variant turnover.

3.7 Conclusions

Overall, this chapter demonstrated toxicity of both D76N β_2m and ΔN6 β_2m *in vivo* in *C. elegans*, replicating the aggregation of the proteins observed *in vitro*. The results suggest that this toxicity can be linked to protein aggregation at an organismal level, although further research is needed to fully characterise which tissues are affected by proteotoxic β_2m species. It was also demonstrated that β_2m expression impairs the UPR^{ER}; however, further investigation is needed to understand how β_2m affects proteostasis in the ER and whether this is associated with reduced clearance of aggregated β_2m in the organelle. The data from this thesis chapter could be useful to future research and be used to help find new ways to ameliorate disease such as through the testing of small molecules or protein-based therapies to limit aggregation.

Chapter 4. Expression of Islet Amyloid Polypeptide in *C. elegans*

4.1 Abstract

Type II diabetes mellitus is associated with the deposition of islet amyloid polypeptide (IAPP) deposits surrounding insulin producing β-cells. To further investigate the aggregation and toxicity of this protein *in vivo*, three new *C. elegans* disease models were generated to express variants of varying amyloidogenicity: wild type human IAPP (hIAPP), a highly amyloidogenic mutant S20G and the non-amyloidogenic rat IAPP. Animals expressing the amyloidogenic variants hIAPP and S20G displayed delayed development, shortened lifespan, reduced thrashing rates, increased paralysis, reduced thermotolerance and reduced survival to ER stress. *C. elegans* expressing rat IAPP displayed sensitivity to ER stress but were resistant to heat stress. The phenotypes observed in these models *in vivo* correlates with the aggregation potential of the proteins previously demonstrated *in vitro*, linking amyloid formation with toxicity. Interestingly, co-expression of hIAPP with other amyloidogenic disease models - Aβ and Q35 – protected animals against the toxic paralysis phenotypes associated with these models.

4.2 Introduction

Type II diabetes mellitus (T2DM) is a condition characterised by high blood glucose levels and glucose intolerance (Pillay and Govender, 2013). Defective insulin production and secretion by the pancreatic β-cells in patients leads to long-term consequences including heart disease, strokes and kidney failure. Loss of β-cells has been linked to various pathologies including glucolipotoxicity, islet cholesterol accumulation, and islet inflammation (Stumvoll et al., 2005). Increasing evidence has also implicated the neuroendocrine hormone islet amyloid polypeptide (IAPP) in β-cell dysfunction and disease (Raimundo et al., 2020). Accumulation, aggregation and deposition of IAPP oligomers and amyloid in the surrounding tissues leads to the disruption of normal islet architecture and function, and aids in the pathology of disease. These deposits of IAPP amyloid in the Islets of Langerhans are a histological hallmark of T2DM and are represented in ~90% of patients (Costes, 2018).

IAPP is a 37-amino acid prohormone which plays a role in the regulation of metabolism and glucose homeostasis (Westermark et al., 2011). IAPP is co-secreted with insulin in a 1:100 manner, and works in synergy to stimulate uptake of blood glucose into tissues and inhibit glucose output from the liver, stabilising blood glucose levels (Westermark et al., 2011). IAPP is synthesised as a 89-residue preprohormone and processed by proprotein convertase (PC) 1/3, PC 2, PAM and carboxypeptidase E (Yonemoto et al., 2008) (Figure 4.1). IAPP is directed to the endoplasmic reticulum (ER) and cleaved to form proIAPP. ProIAPP is processed in the late Golgi complex, and undergoes amidation of the C-terminal end, and a disulphide bond forms between cysteines at positions two and seven (Westermark et al., 2011) (Figure 4.1).

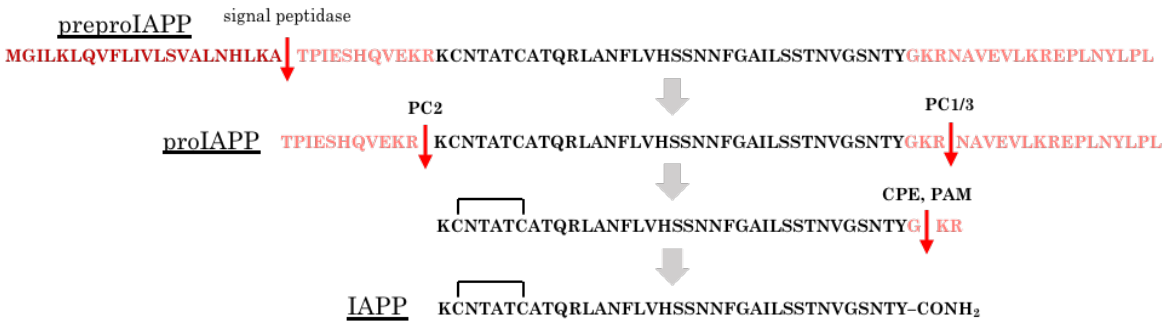

Figure 4.1 Processing of preproIAPP into mature IAPP.
The primary sequence of the 89-residue preproIAPP which is cleaved by signal peptidase to generate proIAPP. proIAPP undergoes cleavage by PC2 and PC1/3 in the ER at the sites indicated by arrows. Further processing by CPE/PAM amidates the C-terminus to generate the 37-residue mature IAPP. The signal peptide sequence of preproIAPP is indicated in dark red and the pro IAPP flanked regions indicated in light red.

4.2.1 *In vitro* assembly

Various studies to uncover the amyloid assembly pathway of IAPP have been performed *in vitro*. Native hIAPP is an intrinsically disordered, positively charged, hydrophobic peptide with weak sampling of α-helical states across residues 5-22 (Williamson et al., 2009). IAPP interaction with a phospholipid bilayer stabilises this helical subdomain and increases the conversion of IAPP to an amyloid form (Apostolidou et al., 2008; Williamson et al., 2009); this is thought to be due to the helix bringing together the amyloidogenic region of hIAPP (residue 20-29), increasing nucleation of the β-strand structure (Williamson et al., 2009). Electrospray ionization-ion mobility spectrometry-mass spectrometry (ESI-IMS-MS) of IAPP oligomers has identified oligomeric species up to

hexamers of IAPP (Young et al., 2014). These early pre-amyloid lag phase oligomers are cytotoxic, and reduce β-cell viability (Abedini et al., 2016). Amyloid deposits of IAPP, like many other amyloid deposits, contain serum amyloid P component (SAP), apolipoprotein E (apoE), and the heparan sulphate proteoglycan (HSPG) perlecan (Conde-Knape, 2001; Vidal et al., 2003). The interaction of IAPP and SAP or apoE does not appear to be vital in amyloid deposition; however, the glycosaminoglycan (GA) component of HSPGs has been shown to accelerate amyloid formation of IAPP and the partially processed form proIAPP *in vitro* (Jha et al., 2011).

4.2.1.1 *S20G*

Mutations in human IAPP have been shown to increase its aggregation propensity. The naturally occurring S20G mutation has been associated with early onset diabetes (Sakagashira et al., 1996). S20G IAPP has a higher aggregation propensity than hIAPP *in vitro* (Ma et al., 2001; Morita et al., 2013). It is thought this increased amyloidogenicity is due to increased local flexibility, or to conformational pre-organisation in the monomer prior to self-assembly (Xu et al., 2009). Furthermore, the peptide segment between amino acids 19-29 of the hIAPP-S20G variant forms pairs of β-sheets that share structural similarity to full length hIAPP fibrils. In contrast, the peptide segment between amino acids 15-25 of hIAPP forms non-toxic labile β-sheets (Krotee et al., 2017). Expression of the hIAPP-S20G mutant in mouse β-cells caused increased β-cell apoptosis, decreased β-cell area and impaired insulin release (Meier et al., 2016). Furthermore, downregulation of insulin in cells enhanced cytotoxicity in cells, a mechanism that is mimicked in hIAPP cytotoxicity (Morita et al., 2013).

4.2.1.2 *Rat IAPP*

As discussed, IAPP can form into amyloid in humans; however, this is not the case for all species. Rats express a form of IAPP which cannot form amyloid fibrils (Betsholtz et al., 1989). Protein sequences of rat and human IAPP are similar but differ mainly in the 20-29 region. In particular, the three proline residues (positions 25, 28, and 29) and the His-18 to Arg substitution in rat IAPP are thought to disrupt hydrogen bonding and intermolecular β-sheet formation, inhibiting amyloid formation (Betsholtz et al., 1989). Indeed, replacement of His-18 in hIAPP with Arg decreases the amyloidogenic nature of the protein (Abedini and Raleigh, 2005). Moreover, the rat IAPP sequence gives rise to a lower bend angle between the two α-helices of the molecule. In hIAPP and the S20G

mutant, it is a more pronounced bend that favours amyloid formation (Duan et al., 2012; Nanga et al., 2011). Rat IAPP was also found to be an inhibitor of hIAPP amyloid formation, as it slowed growth rate, reduced the amount of fibrils in a dose dependent manner and altered the morphology of fibrils (Cao et al., 2010).

4.2.1.3 *ProIAPP*

Upon translation, IAPP is targeted to the endoplasmic reticulum (ER), where proIAPP is converted to mature IAPP (Figure 4.1). ProIAPP has also been shown to be highly fibrillogenic (Exley et al., 2010). Increased concentrations of proIAPP in the ER has been shown to induce ER stress, activating stress responses in the UPR which can lead to cellular death (Westermark et al., 2011). ProIAPP is thought to initiate aggregation into amyloid fibrils, triggering aggregates in secretory granules of β-cells (Paulsson et al., 2006). Inhibition of processing of proIAPP into mature IAPP in murine cell models has also been shown to lead to rapid formation of intracellular amyloid suggesting this variant is important in aggregation and disease progression (Paulsson et al., 2006).

4.2.2 Mechanisms of IAPP-induced toxicity

IAPP has been shown to induce islet cell apoptosis that is characterised by pancreatic β-cell death, plasma membrane blebbing, chromatin condensation, and DNA condensation (Abedini and Schmidt, 2013). A number of different mechanisms have been proposed as to how IAPP exerts β-cell toxicity. IAPP aggregates into a number of different species which can induce differential cellular effects. However, the literature positions the oligomeric species of IAPP as the main culprit in the progression of disease, inducing a higher amount of damage.

IAPP toxicity mechanisms are further complicated as the initiation site of amyloid formation is controversial. Amyloid deposits in T2DM patients are found extracellularly; therefore it could be assumed that IAPP forms into amyloid extracellularly and this is supported through studies using cultured mouse islets (Aston-Mourney et al., 2011). Reagents increasing IAPP secretion but not effecting IAPP levels increased the amyloid formation and toxicity of IAPP, while inhibition had the reverse effect (Aston-Mourney et al., 2011). Studies have revealed that applying hIAPP peptides to primary cultures of human pancreatic islets causes increased expression of chaperones in the ER stress response pathway and a reduction in proteasome activity contributing to cellular apoptosis

(Casas et al., 2007). Oligomeric species of hIAPP have also been shown to permeabilise membranes, forming an "IAPP amyloid pore". This pore is temporally correlated with the formation of early IAPP oligomers, and is not induced by fibrillar IAPP (Anguiano et al., 2002). IAPP interacts with membranes through the N-terminal region, and this interaction markedly accelerates fibre formation (Knight et al., 2006). These membrane traversing-pores cause toxicity through the entry of calcium ions (Anguiano et al., 2002).

Other studies that over-express hIAPP *in vivo* point to an intracellular origin of toxicity (Gurlo et al., 2010). Toxicity caused by intracellular aggregates has been shown to activate the JNK pathway and mediate β-cell apoptosis. This pathway can be activated by a range of events such as ER stress, ROS formation, oxidative stress, increases in glucose concentration and the production of pro-inflammatory cytokines (Gurlo et al., 2010). Moreover, interaction between IAPP and Fas – another downstream signalling pathway – has been shown to lead to caspase 3 activation and cell death (Park et al., 2012; Subramanian et al., 2012). Studies inhibiting caspase 3 have been shown to protect β-cells against IAPP-induced cell death *in vivo* (Law et al., 2010; Park et al., 2012). Other intracellular proteotoxic effects of IAPP aggregation include the induction of the ER and oxidative stress pathway (Huang et al., 2007; Zraika et al., 2009). Moreover, patients with T2DM have reduced ubiquitin carboxyl-terminal hydrolase L1 (UCH-L1) protein levels, thought to be caused by hIAPP aggregation that leads to ER stress and apoptosis (Costes et al., 2011). These intracellular effects are thought to destroy β-cells, releasing amyloid into the extracellular matrix from where it can provide seeds for further fibril growth.

In β-cells, autophagy is important for maintaining the secretory granule population and removal of damaged mitochondria and other foreign material in the cytoplasm. In hIAPP transgenic mouse islets, hIAPP bound to p62, a protein essential for targeting proteins for autophagy, suggesting hIAPP fibrils are recognised for degradation via autophagy (Rivera et al., 2014). Furthermore, expression of hIAPP in a mouse β-cell line caused the formation of autophagosomes, whereby treatment with rapamycin – an inhibitor of autophagy – increased the viability of cells (Morita et al., 2011).

4.2.3 *In vivo* IAPP models

Various animal models have been utilised in research of IAPP aggregation and toxicity. Transgenic technology has been used to generate many rodent models which overexpress

hIAPP to investigate adverse effects of hIAPP aggregation on β-cell destruction. Initial mouse models noted the presence of abnormal hIAPP aggregates in β-cell secretory granules, but the models did not develop diabetes (De Koning et al., 1994). However, when bred to homozygosity, transgenic mice developed diabetes spontaneously, and demonstrated a rapid decline in β-cell production. This decline preceded the development of amyloid surrounding islets, and supported *in vitro* findings that small IAPP oligomers were the cytotoxic species (Janson et al., 1996). Other rodent models include the HIP rat model, that rapidly develops diabetes within the first two months of life when homozygous, correlating with a rapid decline in β-cell mass although no extracellular amyloid is observed. In the hemizygous model, the animal develops diabetes over 5-10 months, developing the presence of extensive extracellular amyloid deposits and an increase in β-cell apoptosis (Butler et al., 2004).

The model organism *Caenorhabditis elegans* has been used before as a model system for investigating IAPP aggregation and toxicity *in vivo* (Aldras et al., 2019; Rosas et al., 2016). Modelling disease in *C. elegans* provides a less expensive and simpler system to the traditional rat model, whereby the short ~3-day life cycle allows for an easier system to study the effects of IAPP expression on ageing throughout the entire lifespan of the animal. Rosas and colleagues utilised expression of proIAPP with a yellow fluorescent protein (YFP) tag on the C-terminal end of the protein in the body wall muscle of the animals. Their model displayed insoluble YFP aggregates throughout the animal during ageing, and a delayed development phenotype. Co-expression of Hsp72 in the animals improved this aggregation, decreasing the number of insoluble aggregates observed (Rosas et al., 2016). An inducible IAPP *C. elegans* model has also been generated which utilised the *hsp-16.2* promoter for expression in the neurons, pharyngeal muscle and hypodermal cells upon heat induction. This model displayed defects in sensory behaviour and was used to investigate transcriptional changes associated with hIAPP and demonstrated profile changes in diverse physiologically responses (Aldras et al., 2019).

4.2.4 IAPP and other amyloidogenic diseases

Several studies have implicated IAPP in the progression of the amyloidogenic disease Alzheimer's disease (AD). A genome-wide study has revealed that IAPP gene polymorphism is associated with brain amyloid burden and cognitive impairment in AD (Jackson et al., 2013). Moreover, the association of IAPP concentration and AD onset in

patients is non-linear. Compared with patients with a low concentration of plasma IAPP, patients with high concentrations of IAPP correlate with lower rate of AD incidence, but patients with extremely high concentration of IAPP have a higher potential to develop AD (Zhu et al., 2019). A number of studies have focussed on the interplay of Amyloid-β (Aβ) - a major component of amyloid plaques in Alzheimer's disease - and IAPP. Indeed in patients suffering both T2DM and AD, IAPP was found in Aβ deposits in the brain (Oskarsson et al., 2015). IAPP and Aβ share 25% sequence identity, that is particularly prominent in regions important for fibril assembly (O'Nuallain et al., 2004). Further, two regions of Aβ (11-21 and 23-37) have high binding affinity to IAPP (Andreetto et al., 2010), and both bind to the amylin receptor. Co-assembly occurs between Aβ and IAPP, and IAPP promotes Aβ aggregation in a seeding-like manner, leading to the formation of cross-seeded oligomers (Andreetto et al., 2010; Young et al., 2015).

4.3 Aims of the chapter

In this chapter, I aimed to generate *C. elegans* disease models of type II diabetes mellitus by expressing different variants of IAPP that possess differing amyloidogenicity *in vitro*. The human wild type IAPP, a mutant protein harbouring the S20G point mutation that increases amyloidogenicity, and the non-amyloidogenic variant rat IAPP were chosen for expression in the body wall muscle of animals. To understand the toxicity of these variants *in vivo*, I aimed to characterise these models for any phenotypes that might be a result of toxic damage including motility, development and lifespan. I further aimed to understand the aggregation and interaction of IAPP with other amyloidogenic proteins by co-expressing hIAPP with other amyloidogenic proteins Amyloid-β and Q35.

4.4 Methods

4.4.1 *C. elegans* strains and maintenance

Strain name	Genotype
AM167 (Q35)	rmIs156 *[unc-54p::Q35::YFP]*
GMC101 ($A\beta_{1-42}$)	dvIs100*[unc-54p::A-beta-1-42::unc-54 3'-UTR + mtl-2p::GFP]*
N2 (Bristol)	Wild type
PVH180	pccEx012*[myo-3p::WT IAPP::unc-54 3'UTR + myo-2p::RFP]*
PVH181	pccEx013*[myo-3p::S20G IAPP::unc-54 3'UTR + myo-2p::RFP]*
PVH182	pccEx024*[myo-2p::mCherry*]
PVH222	pccEx025*[myo-3p::rat IAPP::unc-54 3'UTR + myo-2p::RFP]*
PVH223	dvIs100*[unc-54p::A-beta-1-42::unc-54 3'-UTR + mtl-2p::GFP];* pccEx012*[myo-3p::WT IAPP::unc-54 3'UTR + myo-2p::RFP]*
PVH224	dvIs100*[unc-54p::A-beta-1-42::unc-54 3'-UTR + mtl-2p::GFP];* pccEx013*[myo-3p::S20G IAPP::unc-54 3'UTR + myo-2p::RFP]*
PVH225	rmIs156 *[unc-54p::Q35::YFP]* pccEx012*[myo-3p::WT IAPP::unc-54 3'UTR + myo-2p::RFP]*

Table 4.1 *C. elegans* strains used in Chapter 4 and their genotypes

4.4.2 Generation of an IAPP-expressing transgenic vector

The *C. elegans* expression vector pPD95_75 (Fire lab, Addgene) was digested with HindII and SalI, and the body wall promoter sequence *myo-3p* inserted. cDNA of hIAPP, S20G and rat including their signal peptide sequence and pro regions were made by Eurofin Scientific. Using the SalI and EcoRI restriction sites, the preproIAPP variant sequences were cloned into the vector downstream of the *myo-3p* promoter, which removed the GFP sequence from the vector. Successful constructs were sequenced and analysed to verify the correct sequence.

4.4.3 Soluble/insoluble protein fractionation

Animals were aged to day 1 or day 8 adults using FUdR plates (Chapter 2.1.4). Nematodes were collected using M9 buffer, and resuspended in lysis buffer (20 mM Tris, pH 7.5, 10 mM β-mercaptoethanol, 0.5% (v/v) Triton X-100, complete protease inhibitor (Roche)). Extracts were shock frozen in liquid nitrogen, and the frozen nematode pellet was ground

using a motorized pestle, then lysed on ice in the presence of 0.0025 U/mL benzonase (Sigma). Lysates were centrifuged at 1000 rpm for 1 min in a tabletop centrifuge and the supernatant was extracted. 2% (v/v) N-Lauroylsarcosine was added to the supernatant and was ultracentrifuged at 100,000 *g* for 1 hour at 4°C. The supernatant was removed, and the resulting pellet was resuspended in the same volume of dH_2O as the supernatant.

4.4.4 Silver-Stain

Nematode extracts were run on an 4-20% (w/v) SDS-PAGE gel (BioRad). The gel was fixed in solution A (50% (v/v) ethanol, 10% (v/v) acetic acid) for 30 minutes, then incubated in solution B (5% (v/v) ethanol, 1% (v/v) acetic acid) for 15 minutes on a gentle rocker. The gel was washed in dH_2O three times for 5 minutes, and then incubated in solution D (0.02 g sodium thiosulphate in 100 mL dH_2O) for 2 minutes while gently rocking. The gel was washed again in dH_2O three times for 30 seconds, then incubated in solution E (0.2 g silver nitrate, 75 µL formaldehyde in 100 mL dH_2O) for 20 minutes. After three washes in dH_2O for 20 seconds, the gel was developed in solution F (6 g sodium carbonate, 50 µL formaldehyde, 0.2 mL solution C in 100 mL dH_2O) until protein bands could be visualised and the reaction was stopped using solution G (5% (v/v) acetic acid). The gel was then stored in dH_2O and imaged.

4.4.5 Western blot analysis

Nematodes were collected and lysed on ice using a motorised pestle in lysis buffer (150mM NaCl, 50 mM Tris pH 7.4, 1 mM EDTA, 0.1% (v/v) NP-40). Extracts were centrifuged at 13,000 rpm for 1 minute to pellet the carcasses and the supernatant collected. The protein extract was run on a 10% (w/v) Tris-Tricine gel and proteins were electro-transferred to 0.22 µM nitrocellulose membranes. The blots were blocked using 5% (w/v) milk overnight, washed four times in PBS/Tween (0.1% v/v) for 5 minutes, then probed with primary anti-human amylin mouse polyclonal antibody (R10/99, Invitrogen) at a 1:1000 (v/v) dilution in PBS/Tween (0.1% v/v) and 1% milk for 2 hours. Blots were washed then probed with 1:10000 (v/v) dilution HRP-conjugated goat anti-mouse secondary antibody (Invitrogen) for 1 hour. Blots were developed using ECL (Fisher) and images were exposed onto film.

4.4.6 Aggregation assay

Age-synchronised *C. elegans* (n > 30) expressing *unc-54p*::Q35::YFP (Q35) were imaged using a Leica MZ10F fluorescent stereoscope with a YFP filter and the number of

aggregates was counted each day of adulthood (L4 = day 0). Aggregates defined as fluorescent foci were brighter and clearly distinguishable from background YFP fluorescence (Morley et al., 2002).

Methods for the following experiments can be found in the Methods chapter (Chapter 2):

C. elegans maintenance	Chapter 2.1
Developmental assay	Chapter 2.2.1
Lifespan	Chapter 2.2.3
Paralysis assay	Chapter 2.2.4
Thrashing assay	Chapter 2.2.5
Thermotolerance	Chapter 2.2.6
ER Stress survival	Chapter 2.2.7
Immunostaining	Chapter 2.3.1
X-34 staining	Chapter 2.3.2
RT-qPCR	Chapter 2.4

4.5 Results

4.5.1 Generation of IAPP-expressing *C. elegans* strains

To study the aggregation and proteotoxicity of IAPP *in vivo*, we generated three new transgenic *C. elegans* strains expressing different variants of IAPP, including human wild type IAPP (hIAPP), the single point highly amyloidogenic variant S20G, or the non-aggregation prone variant rat IAPP (Figure 4.2b). To generate expression constructs targeted to the muscle, the body wall muscle promoter *myo-3p* was inserted into the pPD95_75 *C. elegans* expression vector using HindII and SalI (Figure 4.2a). Next, cDNA encoding either the human wild type preproIAPP, human S20G preproIAPP or rat preproIAPP - which contains the gene of interest, its pro regions and the signal peptide sequence – was inserted into the myo-3p-pPD95_75 vector using SalI and EcoRI sites to generate *myo-3p*::preproIAPP *C. elegans* transgenes (Figure 4.2a). Transgenes were microinjected in the gonad of wild type (N2) animals alongside the co-injection marker *myo-2p*::*mCherry* which causes red fluorescence in the pharynx of animals. A marker control was also generated, where the co-injection marker (*myo-2::mCherry)* alone was injected into animals and subsequently used as a negative control (marker control).

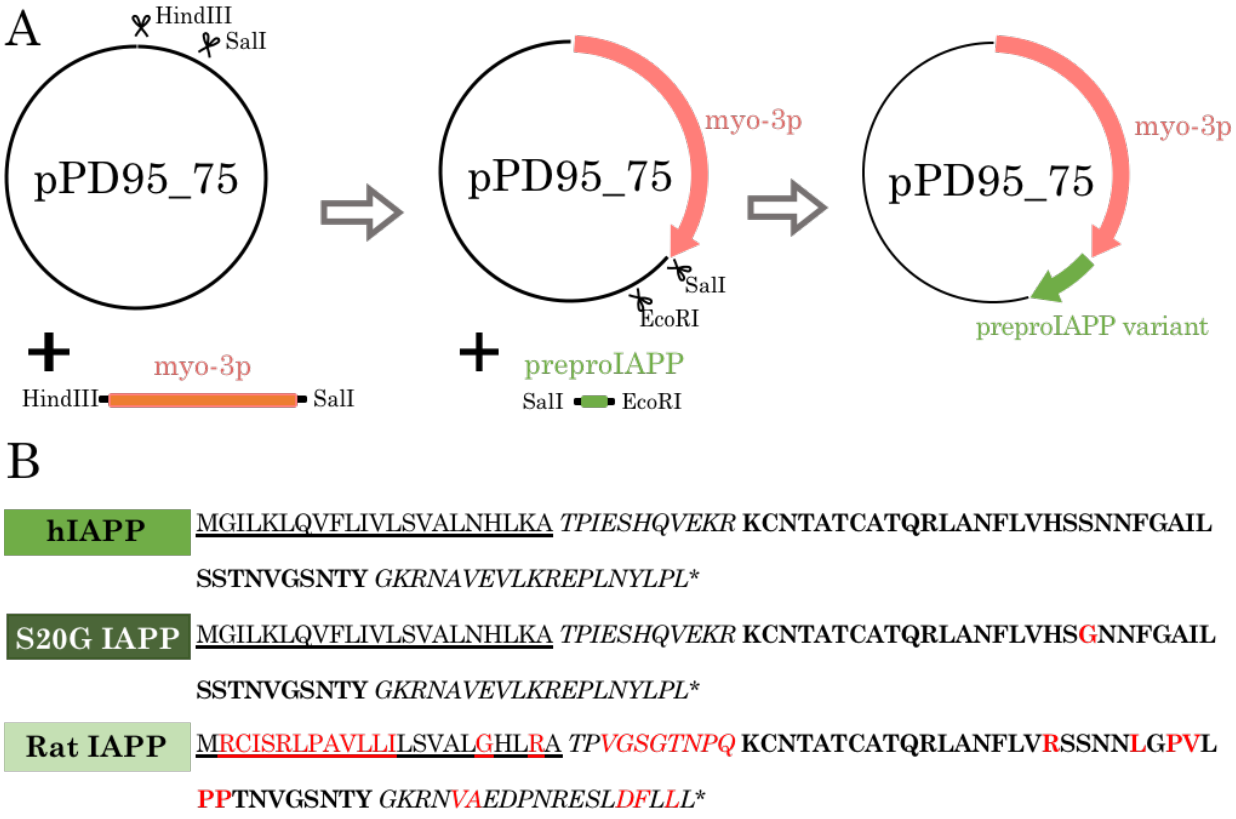

Figure 4.2 Generation of plasmids for the expression of different variants of IAPP in *Caenorhabditis elegans*.
A) Cloning strategy for the generation of a plasmid encoding variants of IAPP under the control of the body wall muscle promoter *myo-3p*. The protomer *myo-3p* was cloned into the HindIII and SalI restriction sites of the pPD95_75 *C. elegans* vector. The resulting constructs were digested with SalI and EcoRI and cDNA of the human prepro hIAPP, S20G IAPP or rat IAPP were then cloned in to generate the hIAPP, S20G IAPP and rat IAPP transgenes. B) hIAPP, S20G IAPP and rat IAPP human prepro amino acid sequences. The signal peptide amino acid sequence (1-22) is underlined. The pro regions of the amino acid sequence (23-33; 71-89) are in italics. Any differences between the amino acid sequences compared with hIAPP are in red.

4.5.2 RNA expression characterisation of IAPP-expressing transgenic strains

Extrachromosomal lines for each construct were established by selecting *C. elegans* expressing the *myo-2p*::*mCherry* co-injection marker in the pharynx. To confirm that these lines expressed the IAPP transgene as expected, quantitative real time PCR (qRT-PCR) was performed on each strain using primers for human IAPP sequence (hIAPP or S20G IAPP), or the primers for the rat IAPP sequence (rat IAPP). Expression of IAPP in control animals expressing the co-injection marker only (MC), did not have any significant effect on IAPP levels. (Figure 4.3a and 4.3b). Transgenic animals expressing either hIAPP, S20G IAPP or rat IAPP were observed to have 34000-, 4000- and 10000-fold increased mRNA levels of IAPP respectively, compared with wild type (N2) animals. Therefore, this validated the transgenes were successfully expressed in the disease models.

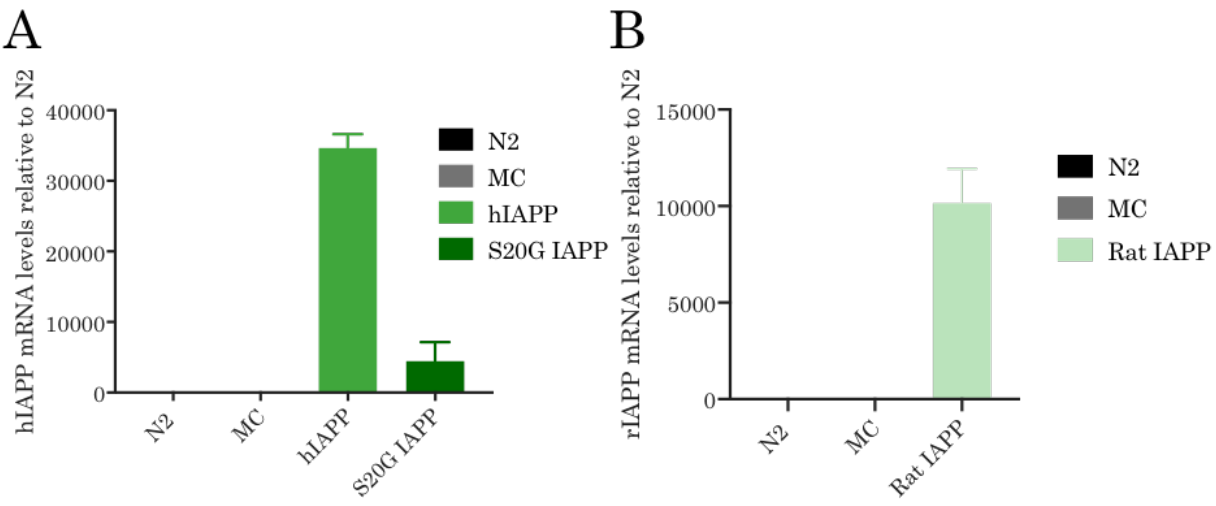

Figure 4.3 IAPP RNA expression in the IAPP-expressing transgenic *C. elegans* strains.
A) Transcript levels of IAPP in adult transgenic animals transfected with the marker control (MC) or vectors for the expression of hIAPP or S20G IAPP compared with a wildtype (N2) control. Quantitative RT-PCR using primers for hIAPP (Chapter 2.4, Table 2.2) coding sequence was performed on day 1 adults. Data represent the mean of three independent experiments. Error bars = ±SEM. B) Transcript levels of IAPP in adult transgenic animals transfected with the marker control (MC) or rat IAPP compared with wild type (N2). Quantitative RT-PCR using primers for rat IAPP (Chapter 2.4, Table 2.2) coding sequence was performed on day 1 adults. Data represents the mean of three independent experiments. Error bars = ±SEM

4.5.3 IAPP could not be detected in transgenic strains using western blot methods

The presence of the IAPP gene transcript in IAPP-expressing *C. elegans* models generated (Figure 4.3) confirms successful transcript expression but does not necessarily correlate to protein expression in our disease models. To confirm this, western blot analysis was performed on IAPP-expressing *C. elegans* strains using antibodies specific for the IAPP protein. However, IAPP protein could not be detected in either control strains or the hIAPP- and S20G-expressing disease models (Figure 4.4a). As IAPP is a relatively small protein (3904.5 MW), it was questioned whether the protein was transferring through the nitrocellulose membrane. A western blot was therefore performed on differing amounts of synthetic IAPP. Protein transfer from the gel to the nitrocellulose membrane was confirmed by Ponceau red staining, before antibody staining with IAPP. Ponceau Red staining detected the presence of protein at the correct molecular weight in the 25 ng, 12.5 ng and 2.5 ng samples, confirming the protein had transferred onto the membrane (Figure 4.4b). However, subsequent antibody staining of the same membrane did not yield any detectable bands (Figure 4.4b). These results suggest that the antibody used for this western blot analysis could not detect the protein at the concentrations required for analysis.

IAPP protein expression could not be detected in the transgenic strains generated. However, the protein could still be expressed and affect the aggregation of endogenous proteins in these strains. To explore this, soluble and insoluble fractions of protein extracts of aged (day 8) adult nematodes of IAPP variant expressing strains and control strains (N2 and MC) were prepared and examined using SDS-PAGE and silver staining (Figure 4.4c). The ratio of insoluble to soluble proteins in the samples were calculated (Figure 4.4d). In the wild type and marker control strains, a similar ratio of insoluble/soluble fractions of 0.36 ±0.02 and 0.31 ±0.04 respectively was observed (Figure 4.4d). Both the hIAPP- (0.41 ±0.05) and rat IAPP- (0.35± 0.003) expressing strains displayed similar insoluble/soluble ratios compared with the wild type control strain (Figure 4.4d). Expression of the highly amyloidogenic IAPP variant S20G correlated with a significantly increased insoluble/soluble protein ratio of 0.54 ±0.03, suggesting that expression of S20G but not hIAPP or rat IAPP leads to widespread global protein aggregation within the organism.

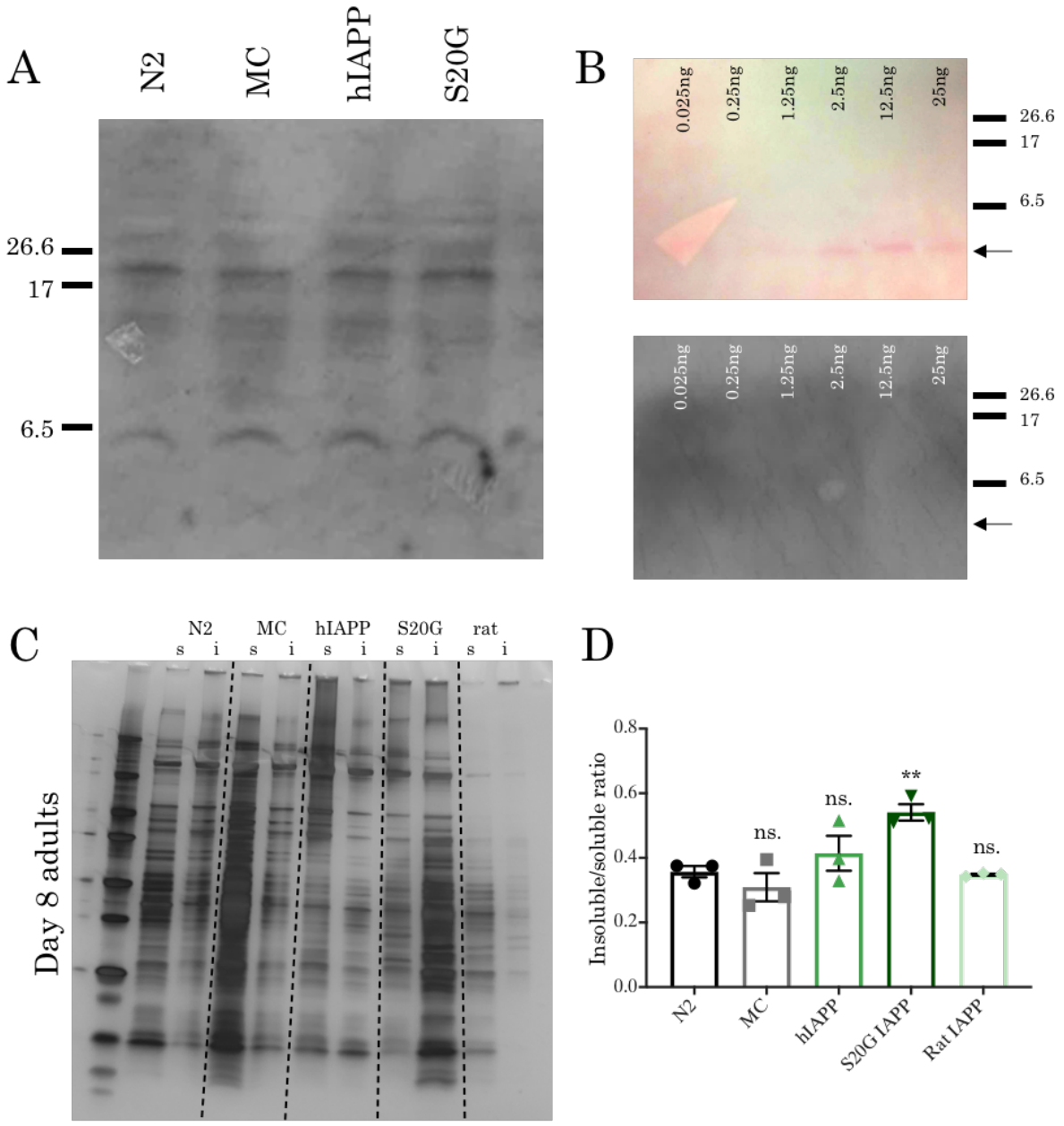

Figure 4.4 Western blot analysis of IAPP-expressing transgenic *C. elegans*.
A) Western blot of wild type (N2), marker control (MC), hIAPP-expressing or S20G-expressing transgenic animals. Anti-amylin antibodies (R10/99, Invitrogen) were used to in a 1:1000 ratio to detect IAPP. Bands shown are non-specific staining. B) Ponceau red staining (Top) and western blot staining (bottom) of 0.0025ng, 0.25ng, 1.25ng, 2.5ng, 12.5ng or 25ng of synthetic IAPP. Arrows denote the expected weight of IAPP. C) Representative silver stain of the soluble and insoluble fractions of day 8 adult nematodes. Protein was extracted from nematodes and ultracentrifuged for 1 hour at 100,000 x *g*. The soluble fraction (s) and insoluble fraction (i) were run on an SDS-PAGE, stained using silver nitrate and imaged. D) Quantification of protein levels in C. Density of lanes were analysed using ImageJ, and fraction of insoluble protein calculated using [density of insoluble]/[density of soluble + density of insoluble] (n=3).

4.5.4 **Localisation and aggregation of IAPP in IAPP-expressing transgenic *C. elegans***

As IAPP expression could not be detected by western blot analysis in the strains using an anti-amylin antibody, a different approach was required to detect the protein. The IAPP-expressing strains were immuno-stained using an anti-amylin antibody conjugated to Alexa-647 and the protein delivery reagent Pulsin. Pulsin has been previously described to limit degradation of proteins in the gut and promote absorption into body tissues of *C. elegans* (Perni et al., 2017). In wild type (N2) animals, some non-specific staining was observed throughout the gut, suggesting little presence of IAPP throughout the animal (Figure 4.5a). Interestingly, animals expressing hIAPP in the body wall muscle were observed to have fluorescence signal in the body wall muscle of animals, specifically surrounding the vulva muscle (Figure 4.5a). This suggests hIAPP is present in the body wall muscle of the animals.

Another useful localisation technique in amyloid disease models is staining with the amyloid binding dye X-34. X-34 stains amyloid deposits, which allows for the depiction of both the localisation of deposits and the presence of amyloid species in the animal (Link et al., 2001). In wild type (N2) animals, the presence of any foci could not be detected in the body wall muscle of the head region of animals (Figure 4.5b). It is worth noting however, that non-specific staining was observed throughout the entire wild type (N2) animals, in particular in the intestine. Transgenic animals expressing hIAPP were observed to possess small foci in the outer region of the head, indicating the formation of amyloidogenic species in this region. Further experiments to identify whether expression of S20G or rat IAPP yield similar results are required to draw comparisons between strains.

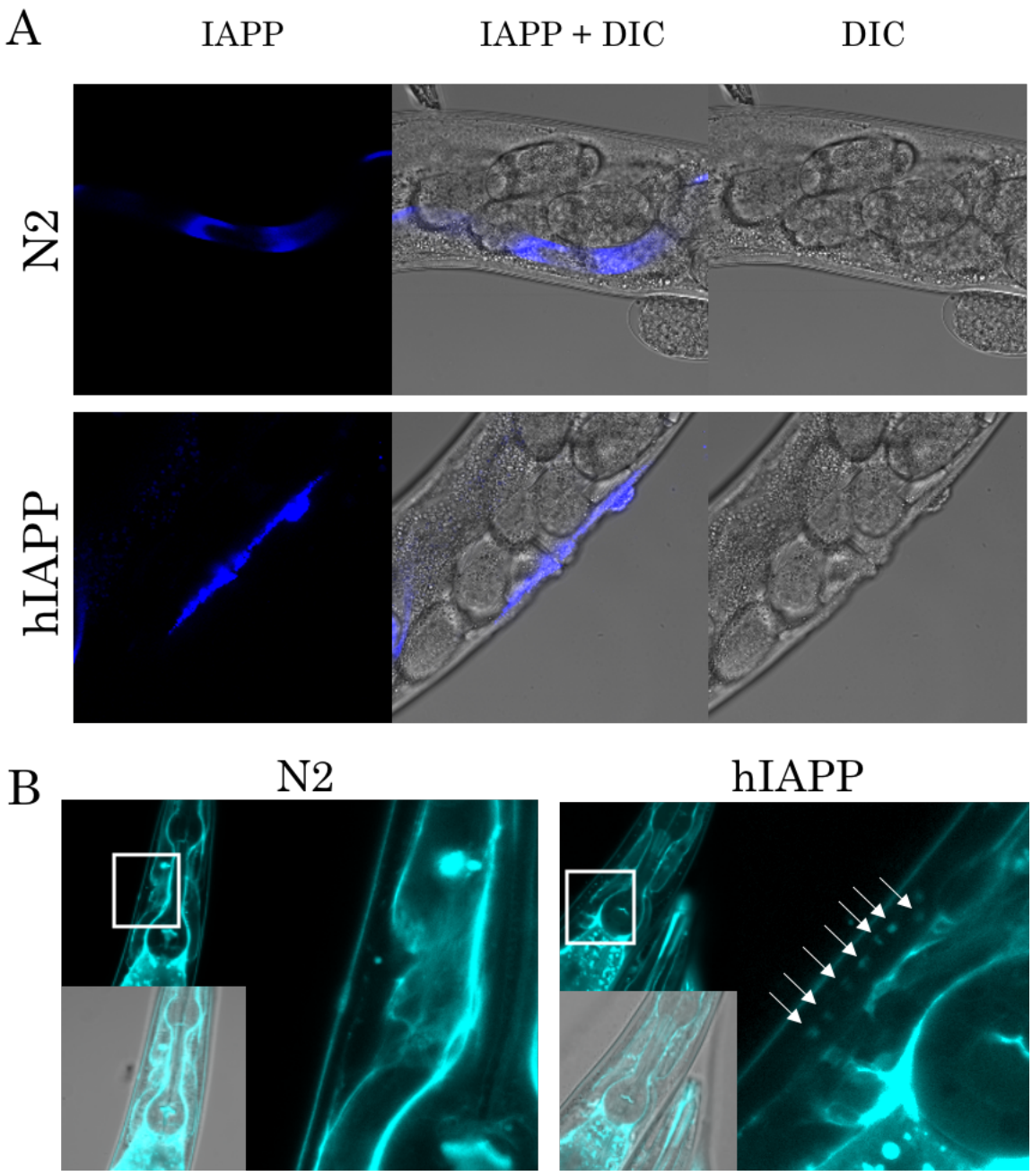

Figure 4.5 Localisation of aggregates in hIAPP-expressing transgenic *C. elegans*.
A) Immunofluorescence of day 1 adult wild type (N2) and hIAPP-expressing transgenic *C. elegans* using anti-amylin (Invitrogen) antibodies. Images show are fluorescence imaging, brightfield and overlay B) Representative images of X-34 staining of day 5 adult wild type (N2) or hIAPP expressing transgenic animals. Immunofluorescence images and overlay with bright field are depicted. White arrows indicate foci. All images shown were obtained using a Zeiss LSM880 confocal microscope.

4.5.5 Expression of hIAPP and S20G IAPP but not rat IAPP delays development in *C. elegans*

After establishing the *C. elegans* strains expressing different IAPP variants, it was next questioned whether expression of these proteins could affect the behavioural characteristics of the animals. Previous studies using hIAPP-expressing *C. elegans* have noted a delay in the development of the animals (Rosas et al., 2016), and thus it was questioned whether the disease models generated in this chapter caused a similar phenotype. When the developmental stage of animals was analysed 65 hours after egg laying, 93.4% (± 1.3) of wild type (N2) animals had reached the adult stage (Figure 4.6a). Likewise, expression of the marker control (MC) or the non-amyloidogenic rat IAPP in animals did not affect development, where 91.6% (± 2.8) and 93.7 (± 0.7) of animals also reached adult stage after 65 hours respectively (Figure 4.6a). Remarkably, in transgenic animals expressing either hIAPP or S20G IAPP, 74.3% (± 4.3) and 36.8% (± 3.3) of animals reached adult stage, a significant decrease compared with wild type (N2) animals (Figure 4.6a). This was consistent with the previous literature implicating hIAPP expression in developmental toxicity (Rosas et al., 2016), and further confirms the toxic nature of S20G IAPP *in vivo*. Further, as a stronger phenotype was demonstrated in S20G IAPP-expressing animals, this could provide a link between its *in vitro* amyloidogenicity and the toxicity it exerts *in vivo*.

As a developmental delay was observed in IAPP-expressing animals, it was next questioned whether the disease models also displayed differences in lifespan. To measure lifespan, the survival of animals was monitored every other day from L4 stage until death. Wild type (N2) animals had a maximal lifespan of 37 days (Figure 4.6b and 4.6c), and a mean lifespan of 18.7 ±0.6. Expression of the marker control (MC) in animals did not significantly affect the lifespan, where a mean lifespan of 17.6 ±0.5 was observed in the population (Figure 4.6d). Consistent with previous results showing expression of rat IAPP has no effect on development, no significant effect on the mean lifespan was observed in rat IAPP-expressing animals (18.5 ±0.8) compared with wild type (N2) animals (Figure 4.6c). Expression of either hIAPP or S20G IAPP in animals correlated with a decreased mean lifespan, where animals on average lived for 13.7 ±0.4 and 15.3 ±0.6 days respectively (Figure 4.6c). Together these results suggest that expression of either hIAPP or S20G IAPP reduced the mean lifespan. The phenotypes in development and the reduced lifespan observed in hIAPP- and S20G IAPP-expressing animals could represent toxic damage caused by the aggregation of amyloid species in these models.

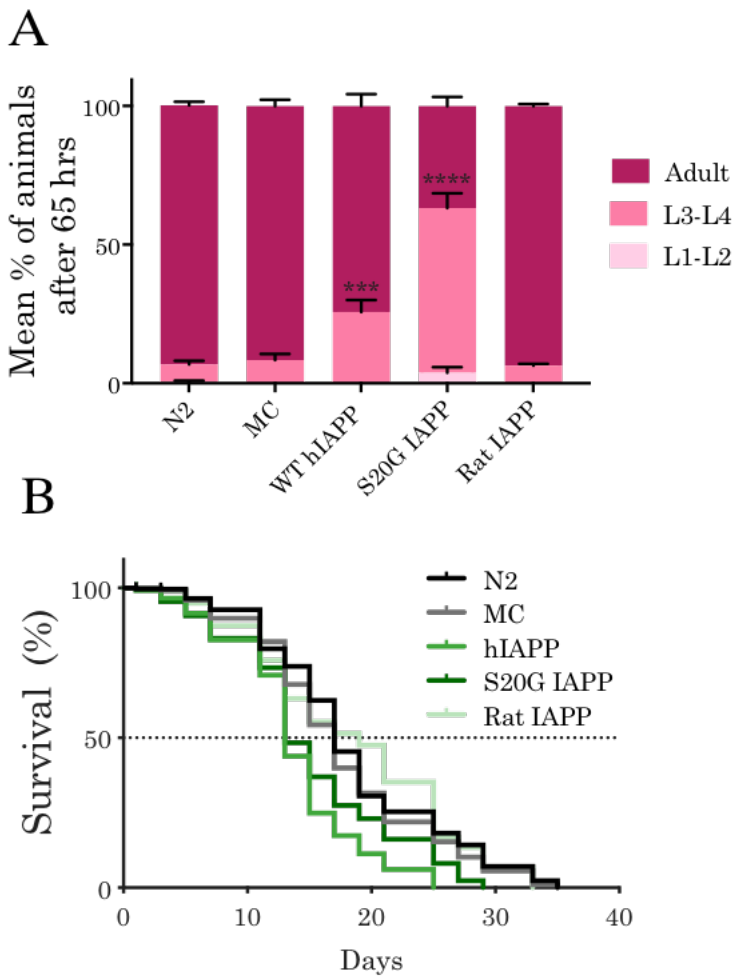

C

	Mean		Age in days at % mortality					P-value
	Days	S.E.	25%	50%	75%	90%	100%	
N2	18.70	0.58	13.00	17.00	25.00	29.00	37.00	
MC	17.55	0.53	13.00	17.00	21.00	27.00	33.00	0.1105
hIAPP	13.66	0.39	11.00	13.00	15.00	21.00	25.00	>0.0005
S20G IAPP	15.25	0.56	11.00	13.00	19.00	25.00	29.00	>0.0005
Rat IAPP	18.52	0.77	13.00	19.00	25.00	29.00	33.00	0.6384

Figure 4.6 Developmental phenotypes of IAPP-expressing *C. elegans* strains.
A) Development of hIAPP, S20G IAPP and rat IAPP -expressing transgenic nematodes compared with wild type (N2) and marker control (MC) nematodes 65 hours after eggs have been laid. Data is expressed as the percentage of total nematodes on the plate at each developmental stage. Three independent experiments were performed (n=100 animals per experiment). **p<0.005 ***p<0.001 B) Survival curves of wildtype (N2), marker control (MC), hIAPP, S20G IAPP and rat IAPP transgenic *C. elegans*. Adults were placed on seeded OP50-1 plates from L4 stage, cultured at 20°C and transferred every other day. Survival rate was scored and expressed as percentage survival. Plots are representative of three independent experiments (n=80). C) Mean lifespan of wildtype (N2), marker control (MC), hIAPP, S20G IAPP and rat IAPP transgenic *C. elegans*. Data from B) was analysed using OASIS 2 (Han et al., 2016) and mean lifespan, standard error and age in days at 35%, 50%, 75%, 90% and 100% mortality is displayed. P-value displayed is in comparison with wild type (N2) strain.

4.5.6 Expression of hIAPP or S20G IAPP but not rat IAPP affects locomotion in *C. elegans*

Because all hIAPP variants are expressed in the body wall muscle, an obvious phenotype of toxic damage could be disruption to the locomotory action of the animals. To explore this further, animals were monitored for 8 days and the paralysis was recorded. Wild type (N2) animals were observed to paralyse starting at day 4 of adulthood, and by day 8 of adulthood ~17% of animals were paralysed (Figure 4.7a). Similarly, expression of the marker control (MC) or the non-amyloidogenic variant rat IAPP in animals did not significantly affect paralysis compared with wild type (N2) animals, where ~17% of animals were paralysed at day 8 of adulthood (Figure 4.7a). Expression of the hIAPP transgene led to an increased paralysis at day 8 of adulthood, where ~29% of animals were paralysed (Figure 4.7a). Likewise, the expression of S20G IAPP affected paralysis compared with wild type (N2) animals, as animals started paralysing two days earlier, and ~32% of animals were paralysed after 8 days of adulthood (Figure 4.7a). The paralysis observed in hIAPP- and S20G IAPP-expressing animals is indicative of toxic damage to muscle cells.

The locomotion of animals was further explored using thrashing assays which record the frequency of body bends an animal performs in liquid. The thrashing rate was recorded at day 1 and day 8 of adulthood in order to assess any age-related consequence of IAPP expression. In wild type (N2) animals, a thrashing rate of 1.11 ±0.05 body bends per second (BBPS) was recorded at day 1 of adulthood which decreased to 0.90 ±0.05 BBPS at day 8 of adulthood (Figure 4.7b). Expression of the marker control (MC) did not significantly affect the motility of animals compared with wild type (N2) and a thrashing rate of 1.21 ±0.07 BBPS was observed at day 1 and 0.88 ±0.07 BBPS at day 8 (Figure 4.7b). Likewise, the expression of rat IAPP had no significant effect on motility, where 1.15 ±0.07 BBPS at day 1 and 0.85 ±0.08 BBPS at day 8 of adulthood was recorded (Figure 4.7b). Expression of hIAPP in *C. elegans* did not significantly affect the thrashing rate of animals at day 1 of adulthood (1.19 ±0.07 BBPS) compared with wild type (N2) nematodes; however, at day 8 of adulthood the thrashing rate was significantly decreased (0.57 ±0.08 BBPS) compared with wild type (N2) animals (Figure 4.7b). Intriguingly, the expression of S20G IAPP affected the thrashing rate of animals at day 1 and day 8 of adulthood, where a thrashing rate of 0.92 ±0.03 BBPS at day 1 and 0.51 ±0.07 BBPS at day 8 of adulthood was observed (Figure 4.7b). Combined, these results demonstrate the toxicity associated with the expression of WT hIAPP and S20G IAPP in *C. elegans*.

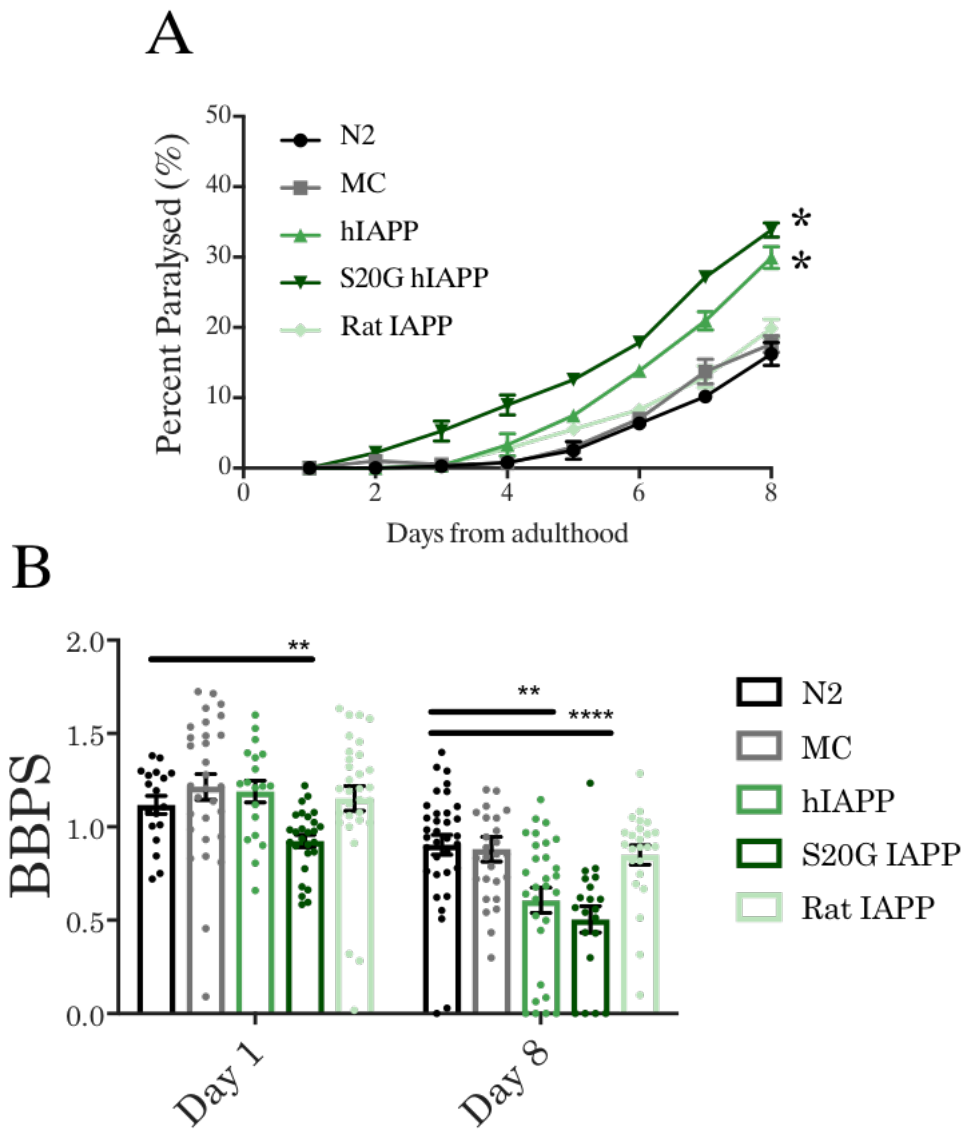

Figure 4.7 Locomotion phenotypes of IAPP-expressing *C. elegans* strains.
A) Paralysis assays of *C. elegans* expressing either hIAPP, S20G IAPP, rat IAPP or the marker control (MC) compared with wild type (N2) animals at 20°C. Paralysis data represents the SEM of 3 independent biological repeats (n=100 animals). Statistical significance was determined using the Wilcoxon matched-paired signed rank test. * $p<0.05$ B) Thrashing rates of wild type (N2), marker control (MC), hIAPP, S20G IAPP and rat IAPP transgenic *C. elegans* at day 1 and day 8 of adulthood. Data represents the number of full body bends per second (BBPS) in M9 (n=30 animals). Data is given as a mean of the number of body bends per second ±SEM. A student's t test was used to assess significance: **$p<0.01$, ***$p<0.005$

4.5.7 Expression of hIAPP and S20G IAPP but not rat IAPP impairs *C. elegans* thermotolerance

In order to cope with external stressors, organisms have developed specialised defence pathways which become transcriptionally activated during times of stress. Of these, the heat shock response mitigates against the increased protein misfolding and aggregation that occurs under environmental stress such as increased temperature. To understand the effect of IAPP expression on the ability of *C. elegans* to cope with thermal stress, survival assays were performed under heat stress conditions of 35°C for 6 hours. Wild type (N2) animals display a 30% (± 2.8) survival rate after a 6-hour heat shock (Figure 4.8). Both expression of the marker control (MC), or the non-amyloidogenic rat IAPP had no significant effect on survival, where survival rates were 27% (± 0.5) and 27% (± 2.3) respectively (Figure 4.8). Expression of the hIAPP however, correlated with a decrease in heat stress survival to 20% (± 1.7) (Figure 4.8). Moreover, *C. elegans* expressing the highly amyloidogenic variant S20G displayed a significantly decreased survival rate, where just 11% (±1.4) of animals survived the 6-hour heat shock (Figure 4.8). Concurrent with the developmental and motility phenotypes in both hIAPP- and S20G IAPP-expressing animals, these results suggest that expression of these amyloidogenic proteins cause toxic damage *in vivo*.

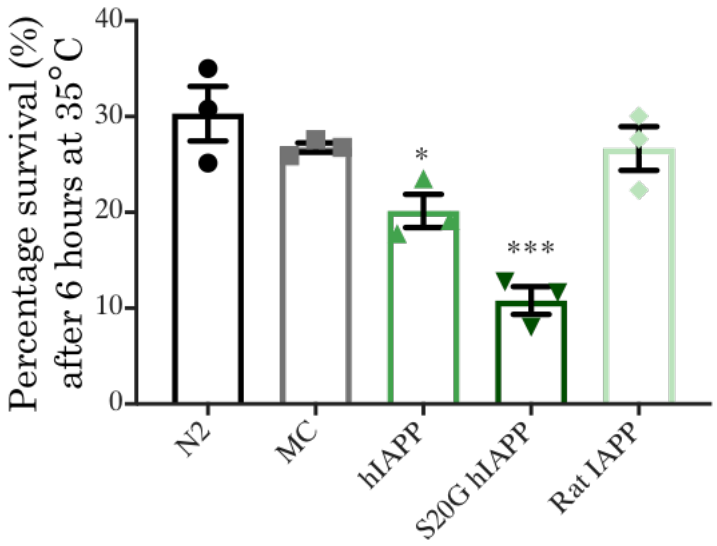

Figure 4.8 Animals expressing amyloidogenic IAPP are thermosensitive.
Survival rates of wild type (N2), marker control (MC), hIAPP, S20G IAPP and rat IAPP strains after thermal stress. Day 1 adults were placed onto seeded OP50-1 and incubated at 35°C for 6 hours. Animals were left to recover for 16 hours and scored for survival. Three independent experiments were performed (n=50 animals per experiment). A student's t test was used to assess significance *p<0.01 ***p<0.001

4.5.8 Expression of hIAPP, S20G IAPP and rat IAPP impairs *C. elegans* ER stress survival

As expression of either the wild type or S20G variant of IAPP affected the ability of the animals to cope with heat stress, it was next questioned whether the expression of these proteins could also affect other stress response pathways. As IAPP is a pro-hormone that is post-translationally modified throughout the ER secretory pathway in order to generate the mature 37 amino acid IAPP protein (Raimundo et al., 2020) the ER stress response could be affected. Several studies have linked the trafficking of IAPP through the ER with the early amyloid formation and toxicity (Raleigh et al., 2017). In particular, proIAPP can form amyloidogenic species and aggregates in the ER and so cause cellular damage (Exley et al., 2010; Paulsson et al., 2006; Paulsson and Westermark, 2005). To investigate whether expression of hIAPP, S20G IAPP and rat IAPP affects the ER stress response, the transgenic animals were exposed to tunicamycin. Tunicamycin is a glycosylation inhibitor that perturbs protein folding in the ER and elicits an ER stress response (Harding et al., 2003). Animals were treated with 50 µg/mL tunicamycin cultures for either 6 or 10 hours and the survival of the animals was scored. The control strains N2 and MC displayed similar survival response to tunicamycin, with 86.3% (± 0.9) and 87.4% (± 2.4) survival after 6 hours of treatment and 81.6% (± 1.2) and 80.2% (±4.4) survival after 10 hours treatment (Figure 4.9a). After 6 hours of treatment, hIAPP (79.9% ±2.8) and rat IAPP (86.1% ±2.6) expressing nematodes displayed similar survival rates to the control strains; however, strains expressing S20G IAPP displayed a small but significant decrease in the percentage of animals surviving treatment with 75.8% (±1.1) survival (Figure 4.9a). When hIAPP, S20G IAPP and rat IAPP were treated with tunicamycin for a longer period of time (10 hours), all three IAPP variant strains displayed significantly reduced ER stress survival compared with the wild type (N2) strain of 44.7% (±4.6), 50.9% (±5.9) and 50.2% (±5.9) respectively. This impairment in ER stress survival suggests that these proteins could be impairing the ER stress response.

As an ER stress response phenotype was observed in all IAPP variant expressing strains, it was next questioned whether this could be linked to reduced chaperone expression in the ER. The ER Hsp70 BiP homolog, *hsp-4*, is upregulated upon ER stress in an IRE-1 and XBP-1 dependent manner (Taylor and Dillin, 2013). The mRNA levels of *hsp-4* were measured using quantitative RT-PCR at both basal levels and under ER stress conditions and analysed relative to basal *hsp-4* wild type (N2) levels (Figure 4.10b and 4.10c). During normal growth conditions, the marker control strain (MC) expressed *hsp-4* levels

(0.95±0.09) similar to wild type animals (N2) (Figure 4.9b). When tunicamycin was applied to both the wild type (N2) and marker control (MC) strains, a significant upregulation of *hsp-4* to 2.73 (±0.53) and 2.49 (±0.41) was observed respectively (Figure 4.9c). Although basal *hsp-4* levels of hIAPP (0.87 ±0.15) were not significantly different compared with wild type (N2) levels, upon treatment with tunicamycin *hsp-4* levels (1.02 ±0.09) did not significantly increase. Basal levels of *hsp-4* transcripts in S20G IAPP expressing nematodes were significantly reduced (0.74 ±0.08) compared with the control strain and did not significantly increase upon ER stress (0.74 ±0.20) (Figure 4.9c). Expression of the non-amyloidogenic rat IAPP did not affect basal *hsp-4* levels (0.99 ±0.02) compared with wild type strain or significantly affect *hsp-4* levels when ER stress was applied (1.90 ±0.23). This suggests that the ER chaperone response in hIAPP- and S20G IAPP-expressing strains could be impaired.

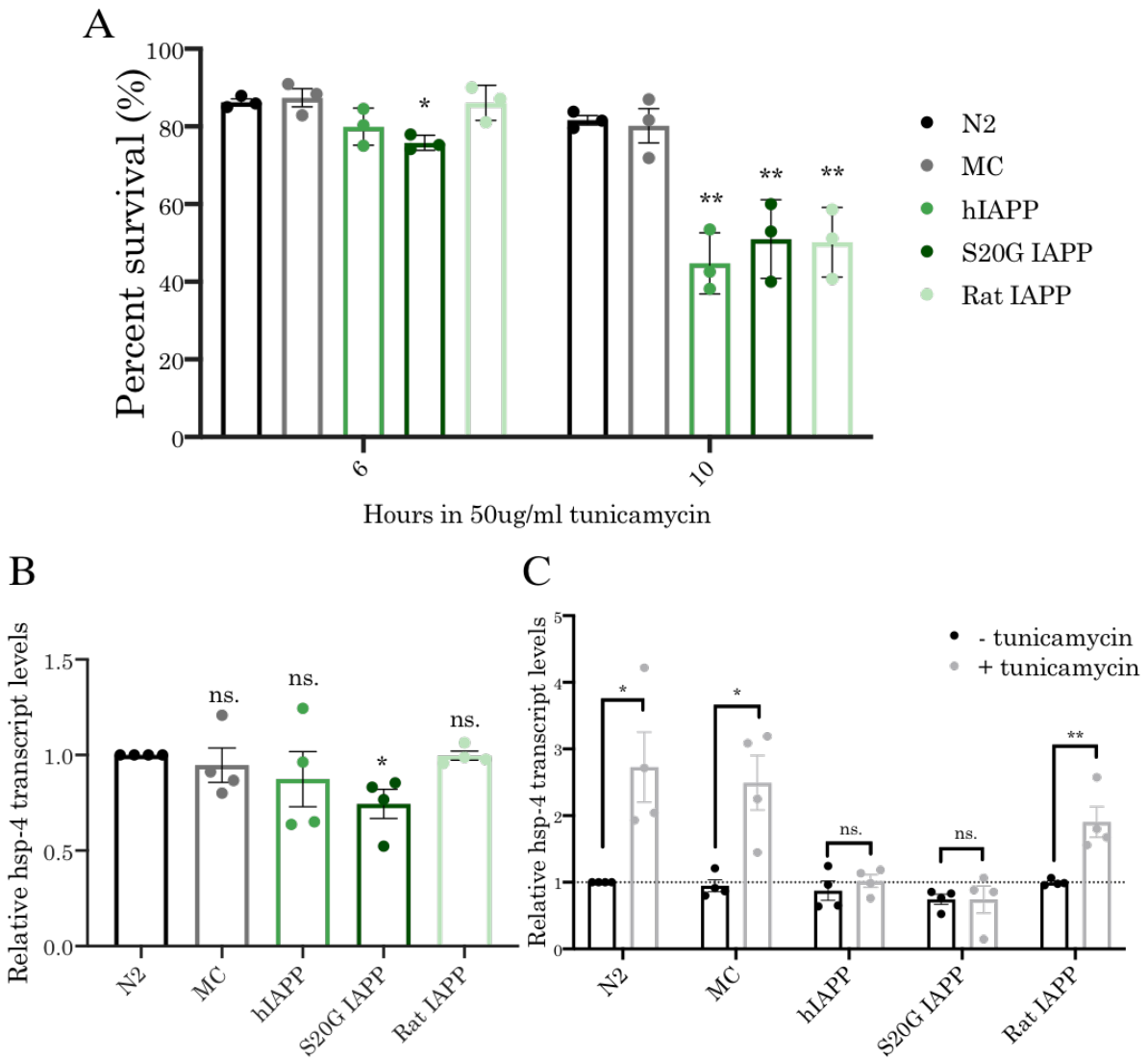

Figure 4.9 Animals expressing amyloidogenic IAPP have a reduced survival under ER stress.

A) Survival rates of wild type (N2), marker control (MC), hIAPP, S20G IAPP and rat IAPP strains after 6- and 10-hours ER stress. Day 1 adults were incubated in 50 µg/mL tunicamycin for either 6 or 10 hours then recovered on plates for 16 hours, and survival was scored. Three independent experiments were performed (n=40 animals per experiment). Error bars represent mean ±SEM. B) Transcript levels of *hsp-4* in day 1 adult marker control (MC), hIAPP, S20G IAPP and rat IAPP transgenic *C. elegans* compared with wild type (N2). Levels were measured through quantitative RT-PCR and are given relative to transcript levels in N2 animals, with error bars indicating mean ±SEM. Three independent experiments were performed. C) Transcript levels for *hsp-4* with (+) or without (-) tunicamycin treatment in day 1 adult marker control (MC), hIAPP, S20G IAPP and rat IAPP transgenic *C. elegans* compared with wild type (N2). Day 1 adult animals were incubated in 5 µg/mL tunicamycin cultures for 2 hours, RNA was extracted, and quantitative RT-PCR was performed. Transcript levels shown are relative to N2 animals, with error bars indicating mean ±SEM. Three independent experiments were performed. Experiments were performed and data are displayed as in B). A student's t test was used to assess all significance: *p<0.05 **p<0.001 ns. = not significant

4.5.9 The effect of co-expression of different amyloidogenic proteins in *C. elegans*

The cross-seeding capability between different amyloidogenic proteins has been demonstrated in several instances (Chaudhuri et al., 2019; Dubey et al., 2014; Sarell et al., 2013a) . Heterologous cross-seeding has be reported to occur between amyloid-β (Aβ) and IAPP (O'Nuallain et al., 2004; Oskarsson et al., 2015), Aβ and prion protein (PrP) (Morales et al., 2010) and Aβ and α-synuclein (Köppen et al., 2020). Furthermore, more amyloidogenic variants of proteins have been shown to induce higher aggregation rates in less amyloidogenic variants through cross-seeding, as shown through the increase in rat IAPP amyloidogenicity when S20G is incubated with it (Young et al., 2017). Co-expression studies of amyloidogenic proteins in *C. elegans* are limited, and therefore we sought to explore this phenomenon further by co-expressing IAPP with other amyloidogenic variants.

4.5.10 Co-expression of the amyloidogenic proteins hIAPP and $A\beta_{1-42}$ in the same tissue of *C. elegans* affects the paralysis of animals

The interaction between the amyloidogenic disease related proteins IAPP and Amyloid-β has been proposed to aid in the progression of disease in Alzheimer's patients (Raimundo et al., 2020). To further investigate this interaction, hIAPP-expressing strains were genetically crossed into an $A\beta_{1-42}$-expressing transgenic *C. elegans* model, GMC101 (Figure 4.10a). When transferred to the permissive temperature of 25°C at L4 stage (day 0), animals expressing $A\beta_{1-42}$ display age-dependent paralysis, where ~80% of animals are paralysed after 3 days (Figure 4.10b). Comparatively, under these conditions wild type (N2) animals are not observed to paralyse, where on average 3% of animals are paralysed after 3 days at 25°C (Figure 4.10b). Transgenic IAPP- or S20G IAPP-expressing animals were also observed to induce a paralysis phenotype – although to a lesser extent than $A\beta_{1-42}$-expressing animals – where on average 25% of animals were paralysed after day 3 at 25°C (Figure 4.10b). Remarkably, co-expression of both $A\beta_{1-42}$ and either hIAPP or S20G ameliorated paralysis associated with $A\beta_{1-42}$ toxicity, resulting in 40% animals paralysed at day 3 of adulthood (Figure 4.10b).

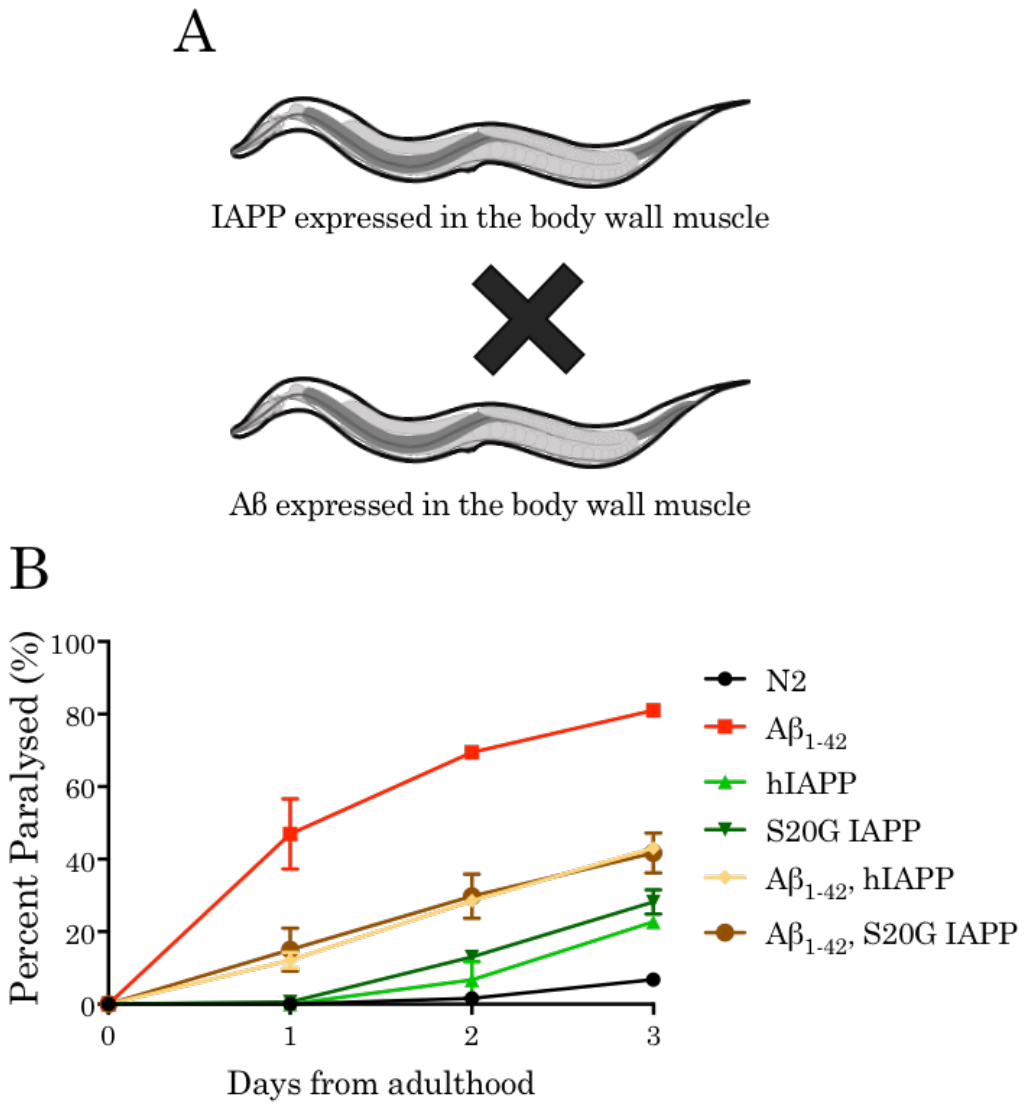

Figure 4.10 hIAPP and Aβ co-expression in the body wall muscle of *C. elegans* reduces the paralysis associated with the Alzheimer's disease model.
A) Graphical representation of the Aß, IAPP cross. hIAPP or S20G IAPP was crossed into the Alzheimer's $A\beta_{1-42}$ disease model (GMC101), where both Aß and IAPP are expressed in the body wall muscles of animals. B) Paralysis assays of *C. elegans* expressing either Aß; hIAPP; S20G IAPP; Aß, hIAPP; Aß, S20G or wildtype (N2) animals at 25°C. Animals were shifted to 25 °C at L4 stage and the number of paralysed nematodes was recorded every day for 3 days. Paralysis data represents the mean ±SEM of 3 independent biological repeats (n=100 animals).

4.5.11 Co-expression of the amyloidogenic proteins hIAPP and Q35-YFP in the same tissue of *C. elegans* affects the aggregation of Q35-YFP protein

The specificity of the beneficial effect of hIAPP was next questioned on another amyloidogenic *C. elegans* disease model. The Huntington's Disease model expressing the expanded polyglutamine chain Q35 tagged with a yellow fluorescent protein (Q35-YFP) has been utilised as a proteostasis sensor in studies before (Gidalevitz et al., 2006). Expression of the Q35-YFP in the body wall muscle of the animal leads to an age-dependent aggregation of fluorescent YFP foci which can be quantified (Morley et al., 2002). Therefore, the hIAPP-expressing transgenic model was crossed into the Q35-YFP body wall muscle disease model, AM167 (Figure 4.11a). The number of YFP foci was monitored in the animals every day for 5 days post vulval development. Animals expressing Q35-YFP were observed to have rapid aggregation and formation of foci, where on average 28.1 ±1.2 aggregates were observed at day 2 and 51.9 ±0.9 aggregates were at day 4 (Figure 4.11b and 14.11c). In comparison, animals expressing both hIAPP and Q35-YFP displayed delayed aggregation progression, where on average 16.9 ±2.1 aggregates were observed in day 2 adults and 41.8 ±1.7 aggregates were observed at day 4 (Figure 4.11b and 4.11c). This suggested that hIAPP expression was delaying Q35-YFP aggregation and could represent a mechanism of suppression. It is important to note however, that the number of aggregates in animals co-expressing Q35-YFP and hIAPP appear to converge with Q35-YFP expressing animals at day 5 (Figure 4.11c). Further experiments are required at later time points beyond day 5 to investigate the aggregation kinetics of animals co-expressing Q35 and hIAPP.

As a delay in aggregation was observed when we co-expressed hIAPP and Q35-YFP, it was next questioned whether this also ameliorated toxicity. To do so, the paralysis of animals over 8 days from the onset of adulthood was assessed. After 6 days, 55% of Q35-YFP expressing animals were paralysed (Figure 4.11d), whereas animals co-expressing hIAPP and Q35-YFP displayed 60% paralysis in a population, and only 40% of animals expressing hIAPP were paralysed at day 6. (Figure 4.11d). Interestingly, no other time points were observed to have a differing percentage of paralysed animals. Our results suggest that co-expression of hIAPP with other amyloidogenic proteins could ameliorate aggregation and toxicity associated with those models. It would therefore be interesting to further dissect this mechanism further and demonstrate whether disruption in aggregation is caused by direct protein aggregation or an indirect cellular response.

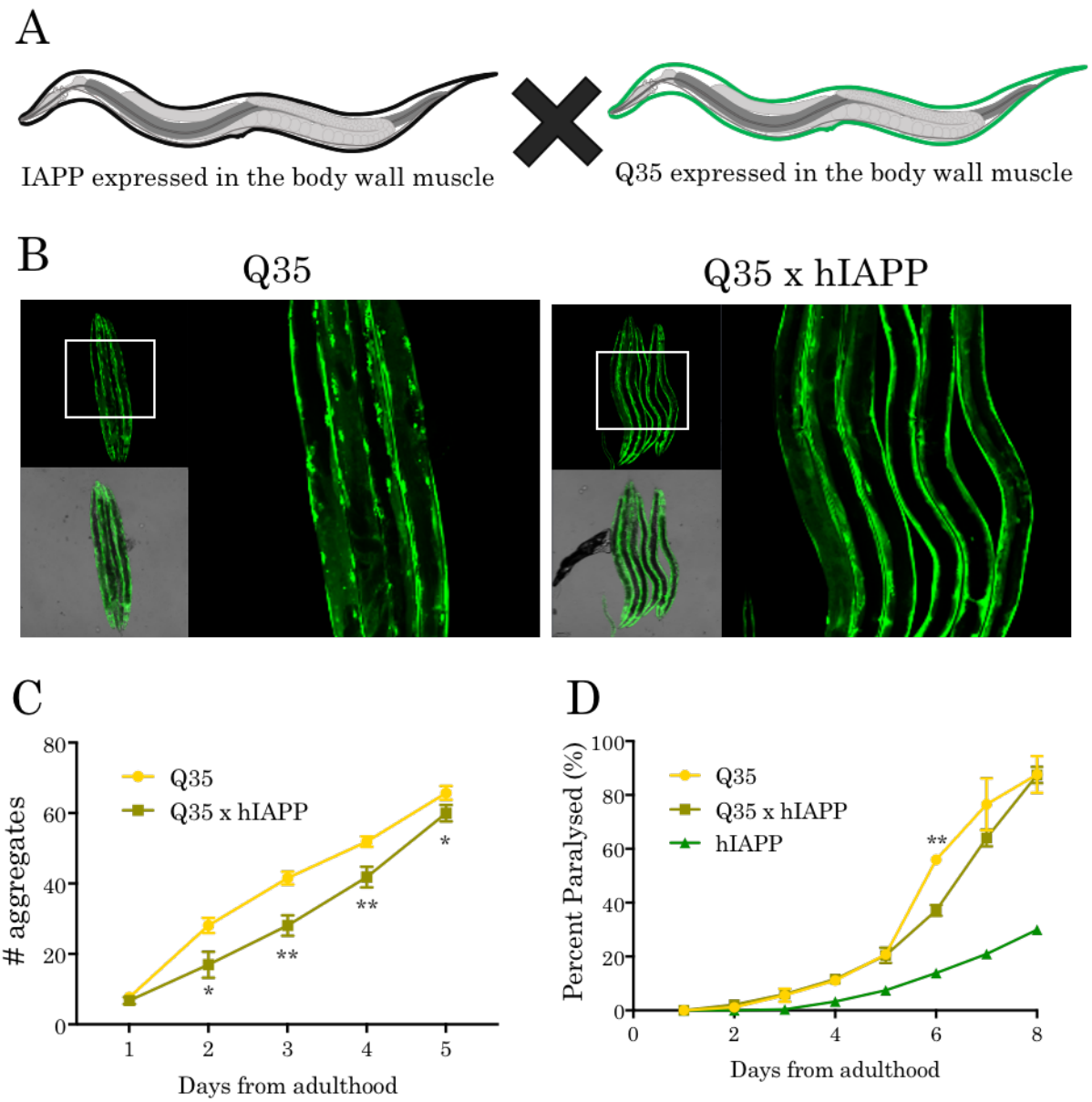

Figure 4.11 hIAPP and Q35 co-expression in the body wall muscle of *C. elegans* reduces the aggregation of Q35-YFP foci and paralysis associated with a Q35 disease model.
A) Graphical representation of the Q35, IAPP cross. hIAPP or S20G IAPP was crossed into the Huntington's Q35 disease model, where Q35 is expressed in the body wall muscles of animals and tagged with YFP. B) Representative confocal images of day 2 adult Q35, hIAPP and Q35 strains. Images were taken on the LSM880 Zeiss microscope using the YFP parameters. C) Quantification of accumulated Q35-YFP in age-synchronised Q35 or Q35, hIAPP animals. The number of Q35-YFP foci was recorded every day from day 1 until day 5 of adulthood. The data represents three independent experiments (n=20 per experiment ±SEM. *p<0.05 **p<0.01 D) Paralysis assays of *C. elegans* expressing either Q35, hIAPP or co-expressing hIAPP and Q35 at 20°C. Paralysis data represents the SEM of 3 independent biological repeats (n=100 animals). **p<0.01

4.6 Discussion

Research in this chapter detailed the generation and characterisation of a new *C. elegans* type 2 diabetes disease model expressing different variants of IAPP including hIAPP, S20G and rat IAPP. Using phenotypic readouts such as motility, development, lifespan and heat stress, I demonstrated that the amyloidogenicity of each variant *in vitro* correlates with toxic effects *in vivo*. Specifically, expression of the highly amyloidogenic variant S20G conferred to greater defects in motility, thermotolerance and development compared with hIAPP. Moreover, expression of the non-amyloidogenic variant rat IAPP was not observed to have little effect on the behavioural phenotypes analysed. This was in line with previous research demonstrating the high amyloidogenicity of the S20G variant (Sakagashira et al., 2000), while the rat IAPP variant does not aggregate or induce toxic damage (Cao et al., 2010). This study further adds to the increasing evidence that the aggregation of proteins into amyloid species induces toxic damage, where the faster a protein aggregates, the more toxic damage is observed.

4.6.1 Expression of hIAPP and S20G IAPP in animals may correlate to increased aggregation

The expression of toxic amyloidogenic protein has been proposed to interact with and impair the proteostasis network (PN) within cells (Hipp et al., 2019). As amyloidogenic proteins can aggregate readily, it has been suggested that this aggregation can overwhelm the PN and sequester away components from the folding of endogenous proteins (Gidalevitz et al., 2006), or impair vital protein degradation pathways (Bennett et al., 2007; Kristiansen et al., 2007; Park et al., 2013). The expression of S20G IAPP in *C. elegans* was shown to correlate with increased protein in the insoluble fraction of aged animals (Figure 4.4). As organisms age, the protein quality network becomes compromised and declines (Ben-Zvi et al., 2009; Walther et al., 2015). The data presented here suggests that expression of the S20G IAPP mutant could exacerbate this decline and cause aberrant folding and widespread proteome aggregation in *C. elegans*. Expression of wild type hIAPP, however, did not affect global protein aggregation in the nematodes, and suggests that the S20G variant might be more amyloidogenic *in vivo* and so replicate the highly amyloidogenic nature of S20G observed previously *in vitro* (Meier et al., 2016; Sakagashira et al., 2000).

It was also noted that the expression of hIAPP in *C. elegans* models coincided with the presence of X-34 positive foci in the head region of the nematodes, indicating the formation of amyloid fibres (Figure 4.5). This is consistent with aggregated foci observed in a previous *C. elegans* model expressing proIAPP tagged with YFP in various tissues of the animal (Rosas et al., 2016). However, although we observed the presence of amyloid deposits in our model, it would be interesting to also analyse the amount of oligomeric species in the animals. Oligomers can be detected by western blot analysis using antibodies specific against amyloid oligomers (such as A11), or dyes that bind to a wider range of amyloid species encompassing oligomeric species. Moreover, it would be interesting to extract the IAPP amyloid deposits from these models (by generating nematode extracts) and analyse their *in vitro* aggregation properties, seeding potential and structure compared with *in vitro* or *ex vivo* fibrils.

A major pitfall in the IAPP disease models presented in this chapter is that IAPP protein could not be detected using a western blot (Figure 4.4). Attempts were made to optimise this protocol; however, the anti IAPP antibody used could not detect synthetic IAPP at relevant concentrations. This might be due to denaturation of the protein in the gels, which could modify the structure and effect binding capabilities of the antibody. Despite these negative results, some signal was detected surrounding the vulva muscles when immunostaining was performed on the animals, indicating the protein is present in the animals (Figure 4.5a). However, as this was localised to the vulva muscle region it poses further questions: is expression of IAPP protein vulval specific or is incomplete immunostaining occurring? To address this, further investigation using different antibodies or alternative techniques are required.

Furthermore, the processing and secretion of preproIAPP in the models needs to be assessed. Although some deposits were observed in the head region of the animal (Figure 4.5), a number of questions still remain surrounding the secretion and processing of the prohormone. The construct for IAPP expression was designed to include both the human signal peptide sequence and the pro region of the IAPP variant in order to replicate the natural processing of the protein. IAPP is normally directed to the secretory pathway via it's signal peptide that is cleaved upon entry to the endoplasmic reticulum (ER) (Paulsson and Westermark, 2005). In the ER proIAPP undergoes processing by the prohormone convertases PC1/3 and PC2, followed by modifications by carboxypeptidase E (CPE) and PAM to generate an amidated C-terminus (Chen et al., 2018). In *C. elegans*, there are four

proprotein convertase genes, of which *egl-3* encodes a PC2-like convertase (Kass et al., 2001). In addition, carboxypeptidase E is also expressed by the *egl-21* gene (Jacob and Kaplan, 2003). However, although abundantly expressed in the neurons of the animal, these are expressed relatively low in the body wall muscle (Jacob and Kaplan, 2003). Therefore, cleavage of proIAPP into mature IAPP may not occur in our model and needs further investigation to resolve. Nevertheless, the study of proIAPP aggregation is still important as the aggregation of proIAPP in the secretory pathway has been proposed to initiate toxic damage in T2DM disease progression (Paulsson et al., 2006). ProIAPP has been identified in intracellular fibrils of IAPP. The accumulation of unprocessed proIAPP in β-cells overwhelms the ER and generates a forward feed-back cycle that promotes oligomerisation, fibril formation and β-cell injury (Paulsson et al., 2006). Cells lacking PC1/3 and PC2 increased amyloid deposition and cell death (Marzban et al., 2006). Together this corroborates the idea that unprocessed proIAPP is important in disease progression.

4.6.2 Expression of IAPP in *C. elegans* causes both cell autonomous and cell non autonomous toxicity

In the models generated in this study, expression of hIAPP and S20G led to a developmental delay. This was consistent with a previously generated *C. elegans* IAPP disease model, where expression of proIAPP tagged with YFP caused a growth retardation phenotype (Rosas et al., 2016). This phenotype may represent cell non autonomous toxicity of IAPP in our model, whereby expression of IAPP in one tissue causes systemic toxicity by affecting multiple cellular processes involved in development. Questions still remain on whether this cell non autonomous toxicity is due to signalling triggered by aggregation of the protein in the muscle cells, or by extracellular protein aggregation that could potentially damage other tissues. As discussed earlier, further experiments are needed to fully understand the secretion of IAPP in the models, enabling conclusions to be drawn about the mechanisms of toxicity.

It was unsurprising that a reduction in motility was observed in animals expressing IAPP (Figure 4.7) variant given that they were engineered to express the aggregation-prone protein in the muscle cells of the animal. Toxicity observed could be due to the interaction of IAPP species with components of the proteostasis network in the muscle cell. Amyloid fibrils are known to sequester away molecular chaperones, which function to prevent the misfolding or refolding of these fibrils (Olzscha et al., 2011). Reduced chaperone function

in muscle cells affects the stability of myosin fibres leading to reduced muscle function (Barral et al., 2002; Frumkin et al., 2014) which could explain the toxic damage caused by hIAPP and S20G expression. This is further exemplified by the rat IAPP strain, where no reduction in locomotory action was observed in animals suggesting there was no toxic damage resulting from expression of the non-amyloidogenic variant. This indicates that it is the amyloidogenic potential of hIAPP and S20G variants that is causing the phenotypes observed. It would therefore be interesting to further investigate the myosin fibres in the disease models, staining of the myosin fibres using dyes such as phalloidin can detect any disruptions to the myosin fibre pattern (Gaiser et al., 2011). This could further demonstrate toxic damage in the cells.

4.6.3 Stress responses may be compromised in IAPP expressing *C. elegans* models

In this chapter, expression of either S20G or hIAPP in *C. elegans* was demonstrated to decrease the thermo stress survival capability of the animal. This could indicate that the proteostasis network (PN) in the animals is impaired. The heat shock response (HSR) is responsible for maintaining the cytoplasmic cellular proteome, and is coordinated by the action of the master regulator heat shock factor 1 (HSF-1) (Abravaya et al., 1992; Nadeau et al., 1993). Environmental stressors such as heat promote protein misfolding, engaging activity of the chaperones HSP-90 and HSP-70 to restore proteins to their native structures (Hipp et al., 2014). The presence of additional aggregation-prone proteins hIAPP and S20G in the models presented in this chapter could be further overwhelming the balance of the proteostasis network under heat stress. Thus, this could possibly explain the decrease in survival observed during heat stress conditions. Further experiments to investigate the response of the proteostasis network are required to gain insight into the molecular mechanisms behind this phenotype. This includes exploring the expression levels of chaperones such as HSP-90 and HSP-70, as well as the effect knockdown of key components of the PN such as HSF-1 has on survival.

This chapter also explored the effect of expression of IAPP variants in *C. elegans* on the UPR^{ER} and demonstrated that expression of hIAPP, S20G IAPP or rat IAPP led to reduced survival under ER stress conditions (Figure 4.9). These results could indicate that hIAPP, S20G IAPP and rat IAPP in the generated transgenic strains are being directed to the ER secretory pathway and affected the stress response pathways there. It was particularly interesting to note that the expression of rat IAPP confers to reduced survival under ER

stress as rat IAPP expression did not correlate with any other phenotypes in the animal. While rat IAPP cannot form into amyloid fibrils, it – like the majority of proteins - has the propensity to aggregate, and this aggregation could explain the phenotype observed. As well as the reduction in ER stress survival of hIAPP and S20G IAPP expressing animals under tunicamycin treatment, an inhibition of *hsp-4* upregulation was observed in these animals as well, suggesting an impairment of the UPR^{ER}. IAPP and ER stress have an established relationship; the accumulation of proIAPP into fibrils has been observed in the secretory pathway where intracellular aggregates have been observed (Paulsson et al., 2006). As previously discussed, a drawback of the data presented in this chapter was the unknown localisation of IAPP within the animal. The ER stress phenotype could indicate that IAPP is not being processed and secreted as normal in our model, instead accumulating in the ER and affecting the stress response pathway there. Future experiments to address the localisation of IAPP in the models including different immunostaining and localisation techniques would be useful in order to understand this phenotype further.

4.6.4 Co-expression of hIAPP with other amyloidogenic protein reduces aggregation in *C. elegans*

Although primarily associated with T2DM, numerous studies have also implicated hIAPP in the progression of Alzheimer's Disease (AD). The literature shows a complicated relationship between expression and aggregation of hIAPP and amyloid plaques formed in AD. In this study, co-expression of hIAPP and $A\beta_{1-42}$ in muscle cells reduced paralysis compared with animals expressing $A\beta_{3-42}$ only (Figure 4.10). This was particularly interesting as a range of clinical studies have implicated high levels of IAPP, or IAPP gene polymorphisms to increase the incidence of AD (Jackson et al., 2013; Zhu et al., 2019).

This chapter demonstrated that hIAPP expression protects animals from $A\beta_{1-42}$– and Q35-associated toxicity. However, it is not clear whether hIAPP directly or indirectly ameliorates the aggregation kinetics of Q35 and/or toxicity of Ab1-42. It is possible that the direct interaction of hIAPP and $A\beta_{1-42}$/Q35 could be delaying aggregation of the proteins. Cross-inhibition of the two proteins could delay the initial nucleation phase of protein aggregation, accounting for the fewer aggregates observed in the Q35 model, and the reduction in paralysis observed in both models. This would be consistent with i*n vitro* studies showing cross-seeding Aβ and hIAPP leads to a delayed initial nucleation stage and an accelerated fibrillisation stage (Hu et al., 2015). However, as the interaction

between IAPP and Q35 has not been explored before, it is unclear whether these two proteins can cross-seed. Experiments including pull-down studies of aggregates are needed to further confirm whether it is indeed direct or indirect consequences of hIAPP expression that is protecting animals against Aβ and Q35 proteo-toxicity.

4.7 Conclusions

To conclude, this study demonstrated that the expression of the amyloidogenic proteins hIAPP or S20G IAPP in *C. elegans* caused toxicity. The toxicity observed here *in vivo* is in accordance with the amyloidogenicity of these variants observed *in vitro*, providing further evidence for the correlation between aggregation and toxicity of these proteins. It was also demonstrated that co-expression of hIAPP could alleviate the toxicity and aggregation associated with an Amyloid-β or Q35 disease model. These observations could provide the basis for future experiments exploring the stress responses associated with amyloidogenic protein expression.

Chapter 5. HSP-90 and Alzheimer's Disease

5.1 Abstract

The interplay of chaperones and protein misfolding is a complex relationship that serves to protect organisms from proteotoxic stress. The metazoan chaperone *hsp-90* has been established to regulate myosin folding in a cell autonomous and cell-non-autonomous manner. Using *C. elegans,* whether this beneficial regulation can also aid against the toxic nature of the Alzheimer's Disease-related protein Amyloid-β (Aβ) was explored. This chapter demonstrates that *hsp-90*, as well as its co-chaperone *sti-1*, can protect against Aβ toxicity. *hsp-90* was further demonstrated to act through cell-non-autonomous signalling via the neurons or intestine to rescue Aβ-associated toxicity in the muscle, and this was coordinated through the GATA zinc-finger transcription factor PQM-1. These results provide further insight into proteostasis dysfunction and could guide potential therapeutic interventions.

5.2 Introduction

Heat shock protein 90 (Hsp90 or HSP-90 in *C. elegans*) is a highly conserved molecular chaperone that is essential for the folding and maintenance of many cellular proteins, including transcription factors, hormone receptors and protein kinases (Zhao et al., 2005). Hsp90 is a homodimeric unit that is composed of three distinct regions (Figure 5.1), a N-terminal domain (NTD) for nucleotide binding, a middle domain (MD) important in client recognition and ATP hydrolysis and a C-terminal domain (CTD), which is required for dimerization (Pearl and Prodromou, 2006). Moreover, the CTD contains a conserved MEEVD sequence that is required for interactions with co-chaperones of the tetratricopeptide repeat (TPR) domain class (Young et al., 1998).

5.2.1 Hsp90 and its co-chaperones

More than 20 co-chaperones interact with Hsp90 in order to facilitate Hsp90 client recognition, binding and biochemical activity (Figure 5.1) (Schmid et al., 2012). STI1/Hop (STI-1 in *C. elegans*) is a Hsp70/Hsp90 co-chaperone that is composed of three TPR domains (TPR1, TPR2A and TPR2B) and two aspartate- and proline- rich domains (DP1 and DP2) (Schmid et al., 2012; Song and Masison, 2005). The multiple TPR domains of

STI1 allow for simultaneous binding of both Hsp90 and Hsp70 and therefore facilitates the successive action of each chaperone to mature client proteins (Taipale et al., 2010). In *C. elegans*, however, the STI1 homolog STI-1 or CeHop (Figure 5.1) contains only the TRP2A-TPR2B-DP2 module and therefore can still bind Hsp70 and Hsp90, but not simultaneously (Gaiser et al., 2009; Song et al., 2009). STI-1 shares approximately 56% sequence identify with human STI1 and is expressed in the pharynx, intestine, nervous system and muscle in all developmental stages (Song et al., 2009). Through the use of a *sti-1 (jh125)* null mutant, STI-1 has also been shown to be important in ageing and the heat stress response in *C. elegans* (Song et al., 2009).

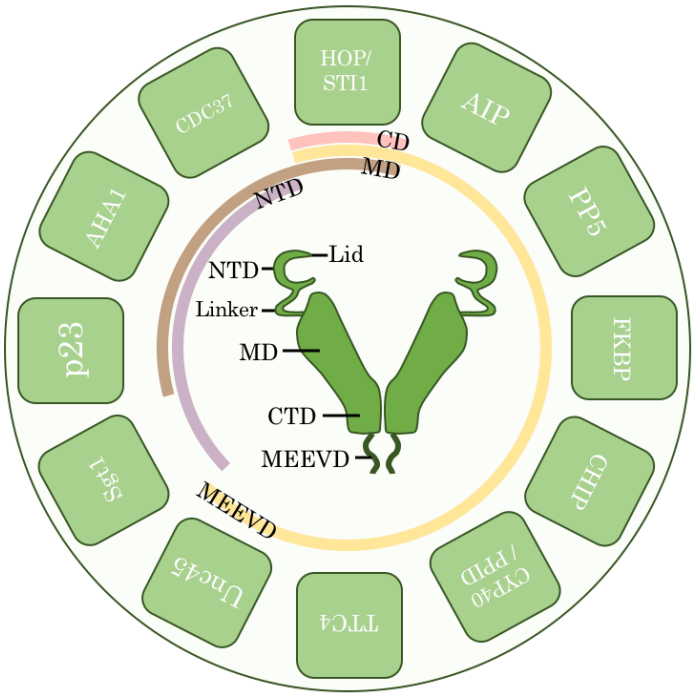

Protein	Human gene	*C. elegans* gene
Hsp90	HSP90AA1, HSP90AB1	*daf-21*
Hop/Sti1	STIP1	*sti-1*
AIP	AIP, AIPL1	C56C10.10
PP5	PPP5C	*pph-5*
FKBPs	FKBP4, FKBP5	*fkb-6*
CHIP	STUB1	*chn-1*
CYP40/PPID	PPID	*cyn-2*
TTC4	TTC4	C17G10.2
Unc45	UNC45A, UNC45B	*unc-45*
Sgt1	SGTA, SGTB, SUGT1	*sgt-1*
P23	PTGES3	ZC395.10
AHA1	AHSA1	C01G10.8
CDC37	CDC37	*cdc-37*

Figure 5.1 HSP-90 and its co-chaperones.
Left. Hsp90 is composed of three domains, the N-terminal Domain (NTD), containing the lid and a linker to the Middle Domain (MD), which connects to the C-terminal Domain (CTD), containing a MEEVD binding sequence for co-chaperone binding. A selection of Hsp90 co-chaperones and the regions they bind to are illustrated. *Right.* Table of Hsp90 and its co-chaperones detailing their corresponding Human genes and *C. elegans* orthologs.

5.2.2 Hsp90 and neurodegenerative disease

Hsp90 has been shown to play diverse roles in many neurodegenerative diseases, including the most common form of dementia, Alzheimer's disease (AD) (Brehme et al., 2014; Chen et al., 2014; Evans et al., 2006; Kakimura et al., 2002; Wang et al., 2017). In AD, two types of protein aggregates form in the brain, extracellular plaques of Amyloid-β

(Aβ) and intraneuronal neurofibrillary tangles (NFT) of the microtubule-associated protein tau (Huang and Mucke, 2012). Analysis of Alzheimer's patients brains uncovered a chaperome subnetwork that is suppressed with ageing and in AD patients, of which Hsp90 and Sti1 were members of a 16 component chaperone "core-network" (Brehme et al., 2014). This core-network was confirmed in both an Alzheimer's and Huntington's *C. elegans* disease model, identifying *hsp-90* (the *C. elegans* Hsp90 ortholog) and *sti-1* amongst others, as genes that control the Aβ-associated motility phenotype observed in animals (Brehme et al., 2014). This research is supported by i*n vitro* studies which demonstrated that Hsp90 can block early stage Aβ self-assembly (Evans et al., 2006). Moreover, Hsp90, as well as Hsp70 and Hsp32, can increase the phagocytotic activity of microglia, and promote the clearance of Aβ peptides (Kakimura et al., 2002). However, balance of this activity is critical, as chronic induction of microglia is a hallmark of AD and contributes to neuronal damage (Wang et al., 2015).

Although Hsp90 has been shown to be directly beneficial to the inhibition and toxicity of Aβ aggregation *in vitro* and in *C. elegans* models, due to the complex nature of the brain and the proteins that Hsp90 affects, downregulation of Hsp90 in AD can stimulate beneficial effects as well. Use of the Hsp90 inhibitors 17-AAG and OS47720 in AD mouse models have been shown to improve synaptic protection and memory loss through the activation of HSF1 and the upregulation of synaptic genes (Chen et al., 2014; Wang et al., 2017).

Although it was not explored in this chapter, it is also worth mentioning that Hsp90 plays a role in the accumulation of tau and other amyloidogenic proteins (Blair et al., 2013; Dickey et al., 2007; Jinwal et al., 2010; Luo et al., 2007; Salminen et al., 2011). Studies have shown that Hsp90 and its co-chaperones regulate tau phosphorylation and dephosphorylation (Salminen et al., 2011). Hsp90 inhibitors in cellular and mouse models of tauopathies have been shown to reduce the toxicity of tau, and reduced the amount of aggregated tau observed (Dickey et al., 2007; Luo et al., 2007). Furthermore, Hsp90 in complex with the co-chaperone FKBP51 protects tau from proteasomal degradation, promoting neurotoxic tau accumulation (Blair et al., 2013; Jinwal et al., 2010).

5.2.3 Sti1 and neurodegenerative disease

The role of Sti1 in neurodegenerative diseases has also been explored before (Ambegaokar and Jackson, 2011; Maciejewski et al., 2016; Ostapchenko et al., 2013; Wolfe et al., 2013). Sti1 plays an important role in the clearance of tau protein, whereby loss-of-function mutations in STI1 in a *Drosophila melanogaster* model of tauopathy triggers the accumulation of tau (Ambegaokar and Jackson, 2011). Further, knockdown of Sti1 in a Huntingtin Q103 yeast model exacerbated toxicity and hindered the packaging of Htt into foci, while elevation of Sti1 suppressed toxicity and promoted the organisation of small Htt103Q foci into larger assemblies, suggesting that Sti1 acts to buffer proteotoxicity through spatial re-organisation (Wolfe et al., 2013).

As well as the critical functionality of Sti1 in Hsp70/Hsp90 machinery, further research on Sti1 has focussed on the extracellular effects of the interaction between Sti1 and the cellular prion protein (PrP^c). PrP^c is anchored to cell membranes by glycosylphosphatidylinositol (GPI) and serves as a molecular scaffold protein, organising signalling complexes (Linden et al., 2008). In order to interact with PrP^c, Sti1 is secreted via exosomes, and can interact with the PrP^c on the surface of neurons, causing effects on cell growth and survival (Hajj et al., 2013). In Alzheimer's disease, PrP^c has been shown to help transmit neurotoxic signals of soluble oligomers of Aβ (AβO) (Ostapchenko et al., 2013), which are well recognised to be toxic to synapses and thought to increase early plaque formation (Ferreira and Klein, 2011). *In vitro* studies have uncovered the ability of Sti1 to inhibit AβO binding to PrP^c, and prevent AβO-induced synaptic loss and death in cultured mouse neurons (Ostapchenko et al., 2013). Interestingly, Hsp90 interaction with Sti1 decreases the PrP^c-dependent STI1 neuroprotection observed, suggesting that Hsp90 may interfere with the interaction between STI1 and PrP^c (Maciejewski et al., 2016).

5.2.4 Transcellular chaperone signalling

In order to preserve proteostasis in multicellular organisms, a coordinated activation of the protective PN components is required. Thus, when cells are stressed in one tissue of the animal, this can trigger a stress signalling response that leads to altered chaperone expression in cells distinct from the stressed sender cell and is known as transcellular chaperone signalling (TCS). Previous research has utilised the nematode *C. elegans* to understand the cell-non-autonomous activity of chaperones across tissues, including the action of ER chaperone XBP-1, and HSP-90 which is explored further in this chapter

(Taylor and Dillin, 2013; Van Oosten-Hawle et al., 2013). HSP-90 expression in the intestine or neurons can suppress misfolding of myosin temperature-sensitive (ts) mutants in the muscle cells of the animals, and was shown to be controlled by the FoxA transcription factor PHA-4 (Van Oosten-Hawle et al., 2013). Following on from this, the GATA-transcription factor PQM-1 and innate immunity-associated transmembrane protein CLEC-41 were shown to be involved in the TCS associated with neuronal HSP-90 expression, and the aspartic protease ASP-12 with the intestinal HSP-90 TCS (O'Brien et al., 2018), of which data presented in this chapter contributed to.

5.3 Aims of this chapter

Chapter 5 aimed to investigate the cell nonautonomous activity of HSP-90 and its co-chaperone STI-1 to protect the roundworm nematode *C. elegans* from Aβ-associated toxicity. Further, I wanted to uncover if HSP-90 could cell-non-autonomously protect *C. elegans* from proteotoxic stress induced from $A\beta_{3\text{-}42}$ expression in the muscle and sought to uncover the signalling molecules that are involved with this process.

5.4 Methods

5.4.1 *C. elegans* strains

Strain name	Genotype
AM986	rmIs 345[*vha-6p::HSP-90::RFP*]
AM987	rmIs 346[*F25B3.3::HSP-90::RFP*]
AM988	rmIs347[*unc-54p::HSP-90::RFP*]
CL2006	dvIs2 [pCL12(*unc-54/human Abeta peptide 1-42 minigene) + pRF4*]
N2 (Bristol)	Wild type
PP11972	*unc-54p::STI-1::GFP*
PVH40	dvIs2 [*pCL12(unc-54p/human Abeta peptide 1-42 minigene) + pRF4*]; *unc-54p::STI-1::GFP*
PVH50	dvIs2 [pCL12(*unc-54p/human Abeta peptide 1-42 minigene) + pRF4]; rmIs347[unc-54p::HSP-90::RFP*]
PVH59	pkIs2386 [*unc-54p::alpha-synuclein::YFP + unc-119(+)]; rmIs347[unc-54p::HSP-90::RFP*]
PVH71	dvIs2 [pCL12(*unc-54p/human Abeta peptide 1-42 minigene) + pRF4]; unc-54p::STI-1::GFP; rmIs347[unc-54p::HSP-90::RFP*]
PVH85	dvIs2 [pCL12(*unc-54/human Abeta peptide 1-42 minigene) + pRF4]; rmIs 346[F25B3.3::HSP-90::RFP*];
PVH86	dvIs2 [pCL12(*unc-54/human Abeta peptide 1-42 minigene) + pRF4]; rmIs 345[vha-6p::HSP-90::RFP*]

Table 5.1 *C. elegans* strains used in Chapter 5 and their genotypes.

5.4.2 RNAi silencing of genes

RNAi plates were made using standard NGM protocol with the addition of 1 mM IPTG and the replacement of streptomycin with 100 µg/mL Ampicillin. Overnight cultures of HT115 containing target RNAi constructs (gifted from Ahringer lab) were made and 1 mM IPTG was added 3 hours before seeding to induce RNAi expression. Plates were seeded with 200 µL of cultures and left to dry for at least a day before use. Animals were placed onto control (L4440) or target RNAi plates at L4 stage and then analysed for paralysis.

For the following methods see the Materials and Methods Chapter:

Paralysis assay Chapter 2.2.4

RT-qPCR Chapter 2.4

5.5 Results

5.5.1 The cell autonomous action of HSP-90 on Aβ-associated toxicity

The *C. elegans* strain CL2006 (*unc-54p*::human $A\beta_{3-42}$) expresses human $A\beta_{3-42}$ in the body wall muscle of the animal which leads to a progressive, age-dependent aggregation resulting in toxicity observed through decreased motility and paralysis (Link, 1995; McColl et al., 2012). Modulation of various PN components have been shown to suppress or exacerbate the Aβ toxicity associated with this *C. elegans* disease model, including HSP-90 and HSP-16.2 (Brehme et al., 2014; Fonte et al., 2008; Muñoz-Lobato et al., 2014; Sorrentino et al., 2017).

In order to explore the relationship between HSP-90 (or DAF-21 in *C. elegans*) expression and the toxicity of Aβ in these models, CL2006 ($A\beta_{3-42}$) was genetically crossed (Chapter 2.1.2) into the HSP-90 body wall muscle overexpression strain AM988 ($HSP\text{-}90^{bwm}$) to generate the strain PVH50 (Aβ; $HSP\text{-}90^{bwm}$). The resulting strain combines both the overexpression of HSP-90 and the expression of $A\beta_{3-42}$ in the same tissue of the animal - the body wall muscle. Animals were assessed for paralysis from the onset of adulthood for 8 days. The overexpression of HSP-90 alone had no effect on the percentage of paralysed animals compared with wildtype (N2) controls (Figure 5.2a). However, the overexpression of HSP-90 in the $A\beta_{3-42}$ model significantly suppressed the associated progressive paralysis observed in the Alzheimer's strain reducing the percentage of paralysed animals at day 8 of adulthood from 50% to 15% (Figure 5.2a).

Moreover, the cytosolic HSP-90 gene *hsp-90* was knocked down using RNAi in both the $A\beta_{3-42}$ strain and the N2 wildtype strain at L4 stage and the paralysis of the animals were assessed for 8 days afterwards (Figure 5.2b). Interestingly, knockdown of *hsp-90* in both strains caused a comparable severe paralysis phenotype in the animals, whereby 80% of animals were paralysed after 8 days. HSP-90 has been shown previously to be essential for myosin folding and muscle cell integrity (Frumkin et al., 2014). Our data confirmed this result, as animals treated with *hsp-90* RNAi exhibit an age-dependent paralysis comparable to Aβ-expressing nematodes (Figure 5.2b). One possible explanation of these results could be the increased folding load in the muscle cells caused by Aβ, whereby HSP-90 is sequestered away from maintaining the folding of myosin and towards the folding of Aβ. This disrupts muscle cell integrity and causes collapse observed through increased

paralysis. Therefore, maintaining the expression of HSP-90 to cope with both myosin and Aβ misfolding is crucial in protecting the proteome during aging.

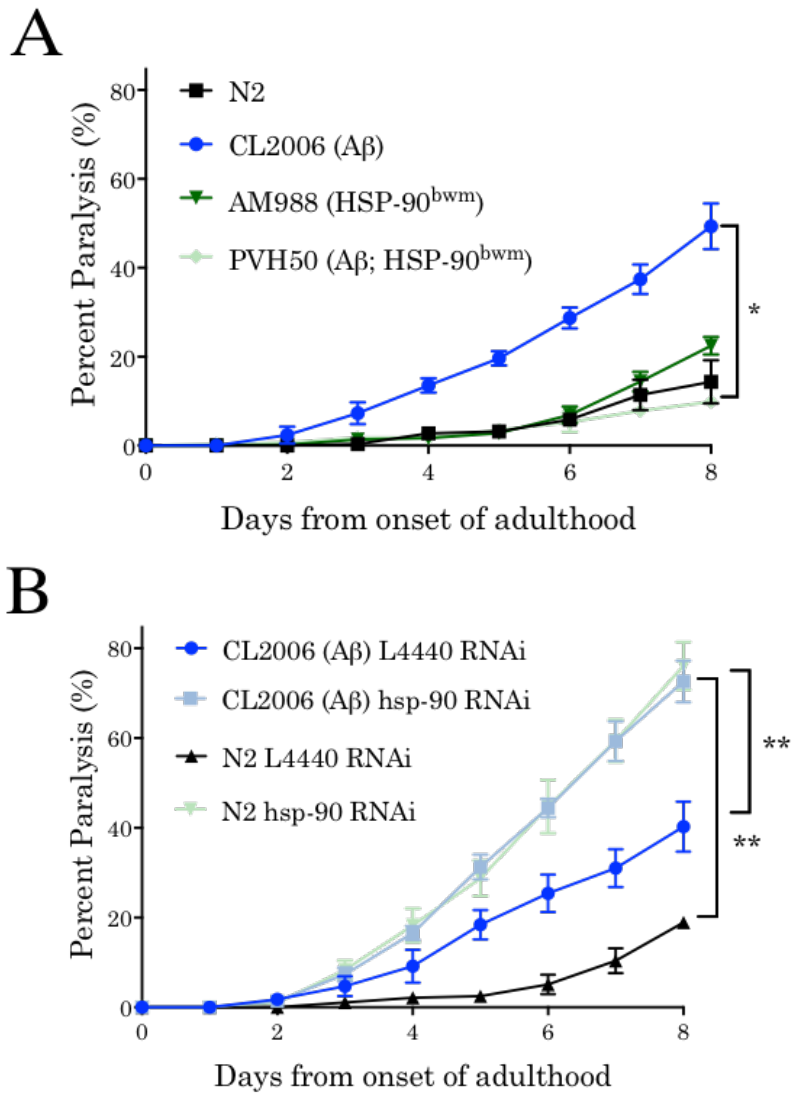

Figure 5.2 Paralysis phenotypes of *C. elegans* Alzheimer's models with modulated HSP-90 expression.
A) Paralysis assays of *C. elegans* expressing Aβ$_{3-42}$ in the body wall muscle compared with wild type (N2), HSP-90^{bwm} overexpression or Aβ$_{3-42}$; HSP-90^{bwm}. B) Paralysis assays of wild type *C. elegans* (N2) or *C. elegans* expressing Aβ$_{3-42}$ (CL2006) on control L4440 RNAi or *hsp-90* RNAi. Paralysis data represents the SEM of 3 biological replicates (n=100 animals). Statistical significance was determined using the Wilcoxon matched-paired signed rank test. * $p<0.05$ **$p<0.01$

5.5.2 Chaperone expression levels in HSP-90 overexpression models

Chaperones have been shown to work in complex networks, whereby upregulation of one chaperone can influence the expression of other chaperones or co-chaperones both cell autonomously and cell-non-autonomously (Taylor and Dillin, 2013; Van Oosten-Hawle et al., 2013). Therefore, I asked whether the overexpression of *hsp-90* can modulate the expression of other chaperone proteins, and aid in maintaining proteostasis. As expected, cytosolic *hsp-90* was significantly upregulated in all strains where HSP-90 has been overexpressed: the HSP-90^{bwm}, Aβ; HSP-90^{bwm}, and Aβ; HSP-90^{bwm}; STI-1o/e strains had increased *hsp-90* transcript levels of 4-, 9- and 4-fold respectively compared with the wildtype (N2) control (Figure 5.3b). However, in the Aβ strain, although *hsp-90* expression appears to be upregulated, this was not significant (Figure 5.3a). Transcript levels of the HSP-90 co-chaperone gene *sti-1* was significantly upregulated 3-fold in only the Aβ; HSP-90^{bwm}; STI-1o/e strain (Figure 5.3b). Levels of the constitutively expressed Hsp70 gene *hsp-1* were not significantly up- or down-regulated in any strains compared with the wildtype (N2) control (Figure 5.3d). However, levels of the stress-inducible *hsp-70* gene *C12C8.1* were upregulated 40- and 10- fold respectively in the Aβ and Aβ; HSP-90^{bwm} strains, but was not significant in the HSP-90^{bwm} and Aβ; STI-1o/e; HSP-90^{bwm} strains (Figures 5.3c and 5.3d). The upregulation of the inducible *hsp-70* gene C12C8.1 in the Aβ and Aβ; HSP-90^{bwm} strain could be a response to the increased load on the PN components due to the expression and aggregation of Aβ in this strain. The increased folding load from the expression and misfolding of Aβ could be sequestering HSP-70 and HSP-90 and thus inducing the heat shock response (HSR). The HSR is activated in the shortage of cytosolic HSP-70 and HSP-90 and could be upregulating chaperones such as HSP-70 in order to maintain proteostasis.

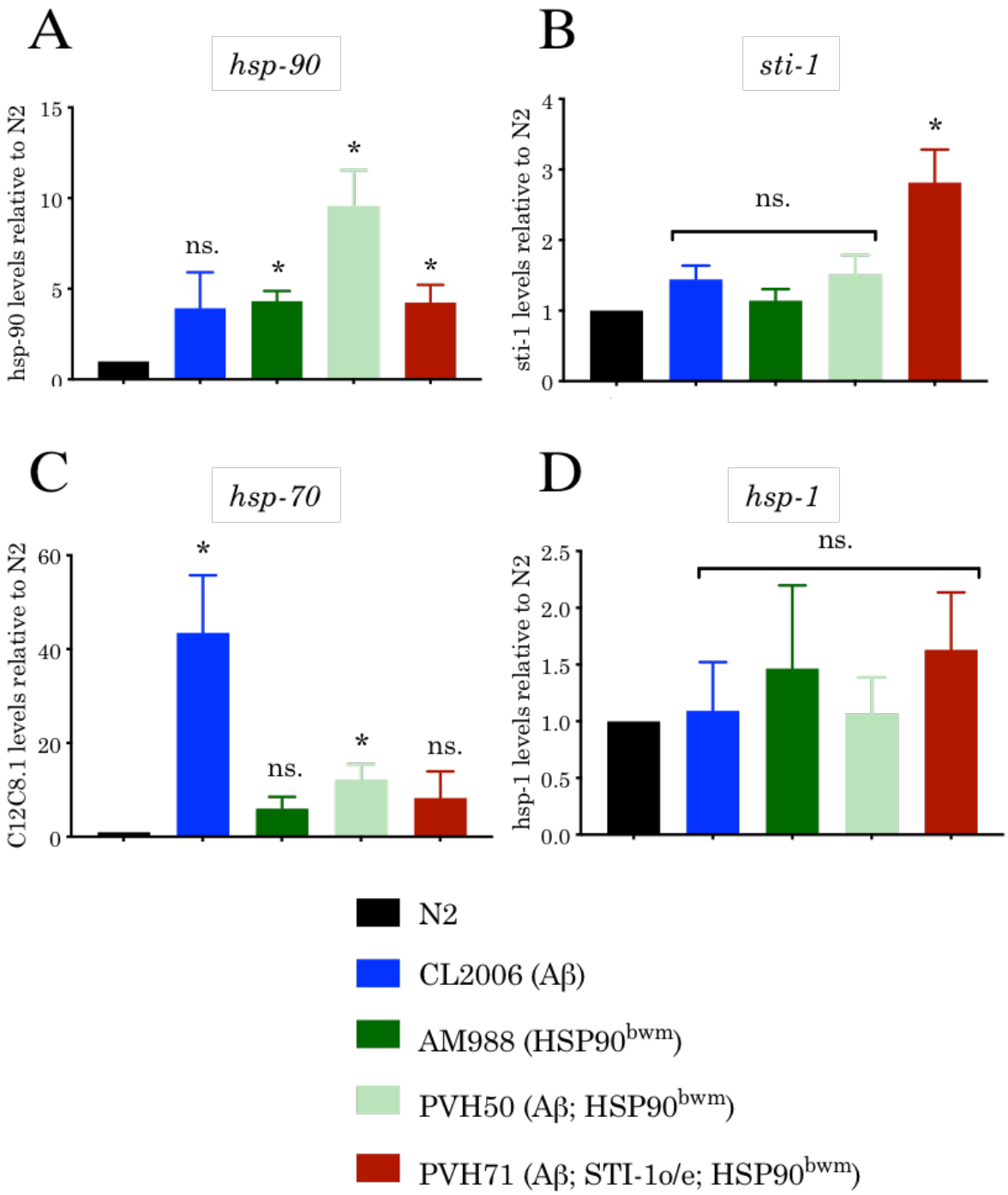

Figure 5.3 mRNA levels of chaperone genes in wild type (N2), Aβ$_{3-42}$ (CL2006), HSP-90^{bwm} overexpression, Aβ$_{3-42}$; HSP-90^{bwm} or Aβ$_{3-42}$; HSP-90^{bwm}; STI-1o/e.
mRNA levels of chaperone genes A) *hsp-90* mRNA expression of all strains compared with the wild type (N2) control. B) *sti-1* mRNA expression of all strains compared with the wild type (N2) control. C) *hsp-70* mRNA expression of all strains compared with the wild type (N2) control. D) *hsp-1* mRNA expression of all strains compared with the wild type (N2) control. All bar graphs are representative of the mean of three independent experiments, error bars represent ± SEM. p*<0.05 ns, not significant.

5.5.3 The effect of the HSP-90 co-chaperone STI-1 on Aβ-associated toxicity

The HSP-70/HSP-90 co-chaperone STI-1 has been shown to be required for both muscle cell integrity and the safeguarding of the proteome from Aβ-toxicity in *C. elegans* (Brehme et al., 2014; Frumkin et al., 2014). To further evaluate the potential of STI-1 to modulate Aβ-toxicity, the STI-1o/e strain (PPI1972) was crossed into the $A\beta_{3\text{-}42}$-expressing Alzheimer's disease strain (CL2006) to generate the strain PVH40 (Aβ; STI-1o/e). This strain alleviated the paralysis phenotype associated with $A\beta_{3\text{-}42}$ expression from 45% of animals paralysed at day 8 of adulthood to 20% paralysed (Figure 5.4a). Furthermore, the overexpression of STI-1 alone did not significantly affect nematode motility compared with the wildtype (N2) control (Figure 5.4a).

Knockdown of *sti-1* has been shown previously to affect the motility of an Alzheimer's strain and a *unc-45* mutant strain (Brehme et al., 2014; Frumkin et al., 2014). Knockdown of *sti-1* in the $A\beta_{3\text{-}42}$ model resulted in a 10% increase in the percentage of paralysed animals at day 10 of adulthood compared with $A\beta_{3\text{-}42}$ nematodes on control RNAi (Figure 5.4b). However, knockdown of *sti-1* in the wildtype (N2) strain had no significant effect on the paralysis of the animals (Figure 5.4b), similar to previous literature (Frumkin et al., 2014). Combined, these results potentially indicate that STI-1 may not be essential in maintaining muscle integrity under normal conditions; however, when the muscle cell is under stress – for example under the proteotoxic stress induced by $A\beta_{3\text{-}42}$ expression - STI-1 is required to protect the proteome. This is consistent with previous research that investigated the upregulation of STI-1 during heat stress (Song et al., 2009).

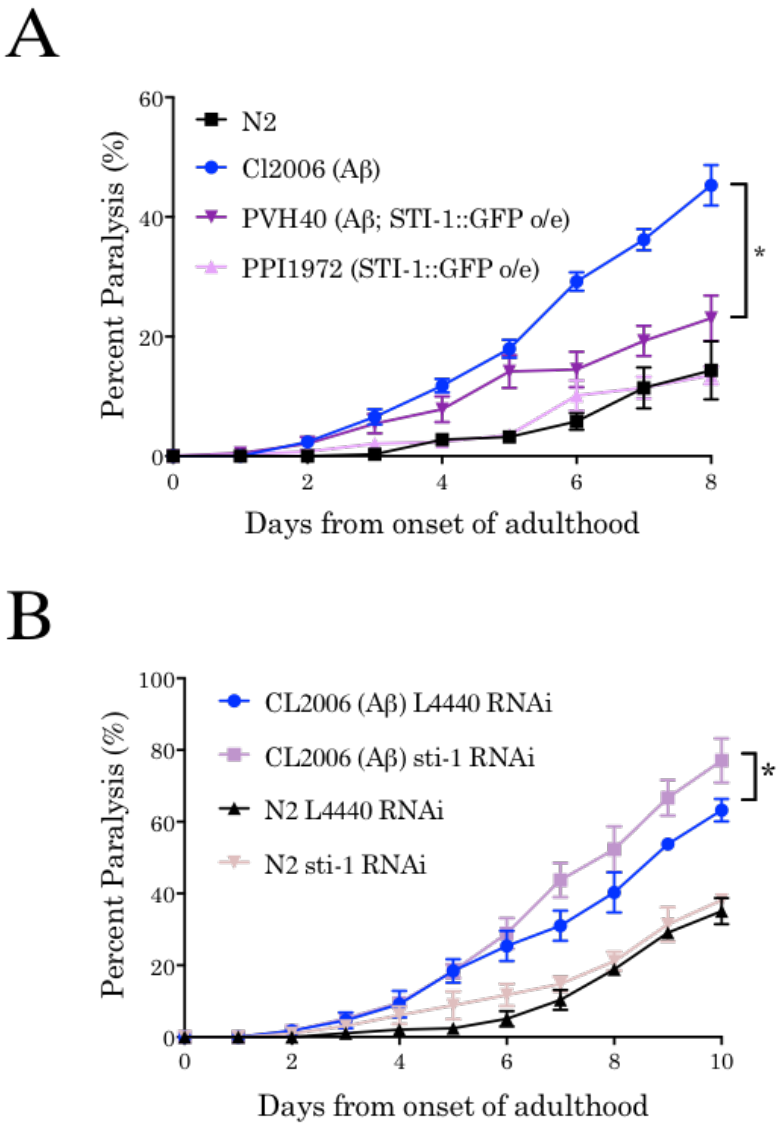

Figure 5.4 Paralysis phenotypes of *C. elegans* Alzheimer's models with modulated STI-1 expression.

A) Paralysis assays of *C. elegans* expressing $A\beta_{3\text{-}42}$ in the body wall muscle compared with wild type (N2), STI-1^{bwm} overexpression or $A\beta_{3\text{-}42}$; STI-1^{bwm}. B) Paralysis assays of wild type *C. elegans* (N2) or *C. elegans* expressing $A\beta_{3\text{-}42}$ (CL2006) on control (L4440) RNAi or *sti-1* RNAi. Paralysis data represents the SEM of 3 biological replicates (n=100 animals). Statistical significance was determined using the Wilcoxon matched-paired signed rank test. * $p<0.05$ **$p<0.01$

5.5.4 Chaperone expression levels in STI-1 overexpression strains

Similarly to the HSP-90 overexpression strains at the start of this chapter, I next asked whether STI-1 overexpression affected the expression other chaperone genes. RT-qPCR analysis showed a significant increase of 2.5-fold in the transcript levels of *sti-1* in both the STI-1o/e and Aβ; STI-1o/e strains and a 3-fold increase in the Aβ; STI-1o/e; HSP-90o/e strain; while the Aβ strain did not display any significant increase in *sti-1* levels (Figure 5.5b). The Aβ; STI-1o/e; HSP-90o/e strain displayed a 4-fold increase in *hsp-90* transcript levels, while the other strains did not significantly upregulate *hsp-90* (Figure 5.5a). Levels of stress-inducible *hsp-70* were significantly upregulated 40-fold in the Aβ strain, but not any of the other strains (Figure 5.5c). Further, the constitutively expressed Hsp70 gene *hsp-1* did not show any significantly up- or down-regulation in any of the strains analysed (Figure 5.5d). Therefore, apart from the expected increase in *sti-1* expression, these results suggest *sti-1* overexpression does not actively regulate any of the chaperone subset analysed. This indicates the protective effects of *sti-1* overexpression might be direct effects, and not indirectly impacting $A\beta_{3\text{-}42}$ folding through the upregulation of other chaperones, although more research into the expression of other genes is required to confirm this.

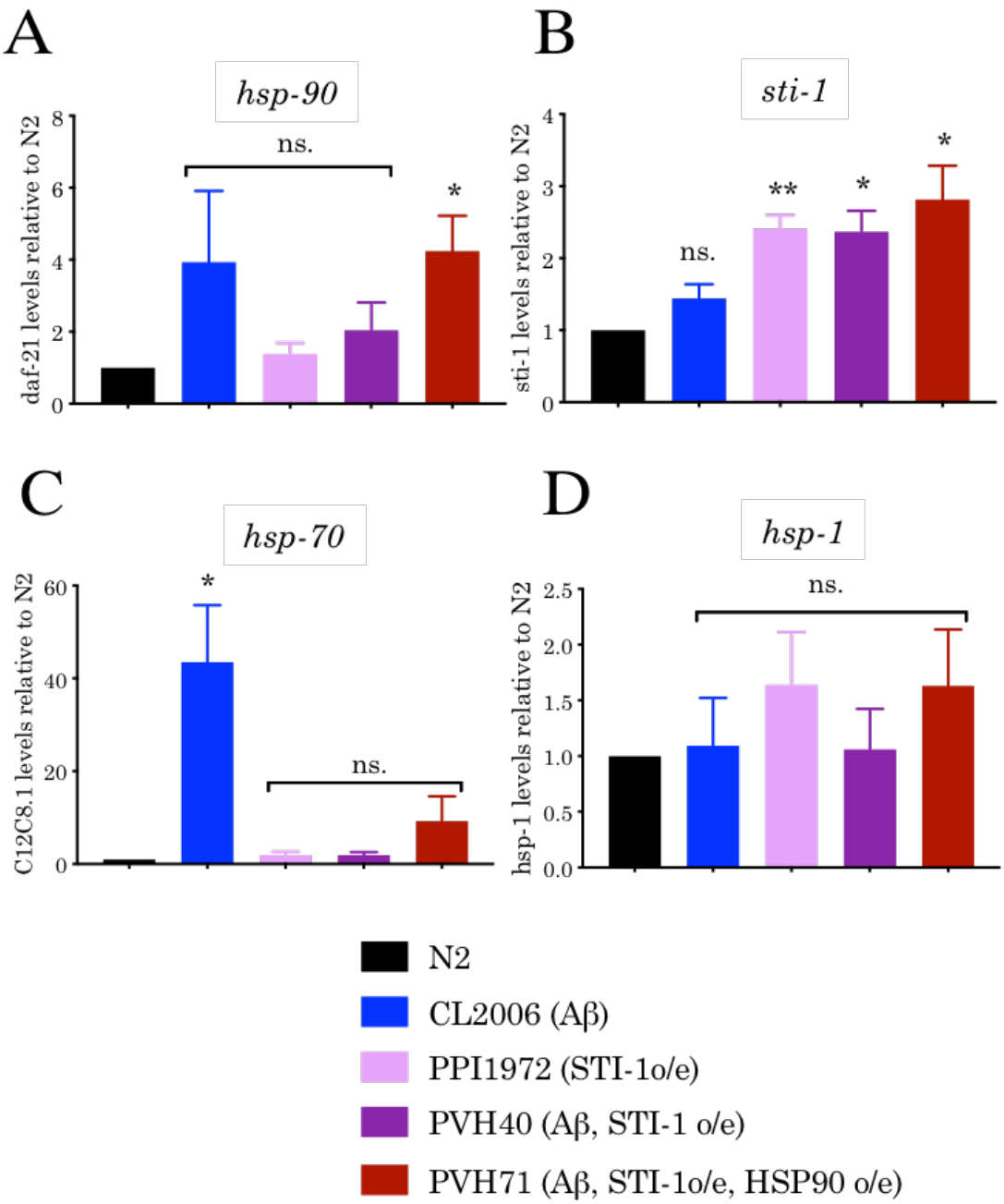

Figure 5.5 mRNA levels of chaperone genes in wild type (N2), Aβ$_{3-42}$ (CL2006), STI-1o/e, Aβ$_{3-42}$; STI-1o/e or Aβ$_{3-42}$; HSP-90bwm; STI-1.
A) *hsp-90* mRNA expression of all strains compared with the wild type (N2) control. B) *sti-1* mRNA expression of all strains compared with the wild type (N2) control. C) *C12C8.1* mRNA expression of all strains compared with the wild type (N2) control. D) *hsp-1* mRNA expression of all strains compared with the wild type (N2) control. All bar graphs are representative of the mean of three independent experiments, error bars represent ± SEM. p*<0.05 p**<0.01 ns. = not significant

5.5.5 The cell-non-autonomous action of HSP-90 on Aβ-associated toxicity

Multicellular organisms employ transcellular chaperone signalling (TCS) of PN components in order to maintain the proteome across all tissues of the animal. In *C. elegans,* modulation of the essential molecular chaperone HSP-90 has been shown to activate TCS (O'Brien et al., 2018; Van Oosten-Hawle et al., 2013). Overexpression of HSP-90 in the intestine or neurons of *C. elegans* has been shown to elevate misfolding in muscle cells induced in myosin temperature-sensitive mutants (Van Oosten-Hawle et al., 2013). Here, it was questioned if the cell-non-autonomous action of HSP-90 can also alleviate the toxicity associated with the expression of the aggregation-prone protein amyloid-β, and which signalling molecules are involved in this response.

5.5.6 Intestinal specific upregulation of HSP-90 rescues Aβ-associated toxicity

To explore the cell-non-autonomous relationship of HSP-90 further, the HSP-90 intestinal overexpression strain AM986 (HSP-90^{int}) was crossed into the Alzheimer's disease model CL2006, where A$\beta_{3\text{-}42}$ is expressed in the body wall muscle, to generate the strain PVH86 (Aβ; HSP-90^{int}). The overexpression of HSP-90 in the intestines of the Alzheimer's disease model significantly reduced the number of paralysed animals observed during ageing, where 25% of animals were paralysed at day 8 of adulthood in the Aβ; HSP-90^{int} strain compared with 50% in the Aβ Alzheimer's disease model (Figure 5.6). This demonstrates intestinal HSP-90 TCS is beneficial to the prevention of Aβ misfolding in the distal body wall muscle tissue and furthers our understanding of the effects of intestinal TCS.

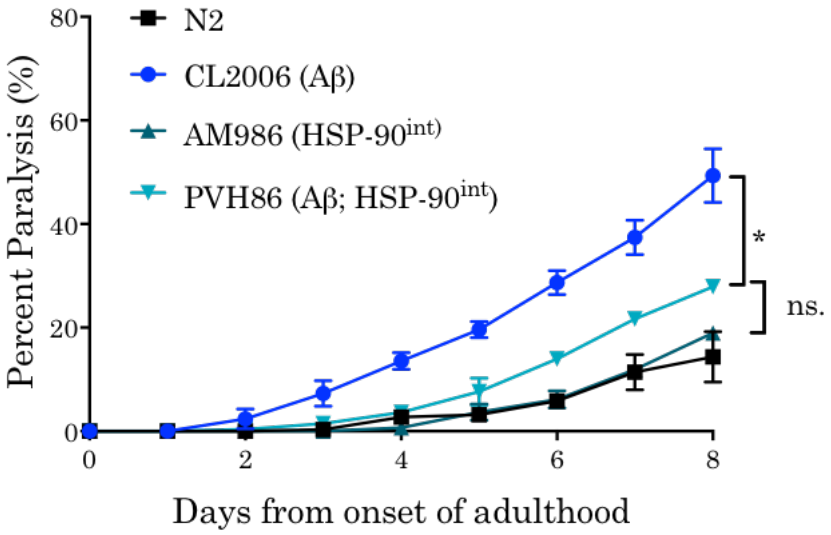

Figure 5.6 Paralysis phenotypes of *C. elegans* Alzheimer's models with modulated tissue-specific HSP-90 expression
A) Paralysis assays of *C. elegans* expressing Aβ$_{3-42}$ in the body wall muscle compared with wild type (N2), intestinal specific expression of HSP-90 (HSP-90^{int}) or Aβ$_{3-42}$; HSP-90^{int}. Paralysis data represents the SEM of 3 biological replicates (n=100 animals). Statistical significance was determined using the Wilcoxon matched-paired signed rank test. * $p<0.05$ ns, not significant.

5.5.7 Neuronal specific upregulation of HSP-90 rescues Aβ-associated toxicity and is mediated by *pqm-1*

Next it was explored whether this protective effect was also apparent when HSP-90 was overexpressed in the neurons of the animals. To address this the tissue-specific neuronal HSP-90 overexpression strain AM987 (HSP-90^{neuro}) was genetically crossed into the Alzheimer's disease model CL2006 which expresses Aβ$_{3-42}$ in the body wall muscle of the animal to generate the strain PVH85 (Aβ; HSP-90^{neuro}). Neuronal HSP-90 overexpression alleviated the paralysis phenotype seen in the Aβ$_{3-42}$ strain to levels similar to wild type (N2) (Figure 5.7a). The percentage of animals paralysed at day 8 of adulthood were reduced from 50% in the Aβ strain to 20% in the Aβ; HSP-90^{neuro} strain (Figure 5.7a).

Building on this, I sought to uncover the signalling molecules involved in the cell-non-autonomous action of HSP-90 observed through the overexpression of HSP-90 in the neurons of *C. elegans*. The FoxA transcription factor *pha-4* has been previously identified by chromatin immunoprecipitation to bind to the promoter of *hsp-90* and to regulate cell-non-autonomous *hsp-90* expression in a myosin ts mutant (Celniker et al., 2009; Van Oosten-Hawle et al., 2013). Knock-down of *pha-4* expression through RNAi in the Aβ,

HSP-90^{neuro} strain reversed the protective effect of neuronal HSP-90 overexpression on the Alzheimer's disease model and increased the percentage of paralysed animals on day 8 of adulthood from 25% to 45% (Figure 5.7b). Knock-down of *pha-4* in the Aβ_{3-42}-expressing Alzheimer's disease strain also caused an increase in the percentage of paralysed animals during ageing, from 40% of animals paralysed at day 8 of adulthood on control RNAi to 65% of animals paralysed on *pha-4* RNAi (Figure 5.7b). Therefore, this suggests that *pha-4* knockdown might be affecting Aβ misfolding in a separate pathway to neuronal HSP-90 TCS in order to mediate protein folding in the muscle.

Through RNAseq analysis of the HSP-90^{neuro} strain, our group identified 34 genes to be significantly upregulated, of which a motif with the consensus sequence AGATAACA or TGTTATCT was found to be enriched in the promoter regions of 27 of the 34 upregulated genes (O'Brien et al., 2018). This motif resembled the GATA-like binding site for the zinc-finger transcription factor PQM-1, and therefore we asked whether this transcription factor could be involved in TCS. Using RNAi, *pqm-1* was knocked down in Aβ; HSP-90^{neuro} strain, and remarkably exacerbated paralysis, reversing the protective effect of neuron-induced TCS, from 20% of animals paralysed at day 8 of adulthood to 40% of animals paralysed (Figure 5.7c). Interestingly, knockdown of *pqm-1* in an Aβ_{3-42} Alzheimer's disease strain had no significant effect on the percentage of animals paralysed, indicating that this transcription factor is not essential for general muscle cell integrity but is likely required for TCS-mediated protection against amyloid toxicity.

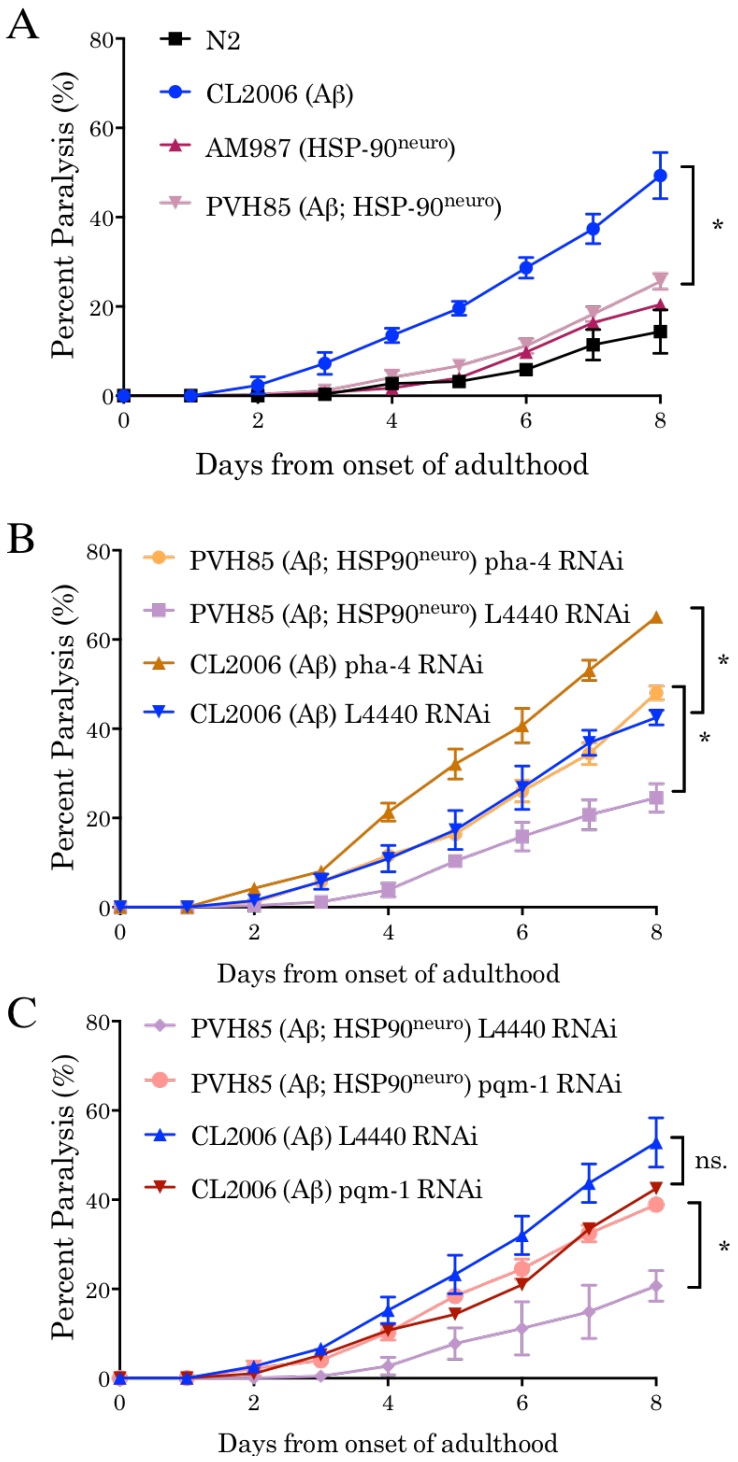

Figure 5.7 Overexpression of HSP-90 in the neurons of an Alzheimer's model rescues its paralysis phenotype, and is modulated through knocking down *pqm-1* or *pha-4*.
A) Paralysis assays of *C. elegans* expressing Aβ$_{3\text{-}42}$ in the body wall muscle compared with wild type (N2) or neuronal specific expression of HSP-90 (HSP-90^{neuro}) or Aβ$_{3\text{-}42}$; HSP-90^{neuro}. B) Paralysis assays of CL2006 (Aβ$_{3\text{-}42}$) or Aβ$_{3\text{-}42}$; HSP-90^{neuro} on control (L4440) RNAi or *pha-4* RNAi C) Paralysis assays of CL2006 (Aβ$_{3\text{-}42}$) or Aβ$_{3\text{-}42}$; HSP-90^{neuro} on control (L4440) RNAi or *pqm-1* RNAi. Paralysis data represents the SEM of 3 biological replicates (n=100 animals). Statistical significance was determined using the Wilcoxon matched-paired signed rank test. * $p<0.05$ ** $p<0.01$

5.6 Discussion

Molecular chaperones are highly conserved across organisms and their function is essential for proteome maintenance during aging. The analysis presented in this chapter, modulating the expression HSP-90 and its co-chaperone STI-1 in *C. elegans* has validated their role in maintaining cellular proteostasis during aging in a cell-autonomous and cell-non-autonomous manner. Elevation of both HSP-90 and STI-1 levels in an Alzheimer's *C. elegans* disease model was shown to alleviate the age-associated paralysis phenotype characteristic for this disease model (Figures 5.2a and 5.4a). Further, it was demonstrated that knockdown of these two components of the PN exacerbated the paralysis phenotype observed in the Aβ-expressing disease model (Figures 5.2b and 5.4b). Together, these results indicate that HSP-90 and STI-1 are crucial in protecting the cell against Aβ misfolding and aggregation. This is consistent with previous research performed by Brehme and colleagues, who knocked down both HSP-90 and STI-1 in both an Alzheimer's and a Huntington's disease model of *C. elegans* and observed a reduction in the thrashing rate of animals at day 4 of adulthood compared with the disease model alone (Brehme et al., 2014). Moreover, *in vitro* studies using human Hsp90 and Aβ, suggested that Hsp90 is involved in Aβ oligomer assembly (Evans et al., 2006), and our group further demonstrated that HSP-90 overexpression reduced the amount of Aβ oligomers in *C. elegans* (O'Brien et al., 2018). As STI1 has also been previously shown to protect neuronal cells and an AD mouse model from the toxic effects of Aβ oligomers (Ostapchenko et al., 2013), it is likely that STI-1 and HSP-90 overexpression in our $A\beta_{3\text{-}42}$ *C. elegans* model reduces the amount of toxic oligomer species in the animals, reducing muscle damage and alleviating the paralysis phenotype observed. Further investigation probing the toxic species in our disease models using anti-oligomer antibodies would aid in the understanding of this.

5.6.1 Knockdown of HSP-90 but not its co-chaperone STI-1 causes an increased paralysis phenotype in both an Alzheimer's model and wild type *C. elegans*

Knockdown of HSP-90 caused widespread paralysis in the wild type (N2) control strain and the Alzheimer disease model (Figure 5.2b). This is unsurprising considering the key role HSP-90 has been shown to play in maintaining correct myosin folding (Barral et al., 2002; Frumkin et al., 2014; Gaiser et al., 2011). HSP-90, in conjunction with UNC-45 has been shown previously to control the assembly of myosin filaments (Barral et al., 2002). The down-regulation of either HSP-90 or UNC-45 causes a reduction in motility -measured

by the thrashing rate of animals - and the accumulation of aggregate-like myosin in the muscle cells of animals (Gaiser et al., 2011). It is therefore hard to differentiate the effects of increased Aβ misfolding and toxicity when HSP-90 is knocked down, from the effects of ineffective myosin folding causing paralysis. However, as overexpression of HSP-90 in the body wall muscle alleviates paralysis associated with the Alzheimer's disease model, and was shown by other members of the group to reduce the amount of Aβ oligomers present in the animals (O'Brien et al., 2018), it is likely that HSP-90 also plays a vital role in reducing misfolding and toxicity associated with Aβ.

On the other hand, knockdown of *sti-1* in the wild type (N2) strain did not have an effect on the paralysis of the animals (Figure 5.4b), suggesting it plays a less important role in maintaining muscular homeostasis than *hsp-90* in *C. elegans*. This is further exemplified through the knockdown of *sti-1* in the Alzheimer's disease model where a 10% increase in the percentage of paralysed animals was observed at day 10 of adulthood compared with 30% increase observed when HSP-90 was silenced (Figure 5.2a and 5.4a). Indeed, previous literature has implicated STI-1 in muscle cell integrity and regulation, but only when paired with *unc-45* knockdown (Frumkin et al., 2014). It has been purposed this effect observed could be mediated through the interaction of HSP-90, STI-1 and UNC-45; however, pull-down of STI-1 revealed an interaction with HSP-90 but not UNC-45 (Frumkin et al., 2014). Further reports of the relationship between STI-1 and HSP-90 have revealed that *sti-1* knockdown correlates with an upregulation in *hsp-90* transcripts (Burga et al., 2019). This interplay with *hsp-90* could be responsible for both the lack of effect of STI-1 knockdown in the wild type strain, and the reduced protective effect observed when STI-1 is knocked down in the Alzheimer's model, where the effects of STI-1 knockdown on Aβ could be partially mitigated by up-regulation of HSP-90.

As STI-1 modulation only effected animals under increased stressed conditions due to Aβ aggregation, another possible explanation of the results could be that STI-1 function is strongly linked to the stress response. Indeed, STI-1 has been previously shown to be upregulated in response to heat stress, and has a potential heat shock element sequence (TTCTa/cGAA) upstream of the start codon (Song et al., 2009). This points to the involvement of STI-1 in the stress response pathway, although overexpression STI-1 did not induce the transcript expression of a subset of chaperone genes (C12C8.1, *hsp-1* or *daf-21*), likewise HSP-90 overexpression did not upregulate *sti-1* expression. Other genes could be involved in this response, and further investigation, such as the co-

immunoprecipitation of STI-1 with either HSP-70 or HSP-90 is needed to provide a complete picture. Overall however, it seems likely STI-1 is important in times of stress, in order to maintain protein stability and inhibit protein aggregation.

5.6.2 Transcellular chaperone signalling can be used to improve phenotypes associated with Amyloid-β

As well as providing beneficial effects to proteostasis through cell autonomous means, this study demonstrated the upregulation of HSP-90 in distal tissues can also induce a cell-non-autonomous protective response against Aβ aggregation. HSP-90 overexpression in the intestines or the neurons of the animals can alleviate the toxicity of Aβ observed through monitoring the paralysis of animals (Figures 5.6 and 5.7a). This is consistent with the previously observed protective effect observed towards the misfolding of metastable myosin in the muscle (Van Oosten-Hawle et al., 2013). This previous study also identified the FoxA transcription factor *pha-4* to be required for TCS, as TCS-induced cell nonautonomous *hsp-90* expression is reduced when *pha-4* is knocked down (Van Oosten-Hawle et al., 2013). In the HSP-90^{neuro} Alzheimer's TCS model, a reduction in the protective cell-non-autonomous action of HSP-90 was observed, which is consistent with this conclusion. However, when *pha-4* was knocked down using RNAi in the Alzheimer's disease model, an increase in paralysed nematodes was observed during ageing (Figure 5.7b). This might instead suggest that PHA-4 is not TCS-specific and instead involved in a separate pathway to regulate the misfolding of proteins in the muscle. It has been widely reported that PHA-4 controls other stress response pathways, including the insulin-like signalling (IIS) and the unfolded protein response pathway of the endoplasmic reticulum (UPR^{ER}) (Matai et al., 2019; Shpigel et al., 2019). It is thus possible that these pathways are regulating the response observed in the nematodes. It would therefore be interesting to further explore *pha-4* in the context of cellular proteostasis and Aβ toxicity and identify the pathway upon which protein misfolding is exacerbated in our model.

Following on from this, we also identified the novel signalling component of transcellular activation of *hsp-90*, PQM-1. Research from the group used RNAseq and motif analysis to identify this GATA-transcription factor as a possible signalling molecule in neuronal-activated HSP-90 TCS (O'Brien et al., 2018). PQM-1 has been shown previously to control development and longevity, and to display opposing patterns of nuclear localisation to DAF-16 (Tepper et al., 2013). Our group also explored the localisation of PQM-1 further, showing a higher percent of PQM-1 in HSP-90^{neuro} animals to be localised in the nucleus

in the than in the control animals (O'Brien et al., 2018). Subsequently, it was shown that PQM-1 aids in the protective TCS response seen through HSP-90^{neuro} expression, where knock down of PQM-1 ablates the protective nature of neuronal TCS (Figure 5.7c). As knockdown in the Alzheimer's disease model did not also increase the amount of paralysed animals, PQM-1 is likely to act in this cell-non-autonomous pathway and regulate the protective effect of TCS observed.

5.7 Conclusions

Overall, this chapter has demonstrated the beneficial effects of HSP-90 and its co-chaperone STI-1 towards the toxicity associated with $A\beta_{3\text{-}42}$ expression. As protein misfolding diseases are responsible for a large number of debilitating conditions and deaths each year, the development of new therapeutics is vital. The beneficial effects of HSP-90 (Hsp90) and STI-1 (STI1) need to be further explored in more relevant human systems, especially in the light of developing these PN components for therapeutic interventions. Moreover, targeting of the PQM-1 TCS pathway using genetic or small molecule interventions could also provide another possible route for therapeutics for the treatment of protein misfolding diseases.

Chapter 6. Conclusions and Future Directions

The formation of amyloid species and their toxic effects have been well documented in the progression of many diseases; however, many questions still remain as to the mechanisms of amyloid toxicity and the cellular response mechanisms an organism employs to combat this. The utilisation of *C. elegans* as a model organism for amyloid disease research has been well established in respect to gaining further understanding of these topics. The majority of *C. elegans* research has focused on neurological conditions, and therefore systemic amyloid diseases such as DRA and T2DM have limited disease models in comparison (Aldras et al., 2019; Diomede et al., 2012; Faravelli et al., 2019; Rosas et al., 2016). To address this, the thesis research presented here displays the generation and characterisation of new amyloid disease models expressing proteins associated with either the systemic amyloid diseases DRA or T2DM (Chapters 3 and 4), and further delves into the effects of amyloid protein aggregation and the cellular response to combat these (Chapters 3, 4 and 5).

6.1 Phenotypes of amyloid protein expression in *C. elegans*

Overall, this research has demonstrated the benefits on using the model organism *C. elegans* in studying the relationship of amyloid aggregation and toxicity. These models provide a simple system from which to study the aggregation of amyloidogenic proteins and how this contributes to toxicity from which implications to human disease can be translated. It is interesting to observe that the highly amyloidogenic disease linked mutations D76N β_2m and S20G IAPP confer to stronger toxic phenotypes in the models presented (Chapters 3 and 4), and replicate *in vitro* research (Ma et al., 2001; Mangione et al., 2013). Further research into the mechanism of toxicity of these variants would be interesting to disseminate whether these phenotypes are due to higher rates of aggregation as previously thought, or due to a different mechanism of toxicity.

Expression of highly amyloidogenic variants of both β_2m (D76N and ΔN6) and IAPP (hIAPP and S20G) were demonstrated to affect motility of *C. elegans* in an age-dependent as shown by the increase in paralysed animals with age and reduction of the thrashing rate of the nematode (Chapter 3.8 and 4.7). Locomotion phenotypes are also observed in other *C. elegans* disease models expressing amyloid proteins in the body wall muscle of

animals such as in those expressing amyloid-β (Brehme et al., 2014; Fay et al., 1998; Link, 1995; McColl et al., 2012), α-synuclein (Kuwahara et al., 2008; van Ham et al., 2010; Van Ham et al., 2008) and polyglutamine expansions (Morley et al., 2002; Wang et al., 2006). As similar defects were observed between models, these observations might point towards a common mechanism of toxicity that underlies motility defects between the amyloidogenic proteins. Amyloidogenic proteins have been known to sequester chaperone components, disrupting normal cellular processes such as myosin folding and integrity, which could explain the common phenotype.

6.2 The proteostasis network and amyloid

Throughout this thesis, the role of the proteostasis network (PN) has been highlighted to be critical in amyloid aggregation and toxicity. In particular, expression levels of the ER-resident chaperone *hsp-4* (Human ortholog of BiP*)* were found to be reduced in *C. elegans* models expressing β_2m proteins (WT β_2m, D76N β_2m and ΔN6 β_2m) and amyloidogenic IAPP variants (hIAPP and S20G IAPP) (Chapter 3.10 and Chapter 4.9). Interestingly, when ER stress was applied to the models, strains expressing WT β_2m, D76N β_2m, hIAPP and S20G IAPP *hsp-4* transcripts were not induced (Chapter 3.10 and Chapter 4.9). In these amyloid models β_2m and IAPP expression constructs harboured a signal sequence, which allows to target the protein to the ER and the secretory pathway. The reduced ER stress survival and impaired *hsp-4* transcript response in the strains could point to common mechanism whereby upon entering the ER, the initiation of aggregation occurs and impairs stress responses. This is consistent with previous studies that demonstrate that amyloid aggregation can affect the ER (Chien et al., 2010; Hull et al., 2009). Future experiments to explore this phenomenon are needed, such as to investigate whether reduced ER stress survival is further exacerbated in an *ire-1* mutant or rescued in an *xbp-1s* mutant, which shows elevated hsp-4 levels and ER stress survival rates throughout aging (Taylor and Dillin, 2013). These strains could be used to exacerbate the phenotypes associated with amyloidogenic protein expression and understand the relationship between these ER components and the expression of these proteins further.

Chapter 5 demonstrated the importance of HSP-90 function on amyloid-β toxicity. The proteostasis network has been shown numerous times to be vital in protecting the organism against proteotoxic damage from the expression of aggregation-prone proteins (Hipp et al., 2014). These results also tie in with previous research showing that Hsp90

can modulate protein aggregation (Brehme et al., 2014; Evans et al., 2006; Luo et al., 2007). However, it would also be interesting to explore whether these chaperone responses are common across the amyloid models presented here. Experiments could include RT-qPCR experiments to analyse the levels of *hsp-90* in the IAPP and β_2m models generated in this study in order to understand whether *hsp-90* has a generic role to play in preventing amyloid aggregation. It would also be interesting to explore whether HSP-90 overexpression or knockdown could exacerbate or alleviate the phenotypes we observed. Furthermore, *hsp-4* expression and the ER stress response could be explored in the intracellular amyloid-β expressing strains; presence of an ER stress survival phenotype in this model could allude to an intracellular effect on the ER response or lack thereof could implicate the targeting of IAPP and β_2m to the secretory pathway in the response observed.

6.3 Screening of therapeutics

The generation of new disease models of amyloid diseases provides many avenues for future research. As there are limited *in vivo* models of systemic amyloidosis - in particular for β_2m models - an obvious direction could be for small molecule drug screening. Traditional *in vitro* methods such as ThT assays, NMR and mass spectrometry analysis are useful in screening large numbers of therapeutics and understanding their mechanism of action against amyloid aggregation. Cellular based assays are also useful in screening therapeutics and can provide a clearer picture on the efficacy of a drug. However, the efficacy and in particular the safety and toxicity of many of these therapeutics differs considerably in an organismal environment and therefore *in vivo* disease models such as the ones presented in this thesis are required. Similar screening studies have been performed in numerous *C. elegans* amyloid models (Chen et al., 2015; Lublin and Link, 2013; Miyasaka et al., 2016; Perni et al., 2017). An example of this includes an $A\beta_{42}$ Alzheimer's model where the drug Bexarotene was discovered to reduce amyloid aggregation through a chemical kinetics-based strategy (Habchi et al., 2016). The drug was subsequently tested on neuroblastoma cells which displayed a delay the formation of toxic species and when applied to a *C. elegans* model of $A\beta_{42}$-mediated toxicity, Bexarotene suppressed $A\beta_{42}$ deposition and ameliorated the reduced motility observed in the model (Habchi et al., 2016).

A major problem for the treatment of amyloid diseases is that as the aggregating amyloid fibres are highly ordered and thermodynamically stable, they are difficult to disaggregate or remove (Tipping et al., 2015). As amyloid proteins undergo conformational changes on different timescales *in vivo* compared to *in vitro* studies, challenges arise from the highly heterogeneous toxic body of oligomers that are generated on pathway to fibril formation. These oligomers are thought to be the leading cause of cellular toxicity, and play an important role in the pathogenesis of many amyloid diseases (Chiti and Dobson, 2017; Glabe, 2006; Stefani, 2012). Therefore, the timing of drug administration in amyloid diseases is crucial to the efficacy. As well as standard therapeutic screening using the β_2m and IAPP models, future studies could focus on the timing of administration of therapeutics. By administering therapeutics at various time points in the lifecycle of the organism, it would provide information about not only the efficacy of the therapeutic but the species the drug acts upon.

6.4 Limitations and improvements to research

Although the models generated in this study are useful in modelling the aggregation and subsequent toxicity of both β_2m and IAPP variants, there are several improvements that could be made to both models. The expression of the amyloidogenic proteins could be explored in other tissues using different tissue specific promoters. In particular, it would be interesting to express IAPP in the neurons of animals. Before IAPP is secreted, it undergoes several steps involving several auxiliary factors including pro-hormone convertases in order to generate the mature form of the protein (Chen et al., 2018). In *C. elegans* factors such as PC2 and CPE are abundantly expressed in the neurons of the animal (Jacob and Kaplan, 2003; Kass et al., 2001) and therefore could represent a better tissue for IAPP to be expressed and secreted in. Future studies could also focus on expressing β_2m in the neurons of the animal, in order to discriminate differences in toxicity between different tissue types.

Although all amyloid disease models generated throughout this study where designed to secrete the disease protein extracellularly, it was not established whether this was the case. Future experiments need to concentrate on determining on the localisation of the proteins in the animal. This could be through improved immuno-staining techniques and different amyloid binding dyes. The localisation of the protein throughout the animal is critical in understanding the nature of toxicity throughout the animal. If found to be

extracellular, it would be interesting to determine if the expression of these amyloidogenic proteins are capable of inducing other cell-non-autonomous effects such as the neuronal phenotype of nociception. This has been demonstrated in other models such as a TTR-expressing *C. elegans* model, that demonstrated cell-non-autonomous nociception neuronal phenotypes when TTR was expressed and secreted in the body wall muscle (Madhivanan et al., 2018). Furthermore, it would be interesting to explore the extracellular proteostasis network, and the effect of expression of the β_2m or IAPP variants on this. A recent study has shown that extracellular proteostasis prevents pathogenic attack, and utilised the extracellular protein lipid-binding protein 2 (LBP-2) as a sensor for extracellular protein aggregation (Gallotta et al., 2020). To understand whether the models presented in this thesis also affected extracellular protein aggregation, future studies could focus on exploring whether IAPP and β_2m expression in the models generated could affect the extracellular aggregation of LBP-2 and reveal more information about the aggregation of these proteins.

Throughout this thesis, the phenotypic effects of amyloidogenic protein expression was described. However, with the exception of insoluble fractionation of the protein in the β_2m models demonstrating aggregated species (Chapter 3.4), there was little other evidence to pinpoint the exact nature of the species. As different amyloid species contribute to different cellular effects within a disease, future research should work on disseminating the species contained within the model to gain further understanding of the mechanism of amyloid toxicity. This could include using oligomer or fibril specific antibodies – such as the anti-amyloid antibody WO1 (O'Nuallain and Wetzel, 2002) and the anti-oligomer antibody A11 (Kayed et al., 2007) - to obtain a picture of the species populations in the models. Further research could even consider a more in depth look into the fibrils at atomic resolution employing techniques to pull down amyloid fibres and analyse their structures using cryo-EM. Recent research on Aβ fibrils from patient brain tissue has shown that these *in vivo* fibrils differ significantly from previous research on fibrils formed *in vitro* (Kollmer et al., 2019). Establishing and comparing the structural composition of the fibrils formed in *in vivo* disease models to patient samples would be beneficial in generating new better amyloid models and understanding the complex nature of the diseases involved.

Bibliography

Abedini, A., Plesner, A., Cao, P., Ridgway, Z., Zhang, J., Tu, L.H., Middleton, C.T., Chao, B., Sartori, D.J., Meng, F., Wang, H., Wong, A.G., Zanni, M.T., Verchere, C.B., Raleigh, D.P., Schmidt, A.M., 2016. Time-resolved studies define the nature of toxic IAPP intermediates, providing insight for anti-amyloidosis therapeutics. Elife 5, 1–28.

Abedini, A., Raleigh, D.P., 2005. The role of His-18 in amyloid formation by human islet amyloid polypeptide. Biochemistry 44, 16284–16291.

Abedini, A., Schmidt, A.M., 2013. Mechanisms of islet amyloidosis toxicity in type 2 diabetes. FEBS Lett. 587, 1119–1127.

Abravaya, K., Myers, M.P., Murphy, S.P., Morimoto, R.I., 1992. The human heat shock protein hsp70 interacts with HSF, the transcription factor that regulates heat shock gene expression. Genes Dev. 6, 1153–1164.

Åkerfelt, M., Morimoto, R.I., Sistonen, L., 2010. Heat shock factors: Integrators of cell stress, development and lifespan. Nat. Rev. Mol. Cell Biol. 11, 545–555.

Aldras, Y., Singh, S., Bode, K., Bhowmick, D.C., Jeremic, A., O'Halloran, D.M., 2019. An inducible model of human amylin overexpression reveals diverse transcriptional changes. Neurosci. Lett. 704, 212–219.

Almeida, Z.L., Brito, R.M.M., 2020. Structure and aggregation mechanisms in amyloids. Molecules 25.

Ambegaokar, S.S., Jackson, G.R., 2011. Functional genomic screen and network analysis reveal novel modifiers of tauopathy dissociated from tau phosphorylation. Hum. Mol. Genet. 20, 4947–4977.

Amin, J., Ananthan, J., Voellmy, R., 1988. Key features of heat shock regulatory elements. Mol. Cell. Biol. 8, 3761–3769.

Andersen, C.B., Hicks, M.R., Vetri, V., Vandahl, B., Rahbek-Nielsen, H., Thøgersen, H., Thøgersen, I.B., Enghild, J.J., Serpell, L.C., Rischel, C., Otzen, D.E., 2010. Glucagon fibril polymorphism reflects differences in protofilament backbone structure. J. Mol. Biol. 397, 932–946.

Andreetto, E., Yan, L.M., Tatarek-Nossol, M., Velkova, A., Frank, R., Kapurniotu, A., 2010. Identification of hot regions of the Aß-IAPP Interaction interface as high-affinity binding sites in both cross- and self-association. Angew. Chemie - Int. Ed. 49, 3081–3085.

Anfinsen, C.B., 1973. Principles that govern the folding of protein chains. Science. 181, 223–230.

Anfinsen, C.B., Haber, E., Sela, M., White, F.H., 1961. The kinetics of formation of native ribonuclease during oxidation of the reduced polypeptide chain. Proc. Natl. Acad. Sci. U. S. A. 47, 1309–1314.

Anguiano, M., Nowak, R.J., Lansbury, P.T., 2002. Protofibrillar islet amyloid polypeptide permeabilizes synthetic vesicles by a pore-like mechanism that may be relevant to type II diabetes. Biochemistry 41, 11338–11343.

Apostolidou, M., Jayasinghe, S.A., Langen, R., 2008. Structure of α-helical membrane-bound human islet amyloid polypeptide and its implications for membrane-mediated misfolding. J. Biol. Chem. 283, 17205–17210.

Argilés, A., Garcia, M., Demaille, J.G., Mourad, G., Collins, B., Kerr, P.G., Mourad, G., 1994. Cells surrounding haemodialysis-associated amyloid deposits are mainly macrophages. Nephrol. Dial. Transplant. 9, 662–667.

Arispe, N., Rojas, E., Pollard, H.B., 1993. Alzheimer disease amyloid ß protein forms calcium channels in bilayer membranes: Blockade by tromethamine and aluminum. Proc. Natl. Acad. Sci. U. S. A. 90, 567–571.

Ash, P.E.A., Zhang, Y.J., Roberts, C.M., Saldi, T., Hutter, H., Buratti, E., Petrucelli, L., Link, C.D., 2010. Neurotoxic effects of TDP-43 overexpression in *C. elegans*. Hum. Mol. Genet. 19, 3206–3218.

Ashkavand, Z., Sarasija, S., Ryan, K.C., Laboy, J.T., Norman, K.R., 2020. Corrupted ER-mitochondrial calcium homeostasis promotes the collapse of proteostasis. Aging Cell 19, 1–13.

Aston-Mourney, K., Hull, R.L., Zraika, S., Udayasankar, J., Subramanian, S.L., Kahn, S.E., 2011. Exendin-4 increases islet amyloid deposition but offsets the resultant beta-cell toxicity in human islet amyloid polypeptide transgenic mouse islets. Diabetologia 54, 1756–1765.

Bailey, R.R., Peddie, B.A., 1985. Enoxacin for the treatment of urinary tract infection. N. Z. Med. J. 98, 286–288.

Balchin, D., Hayer-Hartl, M., Hartl, F.U., 2016. In vivo aspects of protein folding and quality control. Science 353, aac4354.

Baler, R., Dahl, G., Voellmy, R., 1993. Activation of human heat shock genes is accompanied by oligomerization, modification, and rapid translocation of heat shock transcription factor HSF1. Mol. Cell. Biol. 13, 2486–2496.

Barral, J.M., Hutagalung, A.H., Brinker, A., Hartl, F.U., Epstein, H.F., 2002. Role of the myosin assembly protein UNC-45 as a molecular chaperone for myosin. Science. 295, 669–671.

Baskoylu, S.N., Yersak, J., O'Hern, P., Grosser, S., Simon, J., Kim, S., Schuch, K., Dimitriadi, M., Yanagi, K.S., Lins, J., Hart, A.C., 2018. Single copy/knock-in models of ALS SOD1 in *C. elegans* suggest loss and gain of function have different contributions to cholinergic and glutamatergic neurodegeneration. PLoS Genet. 14, 1–28.

Ben-Zvi, A., Miller, E.A., Morimoto, R.I., 2009. Collapse of proteostasis represents an early molecular event in *Caenorhabditis elegans* aging. Proc. Natl. Acad. Sci. 106, 14914–14919.

Bennett, E.J., Shaler, T.A., Woodman, B., Ryu, K.Y., Zaitseva, T.S., Becker, C.H., Bates, G.P., Schulman, H., Kopito, R.R., 2007. Global changes to the ubiquitin system in Huntington's disease. Nature 448, 704–708.

Benseny-Cases, N., Karamanos, T.K., Hoop, C.L., Baum, J., Radford, S.E., 2019. Extracellular matrix components modulate different stages in ß2-microglobulin amyloid formation. J. Biol. Chem. 294, 9392–9401.

Berendzen, K.M., Durieux, J., Shao, L.W., Tian, Y., Kim, H. eui, Wolff, S., Liu, Y., Dillin, A., 2016. Neuroendocrine Coordination of Mitochondrial Stress Signaling and Proteostasis. Cell 166, 1553-1563.e10.

Betsholtz, C., Christmansson, L., Engström, U., Rorsman, F., Svensson, V., Johnson, K.H., Westermark, P., 1989. Sequence divergence in a specific region of islet amyloid polypeptide (IAPP) explains differences in islet amyloid formation between species. FEBS Lett. 251, 261–264.

Bharadwaj, S., Ali, A., Ovsenek, N., 1999. Multiple Components of the HSP90 Chaperone Complex

Function in Regulation of Heat Shock Factor 1 In Vivo. Mol. Cell. Biol. 19, 8033–8041.

Blair, L.J., Nordhues, B.A., Hill, S.E., Scaglione, K.M., O'Leary, J.C., Fontaine, S.N., Breydo, L., Zhang, B., Li, P., Wang, L., Cotman, C., Paulson, H.L., Muschol, M., Uversky, V.N., Klengel, T., Binder, E.B., Kayed, R., Golde, T.E., Berchtold, N., Dickey, C.A., 2013. Accelerated neurodegeneration through chaperone-mediated oligomerization of tau. J. Clin. Invest. 123, 4158–4169.

Brais, B., Bouchard, J.-P., Xie, Y.G., Rochefort, D.L., Chrétien, N., Tomé, F.M.S., Lafrenière, R.G., Rommens, J.M., Uyama, E., Nohira, O., Blumen, S., Korcyn, A.D., Heutink, P., Mathieu, J., Duranceau, A., Codère, F., Fardeau, M., Rouleau, G.A., 1998. Short GCG expansions in the PABP2 gene cause oculopharyngeal muscular dystrophy. Nat. Genet. 18, 164–167.

Brandt, R., Gergou, A., Wacker, I., Fath, T., Hutter, H., 2009. A *Caenorhabditis elegans* model of tau hyperphosphorylation: Induction of developmental defects by transgenic overexpression of Alzheimer's disease-like modified tau. Neurobiol. Aging 30, 22–33.

Brehme, M., Voisine, C., Rolland, T., Wachi, S., Soper, J.H., Zhu, Y., Orton, K., Villella, A., Garza, D., Vidal, M., Ge, H., Morimoto, R.I., 2014. A chaperome subnetwork safeguards proteostasis in aging and neurodegenerative disease. Cell Rep. 9, 1135–1150.

Brenner, S., 1974. The genetics of *Caenorhabditis elegans*. Genetics 77, 71–94.

Brignull, H.R., Moore, F.E., Tang, S.J., Morimoto, R.I., 2006. Polyglutamine proteins at the pathogenic threshold display neuron-specific aggregation in a pan-neuronal *Caenorhabditis elegans* model. J. Neurosci. 26, 7597–7606.

Burga, A., Ben-David, E., Lemus Vergara, T., Boocock, J., Kruglyak, L., 2019. Fast genetic mapping of complex traits in *C. elegans* using millions of individuals in bulk. Nat. Commun. 10.

Butler, A.E., Jang, J., Gurlo, T., Carty, M.D., Soeller, W.C., Butler, P.C., 2004. Diabetes due to a progressive defect in ß-cell mass in rats transgenic for human islet amyloid polypeptide (HIP rat): A new model for type 2 diabetes. Diabetes 53, 1509–1516.

Calfon, M., Zeng, H., Urano, F., Till, J.H., Hubbard, S.R., Harding, H.P., Clark, S.G., Ron, D., 2002. IRE1 couples endoplasmic reticulum load to secretory capacity by processing the XBP-1 mRNA (Nature (2002) 415 (92-96)). Nature 420, 202.

Cao, P., Meng, F., Abedini, A., Raleigh, D.P., 2010. The ability of rodent islet amyloid polypeptide to inhibit amyloid formation by human islet amyloid polypeptide has important implications for the mechanism of amyloid formation and the design of inhibitors. Biochemistry 49, 872–881.

Casas, S., Gomis, R., Gribble, F.M., Altirriba, J., Knuutila, S., Novials, A., 2007. Impairment of the ubiquitin-proteasome pathway is a downstream endoplasmic reticulum stress response induced by extracellular human islet amyloid polypeptide and contributes to pancreatic B-Cell apoptosis. Diabetes 56.

Celniker, S.E., Dillon, L.A.L., Gerstein, M.B., Gunsalus, K.C., Henikoff, S., Karpen, G.H., Kellis, M., Lai, E.C., Lieb, J.D., MacAlpine, D.M., Micklem, G., Piano, F., Snyder, M., Stein, L., White, K.P., Waterston, R.H., 2009. Unlocking the secrets of the genome. Nature 459, 927–930.

Chaudhuri, P., Prajapati, K.P., Anand, B.G., Dubey, K., Kar, K., 2019. Amyloid cross-seeding raises new dimensions to understanding of amyloidogenesis mechanism. Ageing Res. Rev. 56, 100937.

Chen, X., Barclay, J.W., Burgoyne, R.D., Morgan, A., 2015. Using *C. elegans* to discover therapeutic compounds for ageing-associated neurodegenerative diseases. Chem. Cent. J. 9, 65.

Chen, Y.-C., Taylor, A.J., Verchere, C.B., 2018. Islet prohormone processing in health and disease. Diabetes, Obes. Metab. 20, 64–76.

Chen, Y., Wang, B., Liu, D., Li, J.J., Xue, Y., Sakata, K., Zhu, L. -q., Heldt, S.A., Xu, H., Liao, F.-F., 2014. Hsp90 chaperone Inhibitor 17-AAG attenuates Aß-induced synaptic toxicity and memory impairment. J. Neurosci. 34, 2464–2470.

Chien, V., Aitken, J.F., Zhang, S., Buchanan, C.M., Hickey, A., Brittain, T., Cooper, G.J.S., Loomes, K.M., 2010. The chaperone proteins HSP70, HSP40/DnaJ and GRP78/BiP suppress misfolding and formation of ß-sheet-containing aggregates by human amylin: a potential role for defective chaperone biology in Type 2 diabetes. Biochem. J. 432, 113–21.

Chiti, F., De Lorenzi, E., Grossi, S., Mangione, P., Giorgetti, S., Caccialanza, G., Dobson, C.M., Merlini, G., Ramponi, G., Bellotti, V., 2001. A partially structured species of ß2-microglobulin Is significantly populated under physiological conditions and involved in fibrillogenesis. J. Biol. Chem. 276, 46714–46721.

Chiti, F., Dobson, C.M., 2017. Protein misfolding, amyloid formation, and human disease: A summary of progress over the last decade. Annu. Rev. Biochem. 86, 27–68.

Conde-Knape, K., 2001. Heparan sulfate proteoglycans in experimental models of diabetes: A role for perlecan in diabetes complications. Diabetes. Metab. Res. Rev. 17, 412–421.

Costes, S., 2018. Targeting protein misfolding to protect pancreatic beta-cells in type 2 diabetes. Curr. Opin. Pharmacol. 43, 104–110.

Costes, S., Huang, C.J., Gurlo, T., Daval, M., Matveyenko, A. V., Rizza, R.A., Butler, A.E., Butler, P.C., 2011. ß-cell dysfunctional ERAD/ubiquitin/proteasome system in type 2 diabetes mediated by islet amyloid polypeptide-induced UCH-L1 deficiency. Diabetes 60, 227–238.

Das, M., Mei, X., Jayaraman, S., Atkinson, D., Gursky, O., 2014. Amyloidogenic mutations in human apolipoprotein A-I are not necessarily destabilizing - A common mechanism of apolipoprotein A-I misfolding in familial amyloidosis and atherosclerosis. FEBS J. 281, 2525–2542.

De Koning, E.J.P., Höppener, J.W.M., Verbeek, J.S., Oosterwijk, C., Van Hulst, K.L., Baker, C.A., Lips, C.J.M., Morris, J.F., Clark, A., 1994. Human islet amyloid polypeptide accumulates at similar sites in islets of transgenic mice and humans. Diabetes 43, 640–644.

Dearborn, A.D., Wall, J.S., Cheng, N., Heymann, J.B., Kajava, A. V., Varkey, J., Langen, R., Steven, A.C., 2016. α-Synuclein amyloid fibrils with two entwined, asymmetrically associated protofibrils. J. Biol. Chem. 291, 2310–2318.

Dickey, C.A., Burrows, F., Petrucelli, L., Dickey, C.A., Kamal, A., Lundgren, K., Klosak, N., Bailey, R.M., Dunmore, J., Ash, P., Shoraka, S., Zlatkovic, J., Eckman, C.B., Patterson, C., Dickson, D.W., Jr, N.S.N., Hutton, M., Burrows, F., Petrucelli, L., 2007. The high-affinity HSP90-CHIP complex recognizes and selectively degrades phosphorylated tau client proteins. J. Clin. Invest. 117, 648–658.

Diomede, L., Soria, C., Romeo, M., Giorgetti, S., Marchese, L., Mangione, P.P., Porcari, R., Zorzoli, I., Salmona, M., Bellotti, V., Stoppini, M., 2012. *C. elegans* expressing human ß2-microglobulin: A novel model for studying the relationship between the molecular assembly and the toxic phenotype. PLoS One 7.

Dobson, C.M., 2004. Principles of protein folding, misfolding and aggregation. Semin. Cell Dev. Biol. 15, 3–16.

Doherty, C.P.A., Ulamec, S.M., Maya-Martinez, R., Good, S.C., Makepeace, J., Khan, G.N., van Oosten-Hawle, P., Radford, S.E., Brockwell, D.J., 2020. A short motif in the N-terminal region of α-synuclein is critical for both aggregation and function. Nat. Struct. Mol. Biol. 27, 249–259.

Duan, M., Fan, J., Huo, S., 2012. Conformations of Islet Amyloid Polypeptide monomers in a membrane environment: Implications for fibril formation. PLoS One 7.

Dubey, K., Anand, B.G., Temgire, M.K., Kar, K., 2014. Evidence of rapid coaggregation of globular proteins during amyloid formation. Biochemistry 53, 8001–8004.

Durieux, J., Wolff, S., Dillin, A., 2011. The cell-non-autonomous nature of electron transport chain-mediated longevity. Cell 144, 79–91.

Eckert, A., Pagani, L., 2011. Amyloid-beta interaction with mitochondria. Int. J. Alzheimers. Dis. 2011.

Eichner, T., Kalverda, A.P., Thompson, G.S., Homans, S.W., Radford, S.E., 2011. Conformational conversion during amyloid formation at atomic resolution. Mol. Cell 41, 161–172.

Eichner, T., Radford, S.E., 2009. A generic mechanism of ß2-microglobulin amyloid assembly at neutral pH involving a specific proline switch. J. Mol. Biol. 386, 1312–1326.

Englander, S.W., Mayne, L., 2017. The case for defined protein folding pathways. Proc. Natl. Acad. Sci. U. S. A. 114, 8253–8258.

Esposito, G., Michelutti, R., Verdone, G., Viglino, P., ÁNdez, H.H., Robinson, C. V., Amoresano, A., Piaz, F.D., Monti, M., Pucci, P., Mangione, P., Stoppini, M., Merlini, G., Ferri, G., Bellotti, V., 2000. Removal of the N-terminal hexapeptide from human ß2-microglobulin facilitates protein aggregation and fibril formation. Protein Sci. 9, 831–845.

Evans, C.G., Wisén, S., Gestwicki, J.E., 2006. Heat shock proteins 70 and 90 inhibit early stages of amyloid ß-(1-42) aggregation in vitro. J. Biol. Chem. 281, 33182–33191.

Exley, C., House, E., Patel, T., Wu, L., Fraser, P.E., 2010. Human pro-islet amyloid polypeptide (ProIAPP1-48) forms amyloid fibrils and amyloid spherulites in vitro. J. Inorg. Biochem. 104, 1125–1129.

Faber, P.W., Voisine, C., King, D.C., Bates, E.A., Hart, A.C., 2002. Glutamine/proline-rich PQE-1 proteins protect *Caenorhabditis elegans* neurons from huntingtin polyglutamine neurotoxicity. Proc. Natl. Acad. Sci. U. S. A. 99, 17131–6.

Fan, H.C., Ho, L.I., Chi, C.S., Chen, S.J., Peng, G.S., Chan, T.M., Lin, S.Z., Harn, H.J., 2014. Polyglutamine (PolyQ) diseases: Genetics to treatments. Cell Transplant. 23, 441–458.

Faravelli, G., Raimondi, S., Marchese, L., Partridge, F.A., Soria, C., Mangione, P.P., Canetti, D., Perni, M., Aprile, F.A., Zorzoli, I., Di Schiavi, E., Lomas, D.A., Bellotti, V., Sattelle, D.B., Giorgetti, S., 2019. *C. elegans* expressing D76N ß2-microglobulin: a model for in vivo screening of drug candidates targeting amyloidosis. Sci. Rep. 9, 1–10.

Fawcett, T.W., Sylvester, S.L., Sarge, K.D., Morimoto, R.I., Holbrook, N.J., 1994. Effects of neurohormonal stress and aging on the activation of mammalian heat shock factor 1. J. Biol. Chem. 269, 32272–32278.

Fay, D.S., Fluet, a, Johnson, C.J., Link, C.D., 1998. In vivo aggregation of beta-amyloid peptide variants. J. Neurochem. 71, 1616–1625.

Ferreira, S.T., Klein, W.L., 2011. The Aß oligomer hypothesis for synapse failure and memory loss

in Alzheimer's disease. Neurobiol. Learn. Mem. 96, 529–543.

Ferrone, F., 1999. Analysis of protein aggregation kinetics. Methods Enzymol. 309, 256–274.

Fire, A., Xu, S., Montgomery, M.K., Kostas, S.A., Driver, S.E., Mello, C.C., 1998. Potent and specific genetic interference by double-stranded RNA in *Caenorhabditis elegans*. Nature 391, 806–811.

Fitzpatrick, A.W.P., Falcon, B., He, S., Murzin, A.G., Murshudov, G., Garringer, H.J., Crowther, R.A., Ghetti, B., Goedert, M., Scheres, S.H.W., 2017. Cryo-EM structures of tau filaments from Alzheimer's disease. Nature 547, 185–190.

Fonte, V., Kapulkin, W.J., Taft, A., Fluet, A., Friedman, D., Link, C.D., 2002. Interaction of intracellular ß amyloid peptide with chaperone proteins. Proc. Natl. Acad. Sci. 99, 9439–9444.

Fonte, V., Kipp, D.R., Yerg, J., Merin, D., Forrestal, M., Wagner, E., Roberts, C.M., Link, C.D., 2008. Suppression of in vivo B-amyloid peptide toxicity by overexpression of the HSP-16.2 small chaperone protein. J. Biol. Chem. 283, 784–791.

Frakes, A.E., Metcalf, M.G., Tronnes, S.U., Bar-Ziv, R., Durieux, J., Gildea, H.K., Kandahari, N., Monshietehadi, S., Dillin, A., 2020. Four glial cells regulate ER stress resistance and longevity via neuropeptide signaling in *C. elegans*. Science. 367, 436–440.

Frumkin, A., Dror, S., Pokrzywa, W., Bar-Lavan, Y., Karady, I., Hoppe, T., Ben-Zvi, A., 2014. Challenging muscle homeostasis uncovers novel chaperone interactions in *Caenorhabditis elegans*. Front. Mol. Biosci. 1, 21.

Gaiser, A.M., Brandt, F., Richter, K., 2009. The non-canonical Hop protein from *Caenorhabditis elegans* exerts essential functions and forms binary complexes with either Hsc70 or Hsp90. J. Mol. Biol. 391, 621–634.

Gaiser, A.M., Kaiser, C.J.O., Haslbeck, V., Richter, K., 2011. Downregulation of the Hsp90 system causes defects in muscle cells of *Caenorhabditis elegans*. PLoS One 6.

Gaiser, A.M., Kretzschmar, A., Richter, K., 2010. Cdc37-Hsp90 complexes are responsive to nucleotide-induced conformational changes and binding of further cofactors. J. Biol. Chem. 285, 40921–40932.

Gallotta, I., Sandhu, A., Peters, M., Haslbeck, M., Jung, R., Agilkaya, S., Blersch, J.L., Rödelsperger, C., Röseler, W., Huang, C., Sommer, R.J., David, D.C., 2020. Extracellular proteostasis prevents aggregation during pathogenic attack. Nature 584, 410–414.

Geddes, A.J., Parker, K.D., Atkins, E.D.T., Beighton, E., 1968. "Cross-ß" conformation in proteins. J. Mol. Biol. 32, 343–358.

Gejyo, F., Yamada, T., Odani, S.-, Arakawa, M., Kunitomo, T., Kataoka, H., Suzuki, M., Hirasawa, Y., Shirahama, T., Cohen, A.S., Schmid, K., 1985. A new form of amyloid protein associated with chronic hemodialysis was identified as ß2-microglobulin. Biochem. Biophys. Res. Commun. 129, 701–706.

Gidalevitz, T., Ben-Zvi, A., Ho, K.H., Brignull, H.R., Morimoto, R.I., 2006. Progressive disruption of cellular protein folding in models of polyglutamine diseases. Science. 311, 1471–1474.

Gidalevitz, T., Krupinski, T., Garcia, S., Morimoto, R.I., 2009. Destabilizing protein polymorphisms in the genetic background direct phenotypic expression of mutant SOD1 toxicity. PLoS Genet. 5.

Glabe, C.G., 2006. Common mechanisms of amyloid oligomer pathogenesis in degenerative disease.

Neurobiol. Aging 27, 570–575.

Goodchild, S.C., Sheynis, T., Thompson, R., Tipping, K.W., Xue, W.F., Ranson, N.A., Beales, P.A., Hewitt, E.W., Radford, S.E., 2014. β2-microglobulin amyloid fibril-induced membrane disruption is enhanced by endosomal lipids and acidic pH. PLoS One 9.

Guo, Y., Guettouche, T., Fenna, M., Boellmann, F., Pratt, W.B., Toft, D.O., Smith, D.F., Voellmy, R., 2001. Evidence for a mechanism of repression of Heat Shock Factor 1 transcriptional activity by a multichaperone complex. J. Biol. Chem. 276, 45791–45799.

Gurlo, T., Ryazantsev, S., Huang, C.J., Yeh, M.W., Reber, H.A., Hines, O.J., O'Brien, T.D., Glabe, C.G., Butler, P.C., 2010. Evidence for proteotoxicity in β cells in type 2 diabetes: Toxic islet amyloid polypeptide oligomers form intracellularly in the secretory pathway. Am. J. Pathol. 176, 861–869.

Gursky, O., Mei, X., Atkinson, D., 2012. The crystal structure of the C-terminal truncated apolipoprotein A-I sheds new light on amyloid formation by the N-terminal fragment. Biochemistry 51, 10–18.

Habchi, J., Arosio, P., Perni, M., Costa, A.R., Yagi-Utsumi, M., Joshi, P., Chia, S.K.R., Cohen, S.I.A., Müller, M.B.., Linse, S., Nollen, E.A.A., Dobson, C.M., Knowles, T.P.J., Vendruscolo, M., 2016. An anti-cancer drug suppresses the primary nucleation reaction that initiates the formation of toxic Aß aggregates associated with Alzheimer's disease. Sci. Adv. e1501244, 1–13.

Hajdu-Cronin, Y.M., Chen, W.J., Sternberg, P.W., 2004. The L-type cyclin CYL-1 and the heat-shock-factor HSF-1 are required for heat-shock-induced protein expression in *Caenorhabditis elegans*. Genetics 168, 1937–1949.

Hamamichi, S., Rivas, R.N., Knight, A.L., Cao, S., Caldwell, K. a, Caldwell, G. a, 2008. Hypothesis-based RNAi screening identifies neuroprotective genes in a Parkinson's disease model. Proc. Natl. Acad. Sci. U. S. A. 105, 728–733.

Han, S.K., Lee, D., Lee, H., Kim, D., Son, H.G., Yang, J.S., Lee, S.J. V., Kim, S., 2016. OASIS 2: Online application for survival analysis 2 with features for the analysis of maximal lifespan and healthspan in aging research. Oncotarget 7, 56147–56152.

Harding, H.P., Novoa, I., Zhang, Y., Zeng, H., Wek, R., Schapira, M., Ron, D., 2000. Regulated translation initiation controls stress-induced gene expression in mammalian cells. Mol. Cell 6, 1099–1108.

Harding, H.P., Zhang, Y., Zeng, H., Novoa, I., Lu, P.D., Calfon, M., Sadri, N., Yun, C., Popko, B., Paules, R., Stojdl, D.F., Bell, J.C., Hettmann, T., Leiden, J.M., Ron, D., 2003. An integrated stress response regulates amino acid metabolism and resistance to oxidative stress. Mol. Cell 11, 619–633.

Hartl, F.U., Bracher, A., Hayer-Hartl, M., 2011. Molecular chaperones in protein folding and proteostasis. Nature 475, 324–332.

Haynes, C.M., Yang, Y., Blais, S.P., Neubert, T.A., Ron, D., 2010. The matrix peptide exporter HAF-1 signals a mitochondrial UPR by activating the transcription factor ZC376.7 in *C. elegans*. Mol. Cell 37, 529–540.

Haze, K., Yoshida, H., Yanagi, H., Yura, T., Mori, K., 1999. Mammalian transcription factor ATF6 is synthesized as a transmembrane protein and activated by proteolysis in response to endoplasmic reticulum stress. Mol. Biol. Cell 10, 3787–3799.

Hetz, C., Martinon, F., Rodriguez, D., Glimcher, L.H., 2011. The unfolded protein response: Integrating stress signals through the stress sensor IRE1 α. Physiol. Rev. 91, 1219–1243.

Hipp, M.S., Kasturi, P., Hartl, F.U., 2019. The proteostasis network and its decline in ageing. Nat. Rev. Mol. Cell Biol. 20, 421–435.

Hipp, M.S., Park, S.H., Hartl, U.U., 2014. Proteostasis impairment in protein-misfolding and -aggregation diseases. Trends Cell Biol.

Hipp, M.S., Patel, C.N., Bersuker, K., Riley, B.E., Kaiser, S.E., Shaler, T.A., Brandeis, M., Kopito, R.R., 2012. Indirect inhibition of 26S proteasome activity in a cellular model of Huntington's disease. J. Cell Biol. 196, 573–587.

Hoop, C.L., Zhu, J., Bhattacharya, S., Tobita, C.A., Radford, S.E., Baum, J., 2020. Collagen i weakly interacts with the ß-sheets of ß2-microglobulin and enhances conformational exchange to induce amyloid formation. J. Am. Chem. Soc. 142, 1321–1331.

Hu, R., Zhang, M., Chen, H., Jiang, B., Zheng, J., 2015. Cross-seeding interaction between ß-amyloid and human islet amyloid polypeptide. ACS Chem. Neurosci. 6, 1759–1768.

Huang, C., Lin, C., Haataja, L., Gurlo, T., Butler, A.E., Rizza, R.A., Butler, P.C., 2007. High expression rates of human islet amyloid of humans with type 2 but not type 1 diabetes. Diabetes 56, 2016–2027.

Huang, Y., Mucke, L., 2012. Alzheimer mechanisms and therapeutic strategies. Cell 148, 1204–1222.

Hull, R.L., Zraika, S., Udayasankar, J., Aston-Mourney, K., Subramanian, S.L., Kahn, S.E., 2009. Amyloid formation in human IAPP transgenic mouse islets and pancreas, and human pancreas, is not associated with endoplasmic reticulum stress. Diabetologia 52, 1102–1111.

Hutter, H., Vogel, B.E., Plenefisch, J.D., Norris, C.R., Proenca, R.B., Spieth, J., Guo, C., Mastwal, S., Zhu, X., Scheel, J., Hedgecock, E.M., 2000. Conservation and novelty in the evolution of cell adhesion and extracellular matrix genes. Science. 287, 989–1010.

Iadanza, M.G., Jackson, M.P., Hewitt, E.W., Ranson, N.A., Radford, S.E., 2018. A new era for understanding amyloid structures and disease. Nat. Rev. Mol. Cell Biol. 19, 755–773.

Imanikia, S., Özbey, N.P., Krueger, C., Casanueva, M.O., Taylor, R.C., 2019a. Neuronal XBP-1 activates intestinal lysosomes to improve proteostasis in *C. elegans*. Curr. Biol. 29, 2322-2338.e7.

Imanikia, S., Sheng, M., Castro, C., Griffin, J.L., Taylor, R.C., 2019b. XBP-1 remodels lipid metabolism to extend longevity. Cell Rep. 28, 581-589.e4.

Inada, H., Ito, H., Satterlee, J., Sengupta, P., Matsumoto, K., Mori, I., 2006. Identification of guanylyl cyclases that function in thermosensory neurons of *Caenorhabditis elegans*. Genetics 172, 2239–2252.

Jackson, K., Barisone, G.A., Diaz, E., Jin, L.W., DeCarli, C., Despa, F., 2013. Amylin deposition in the brain: A second amyloid in Alzheimer disease? Ann. Neurol. 74, 517–526.

Jackson, S.E., 1998. How do small single-domain proteins fold? Fold. Des. 3, R81–R91.

Jacob, T.C., Kaplan, J.M., 2003. The EGL-21 carboxypeptidase E facilitates acetylcholine release at *Caenorhabditis elegans* neuromuscular junctions. J. Neurosci. 23, 2122–2130.

Jadoul, M., Drüeke, T.B., 2016. ß2-microglobulin amyloidosis: An update 30 years later. Nephrol. Dial. Transplant.

Jakhria, T., Hellewell, A.L., Porter, M.Y., Jackson, M.P., Tipping, K.W., Xue, W.F., Radford, S.E., Hewitt, E.W., 2014. ß2-microglobulin amyloid fibrils are nanoparticles that disrupt lysosomal membrane protein trafficking and inhibit protein degradation by lysosomes. J. Biol. Chem. 289, 35781–35794.

Janson, J., Soeller, W.C., Roche, P.C., Nelson, R.T., Torchia, A.J., Kreutter, D.K., Butler, P.C., 1996. Spontaneous diabetes mellitus in transgenic mice expressing human islet amyloid polypeptide. Proc. Natl. Acad. Sci. U. S. A. 93, 7283–7288.

Jha, S., Patil, S.M., Gibson, J., Nelson, C.E., Alder, N.N., Alexandrescu, A.T., 2011. Mechanism of amylin fibrillization enhancement by heparin. J. Biol. Chem. 286, 22894–22904.

Ji, T., Zhang, X., Xin, Z., Xu, B., Jin, Z., Wu, J., Hu, W., Yang, Y., 2020. Does perturbation in the mitochondrial protein folding pave the way for neurodegeneration diseases? Ageing Res. Rev. 57, 100997.

Jinwal, U.K., Koren, J., Borysov, S.I., Schmid, A.B., Abisambra, J.F., Blair, L.J., Johnson, A.G., Jones, J.R., Shults, C.L., O'Leary, J.C., Jin, Y., Buchner, J., Cox, M.B., Dickey, C.A., 2010. The Hsp90 cochaperone, FKBP51, increases tau stability and polymerizes microtubules. J. Neurosci. 30, 591–599.

Kakimura, J.-I., Kitamura, Y., Takata, K., Umeki, M., Suzuki, S., Shibagaki, K., Taniguchi, T., Nomura, Y., Gebicke-Haerter, P.J., Smith, M.A., Perry, G., Shimohama, S., 2002. Microglial activation and amyloid-ß clearance induced by exogenous heat-shock proteins. FASEB J. 16, 601–603.

Kampinga, H.H., Craig, E.A., 2010. The HSP70 chaperone machinery: J proteins as drivers of functional specificity. Nat. Rev. Mol. Cell Biol. 11, 579–592.

Karamanos, T.K., Jackson, M.P., Calabrese, A.N., Goodchild, S.C., Cawood, E.E., Thompson, G.S., Kalverda, A.P., Hewitt, E.W., Radford, S.E., 2019. Structural mapping of oligomeric intermediates in an amyloid assembly pathway. Elife 8, 1–32.

Karamanos, T.K., Kalverda, A.P., Thompson, G.S., Radford, S.E., 2014. Visualization of transient protein-protein interactions that promote or inhibit amyloid assembly. Mol. Cell 55, 214–226.

Karamanos, T.K., Pashley, C.L., Kalverda, A.P., Thompson, G.S., Mayzel, M., Orekhov, V.Y., Radford, S.E., 2016. A population shift between sparsely populated folding intermediates determines amyloidogenicity. J. Am. Chem. Soc. 138, 6271–6280.

Karpinar, D.P., Balija, M.B.G., Kugler, S., Opazo, F., Rezaei-Ghaleh, N., Wender, N., Kim, H.-Y., Taschenberger, B.H., Heise, H., Kumar, A., Riedel, D., Fichtner, L., Voigt, A., Braus, G.H., Giller, K., Becker, S., Herzig, A., Baldus, M., Jackle, H., Eimer, S., Schulz, J.B., Griesinger, C., Zweckstetter, M., 2009. Pre-fibrillar a-synuclein variants with impaired B-structure increase neurotoxicity in Parkinson's disease models. EMBO J. 28, 3256–3268.

Kass, J., Jacob, T.C., Kim, P., Kaplan, J.M., 2001. The EGL-3 proprotein convertase regulates mechanosensory responses of *Caenorhabditis elegans*. J. Neurosci. 21, 9265–72.

Kayed, R., Head, E., Sarsoza, F., Saing, T., Cotman, C.W., Necula, M., Margol, L., Wu, J., Breydo, L., Thompson, J.L., Rasool, S., Gurlo, T., Butler, P., Glabe, C.G., 2007. Fibril specific, conformation dependent antibodies recognize a generic epitope common to amyloid fibrils and fibrillar oligomers that is absent in prefibrillar oligomers. Mol. Neurodegener. 2, 1–11.

Khan, L.A., Bauer, P.O., Miyazaki, H., Lindenberg, K.S., Landwehrmeyer, B.G., Nukina, N., 2006. Expanded polyglutamines impair synaptic transmission and ubiquitin – proteasome system in *Caenorhabditis elegans*. J. Neurochem. 98, 576–587.

Kirstein, J., Arnsburg, K., Scior, A., Szlachcic, A., Guilbride, D.L., Morimoto, R.I., Bukau, B., Nillegoda, N.B., 2017. In vivo properties of the disaggregase function of J-proteins and Hsc70 in *Caenorhabditis elegans* stress and aging. Aging Cell 16, 1414–1424.

Knight, J.D., Hebda, J.A., Miranker, A.D., 2006. Conserved and cooperative assembly of membrane-bound α-helical states of islet amyloid polypeptide. Biochemistry 45, 9496–9508.

Knowles, T.P.J., Vendruscolo, M., Dobson, C.M., 2014. The amyloid state and its association with protein misfolding diseases. Nat. Rev. Mol. Cell Biol. 15, 384–96.

Kohler, V., Andreasson, C., 2020. Hsp70-mediated quality control : should I stay or should I go ? Biol. Chem. 401, 1233–1248.

Kollmer, M., Close, W., Funk, L., Rasmussen, J., Bsoul, A., Schierhorn, A., Schmidt, M., Sigurdson, C.J., Jucker, M., Fändrich, M., 2019. Cryo-EM structure and polymorphism of Aß amyloid fibrils purified from Alzheimer's brain tissue. Nat. Commun. 10, 1–8.

Köppen, J., Schulze, A., Machner, L., Wermann, M., Eichentopf, R., Guthardt, M., Hähnel, A., Klehm, J., Kriegeskorte, M.C., Hartlage-Rübsamen, M., Morawski, M., von Hörsten, S., Demuth, H.U., Roßner, S., Schilling, S., 2020. Amyloid-beta peptides trigger aggregation of alpha-synuclein in vitro. Molecules 25, 1–18.

Kourie, J.I., Henry, C.L., 2002. Ion channel formation and membrane-linked pathologies of misfolded hydrophobic proteins: The role of dangerous unchaperoned molecules. Clin. Exp. Pharmacol. Physiol. 29, 741–753.

Kraemer, B.C., Burgess, J.K., Chen, J.H., Thomas, J.H., Schellenberg, G.D., 2006. Molecular pathways that influence human tau-induced pathology in *Caenorhabditis elegans*. Hum. Mol. Genet. 15, 1483–1496.

Kraemer, B.C., Zhang, B., Leverenz, J.B., Thomas, J.H., Trojanowski, J.Q., Schellenberg, G.D., 2003. Neurodegeneration and defective neurotransmission in a *Caenorhabditis elegans* model of tauopathy. Proc. Natl. Acad. Sci. 100, 9980–9985.

Kristiansen, M., Deriziotis, P., Dimcheff, D.E., Jackson, G.S., Ovaa, H., Naumann, H., Clarke, A.R., van Leeuwen, F.W.B., Menéndez-Benito, V., Dantuma, N.P., Portis, J.L., Collinge, J., Tabrizi, S.J., 2007. Disease-associated prion protein oligomers inhibit the 26S proteasome. Mol. Cell 26, 175–188.

Krone, M.G., Baumketner, A., Bernstein, S.L., Wyttenbach, T., Lazo, N.D., Teplow, D.B., Bowers, M.T., Shea, J.E., 2008. Effects of familial Alzheimer's disease mutations on the folding nucleation of the amyloid ß-protein. J. Mol. Biol. 381, 221–228.

Krotee, P., Rodriguez, J.A., Sawaya, M.R., Cascio, D., Reyes, F.E., Shi, D., Hattne, J., Nannenga, B.L., Oskarsson, M.E., Philipp, S., Griner, S., Jiang, L., Glabe, C.G., Westermark, G.T., Gonen, T., Eisenberg, D.S., 2017. Atomic structures of fibrillar segments of hIAPP suggest tightly mated ß-sheets are important for cytotoxicity. Elife 6, 1–26.

Kuwahara, T., Koyama, A., Koyama, S., Yoshina, S., Ren, C.H., Kato, T., Mitani, S., Iwatsubo, T., 2008. A systematic RNAi screen reveals involvement of endocytic pathway in neuronal dysfunction in α-synuclein transgenic *C . elegans*. Hum. Mol. Genet. 17, 2997–3009.

Labbadia, J., Morimoto, R.I., 2015. The biology of proteostasis in aging and disease. Annu. Rev. Biochem. 84, 435–464.

Lackie, R.E., Maciejewski, A., Ostapchenko, V.G., Marques-Lopes, J., Choy, W.-Y., Duennwald, M.L., Prado, V.F., Prado, M.A.M., 2017. The Hsp70/Hsp90 chaperone machinery in neurodegenerative diseases. Front. Neurosci. 11, 254.

Lakso, M., Vartiainen, S., Moilanen, A.-M., Sirviö, J., Thomas, J.H., Nass, R., Blakely, R.D., Wong, G., 2003. Dopaminergic neuronal loss and motor deficits in *Caenorhabditis elegans* overexpressing human α-synuclein. J. Neurochem. 86, 165–172.

Langer, T., Lu, C., Echols, H., Flanagan, J., Hayer, M.K., Hartl, F.U., 1992. Successive action of DnaK, DnaJ and GroEL along the pathway of chaperone-mediated protein folding. Nature 356, 683–689.

Law, E., Lu, S., Kieffer, T.J., Warnock, G.L., Ao, Z., Woo, M., Marzban, L., 2010. Differences between amyloid toxicity in alpha and beta cells in human and mouse islets and the role of caspase-3. Diabetologia 53, 1415–1427.

Lejeune, F.X., Mesrob, L., Parmentier, F., Bicep, C., Vazquez-Manrique, R.P., Parker, J.A., Vert, J.P., Tourette, C., Neri, C., 2012. Large-scale functional RNAi screen in *C. elegans* identifies genes that regulate the dysfunction of mutant polyglutamine neurons. BMC Genomics 13, 91.

Leri, M., Bemporad, F., Oropesa-Nuñez, R., Canale, C., Calamai, M., Nosi, D., Ramazzotti, M., Giorgetti, S., Pavone, F.S., Bellotti, V., Stefani, M., Bucciantini, M., 2016. Molecular insights into cell toxicity of a novel familial amyloidogenic variant of ß2-microglobulin. J. Cell. Mol. Med. 20, 1443–1456.

Levinthal, C., 1968. Are there pathways for protein folding? J. Chim. Phys. 65, 44–45.

Li, J., Li, T., Zhang, X., Tang, Y., Yang, J., Le, W., 2013. Human superoxide dismutase 1 overexpression in motor neurons of *Caenorhabditis elegans* causes axon guidance defect and neurodegeneration. Neurobiol. Aging 35, 837–846.

Li, J., Uversky, V.N., Fink, A.L., 2001. Effect of familial Parkinson's disease point mutations A30P and A53T on the structural properties, aggregation, and fibrillation of human α-synuclein. Biochemistry 40, 11604–11613.

Liachko, N.F., Guthrie, C.R., Kraemer, B.C., 2010. Phosphorylation promotes neurotoxicity in a *Caenorhabditis elegans* model of TDP-43 proteinopathy. J. Neurosci. 30, 16208–16219.

Linden, R., Martins, V.R., Prado, M.A.M., Cammarota, M., Izquierdo, I., Brentani, R.R., 2008. Physiology of the prion protein. Physiol. Rev. 88, 673–728.

Lindquist, S., 1986. The Heat Shock Reponse. Annu. Rev. Biochem. 1151–91.

Link, C.D., 1995. Expression of human β-amyloid peptide in transgenic *Caenorhabditis elegans*. Proc. Natl. Acad. Sci. 92, 9368–9372.

Link, C.D., Johnson, C.J., Fonte, V., Paupard, M.C., Hall, D.H., Styren, S., Mathis, C.A., Klunk, W.E., 2001a. Visualization of fibrillar amyloid deposits in living, transgenic *Caenorhabditis elegans* animals using the sensitive amyloid dye, X-34. Neurobiol. Aging 22, 217–226.

Link, C.D., Taft, A., Kapulkin, V., Duke, K., Kim, S., Fei, Q., Wood, D.E., Sahagan, B.G., 2003. Gene expression analysis in a transgenic *Caenorhabditis elegans* Alzheimer's disease model. Neurobiol. Aging 24, 397–413.

Linse, S., 2017. Monomer-dependent secondary nucleation in amyloid formation. Biophys. Rev. 9, 329–338.

Lu, J.X., Qiang, W., Yau, W.M., Schwieters, C.D., Meredith, S.C., Tycko, R., 2013. Molecular structure of ß-amyloid fibrils in alzheimer's disease brain tissue. Cell 154, 1257.

Lublin, A.L., Link, C.D., 2013. Alzheimer's disease drug discovery: In vivo screening using

Caenorhabditis elegans as a model for ß-amyloid peptide-induced toxicity. Drug Discov. Today Technol. 10, e115–e119.

Luo, W., Dou, F., Rodina, A., Chip, S., Kim, J., Zhao, Q., Moulick, K., Aguirre, J., Wu, N., Greengard, P., Chiosis, G., 2007. Roles of heat-shock protein 90 in maintaining and facilitating the neurodegenerative phenotype in tauopathies. Proc. Natl. Acad. Sci. U. S. A. 104, 9511–9516.

Ma, Z., Westermark, G.T., Sakagashira, S., Sanke, T., Gustavsson, Å., Sakamoto, H., Engström, U., Nanjo, K., Westermark, P., 2001. Enhanced in vitro production of amyloid-like fibrils from mutant (S20G) islet amyloid polypeptide. Amyloid 8, 242–249.

Maciejewski, A., Ostapchenko, V.G., Beraldo, F.H., Prado, V.F., Prado, M.A.M., Choy, W.Y., 2016. Domains of STIP1 responsible for regulating PrPC-dependent amyloid-ß oligomer toxicity. Biochem. J. 473, 2119–2130.

Madhivanan, K., Greiner, E.R., Alves-Ferreira, M., Soriano-Castell, D., Rouzbeh, N., Aguirre, C.A., Paulsson, J.F., Chapman, J., Jiang, X., Ooi, F.K., Lemos, C., Dillin, A., Prahlad, V., Kelly, J.W., Encalada, S.E., 2018. Cellular clearance of circulating transthyretin decreases cell-nonautonomous proteotoxicity in *Caenorhabditis elegans*. Proc. Natl. Acad. Sci. 201801117.

Mahadevan, N.R., Rodvold, J., Sepulveda, H., Rossi, S., Drew, A.F., Zanetti, M., 2011. Transmission of endoplasmic reticulum stress and pro-inflammation from tumor cells to myeloid cells. Proc. Natl. Acad. Sci. U. S. A. 108, 6561–6566.

Mangione, P.P., Esposito, G., Relini, A., Raimondi, S., Porcari, R., Giorgetti, S., Corazza, A., Fogolari, F., Penco, A., Goto, Y., Lee, Y.-H., Yagi, H., Cecconi, C., Naqvi, M.M., Gillmore, J.D., Hawkins, P.N., Chiti, F., Rolandi, R., Taylor, G.W., Pepys, M.B., Stoppini, M., Bellotti, V., 2013. Structure, folding dynamics, and amyloidogenesis of D76N ß2-microglobulin. J. Biol. Chem. 288, 30917–30930.

Marciniak, S.J., Yun, C.Y., Oyadomari, S., Novoa, I., Zhang, Y., Jungreis, R., Nagata, K., Harding, H.P., Ron, D., 2004. CHOP induces death by promoting protein synthesis and oxidation in the stressed endoplasmic reticulum. Genes Dev. 18, 3066–3077.

Markaki, M., Tavernakis, N., 2010. Modeling human disease in *C. elegans*. Biotechnol. J. 5, 1261–1276.

Martins, I.C., Kuperstein, I., Wilkinson, H., Maes, E., Vanbrabant, M., Jonckheere, W., Van Gelder, P., Hartmann, D., D'Hooge, R., De Strooper, B., Schymkowitz, J., Rousseau, F., 2008. Lipids revert inert Aß amyloid fibrils to neurotoxic protofibrils that affect learning in mice. EMBO J. 27, 224–233.

Marzban, L., Rhodes, C.J., Steiner, D.F., Haataja, L., Halban, P.A., Verchere, C.B., 2006. Impaired NH2-terminal processing of human proislet amyloid polypeptide by the prohormone convertase PC2 leads to amyloid formation and cell death. Diabetes 55, 2192–2201.

Matai, L., Sarkar, G.C., Chamoli, M., Malik, Y., Kumar, S.S., Rautela, U., Jana, N.R., Chakraborty, K., Mukhopadhyay, A., 2019. Dietary restriction improves proteostasis and increases life span through endoplasmic reticulum hormesis. Proc. Natl. Acad. Sci. U. S. A. 116, 17383–17392.

McColl, G., Roberts, B.R., Gunn, A.P., Perez, K.A., Tew, D.J., Masters, C.L., Barnham, K.J., Cherny, R.A., Bush, A.I., 2009. The *Caenorhabditis elegans* Aß1-42 model of Alzheimer disease predominantly Expresses Aß3-42. J. Biol. Chem. 284, 22697–22702.

McColl, G., Roberts, B.R., Pukala, T.L., Kenche, V.B., Roberts, C.M., Link, C.D., Ryan, T.M., Masters, C.L., Barnham, K.J., Bush, A.I., Cherny, R. a, 2012. Utility of an improved model of amyloid-beta ($Aß_{1-42}$) toxicity in *Caenorhabditis elegans* for drug screening for Alzheimer's disease. Mol. Neurodegener. 7, 57.

Meier, D.T., Entrup, L., Templin, A.T., Hogan, M.F., Mellati, M., Zraika, S., Hull, R.L., Kahn, S.E., 2016. The S20G substitution in hIAPP is more amyloidogenic and cytotoxic than wild-type hIAPP in mouse islets. Diabetologia 59, 2166–2171.

Meisl, G., Kirkegaard, J.B., Arosio, P., Michaels, T.C.T., Vendruscolo, M., Dobson, C.M., Linse, S., Knowles, T.P.J., 2016. Molecular mechanisms of protein aggregation from global fitting of kinetic models. Nat. Protoc. 11, 252–272.

Menaa, C., Esser, E., Sprague, S.M., 2008. ß2-microglobulin stimulates osteoclast formation. Kidney Int. 73, 1275–1281.

Milanesi, L., Sheynis, T., Xue, W.F., Orlova, E. V., Hellewell, A.L., Jelinek, R., Hewitt, E.W., Radford, S.E., Saibil, H.R., 2012. Direct three-dimensional visualization of membrane disruption by amyloid fibrils. Proc. Natl. Acad. Sci. U. S. A. 109, 20455–20460.

Miles, J., Scherz-Shouval, R., van Oosten-Hawle, P., 2019. Expanding the organismal proteostasis network: Linking systemic stress signaling with the innate immune response. Trends Biochem. Sci. 44, 927–942.

Miyasaka, T., Ding, Z., Gengyo-Ando, K., Oue, M., Yamaguchi, H., Mitani, S., Ihara, Y., 2005. Progressive neurodegeneration in *C. elegans* model of tauopathy. Neurobiol. Dis. 20, 372–383.

Miyasaka, T., Xie, C., Yoshimura, S., Shinzaki, Y., Yoshina, S., Kage-Nakadai, E., Mitani, S., Ihara, Y., 2016. Curcumin improves tau-induced neuronal dysfunction of nematodes. Neurobiol. Aging 39, 69–81.

Mogk, A., Kummer, E., Bukau, B., 2015. Cooperation of Hsp70 and Hsp100 chaperone machines in protein disaggregation. Front. Mol. Biosci. 2, 1–10.

Montgomery, M.K., Xu, S., Fire, A., 1998. RNA as a target of double-stranded RNA-mediated genetic interference in *Caenorhabditis elegans*. Proc. Natl. Acad. Sci. U. S. A. 95, 15502–15507.

Morales, R., Estrada, L.D., Diaz-Espinoza, R., Morales-Scheihing, D., Jara, M.C., Castilla, J., Soto, C., 2010. Molecular cross talk between misfolded proteins in animal models of Alzheimer's and prion diseases. J. Neurosci. 30, 4528–4535.

Mori, I., Ohshima, Y., 1995. Neural regulation of thermotaxis in *C. elegans*. Nature 376, 344–348.

Morita, S., Ueyama, M., Sakagashira, S., Shimajiri, Y., Yamana, A., Furuta, M., Sanke, T., 2013. Protective role of human insulin against the cytotoxicity associated with human mutant S20G islet amyloid polypeptide. J. Diabetes Investig. 4, 436–444.

Morley, J.F., Brignull, H.R., Weyers, J.J., Morimoto, R.I., 2002. The threshold for polyglutamine-expansion protein aggregation and cellular toxicity is dynamic and influenced by aging in *Caenorhabditis elegans*. Proc. Natl. Acad. Sci. U. S. A. 99, 10417–10422.

Muñoz-Lobato, F., Rodríguez-Palero, M.J., Naranjo-Galindo, F.J., Shephard, F., Gaffney, C.J., Szewczyk, N.J., Hamamichi, S., Caldwell, K.A., Caldwell, G.A., Link, C.D., Miranda-Vizuete, A., 2014. Protective role of DNJ-27/ERdj5 in *Caenorhabditis elegans* models of human neurodegenerative diseases. Antioxid. Redox Signal. 20, 217–35.

Myers, S.L., Jones, S., Jahn, T.R., Morten, I.J., Tennent, G.A., Hewitt, E.W., Radford, S.E., 2006. A systematic study of the effect of physiological factors on ß2-microglobulin amyloid formation at neutral pH. Biochemistry 45, 2311–2321.

Nadeau, K., Das, A., Walsh, C.T., 1993. Hsp90 chaperonins possess ATPase activity and bind heat

shock transcription factors and peptidyl prolyl isomerases. J. Biol. Chem. 268, 1479–1487.

Nance, J., Frøkjær-Jensen, C., 2019. The *Caenorhabditis elegans* transgenic toolbox, Genetics.

Nanga, R.P.R., Brender, J.R., Vivekanandan, S., Ramamoorthy, A., 2011. Structure and membrane orientation of IAPP in its natively amidated form at physiological pH in a membrane environment. Biochim. Biophys. Acta - Biomembr. 1808, 2337–2342.

Neef, D.W., Jaeger, A.M., Gomez-Pastor, R., Willmund, F., Frydman, J., Thiele, D.J., 2014. A direct regulatory interaction between chaperonin TRiC and stress-responsive transcription factor HSF1. Cell Rep. 9, 955–966.

Nelson, P.T., Alafuzoff, I., Bigio, E.H., Bouras, C., Braak, H., Cairns, N.J., Castellani, R.J., Crain, B.J., Davies, P., Tredici, K. Del, Duyckaerts, C., Frosch, M.P., Haroutunian, V., Hof, P.R., Hulette, C.M., Hyman, B.T., Iwatsubo, T., Jellinger, K.A., Jicha, G.A., Kövari, E., Kukull, W.A., Leverenz, J.B., Love, S., MacKenzie, I.R., Mann, D.M., Masliah, E., McKee, A.C., Montine, T.J., Morris, J.C., Schneider, J.A., Sonnen, J.A., Thal, D.R., Trojanowski, J.Q., Troncoso, J.C., Wisniewski, T., Woltjer, R.L., Beach, T.G., 2012. Correlation of alzheimer disease neuropathologic changes with cognitive status: A review of the literature. J. Neuropathol. Exp. Neurol. 71, 362–381.

Neupert, W., Herrmann, J.M., 2007. Translocation of proteins into mitochondria. Annu. Rev. Biochem. 76, 723–749.

Nillegoda, N.B., Kirstein, J., Szlachcic, A., Berynskyy, M., Stank, A., Stengel, F., Arnsburg, K., Gao, X., Scior, A., Aebersold, R., Guilbride, D.L., Wade, R.C., Morimoto, R.I., Mayer, M.P., Bukau, B., 2015. Crucial HSP70 co-chaperone complex unlocks metazoan protein disaggregation. Nature 524, 247–251.

Nillegoda, N.B., Wentink, A.S., Bukau, B., 2018. Protein disaggregation in multicellular organisms. Trends Biochem. Sci. 43, 285–300.

Nussbaum-Krammer, C.I., Neto, M.F., Brielmann, R.M., Pedersen, J.S., Morimoto, R.I., 2015. Investigating the spreading and toxicity of prion-like proteins using the metazoan model organism *C. elegans*. J. Vis. Exp. 1–15.

O'Brien, D., Jones, L.M., Good, S., Miles, J., Vijayabaskar, M.S., Aston, R., Smith, C.E., Westhead, D.R., van Oosten-Hawle, P., 2018. A PQM-1-mediated response triggers transcellular chaperone signaling and regulates organismal proteostasis. Cell Rep. 23, 3905–3919.

O'Nuallain, B., Wetzel, R., 2002. Conformational Abs recognizing a generic amyloid fibril epitope. Proc. Natl. Acad. Sci. U. S. A. 99, 1485–1490.

O'Nuallain, B., Williams, A.D., Westermark, P., Wetzel, R., 2004. Seeding specificity in amyloid growth Induced by heterologous fibrils. J. Biol. Chem. 279, 17490–17499.

Oeda, T., Shimohama, S., Kitagawa, N., Kohno, R., Imura, T., Shibasaki, H., Ishii, N., 2001. Oxidative stress causes abnormal accumulation of familial amyotrophic lateral sclerosis-related mutant SOD1 in transgenic *Caenorhabditis elegans*. Hum. Mol. Genet. 10, 2013–2023.

Olzscha, H., Schermann, S.M., Woerner, A.C., Pinkert, S., Hecht, M.H., Tartaglia, G.G., Vendruscolo, M., Hayer-Hartl, M., Hartl, F.U., Vabulas, R.M., 2011. Amyloid-like aggregates sequester numerous metastable proteins with essential cellular functions. Cell 144, 67–78.

Oskarsson, M.E., Paulsson, J.F., Schultz, S.W., Ingelsson, M., Westermark, P., Westermark, G.T., 2015. In vivo seeding and cross-seeding of localized amyloidosis: A molecular link between type 2 diabetes and Alzheimer disease. Am. J. Pathol. 185, 834–846.

Ostapchenko, V.G., Beraldo, F.H., Mohammad, A.H., Xie, Y.-F., Hirata, P.H.F., Magalhaes, A.C., Lamour, G., Li, H., Maciejewski, A., Belrose, J.C., Teixeira, B.L., Fahnestock, M., Ferreira, S.T., Cashman, N.R., Hajj, G.N.M., Jackson, M.F., Choy, W.-Y., MacDonald, J.F., Martins, V.R., Prado, V.F., Prado, M.A.M., 2013. The prion protein ligand, stress-inducible phosphoprotein 1, regulates amyloid- oligomer toxicity. J. Neurosci. 33, 16552–16564.

Paravastu, A.K., Leapman, R.D., Yau, W.M., Tycko, R., 2008. Molecular structural basis for polymorphism in Alzheimer's ß-amyloid fibrils. Proc. Natl. Acad. Sci. U. S. A. 105, 18349–18354.

Park, S.H., Kukushkin, Y., Gupta, R., Chen, T., Konagai, A., Hipp, M.S., Hayer-Hartl, M., Hartl, F.U., 2013. PolyQ proteins interfere with nuclear degradation of cytosolic proteins by sequestering the Sis1p chaperone. Cell 154, 134–145.

Park, Y.J., Lee, S., Kieffer, T.J., Warnock, G.L., Safikhan, N., Speck, M., Hao, Z., Woo, M., Marzban, L., 2012. Deletion of Fas protects islet beta cells from cytotoxic effects of human islet amyloid polypeptide. Diabetologia 55, 1035–1047.

Paulsson, J.F., Andersson, A., Westermark, P., Westermark, G.T., 2006. Intracellular amyloid-like deposits contain unprocessed pro-islet amyloid polypeptide (proIAPP) in beta cells of transgenic mice overexpressing the gene for human IAPP and transplanted human islets. Diabetologia 49, 1237–1246.

Paulsson, J.F., Westermark, G.T., 2005. Aberrant processing of human proislet amyloid polypeptide results in increased amyloid formation. Diabetes 54, 2117–2125.

Pearl, L.H., Prodromou, C., 2006. Structure and mechanism of the Hsp90 molecular chaperone machinery. Annu. Rev. Biochem. 75, 271–294.

Pellegrino, M.W., Nargund, A.M., Haynes, C.M., 2013. Signaling the mitochondrial unfolded protein response. Biochim. Biophys. Acta - Mol. Cell Res. 1833, 410–416.

Perni, M., Aprile, F.A., Casford, S., Mannini, B., Sormanni, P., Dobson, C.M., Vendruscolo, M., 2017. Delivery of native proteins into *C. elegans* using a transduction protocol based on lipid vesicles. Sci. Rep. 7, 1–8.

Pieri, L., Madiona, K., Bousset, L., Melki, R., 2012. Fibrillar α-synuclein and huntingtin exon 1 assemblies are toxic to the cells. Biophys. J. 102, 2894–2905.

Pillay, K., Govender, P., 2013. Amylin uncovered: A review on the polypeptide responsible for type II diabetes. Biomed Res. Int. 2013.

Pir, G.J., Choudhary, B., Mandelkow, E., 2017. *Caenorhabditis elegans* models of tauopathy. FASEB J. 31, 5137–5148.

Pir, G.J., Choudhary, B., Mandelkow, E., Mandelkow, E.M., 2016. Tau mutant A152T, a risk factor for FTD/PSP, induces neuronal dysfunction and reduced lifespan independently of aggregation in a *C. elegans* Tauopathy model. Mol. Neurodegener. 11, 1–21.

Porter, M.Y., Routledge, K.E., Radford, S.E., Hewitt, E.W., 2011. Characterization of the response of primary cells relevant to dialysis-related amyloidosis to ß2-microglobulin monomer and fibrils. PLoS One 6.

Prahlad, V., Cornelius, T., Morimoto, R.I., 2008. Regulation of the cellular heat shock response in *Caenorhabditis elegans* by thermosensory neurons. Science. 320, 811–814.

Prahlad, V., Morimoto, R.I., 2011. Neuronal circuitry regulates the response of *Caenorhabditis elegans* to misfolded proteins. Proc. Natl. Acad. Sci. U. S. A. 108, 14204–14209.

Prodromou, C., 2016. Mechanisms of Hsp90 regulation. Biochem. J.

Puchtler, H., Sweat, F., Levine, M., 1961. On the binding of congo red by amyloid. J. Histochem. Cytochem. 10, 355–364.

Raimundo, A.F., Ferreira, S., Martins, I.C., Menezes, R., 2020. Islet amyloid polypeptide: A partner in crime rith Aß in the pathology of Alzheimer's disease. Front. Mol. Neurosci. 13.

Raizen, D.M., Zimmerman, J.E., Maycock, M.H., Ta, U.D., You, Y.J., Sundaram, M. V., Pack, A.I., 2008. Lethargus is a *Caenorhabditis elegans* sleep-like state. Nature 451, 569–572.

Raleigh, D., Zhang, X., Hastoy, B., Clark, A., 2017. The ß-cell assassin: IAPP cytotoxicity. J. Mol. Endocrinol. 59, R121–R140.

Ramot, D., MacInnis, B.L., Goodman, M.B., 2008. Bidirectional temperature-sensing by a single thermosensory neuron in *C. elegans*. Nat. Neurosci. 11, 908–915.

Reimold, A.M., Iwakoshi, N.N., Manis, J., Vallabhajosyula, P., Szomolanyi-Tsuda, E., Gravallese, E.M., Friend, D., Grusby, M.J., Alt, F., Glimcher, L.H., 2001. Plasma cell differentiation requires the transcription factor XBP-1. Nature 412, 300–307.

Relini, A., Canale, C., De Stefano, S., Rolandi, R., Giorgetti, S., Stoppini, M., Rossi, A., Fogolari, F., Corazza, A., Esposito, G., Gliozzi, A., Bellotti, V., 2006. Collagen plays an active role in the aggregation of ß2-microglobulin under physiopathological conditions of dialysis-related amyloidosis. J. Biol. Chem. 281, 16521–16529.

Relini, A., De Stefano, S., Torrassa, S., Cavalleri, O., Rolandi, R., Gliozzi, A., Giorgetti, S., Raimondi, S., Marchese, L., Verga, L., Rossi, A., Stoppini, M., Bellotti, V., 2008. Heparin strongly enhances the formation of ß2-microglobulin amyloid fibrils in the presence of type I collagen. J. Biol. Chem. 283, 4912–4920.

Rendleman, J., Cheng, Z., Maity, S., Kastelic, N., Munschauer, M., Allgoewer, K., Teo, G., Zhang, Y.B.M., Lei, A., Parker, B., Landthaler, M., Freeberg, L., Kuersten, S., Choi, H., Vogel, C., 2018. New insights into the cellular temporal response to proteostatic stress. Elife 7.

Renton, A.E., Majounie, E., Waite, A., Simón-Sánchez, J., Rollinson, S., Gibbs, J.R., Schymick, J.C., Laaksovirta, H., van Swieten, J.C., Myllykangas, L., Kalimo, H., Paetau, A., Abramzon, Y., Remes, A.M., Kaganovich, A., Scholz, S.W., Duckworth, J., Ding, J., Harmer, D.W., Hernandez, D.G., Johnson, J.O., Mok, K., Ryten, M., Trabzuni, D., Guerreiro, R.J., Orrell, R.W., Neal, J., Murray, A., Pearson, J., Jansen, I.E., Sondervan, D., Seelaar, H., Blake, D., Young, K., Halliwell, N., Callister, J.B., Toulson, G., Richardson, A., Gerhard, A., Snowden, J., Mann, D., Neary, D., Nalls, M.A., Peuralinna, T., Jansson, L., Isoviita, V.M., Kaivorinne, A.L., Hölttä-Vuori, M., Ikonen, E., Sulkava, R., Benatar, M., Wuu, J., Chiò, A., Restagno, G., Borghero, G., Sabatelli, M., Heckerman, D., Rogaeva, E., Zinman, L., Rothstein, J.D., Sendtner, M., Drepper, C., Eichler, E.E., Alkan, C., Abdullaev, Z., Pack, S.D., Dutra, A., Pak, E., Hardy, J., Singleton, A., Williams, N.M., Heutink, P., Pickering-Brown, S., Morris, H.R., Tienari, P.J., Traynor, B.J., 2011. A hexanucleotide repeat expansion in C9ORF72 is the cause of chromosome 9p21-linked ALS-FTD. Neuron 72, 257–268.

Reuben, A., 2004. The legend of the lardaceous liver. Hepatology 40, 763–766.

Reynolds, N.P., Adamcik, J., Berryman, J.T., Handschin, S., Zanjani, A.A.H., Li, W., Liu, K., Zhang, A., Mezzenga, R., 2017. Competition between crystal and fibril formation in molecular mutations of amyloidogenic peptides. Nat. Commun. 8.

Richmond, J.E., Davis, W.S., Jorgensen, E.M., 1999. Unc-13 is required for synaptic vesicle fusion in C. elegnas. Nat. Neurosci. 2, 959–964.

Rivera, J.F., Costes, S., Gurlo, T., Glabe, C.G., Butler, P.C., 2014. Autophagy defends pancreatic ß cells from Human islet amyloid polypeptide-induced toxicity. J. Clin. Invest. 124, 3489–3500.

Rosas, P.C., Nagaraja, G.M., Kaur, P., Panossian, A., Wickman, G., Garcia, L.R., Al-Khamis, F.A., Asea, A.A.A., 2016. Hsp72 (HSPA1A) prevents human islet amyloid polypeptide aggregation and Toxicity: A new approach for type 2 diabetes treatment. PLoS One 11.

Rose, A.M., Baillie, D.L., 1979. The effect of temperature and parental age on recombination and nondisjunction in *Caenorhabditis elegans*. Genetics 92, 409–18.

Rousseau, F., Serrano, L., Schymkowitz, J.W.H., 2006. How evolutionary pressure against protein aggregation shaped chaperone specificity. J. Mol. Biol. 355, 1037–1047.

Rüdiger, S., Buchberger, A., Bukau, B., 1997. Interaction of Hsp70 chaperones with substrates. Nat. Struct. Biol. 4, 342–349.

Sakagashira, S., Hiddinga, H.J., Tateishi, K., Sanke, T., Hanabusa, T., Nanjo, K., Eberhardt, N.L., 2000. S20G mutant amylin exhibits increased in vitro amyloidogenicity and increased intracellular cytotoxicity compared to wild-type amylin. Am. J. Pathol. 157, 2101–2109.

Sakagashira, S.S., Hanabusa, T., Shimomura, T., S, H.O., 1996. Missense mutation of amylin gene (S20G) in Japanese NIDDM patients. Diabetes 45, 1279–1281.

Salminen, A., Ojala, J., Kaarniranta, K., Hiltunen, M., Soininen, H., 2011. Hsp90 regulates tau pathology through co-chaperone complexes in Alzheimer's disease. Prog. Neurobiol. 93, 99–110.

Sarell, C.J., Stockley, P.G., Radford, S.E., 2013a. Assessing the causes and consequences of co-polymerization in amyloid formation. Prion 7, 359–368.

Sarell, C.J., Woods, L.A., Su, Y., Debelouchina, G.T., Ashcroft, A.E., Griffin, R.G., Stockley, P.G., Radford, S.E., 2013b. Expanding the repertoire of amyloid polymorphs by co-polymerization of related protein precursors. J. Biol. Chem. 288, 7327–7337.

Sarge, K.D., Murphy, S.P., Morimoto, R.I., 1993. Activation of heat shock gene transcription by heat shock factor 1 involves oligomerization, acquisition of DNA-binding activity, and nuclear localization and can occur in the absence of stress. Mol. Cell. Biol. 13, 1392–1407.

Scarponi, R., Ricardi, M., Albertazzi, V., De Amicis, S., Rastelli, F., Zerbini, L., 2016. Dialysis-related amyloidosis : challenges and solutions. Int. J. Nephrol. Renovasc. Dis. 9, 319–328.

Scheuermann, T., Schulz, B., Blume, A., Wahle, E., Rudolph, R., Schwarz, E., 2003. Trinucleotide expansions leading to an extended poly-l-alanine segment in the poly (A) binding protein PABPN1 cause fibril formation. Protein Sci. 12, 2685–2692.

Schindler, A.J., Schekman, R., 2009. In vitro reconstitution of ER-stress induced ATF6 transport in COPII vesicles. Proc. Natl. Acad. Sci. U. S. A. 106, 17775–17780.

Schmid, A.B., Lagleder, S., Gräwert, M.A., Röhl, A., Hagn, F., Wandinger, S.K., Cox, M.B., Demmer, O., Richter, K., Groll, M., Kessler, H., Buchner, J., 2012. The architecture of functional modules in the Hsp90 co-chaperone Sti1/Hop. EMBO J. 31, 1506–1517.

Schopf, F.H., Biebl, M.M., Buchner, J., 2017. The HSP90 chaperone machinery. Nat. Rev. Mol. Cell Biol. 18, 345–360.

Schröder, M., Kaufman, R.J., 2005. ER stress and the unfolded protein response. Mutat. Res. - Fundam. Mol. Mech. Mutagen. 569, 29–63.

Scior, A., Buntru, A., Arnsburg, K., Ast, A., Iburg, M., Juenemann, K., Pigazzini, M.L., Mlody, B., Puchkov, D., Priller, J., Wanker, E.E., Prigione, A., Kirstein, J., 2018. Complete suppression of Htt fibrilization and disaggregation of Htt fibrils by a trimeric chaperone complex. EMBO J. 37, 282–299.

Sekijima, Y., Wiseman, R.L., Matteson, J., Hammarström, P., Miller, S.R., Sawkar, A.R., Balch, W.E., Kelly, J.W., 2005. The biological and chemical basis for tissue-selective amyloid disease. Cell 121, 73–85.

Shao, L.W., Niu, R., Liu, Y., 2016. Neuropeptide signals cell non-autonomous mitochondrial unfolded protein response. Cell Res. 26, 1182–1196.

Shaye, D.D., Greenwald, I., 2011. Ortholist: A compendium of *C. elegans* genes with human orthologs. PLoS One 6.

Sheynis, T., Friediger, A., Xue, W.F., Hellewell, A.L., Tipping, K.W., Hewitt, E.W., Radford, S.E., Jelinek, R., 2013. Aggregation modulators interfere with membrane interactions of ß2-microglobulin fibrils. Biophys. J. 105, 745–755.

Shirahama, T., Cohen, A.S., 1965. Structure of amyloid fibrils after negative staining and high-resolution electron microscopy. Nature 206, 737–738.

Shpigel, N., Shemesh, N., Kishner, M., Ben-Zvi, A., 2019. Dietary restriction and gonadal signaling differentially regulate post-development quality control functions in *Caenorhabditis elegans*. Aging Cell 18.

Sidrauski, C., Walter, P., 1997. The transmembrane kinase Ire1p is a site-specific endonuclease that initiates mRNA splicing in the unfolded protein response. Cell 90, 1031–1039.

Sipe, J.D., Cohen, A.S., 2000. Review: History of the amyloid fibril. J. Struct. Biol. 130, 88–98.

Smith, H.I., Guthertz, N., Cawood, E.E., Maya-Martinez, R., Breeze, A.L., Radford, S.E., 2020. The role of the IT-state in D76N ß2-microglobulin amyloid assembly: A crucial intermediate or an innocuous bystander? J. Biol. Chem. 295, 12474–12484.

Song, H.O., Lee, W., An, K., Lee, H. suk, Cho, J.H., Park, Z.Y., Ahnn, J., 2009. *C. elegans* STI-1, the homolog of Sti1/Hop, Is involved in aging and stress response. J. Mol. Biol. 390, 604–617.

Song, Y., Masison, D.C., 2005. Independent regulation of Hsp70 and Hsp90 chaperones by Hsp70/Hsp90-organizing protein Sti1 (Hop1). J. Biol. Chem. 280, 34178–34185.

Sorrentino, V., Romani, M., Mouchiroud, L., Beck, J.S., Zhang, H., D'Amico, D., Moullan, N., Potenza, F., Schmid, A.W., Rietsch, S., Counts, S.E., Auwerx, J., 2017. Enhancing mitochondrial proteostasis reduces amyloid-ß proteotoxicity. Nature 552, 187–193.

Stefani, M., 2012. Structural features and cytotoxicity of amyloid oligomers: Implications in Alzheimer's disease and other diseases with amyloid deposits. Prog. Neurobiol. 99, 226–245.

Stiernagle, T., 2006. Maintenance of *C. elegans*. WormBook 1–11.

Strominger, L., Wiley, D.C., Bjorkman, P.J., Saper, M.A., Samraoui, B., Bennett, W.S., 1987. Structure of the human class I histocompatibility antigen, HLA-A2. Nature 329, 506–512.

Stumvoll, M., Goldstein, B.J., van Haeften, T.W., 2005. Type 2 diabetes : principles of pathogenesis and therapy pathophysiology of hyperglycaemia. Lancet 365, 1333–1346.

Subramanian, S.L., Hull, R.L., Zraika, S., Aston-Mourney, K., Udayasankar, J., Kahn, S.E., 2012.

cJUN N-terminal kinase (JNK) activation mediates islet amyloid-polypeptide transgenic mouse islets. Diabetologia 55, 166–174.

Sui, X., Pires, D.E.V., Ormsby, A.R., Cox, D., Nie, S., Vecchi, G., Vendruscolo, M., Ascher, D.B., Reid, G.E., Hatters, D.M., 2020. Widespread remodeling of proteome solubility in response to different protein homeostasis stresses. Proc. Natl. Acad. Sci. U. S. A. 117, 2422–2431.

Sulston, J.E., Schierenberg, E., White, J.G., Thomson, J.N., 1983. The embryonic cell lineage of the nematode *Caenorhabditis elegans*. Dev. Biol. 100, 64–119.

Taipale, M., Jarosz, D.F., Lindquist, S., 2010. HSP90 at the hub of protein homeostasis: emerging mechanistic insights. Nat. Rev. Mol. Cell Biol. 11, 515–28.

Tatum, M.C., Ooi, F.K., Chikka, M.R., Chauve, L., Martinez-Velazquez, L.A., Steinbusch, H.W.M., Morimoto, R.I., Prahlad, V., 2015. Neuronal serotonin release triggers the heat shock response in *C. elegans* in the absence of temperature increase. Curr. Biol. 25, 163–174.

Taylor, R.C., Dillin, A., 2011. Aging as an event of proteostasis collapse. Cold Spring Harb. Perspect. Biol. 3, 1–17.

Taylor, R.C., Dillin, A., 2013. XBP-1 Is a cell-nonautonomous regulator of stress resistance and longevity. Cell 153, 1435–1447.

Teixeira-Castro, A., Ailion, M., Jalles, A., Brignull, H.R., Vilaca, J.L., Dias, N., Rodrigues, P., Oliveira, J.F., Carvalho, A.N., Morimoto, R.I., Maciel, P., 2011. Neuron-specific proteotoxicity of mutant ataxin-3 in *C . elegans* : rescue by the DAF-16 and HSF-1 pathways. Hum. Mol. Genet. 20, 2996–3009.

Teo, E., Ravi, S., Barardo, D., Kim, H.-S., Fong, S., Cazenave-Gassiot, A., Tan, T.Y., Ching, J., Kovalik, J.-P., Wenk, M.R., Gunawan, R., Moore, P.K., Halliwell, B., Tolwinski, N., Gruber, J., 2019. Metabolic stress is a primary pathogenic event in transgenic *Caenorhabditis elegans* expressing pan-neuronal human amyloid beta. Elife 1–25.

Tepper, R.G., Ashraf, J., Kaletsky, R., Kleemann, G., Murphy, C.T., Bussemaker, H.J., 2013. PQM-1 complements DAF-16 as a key transcriptional regulator of DAF-2-mediated development and longevity. Cell 154, 676–690.

Tipping, K.W., van Oosten-Hawle, P., Hewitt, E.W., Radford, S.E., 2015. Amyloid fibres: Inert end-stage aggregates or key players in disease? Trends Biochem. Sci. 40, 719–727.

Treusch, S., Hamamichi, S., Goodman, J.L., Matlack, K.E.S., Chung, C.Y., Baru, V., Shulman, J.M., Parrado, A., Bevis, B.J., Valastyan, J.S., Han, H., Lindhagen-persson, M., Reiman, E.M., Evans, D.A., Bennett, D.A., Olofsson, A., Dejager, P.L., Tanzi, R.E., Caldwell, K.A., Caldwell, G.A., Lindquist, S., 2011. Functional links between Aß toxicity, endocytic trafficking, and Alzheimer's disease risk factors in yeast. Science. 334, 1241–1245.

Tsang, W.Y., Lemire, B.D., 2003. The role of mitochondria in the life of the nematode, *Caenorhabditis elegans*. Biochim. Biophys. Acta - Mol. Basis Dis. 1638, 91–105.

Tsuda, Y., Yamanaka, K., Toyoshima, R., Ueda, M., Masuda, T., Misumi, Y., Ogura, T., Ando, Y., 2018. Development of transgenic *Caenorhabditis elegans* expressing human transthyretin as a model for drug screening. Sci. Rep. 8, 17884.

Tyedmers, J., Mogk, A., Bukau, B., 2010. Cellular strategies for controlling protein aggregation. Nat. Rev. Mol. Cell Biol. 11, 777–788.

Urushitani, M., Kurisu, J., Tsukita, K., Takahashi, R., 2002. Proteasomal inhibition by misfolded mutant superoxide dismutase 1 induces selective motor neuron death in familial amyotrophic

lateral sclerosis. J. Neurochem. 83, 1030–1042.

Valleix, S., Gillmore, J.D., Bridoux, F., Mangione, P.P., Dogan, A., Nedelec, B., Boimard, M., Touchard, G., Goujon, J., Lacombe, C., Lozeron, P., Adams, D., Lacroix, C., Maisonobe, T., Planté-Bordeneuve, V., Vrana, J.A., Theis, J.D., Giorgetti, S., Porcari, R., Ricagno, S., Bolognesi, M., Stoppini, M., Delpech, M., Pepys, M.B., Hawkins, P.N., Bellotti, V., 2012. Hereditary systemic amyloidosis due to Asp76Asn variant ß2-microglobulin. N. Engl. J. Med. 366, 2276–2283.

van Ham, T.J., Holmberg, M.A., van der Goot, A.T., Teuling, E., Garcia-Arencibia, M., Kim, H. eui, Du, D., Thijssen, K.L., Wiersma, M., Burggraaff, R., van Bergeijk, P., van Rheenen, J., Jerre van Veluw, G., Hofstra, R.M.W., Rubinsztein, D.C., Nollen, E.A.A., 2010. Identification of MOAG-4/SERF as a regulator of age-related proteotoxicity. Cell 142, 601–612.

Van Ham, T.J., Thijssen, K.L., Breitling, R., Hofstra, R.M.W., Plasterk, R.H.A., Nollen, E.A.A., 2008. *C. elegans* model identifies genetic modifiers of α-synuclein inclusion formation during aging. PLoS Genet. 4.

Van Oosten-Hawle, P., Porter, R.S., Morimoto, R.I., 2013. Regulation of organismal proteostasis by transcellular chaperone signaling. Cell 153, 1366.

Vartiainen, S., Pehkonen, P., Lakso, M., Nass, R., Wong, G., 2006. Identification of gene expression changes in transgenic *C. elegans* overexpressing human α-synuclein. Neurobiol. Dis. 22, 477–486.

Verdone, G., Corazza, A., Viglino, P., Pettirossi, F., Giorgetti, S., Mangione, P., Andreola, A., Stoppini, M., Bellotti, V., Esposito, G., 2009. The solution structure of human ß2-microglobulin reveals the prodromes of its amyloid transition. Protein Sci. 11, 487–499.

Vidal, J., Verchere, C.B., Andrikopoulos, S., Wang, F., Hull, R.L., Cnop, M., Olin, K.L., LeBoeuf, R.C., O'Brien, K.D., Chait, A., Kahn, S.E., 2003. The effect of apolipoprotein E deficiency on islet amyloid deposition in human islet amyloid polypeptide transgenic mice. Diabetologia 46, 71–79.

Waldherr, S.M., Strovas, T.J., Vadset, T.A., Liachko, N.F., Kraemer, B.C., 2019. Constitutive XBP-1s-mediated activation of the endoplasmic reticulum unfolded protein response protects against pathological tau. Nat. Commun. 10, 1–12.

Wallace, E.W.J., Kear-Scott, J.L., Pilipenko, E. V., Schwartz, M.H., Laskowski, P.R., Rojek, A.E., Katanski, C.D., Riback, J.A., Dion, M.F., Franks, A.M., Airoldi, E.M., Pan, T., Budnik, B.A., Drummond, D.A., 2015. Reversible, specific, active aggregates of endogenous proteins assemble upon heat stress. Cell 162, 1286–1298.

Walter, P., Ron, D., 2011. The unfolded protein response: From stress pathway to homeostatic regulation. Science. 334, 1081–1087.

Walther, D.M., Kasturi, P., Zheng, M., Pinkert, S., Vecchi, G., Ciryam, P., Morimoto, R.I., Dobson, C.M., Vendruscolo, M., Mann, M., Hartl, F.U., 2015. Widespread proteome remodeling and aggregation in aging *C. elegans*. Cell 161, 919–932.

Wang, B., Liu, Y., Huang, L., Chen, J., Li, J. jing, Wang, R., Eunhee, K., Justicia, C., Kazuko, S., Chen, H., Planas, A., Ostrom, R.S., Li, W., Yang, G., McDonald, M.P., Chen, R., Heck, D., Liao, F.-F., 2017. A CNS-permeable Hsp90 inhibitor rescues synaptic dysfunction and memory loss in APP-overexpressing Alzheimer's mouse model via an HSF1-mediated mechanism. Mol. Psychiatry 176, 139–148.

Wang, H., Lim, P.J., Karbowski, M., Monteiro, M.J., 2009. Effects of overexpression of Huntingtin proteins on mitochondrial integrity. Hum. Mol. Genet. 18, 737–752.

Wang, H., Lim, P.J., Yin, C., Rieckher, M., Vogel, B.E., Monteiro, M.J., 2006. Suppression of polyglutamine-induced toxicity in cell and animal models of Huntington's disease by ubiquilin. Hum. Mol. Genet. 15, 1025–1041.

Wang, J., Farr, G.W., Hall, D.H., Li, F., Furtak, K., Dreier, L., Horwich, A.L., 2009a. An ALS-linked mutant SOD1 produces a locomotor defect associated with aggregation and synaptic dysfunction when expressed in neurons of *Caenorhabditis elegans*. PLoS Genet. 5.

Wang, J., Farr, G.W., Zeiss, C.J., Rodriguez-Gil, D.J., Wilson, J.H., Furtak, K., Rutkowski, D.T., Kaufman, R.J., Ruse, C.I., Yates, J.R., Perrin, S., Feany, M.B., Horwich, A.L., 2009b. Progressive aggregation despite chaperone associations of a mutant SOD1-YFP in transgenic mice that develop ALS. Proc. Natl. Acad. Sci. U. S. A. 106, 1392–1397.

Wang, W.Y., Tan, M.S., Yu, J.T., Tan, L., 2015. Role of pro-inflammatory cytokines released from microglia in Alzheimer's disease. Ann. Transl. Med. 3, 1–15.

Wasmer, C., Lange, A., Van Melckebeke, H., Siemer, A.B., Riek, R., Meier, B.H., 2008. Amyloid fibrils of the HET-s(218-289) prion form a β solenoid with a triangular hydrophobic core. Science. 319, 1523–1526.

Weinshenker, D., Garriga, G., Thomas, J.H., 1995. Genetic and pharmacological analysis of neurotransmitters controlling egg laying in *C. elegans*. J. Neurosci. 15, 6975–6985.

Westermark, P., Andersson, A., Westermark, G.T., 2011. Islet amyloid polypeptide, islet amyloid, and diabetes mellitus. Physiol. Rev. 91, 795–826.

Williamson, J.A., Loria, J.P., Miranker, A.D., 2009. Helix stabilization precedes aqueous and bilayer-catalyzed fiber formation in islet amyloid polypeptide. J. Mol. Biol. 393, 383–396.

Winston, W.M., Molodowitch, C., Hunter, C.P., 2002. Systemic RNAi in *C. elegans* requires the putative transmembrane protein SID-1. Science. 295, 2456–2459.

Wolfe, K.J., Rena, H.Y., Trepte, P., Cyr, D.M., 2013. The Hsp70/90 cochaperone, Sti1, suppresses proteotoxicity by regulating spatial quality control of amyloid-like proteins. Mol. Biol. Cell 24, 3588–3602.

World Alzhiemer's Report, 2019. , Alzheimer's Disease International.

Wu, Y., Cao, Z., Klein, W.L., Luo, Y., 2010. Heat shock treatment reduces beta amyloid toxicity in vivo by diminishing oligomers. Neurobiol. Aging 31, 1055–1058.

Wu, Y., Wu, Z., Butko, P., Christen, Y., Lambert, M.P., Klein, W.L., Link, C.D., Luo, Y., 2006. Amyloid-B-induced pathological behaviors are suppressed by ginkgo biloba extract EGb 761 and ginkgolides in transgenic *Caenorhabditis elegans*. J. Neurosci. 26, 13102–13113.

Wyatt, A.R., Yerbury, J.J., Dabbs, R.A., Wilson, M.R., 2012. Roles of extracellular chaperones in amyloidosis. J. Mol. Biol. 421, 499–516.

Xu, W., Jiang, P., Mu, Y., 2009. Conformation preorganization: Effects of S20G mutation on the structure of human islet amyloid polypeptide segment. J. Phys. Chem. B 113, 7308–7314.

Xue, W.F., Hellewell, A.L., Gosal, W.S., Homans, S.W., Hewitt, E.W., Radford, S.E., 2009. Fibril fragmentation enhances amyloid cytotoxicity. J. Biol. Chem. 284, 34272–34282.

Yamamoto, S., Hasegawa, K., Yamaguchi, I., Goto, Y., Gejyo, F., Naiki, H., 2005. Kinetic analysis of the polymerization and depolymerization of β2-microglobulin-related amyloid fibrils in vitro. Biochim. Biophys. Acta - Proteins Proteomics 1753, 34–43.

Ye, J., Rawson, R.B., Komuro, R., Chen, X., Davé, U.P., Prywes, R., Brown, M.S., Goldstein, J.L., 2000. ER stress induces cleavage of membrane-bound ATF6 by the same proteases that process SREBPs. Mol. Cell 6, 1355–1364.

Yonemoto, I.T., Kroon, G.J.A., Dyson, H.J., Balch, W.E., Kelly, J.W., 2008. Amylin proprotein processing generates progressively more amyloidogenic peptides that initially sample the helical state. Biochemistry 47, 9900–9910.

Young, J.C., Obermann, W.M.J., Hartl, F.U., 1998. Specific binding of tetratricopeptide repeat proteins to the C-terminal 12-kDa domain of hsp90. J. Biol. Chem. 273, 18007–18010.

Young, L.M., Cao, P., Raleigh, D.P., Ashcroft, A.E., Radford, S.E., 2014. Ion mobility spectrometry-mass spectrometry defines the oligomeric intermediates in amylin amyloid formation and the mode of action of inhibitors. J. Am. Chem. Soc. 136, 660–670.

Young, L.M., Mahood, R.A., Saunders, J.C., Tu, L.H., Raleigh, D.P., Radford, S.E., Ashcroft, A.E., 2015. Insights into the consequences of co-polymerisation in the early stages of IAPP and Aß peptide assembly from mass spectrometry. Analyst 140, 6990–6999.

Young, L.M., Tu, L.H., Raleigh, D.P., Ashcroft, A.E., Radford, S.E., 2017. Understanding co-polymerization in amyloid formation by direct observation of mixed oligomers. Chem. Sci. 8, 5030–5040.

Zhang, Q., Wu, X., Chen, P., Liu, L., Xin, N., Tian, Y., Dillin, A., 2018. The mitochondrial unfolded protein response is mediated cell-non-autonomously by retromer-dependent Wnt signaling. Cell 174, 870-883.e17.

Zhang, T., Mullane, P.C., Periz, G., Wang, J., 2011. TDP-43 neurotoxicity and protein aggregation modulated by heat shock factor and insulin/IGF-1 signaling. Hum. Mol. Genet. 20, 1952–1965.

Zhao, R., Davey, M., Hsu, Y.C., Kaplanek, P., Tong, A., Parsons, A.B., Krogan, N., Cagney, G., Mai, D., Greenblatt, J., Boone, C., Emili, A., Houry, W.A., 2005. Navigating the chaperone network: An integrative map of physical and genetic interactions mediated by the hsp90 chaperone. Cell 120, 715–727.

Zhu, H., Tao, Q., Ang, T.F.A., Massaro, J., Gan, Q., Salim, S., Zhu, R.Y., Kolachalama, V.B., Zhang, X., Devine, S., Auerbach, S.H., DeCarli, C., Au, R., Qiu, W.Q., 2019. Association of plasma amylin concentration with Alzheimer disease and brain structure in older adults. JAMA Netw. open 2, e199826.

Zou, J., Guo, Y., Guettouche, T., Smith, D.F., Voellmy, R., 1998. Repression of heat shock transcription factor HSF1 activation by HSP90 (HSP90 complex) that forms a stress-sensitive complex with HSF1. Cell 94, 471–480.

Zraika, S., Hull, R.L., Udayasankar, J., Aston-Mourney, K., Subramanian, S.L., Kisilevsky, R., Szarek, W.A., Kahn, S.E., 2009. Oxidative stress is induced by islet amyloid formation and time-dependently mediates amyloid-induced beta cell apoptosis. Diabetologia 52, 626–635.

Zwanzig, R., Szabo, A., Bagchi, B., 1992. Levinthal's paradox. Proc. Natl. Acad. Sci. 89, 20–22.